Heat Vulnerability and Risk Analytics for The Built Environment

by

Norhan Magdy Bayomi

Bachelor of Architecture
Cairo University, 2008

Masters of Science in Architecture
Cairo University, 2012

Masters of Science in Building Technology
Massachusetts Institute of Technology, 2017

Submitted to the Department of Architecture
in Partial Fulfillment of the Requirements for the Degree of

Doctor of Philosophy in Architecture: Building Technology
at the

Massachusetts Institute of Technology

September, 2021

© 2021 Massachusetts Institute of Technology

Signature of Author: _____

Department of Architecture
August 6th, 2021

Certified by: _____

John E. Fernandez
Professor of Building Technology
Thesis Supervisor

Accepted by: _____

Leslie K. Norford
Professor of Building Technology
Chair, Department Committee on Graduate Students

Thesis Supervisor

John E. Fernandez
Professor of Building Technology
Massachusetts Institute of Technology

and readers

Leslie K. Norford
Professor of Building Technology
Massachusetts Institute of Technology

Tarek Rakha
Assistant Professor of Architecture
Georgia Tech

Heat Vulnerability and Risk Analytics for the Built Environment

by

Norhan Magdy Bayomi

Submitted to the Department of Architecture on
August 6th , 2021
in Partial Fulfillment of the Requirements for the Degree of
Doctor of Philosophy in Architecture: Building Technology

ABSTRACT

Climate change risks are considered one of the major global concerns that face humankind in the 21st century. Heatwaves have been identified as one of the deadliest climate hazards, especially in urban areas. Also, extreme heat events have been growing in intensity, duration, and frequency; more risks are expected to affect the urban population. Heat vulnerability assessment in the built environment is a complex process with multiple dynamics and components of human-natural systems and their interaction with the surrounding built environment. These dynamics include social, demographics, urban growth, environmental changes, access to public services, and policy impacts. Yet, there are considerable gaps in the literature on the effect of heat exposure and the built environment as a protective factor from potential vulnerability and risk perspectives.

This dissertation addresses this need by developing a multifaceted and multi-scalar framework for heat vulnerability assessment. The framework is designed to inform decision-makers on the local dimension and the distribution of vulnerable populations by answering two key questions: where and what are the impacts of heat exposure in an urban setting? Who are the most susceptible populations to heat exposure? The dissertation explores vulnerability at multiple levels starting with a detailed assessment of the built environment by integrating the impacts of the physical characteristics of the existing building stock, available urban resources for long-term adaptation, and individuals' adaptive capacity and potential health impacts under varying indoor exposure. Next, a methodology for rapid vulnerability analytics using novel technology such as aerial thermography coupled with Computer Vision (CV) and Machine Learning (ML) techniques to assess the thermal performance of building envelopes to provide actionable data for adaptation strategies at both the building and district levels. Finally, an evaluation framework to assess policy impact on the vulnerability of the urban system during heat events and how delays in the public policy response can increase risk levels.

Thesis Advisor: John E. Fernandez
Title: Professor of Building Technology

In The Name of Allah the Most Gracious the Most Merciful

Acknowledgments

This dissertation would not have been possible without the help, support, and encouragement of my advisor, prof. John E. Fernandez- thanks for giving me the chance to follow and pursue my passion and helping me fulfill my research aspirations; and am excited for whatever comes next. I will always be grateful for his support and for being an exemplary mentor. I have learned a lot from him and hope that I can pay it forward by trying my best to be as great of an adviser to my prospective students as he was to me.

I extend my gratitude to the members of my thesis committee. Professor Leslie Norford, for his insights in heat vulnerability framework development has been invaluable, and his editorial guidance was indispensable to my work on heat exposure analysis. Dr. Tarek Rakha's experience with UAVs and aerial thermography made the rapid analytics efforts possible.

I further would like to thank my colleagues at the Environmental Solutions Initiative, Juan Camilo and Marcela Angel, for their support and assistance in the work in the Bronx; I am forever thankful for believing in this work and supporting me all the way. I want to thank my colleagues in the AIRBEM project, Burak, Yasser, and Eleanna, for their support; it has been a great experience contributing to this project.

I am grateful to the Building Technology program for providing a friendly and inspiring work environment, to the BT faculty and my colleagues for the intellectual support and feedback that helped shape this research and the SA+P staff, Cynthia and Renee, who were always there to help.

I would thank my Egyptian family here at MIT, the MIT Egyptian Students Associations, my friends Randa Azab, Islam Hussein, and Mohamed Ibrahim for their support throughout my journey. I am also thankful to my UROP Mohanned El Kholy for his assistance in developing machine learning models and the work in Cairo, and Ali Ghazal for his valuable help in the development of the MENA heatwave platform. To my friends at Anjunabeats, thank you for believing in me so much and pushing me musically while supporting my academic journey; it has been a true blessing.

Lastly, but most importantly, absolutely none of this would have been possible without my mother's support. Thank you for always believing in me, I see your pride, and I appreciate it. Thank you for always working hard to ensure I can chase my dream. To my dad and brother, may your souls rest in peace; I would not be who I am, where I am, or how I am without you. I doubt I will ever feel as I did when you both were alive, and I know you are taking care of each other until we all unite again; thanks for all you've all done to get me here to this day.

To my brother, Tamer and my father
May your souls rest in peace
And May Almighty Allah dwell you in Jannatul Firdaus

To my Mother
My inspiration

Table of Contents

I.   INTRODUCTION

Climate change risks are considered one of the major global concerns that face humankind in the 21st century. One of the most direct health-related risks arising from climate change is the increased exposure to high ambient temperature (Daniela D'Ippoliti et al., 2010; Antonio Gasparrini & Armstrong, 2011; Guo et al., 2017; J. Y. Lee et al., 2019). Heatwaves have been identified as one of the deadliest climate hazards, especially in urban areas that accommodate populations with specific physical and socioeconomic characteristics (Patz et al., 2001; Pengelly et al., 2007). Heat-related morbidity is primarily extensive in areas with a population with pre-existing medical conditions such as cardiovascular problems and mental disorders (Kovats & Hajat, 2008; Shen, Howe, Alo, & Moolenaar, 1998). The elderly, socially isolated, uneducated, and people living in low-income housing have been highly vulnerable to extreme heat exposure (Balbus & Malina, 2009; Vandentorren et al., 2006). Historical evidence can be found in the Chicago heatwave in 1995 that killed more than 700 persons (Klinenberg, 2003b), and the famous European heatwave in 2003 took more than 22,080 lives (Fouillet et al., 2006, Stone, 2012).

Extreme heat events or heatwaves are defined as an extended period of high temperature that can alter daily lifestyle and have adverse health impacts on affected populations(Ramamurthy, González, Ortiz, Arend, & Moshary, 2017). Heatwaveshave been growing in intensity, duration, and frequency; more risks are expected to affect the urban population. Over the past 15 years, the number of urban communities exposed to extreme heat events has increased to reach around 125 million people by 2016. In 2015 alone, approximately 175 million people worldwide were exposed to excessive heat (Roaf & Nicol, 2017). With the growing concerns of future heat exposure, numerous studies in the literature have developed heat vulnerability indices based on determinants that have heat-related impacts. Most heat vulnerability determinants are found in epidemiological literature, expert interviews, and socioeconomic characteristics utilized as indicators for the high concentration of vulnerable populations. Policymakers rely on vulnerability indices in heat-related adaptation policies (Klein Rosenthal, Kinney, & Metzger, 2014). However, quantitative evaluation of heat vulnerability can provide more insights into the physical and spatial distribution of heat-related risks (Chow, Chuang, & Gober, 2012, Maragno, Fontana, & Musco, 2020).

1.1 Motivation

Increased heat exposure has a detrimental impact on human health, causing an increase in morbidity and mortality (Brooke Anderson & Bell, 2011; Martiello & Giacchi, 2010; Zeng, Li, Cui, Jiang, & Pan, 2016). The effects of extreme heat events have been evident over the past years by several extreme heat events worldwide (Mbokodo, Bopape, Chikoore, Engelbrecht, & Nethengwe, 2020). The 2003 European heatwave and the 2010 Russian heatwave have caused thousands of deaths from heat exposure (Barriopedro, Fischer, Luterbacher, Trigo, & García-Herrera, 2011; Fouillet et al., 2006). In the United States context, the heatwave in California in 2006 took over 600 lives and caused over 16,000 hospital emergency visits from heat (Basu, Pearson, Malig, Broadwin, & Green, 2012). Future projections indicate an increase in heat events' frequency and intensity in the next 20 years (Figure 1-1), posing greater threats to human lives. In cities, health risks from heat exposure are more complicated as heat stress results from numerous factors related to the built environment's physical characteristics that influence urban communities' health and safety. Also, heat-related risks are distributed disproportionately depending on the urban space's physical and socioeconomic factors (Reid et al., 2009). Despite the rising threats from heat exposure, they can be preventable with suitable analysis and warning methods. Since climate change plays a significant role in increasing the frequency of extreme heat events (Field et al., 2012), an improved understanding of areas under potential risks is urgently needed. This would require a better analysis and knowledge of the possible full impacts and the influence of the built environment's physical characteristics.
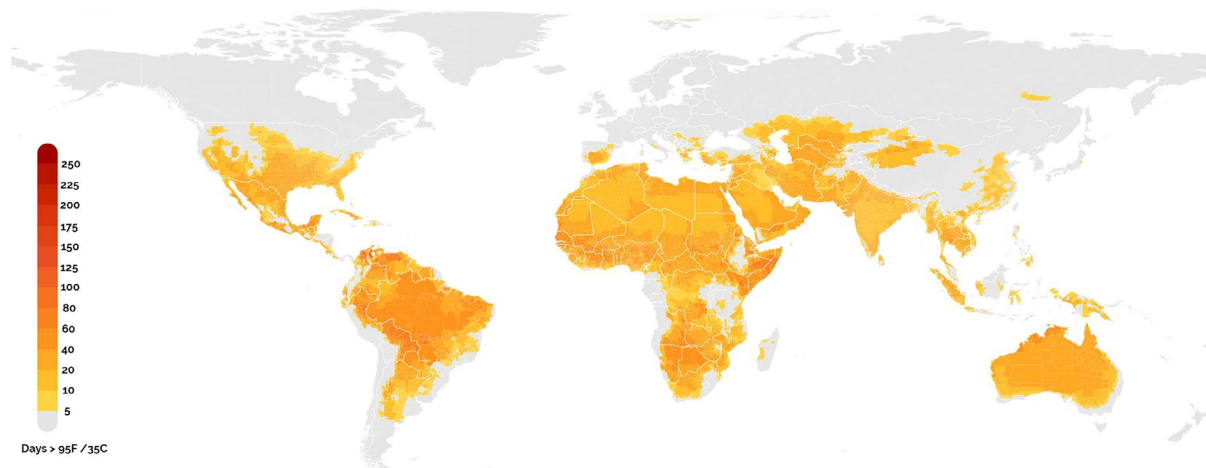
Figure 1-1: Number of days above 95F/32C between 2020-2040 under Business As Usual (RCP 8.5-BAU). (Source: Climate Impact Map).

This dissertation sets out a multi-scalar approach for heat-related vulnerability in cities, emphasizing the impacts of the surrounding built environment's physical characteristics and population adaptive capacity. The remainder of this chapter presents previous efforts from the literature in heat-vulnerability assessment and outlines needs and opportunities to develop a comprehensive framework for heat vulnerability analytics described in the following chapters.

1.1.1 Climate Change Risks and Global Heatwaves

Global warming over the past decades has drastically changed our climate (Perkins-Kirkpatrick & Gibson, 2017). It has been widely established that climate change is considered "the biggest global health threat of the 21st century", posing risks to human lives and the global population's well-being at an escalated rate (Costello et al., 2009). One of the major climate threats is extreme heat events, as they pose significant risks to public health that are well documented in the epidemiologic literature (Baldwin, Dessy, Vecchi, & Oppenheimer, 2019). As a result of climate change, studies have shown that there is a rising trend in the global mean surface air temperature in the past 100 years (Intergovernmental Panel on Climate Change (IPCC), 2013). Consequently, the frequency and intensity of extreme heat events have witnessed a significant increase in the past ten years (Perkins, Alexander, & Nairn, 2012). Furthermore, the World Health Organization (WHO) has identified rising negative impacts from heat exposure in the next 30 years (World Health Organization (WHO), 2018), mainly in locations with poor infrastructure and limited adaptation capacity, as shown in Figure 1-2 below.
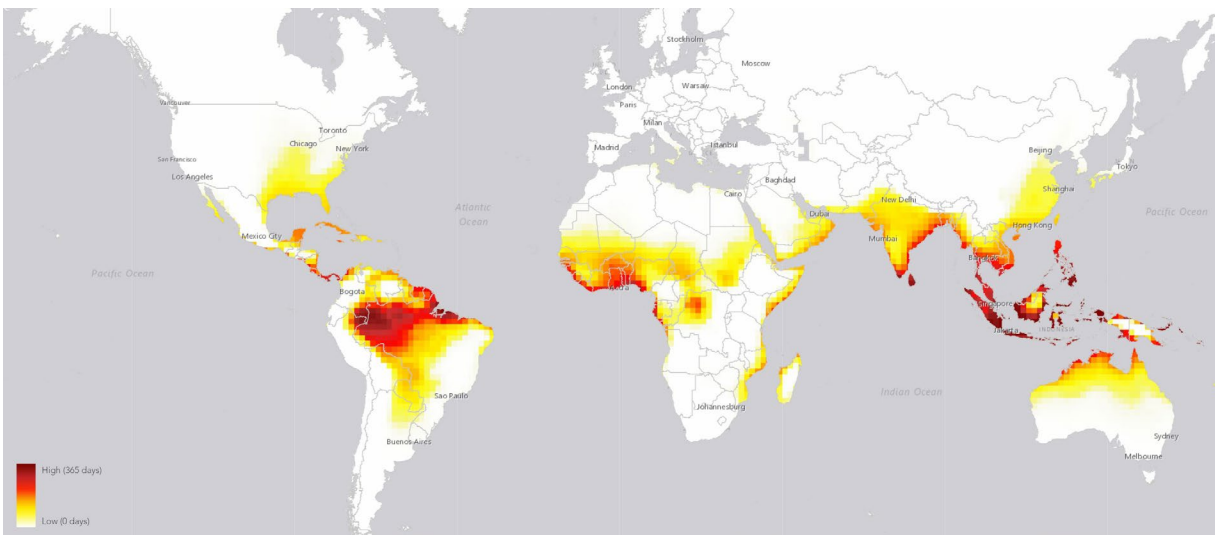
Figure 1-2: Projected deadly heatwaves by 2050 under Business As Usual (BAU) scenario. (Source:(Mora et al., 2017a)).

Regional and multi-country studies have demonstrated that heatwaves have elevated morbidity and mortality (Anderson & Bell, 2009a; Daniela D'Ippoliti et al., 2010; Deschênes & Greenstone, 2011; A. Gasparrini, Guo, & Hashizume, 2015; Merte, 2017). In addition to risks to human health, heatwaves can cause power supply disruption resulting in loss of air conditioning access (Aivalioti, 2015; van der Wiel et al., 2016). Also, prolonged heat exposure associated with heatwaves was found to affect crop production and the efficiency of livestock (Battisti & Naylor, 2009; Lobell, Schlenker, & Costa-Roberts, 2011; Meerburg et al., 2009). Despite these significant impacts, heatwaves do not often get enough media attention as their consequences are not visually vivid. On a city level, most heatwave impacts usually occur in low-income neighborhoods with limited access to air conditioning or areas that accommodate a large portion of the elderly, socially isolated, or racially marginalized populations (Baldwin et al., 2019; Fouillet et al., 2008).

1.1.2 Urban Population and Heat Vulnerability

The projected increase in extreme heat events has raised concerns about potential health risks in cities. Recent literature on heat-related mortality has defined risk as a function of vulnerability (sum of exposure and susceptibility) minus adaptive capacity (Intergovernmental Panel on Climate Change (IPCC), 2013). In climate change science, vulnerability is defined as "the degree to which a system or system component is likely to experience harm due to exposure to a hazard, either perturbation or stress" (B. L. Turner et al., 2003) or "the characteristics of a person or group and their situation that influence their capacity to anticipate, cope with, resist, and recover from the impact of a natural hazard" (Bankoff, Hillorst, & Frerks, 2004). Currently, around 200 million people who live in over 350 cities at an average maximum temperature above 35oC are considered highly vulnerable to future extreme heat exposure (Hoegh-Guldberg et al., 2018). Future climate projections show that by 2050 the number of cities exposed to extreme heat events will increase dramatically (Figure 1-3) (United Nations, 2018).
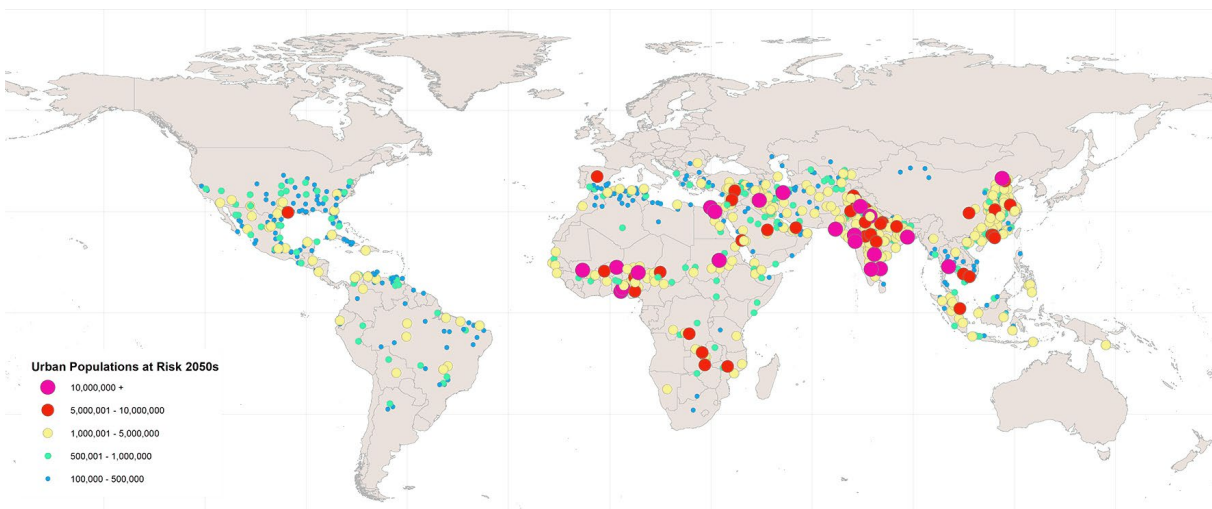
Figure 1-3: Cities with a three consecutive month period where average maximum temperatures exceed 35°C that are projected to extreme heat by the 2050s. (Source: C40 Cities, For cities the heat on).

As a greater proportion of the urban population will be exposed to heat events in the next 30 years, there are speculations on the effectiveness of aggressive heat strategies to lessen or reverse the overall rising trends of increased heat risks in cities (Arbuthnott, Hajat, Heaviside, & Vardoulakis, 2016). These doubts are driven by the immense costs associated with adaptation strategies in cities, primarily based on large-scale quantitative information that doesn't fully capture the complexity of urban conditions or vulnerable populations (Baldwin et al., 2019). Moreover, minimizing the adverse effects of heat events on the vulnerable urban population through targeted strategies is a complicated process that would require highly detailed data on the spatial distribution of highly vulnerable urban populations. Although social factors have been identified in many studies as a primary driver for heat vulnerability, building and urban physical characteristics play a role that has not been thoroughly examined in the literature (Baniassadi et al., 2020). Therefore, there is a need for a vulnerability assessment framework that is based on quantifiable data on the performance of the built environment under heat exposure and thus produces reliable guidelines on where heat adaptation strategies can be prioritized and over what time scale.

1.1.3 Built Environment Impacts on Heat Risks

In the context of extreme heat vulnerability, there has been an interest in heat-related health impacts in urban areas. Complications from extreme heat exposure are experienced at a greater level in cities (Figure 1-4). This is due to the urban heat island (UHI) effect phenomenon, where urban areas are usually warmer than rural surroundings by 1-3oC during the daytime and up to 12oC during the nighttime (Environmental Protection Agency (EPA), 2011; Hondula et al., 2012). This causes urban centers to be more susceptible to heat exposure, leading to greater human health risks, especially in vulnerable populations. In the literature, several studies have examined the city as a whole unit of analysis to compare different cities (Briley, Brown, & Kalafatis, 2015; Lapola, Braga, Di Giulio, Torres, & Vasconcellos, 2019a). Other studies have conducted a more detailed analysis at the city level to examine spatial variability in heat risk across the same city (Apotsos, 2019; de Sherbinin, Schiller, & Pulsipher, 2007). Brown and Walker (2008) have proposed a more detailed framework to examine heat stress as a function of reduced capacity to cope with heat exposure due to surrounding contextual and social factors.
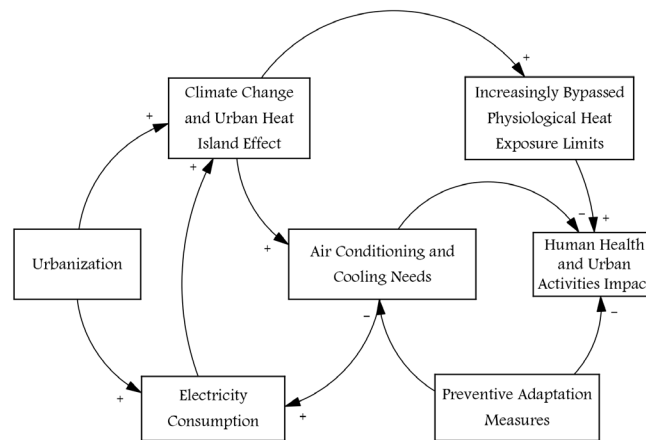
Figure 1-4: Dynamic relationship between heat exposure, urbanization, UHI, and related health impacts.

Housing characteristics have also been linked to potential heat-related health risks (Maller & Strengers, 2011). Building characteristics play a significant role in indoor heat exposure, especially in low-prevalence air-conditioning neighborhoods (Ramamurthy et al., 2017). During heatwaves, indoor air temperature can often exceed outdoor air temperature depending on buildings' thermal inertia (Pyrgou, Castaldo, Pisello, Cotana, & Santamouris, 2017). Heat events can also drive a sharp increase in health service capacity and cooling demand, disrupting cities' health service and power supply similar to what happened in South Korea in 2013 and Germany in 2010 (Aivalioti, 2015). Besides power disruption, heat exposure can influence human productivity, which also comes with great economic losses. The Intergovernmental Panel on Climate Change (IPCC) has identified that reducing human productivity during heatwaves can cause global economic costs of 2 trillion dollars by 2030 (UNDP, 2016). There is currently limited adequate information on how to utilize the physical environment's performance to cope with extreme heat exposure in adaptation planning (Arbuthnott et al., 2016). Thus, to facilitate heat adaptation strategies, there is a necessity for a framework that quantifies the potential heat-related impact with respect to the built environment's performance. This dissertation proposes and tests a vulnerability assessment framework to meet this need.

1.2 State of The Art: Heat Vulnerability Assessment

The IPCC Fourth Assessment Report (AR4) has defined a framework to evaluate climate change vulnerability assessment (IPCC, 2014a; Oppenheimer et al., 2014). The methodology developed by IPCC involves the interaction between exposure (driver of hazard), the susceptibility of a system to a hazard, and adaptive capacity as the sum of vulnerability stimuli. The majority of heat vulnerability studies have utilized the IPCC definition of vulnerability components incorporating: susceptibility, exposure, and adaptive capacity as the sum of vulnerability to a climate hazard (Oppenheimer et al., 2014). There has been a growing interest in examining the relationship between heat vulnerability in urban areas, as illustrated in Figure 1-5 (Hajat & Kosatky, 2010; Vardoulakis et al., 2015). Most of the literature work focused on heat vulnerability assessment from an epidemiological approach to examine how temperature can influence human mortality (Curriero et al., 2002; W. Ma, Chen, & Kan, 2014; McMichael et al., 2008). Other studies have examined heat vulnerability on the spatial level in cities to help policymakers account for spatial variation in climate adaptation planning (Cai, Tang, Chen, & Han, 2019; Hondula, Davis, Saha, Wegner, & Veazey, 2015; Johnson, Stanforth, Lulla, & Luber, 2012).
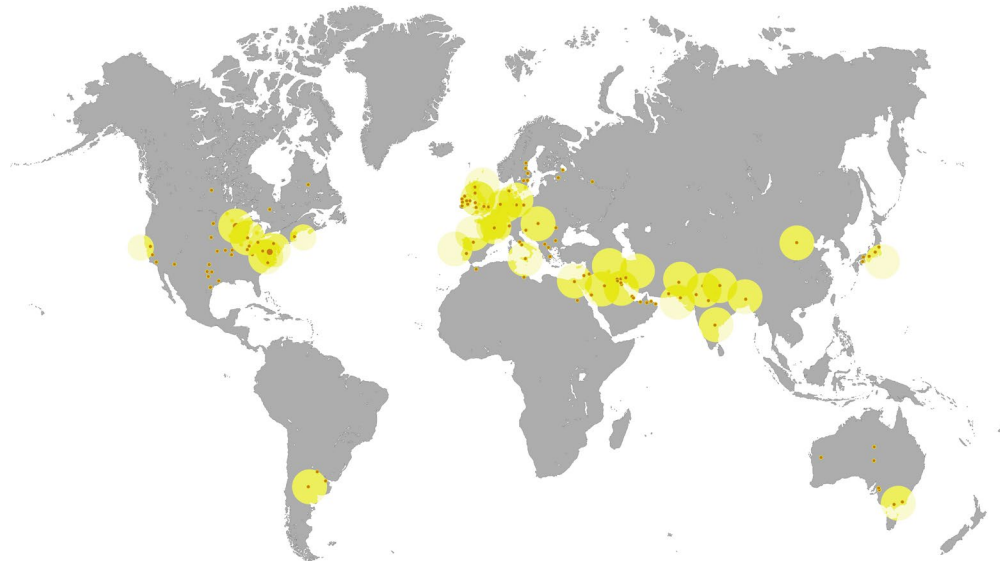
Figure 1-5: Locations of heat-related deaths (orange) and studies on heat vulnerability (yellow) from 2003-2018.

Studies on heat vulnerability assessment have relied significantly on large-scale quantitative information that doesn't fully capture the complexity of urban conditions or vulnerable populations (Brown & Walker, 2008). Romero et al. (2012) have identified 13 factors in the relationship between urban vulnerability and temperature exposure. The study included human-related factors including population density, age, income level, race, education, medical condition, social support, heat acclimatization, adaptation-related parameters such as access to cooling amenities and air conditioning units, and exposure magnitude represented as temperature level. However, there has been limited research on the empirical relationship between urban population susceptibility and heat exposure magnitude from the surrounding physical environment (Arbuthnott et al., 2016). This section presents an overview of existing literature in the field of heat exposure and human vulnerability in urban areas, discusses recent developments of a heat vulnerability assessment framework in cities that are significant for this research, and outlines gaps that this dissertation aims to fulfill.

1.2.1 Heat as a Climate Hazard

A heatwave is denoted as a period, primarily several consecutive days, where the air temperature is significantly higher than the average (Ramamurthy et al., 2017). As previously discussed, heatwaves are one of the significant climate threats to human lives. However, there is still a limited understanding of how we can apply suitable policies to mitigate or lessen heat's impacts on human lives. Climate change plays a significant role in driving heat exposure and its effects on human health. In cities, humans depend mainly on air conditioning to mitigate heat exposure, as there around 1.6 billion units are in operation worldwide (A. Barreca, Clay, Deschenes, Greenstone, & Shapiro, 2016; IEA, 2018). Although air conditioning lessens heat exposure, there is still a potentially high risk in case of power failure from increased demand during extreme heat events (Yu et al., 2012). Although low-income neighborhoods have a high magnitude of heat exposure, these areas tend to have limited air conditioning access. The current increase in heat-related mortality is caused by escalated health risks and limited heat recovery during mega-blackouts (Mora et al., 2017a).
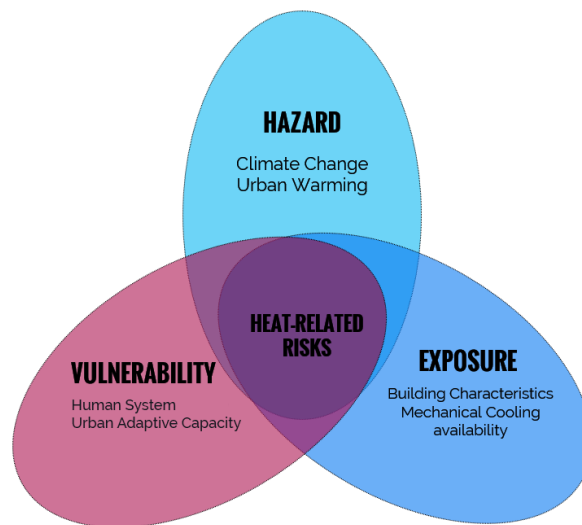
Figure 1-6: Heat-related risks as a function of heat exposure and vulnerability under the scope of climate risk assessment.

In the field of climate risk assessment, health risks are expressed as a function of exposure, hazard, and vulnerability (Figure 1-6). The literature on climate hazard assessment has distinguished between risk resources (climate hazard) and changes in the human system due to risk-shifts over time (Baniassadi, 2019). Vulnerability assessment has been proposed as an indicator that captures the human system's underlying socioeconomic characteristics to evaluate populations' susceptibility to climate hazards and adaptive capacity to cope with heat exposure (Bankoff et al., 2004). In this dissertation, heat is described as a climate hazard characterized by prolonged periods of high temperature with two key drivers: global climate variability and urban development in a changing climate. There are two key components for exposure: outdoor exposure induced from the built environment's characteristics and indoor heat exposure that responds to outdoor heat and is regulated by buildings' physical characteristics and availability of cooling means. Finally, vulnerability represents a framework to examine and analyze how the urban systems' components from the physical built environment and the human system's response can lessen or mitigate heat-related health risks.

1.2.2 Indoor Heat Exposure

It is well documented in the literature that there is a relationship between increased outdoor temperature and human mortality, where mortality increases when the temperature exceeds a specific threshold (Auliciems & Skinner, 1989; Nicholls, Skinner, Loughnan, & Tapper, 2008; Saez, Sunyer, Castellsagué, Murillo, & Antó, 1995). However, indoor temperature can vary significantly compared to measured outdoor temperature during extreme heat events that can substantially affect this relationship in addition to human behavioral adjustments to cope with the heat, as illustrated in Figure 1-7 (Mavrogianni, Davies, Wilkinson, & Pathan, 2010b; Sakka, Santamouris, Livada, Nicol, & Wilson, 2012; White-Newsome et al., 2012; Wright, Young, & Natarajan, 2005). For instance, during summertime, the outdoor temperature at night typically decreases below daytime levels, while indoor temperature usually stays elevated depending on the building's physical and thermal properties (Sakka et al., 2012). Also, indoor air temperature, humidity levels, and airspeed can significantly expose occupants to high levels of heat stress (Pyrgou et al., 2017). Thus, continuous heat exposure can lead to elevated heat-related health risks. Such risks can be lethal to populations with no access to adequate protective measures such as (mechanical ventilation, air conditioning) or those who lack knowledge on suitable behavioral strategies to mitigate heat exposure similar to previous heat events back in 1995 and 2003 (Semenza, 1996; Semenza, McCullough, Flanders, McGeehin, & Lumpkin, 1999; Wright et al., 2005). In addition, recent studies showed that health costs associated with heat events have been increasing drastically and are expected to place an insurmountable burden on the health service system worldwide in the three two decades (Knowlton, Rotkin-Ellman, Geballe, Max, & Solomon, 2011).
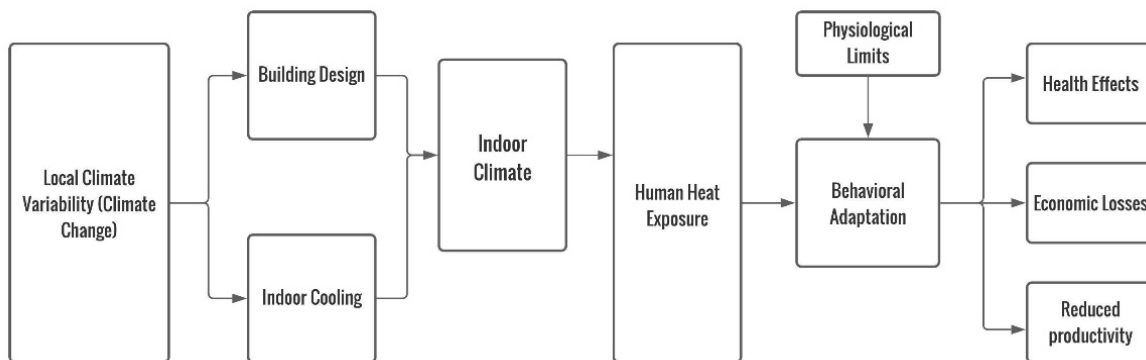
Figure 1-7: Excess heat exposure and related health risks.

There has been a vast literature on the relationship between indoor and outdoor temperature; some studies indicate a linear relationship in naturally ventilated buildings, raising higher risks for the low-income population (Audrey Smargiassi, Fournier, Griot, Baudouin, & Kosatsky, 2008). Rising future temperatures imply that the urban population is expected to experience a prolonged heat exposure period, especially when average people spend around 90% of their time indoors (Klepeis et al., 2001; Leech et al., 2002). Heat stress in buildings is inevitable, driving the urgency to identify a suitable adaptive measure to reduce the health consequences of future heat events.

1.2.3 Urban Heat Stress

The relationship between ambient outdoor temperature and human health is represented as a U-curve shape where heat-related health risks increase exponentially when the temperature exceeds a specific threshold, as shown in Figure 1-8 below (Kenny, Flouris, Yagouti, & Notley, 2019; A. Smargiassi et al., 2009). Numerous studies have investigated the attributable relationship between the urban thermal environment and human mortality during extreme heat events to understand outdoor heat exposure's health effect over time (Curriero et al., 2002; McMichael et al., 2008). Findings from the literature identified several factors that contribute to heat-related health risks in urban areas (Keatinge et al., 2000; Medina-Ramón & Schwartz, 2007; Semenza, 1996), such as climate, location, urban density, seasonal variation, the arrangement of the neighborhoods within the city and time of the year when the heatwave happens, as illustrated in Figure 1-8. Also, urban planning and transportation policies can impact city size and shape and, as a result, influence the magnitude of heat-related risks (Costello et al., 2009; Kenny et al., 2019). Previous studies on mapping heat stress have found an association between urban temperature and mortality during extreme heat events (Kenny et al., 2019; Maller & Strengers, 2011; Stapleton et al., 2014).
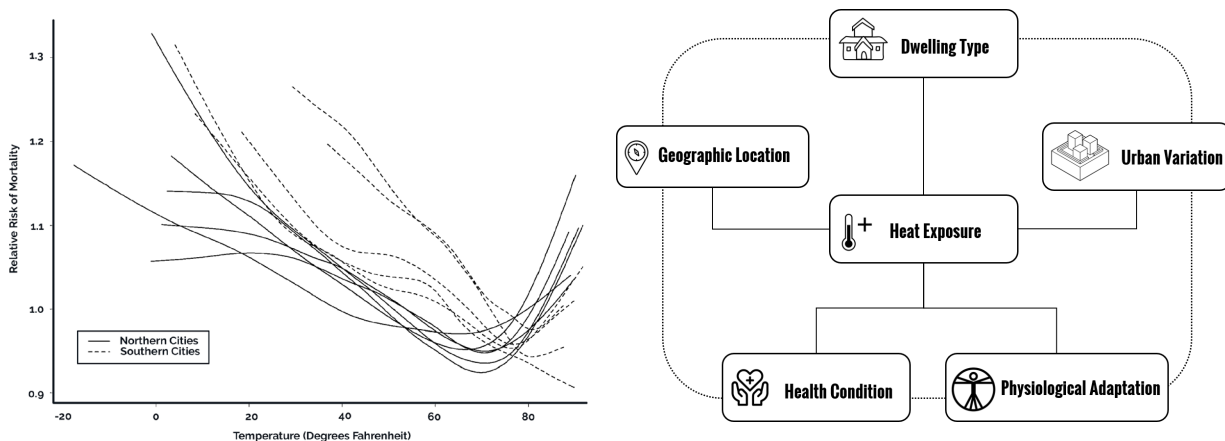
Figure 1-8: Left: Temperature and mortality relative risk function for cities in the U.S. (based on (Curriero et al., 2002) Right: Factors affecting heat exposure and human response in the urban context. (Based on (Kenny et al., 2019).

Scientific communities have applied different assessment frameworks to examine the association between heat exposure in the city and health risks (Jänicke et al., 2019). One of the most common tools is the heat index, which aggregates scores for multiple indicators linked to heat vulnerability into a single score representing vulnerability. Although there is a vast body of literature on UHI and health risks, there is still a limitation in understanding policy impact in reducing heat vulnerabilities (Ketterer & Matzarakis, 2014). Policy planning at the city's scale may affect adaptation strategies and consequently lessen or improve heat-related health impacts. However, evaluating such policy is challenging to examine due to the intricate interaction of multiple physical scales in the city. This includes the physical scale of the built environment and its relationship with the human system and associated socioeconomic variables that can induce a change in inhabitants' behavior during heat exposure and need to be included in heat vulnerability assessment.

1.2.4 Human Adaptive Capacity

Adaptive capacity is one of the heat vulnerability components that significantly influence potential health impacts associated with heat exposure. In climate change science, adaptive capacity or coping capacity is defined as " the ability of people, organizations and systems, using available skills and resources to face and manage adverse conditions, emergencies or disasters" that can "contribute to the reduction of disaster risks." (Intergovernmental Panel on Climate Change (IPCC), 2013). The IPCC fourth assessment report states that that "adaptive capacity is the ability of a system to adjust to climate change [including climate variability and extremes], to moderate potential damages, to take advantage of opportunities or to cope with the consequences." (IPCC, 2014a). In that sense, adaptive capacity is linked to the physical system and the human system's ability to mitigate climate hazard risks, denoted as heat exposure in the dissertation. In urban physical space, adaptive capacity can be categorized into two levels: coping capacity can be determined by the potential to adjust to heat exposure in the long term, whether on the building level through air conditioning or other means of mechanical cooling. In comparison, adaptive capacity is defined by adapting to heat risk in the long term (Maragno, Fontana, & Musco, 2020).
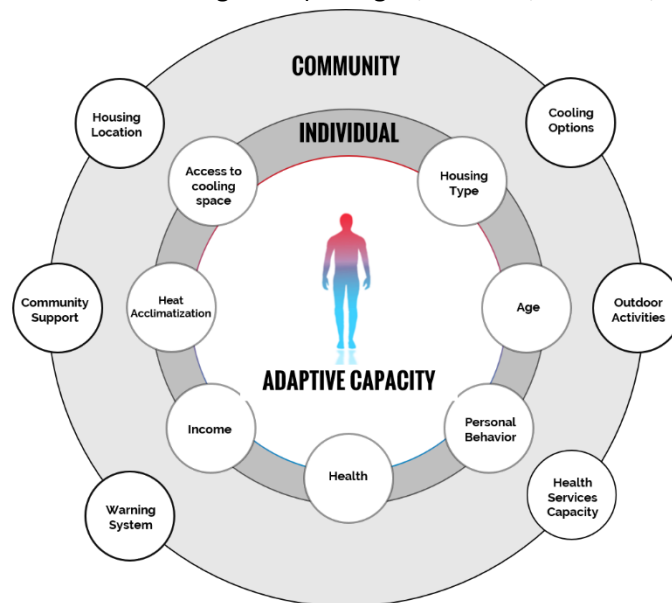
Figure 1-9: Different levels of adaptive capacity within the framework of heat vulnerability assessment in cities.

On the other hand, human systems' adaptive capacity is determined on two levels (Figure 1-9), first an individual adaptive capacity moderated by the socioeconomic, physiological, and psychological characteristics (Brown & Walker, 2008; Lapola et al., 2019a). Second, the surrounding urban community's adaptive capacity is linked to social support and accessibility to health services. Numerous studies have examined multiple strategies to improve urban adaptive capacity under heat exposure, such as green infrastructure utilization, enhancing accessibility to cooling shelters (Sampson et al., 2013). However, there is a limited understanding of how policymakers can better evaluate and improve coping and adaptive capacity with an adequate and targeted plan addressing both the physical and human systems. With climate change is likely exacerbating heat-related health impacts, cities need to prepare better, respond, and avoid heat-induced health risks.

1.3 Research Opportunities

There is an alarming need to respond to health risks associated with extreme heat events (Fuhrmann, Sugg, Konrad, & Waller, 2016). The previous section presented the significant work that has been done in the field of heat-related mortality and vulnerability assessment in cities, especially as it is related to heat-related risks in urban areas and factors driving vulnerability to heat exposure. Previous studies on heat vulnerability assessment established a framework that explored heat risk association with UHI (Ramamurthy et al., 2017; Tomlinson, Chapman, Thornes, & Baker, 2011) and health-risks from indoor overheating and mapping heat vulnerability populations using socioeconomic characteristics (Maller & Strengers, 2011; Pyrgou et al., 2017). However, the most recent findings from the literature report a limited knowledge of the effects of heat exposure on vulnerable populations (Kenny et al., 2019; Lancet, 2015). This limits policymakers' ability to identify suitable adaptation strategies for heat protection and prevention policies to alleviate thermal risks during extreme heat events. Also, the absence of proper adaptation and coping measures to heat would drive higher risks to human mortality and quality of life due to extreme heat exposure that will increase in the absence of climate change.

Furthermore, research findings suggest that even under AC's presence, specific groups of vulnerable populations such as the elderly might be at significant risk from heat stress (Dufour & Candas, 2007). Finally, a lack of quantifiable data corresponds to the intricate relationship between heat exposure due to urban settings' physical characteristics and human adaptive and behavioral response, whether through physiological adaptation or surrounding amenities, to mitigate and lessen health impacts from prolonged heat exposure (Kenny et al., 2019; Lindemann et al., 2017). Gaps in the existing literature on heat vulnerability assessment can be summarized as follows:

- There are considerable gaps in the literature on the effect of heat exposure and buildings as a protective factor from vulnerability and exposure perspectives;
- Existing heat vulnerability frameworks are decoupled from the effects of the physical characteristics of the surrounding built environment;
- Lack of empirical evidence that demonstrates the relationships between heat exposure and health outcomes, especially for vulnerable populations with limited access to adaptation mechanisms;
- Potentials of aerial technology in urban heat vulnerability assessment are not explored in the existing vulnerability frameworks;
- Limited understanding of policy role in heat adaptation planning and how it can lessen or exacerbate potential heat risks.

1.3.1 Research Goal

To address the limitations above, the goal of this research is to develop a multifaceted and multi-scalar framework for the assessment of heat vulnerability that is tailored to integrate the impacts of the physical characteristics of the built environment on the urban level and building level, the available urban resources for long term adaptation, and individual adaptive capacity. This framework is designed to inform decision-makers of the distribution of vulnerable populations, answering two key questions: where and what are the impacts of heat exposure in an urban setting? Who are the susceptible populations? Through analyzing and assessing the relationship between heat exposure, built environment, and social characteristics, we can identify factors that make a given population more vulnerable to heat hazards or prolonged heat exposure.

1.3.2 Hypotheses

The research presented in this dissertation is developed around the premise that there is a need for a multivalent framework to assess heat vulnerability in the urban setting and is based on the following hypotheses, which are revisited in the concluding chapter:

- **Comprehension of Vulnerability:** Including built environment impacts in the vulnerability assessment framework can provide reliable information in adaptation planning;
- **Heat exposure and adaptive capacity limits**: Health impacts from heat exposure vary based on individual physiological factors and the coping and adaptation capacity of the surrounding built environment that needs to be included in heat vulnerability assessment;
- **Rapid vulnerability analytics**: Utilizing aerial technology will help assess heat vulnerability and identify high-risk urban areas and their distribution.
- **Heat adaptation and policy impacts:** Policies and institutional capacities can create conditions associated with increased vulnerability.

1.3.3 Dissertation Overview

This dissertation includes three main parts that examine the components of heat vulnerability assessment, as summarized in Figure 1-10 below: 1) built environment heat vulnerability assessment, 2) rapid vulnerability analytics, and 3) heat adaptation planning.

Chapter 1: Introduction includes research background, literature overview, and research opportunities considered in this dissertation.

Part I. Built Environment heat vulnerability assessment focuses on developing a framework for heat vulnerability assessment in urban settings.

Chapter 2: Built Environment heat vulnerability focuses on two main key outputs: 1) developing a heat vulnerability assessment framework for three levels: urban vulnerability preliminary assessment; detailed analysis; and risk identification, and intervention evaluation and adaptation policy design. 2) Heat vulnerability quantification in urban settings.

Chapter 3: Detailed Assessment of Heat Vulnerability in Low-Income Communities, expands the central framework of heat vulnerability assessment using a case study in Cairo, Egypt, to examine three main topics:

A. Indoor overheating assessment: examines how indoor overheating is modified by the building's physical characteristics and the resulting exposure range.
B. Heat exposure and human adaptive capacity: analyzes heat exposure threshold associated with increased health risks in vulnerable populations.
C. District level heat exposure assessment in Low-Income communities: develops a computational framework for district-level vulnerability assessment and exposure quantification.

Part II. Rapid Vulnerability analytics – Chapter 4: focuses on the applicability of using Unmanned Aerial Vehicles in the larger framework of heat vulnerability assessment on the building scale and urban scale**.**

Part III. Urban Intervention and Policy Design – Chapter 5: examines how different adaptation measures can influence vulnerability level and identify policy's role in long-term adaptation planning.

Chapter 6. Conclusion: summarizes the dissertation's contribution, potential impacts of the proposed vulnerability framework, and future research directions.

	CHAPTER	GAPS	METHODS	OUTCOMES
Context	**1. Introduction**		**Literature review**	Examines research context, gaps & opportuinities
				Understands concepts and theories related to the topic
Heat Vulnerability Assessment	**2. Heat Vulnerability Assessment**	Need for a multiscalar framework for heat vulnerability assessment in urban contexts There are considerable gaps in the literature on the effect of heat exposure and buildings as a protective factor from vulnerability and exposure perspectives	**Systematic literature review, System Dynamics models, Simulation models**	A comprehensive framework for heat vulnerability assessment addressing urban level, building level and policy level A quantitive framework for heat vulnerability assessment taking into account the physical charachteristics of the built environment
	3. Detailed Assessment of Heat Vulnerability	Existing heat vulnerability frameworks are decoupled from the effects of the physical characteristics of the surrounding built environment;	**Simulation models, survey, personal interviews, computational model using Machine learning technqiues**	Examine how indoor heat exposures are modified by building's physical charachteristics and occupants' behavioral adaptation in low-prevalance AC urban communities Evaluates the spatial distribution of heat vulnerability factors and how they relate to large scale district level assessment
		lack of empirical evidence that demonstrates the relationships between heat exposure and health outcomes. Especially for vulnerable populations with limited access to adaptation mechanisms	**In-person monitoring and climatic monitoring**	Examines heat exposure in an existing neigbhourhood in Cairo, Egypt to identify the critical threshold temperatures beyond which heat-related impact are proliferated to potential health risks
Rapid Vulnerability Analytics	**4. Rapid Health Vulnerability Analytics**	Potentials of Aerial technology in urban heat vulnerability assessment are not explored in the existing vulnerability framework	**Simulation models, In-Situ Measurements using UAVs, Survey, Questionnaire**	Examines the applicability of using UAVs technology in the assessment of existing building thermal performance Test UAVs as an approach for heat vulnerability assessment with community engagement in a low-income neighbourhood in Bronx, NYC
Heat Adaptation & Policy Support	**5. Heat Adaptation Planning & Policy Design**	Limited understanding of policy role in heat adaptation planning and how it can lessen or exacerbate potential risks over the long terms	**Literature review, System Dynamic models**	Proposes an integration of multiple urban scale analysticss to improve understanding of human vulnerability to heat. Provides recommendations and policy implications, to decision-makers for heat stress and planning strategies to cope with future environmental change in complex urban systems.
Conclusion	**6. Conclusion**			Summarizes research findings, scientific contributions and recommends direction for future research

Figure 1-10: Synthesis of the dissertation structure and the links between research phases, chapters, goals, gaps, employed methods, and outcomes.

II.   BUILT ENVIRONMENT HEAT VULNERABILITY

There has been limited guidance on heat vulnerability assessment that accounts for the impacts of the built environment. This chapter focuses on developing the framework for heat vulnerability assessment in urban areas, based on integrating three levels of the physical urban space: the urban level, the building level, and human adaptation to heat. Also considered is system dynamics (SD) modeling as an approach for heat vulnerability quantification in urban areas. Therefore, the chapter outlines the dynamics relationship between heat vulnerability components, namely, Susceptibility (S), Coping Capacity (CC), and Adaptive Capacity (AC). Then, a detailed description of the indicators related to each component is presented. The section concludes with an applied case study in Cairo, Egypt, to assess the applicability of using the SD approach in assessing heat vulnerability in urban settings. The second half of the chapter presents a heat vulnerability assessment framework with respect to the physical characteristics of the surrounding urban environment. The framework's central focus is on examining how the physical built environment can influence heat exposure by developing different levels of vulnerability assessment that correspond to heat adaptation needs. For this purpose, heat vulnerability is presented as the causal mechanism between available adaptation amenities in the urban space, the building's performance in mitigating heat, and how occupants cope with heat. The proposed framework has two main objectives: a) explore and identify methods and data to be used in heat vulnerability assessment in urban areas and related health outcomes, b) outline how policymakers can better identify heat adaptation strategies by understanding potential impacts from the built environment. The framework's structure consists of three primary levels of assessment: 1) rapid assessment of heat vulnerability, 2) detailed assessment of indoor heat exposure, and 3) urban intervention and policy development for heat adaptation. Each of the three levels is presented throughout the dissertation with an applied case study. The second part of this chapter discusses the main components of heat vulnerability in the urban context. Finally, the chapter ends with system dynamics as a modeling approach to quantify heat vulnerability using a low-income residential building in Cairo, Egypt, as a case study.

2.1 Heat Vulnerability

The IPCC Working Group II Assessment report outlined the first synthesis of vulnerability as a function of susceptibility, exposure, and adaptive capacity (Hans Martin Füssel & Klein, 2006). Between 2007 and 2014, the perspective on vulnerability has altered to define exposure as a spatial concept tied to the surrounding physical space (Jurgilevich et al., 2017). In climate change science, vulnerability is used to indicate the impact of a climate hazard on the rate and magnitude, duration of exposure, the system's susceptibility, and adaptive capacity (C.Clark, Jager, & Corell, 2000). Accordingly, studies have attempted to develop a framework for vulnerability assessment that considered vulnerability as a function of Susceptibility (S), Exposure (E), and adaptive capacity (AC). These three components are assessed and combined to capture the vulnerability of a climate hazard (UNFCCC, 2016). In this research context, vulnerability is considered a function of an urban area's susceptibility to heat exposure and its adaptive capacity, where vulnerability is calculated using equation (1) as follows:

$$V = \left[\frac{E}{n} + \frac{S}{n}\right] - \left[\frac{AC}{n}\right] \qquad (1)$$

V represents vulnerability, S is the susceptibility, and AC is the adaptative capacity, n is the number of indicators used where all values are normalized between zero and one. This notion of vulnerability is consistent with the Third National Climate Assessment of vulnerability as "Vulnerability is a function of the character, magnitude, and rate of climate variations to which a system is exposed, its sensitivity and adaptive capacity" (Groffman et al., 2014). In the urban context, vulnerability is denoted as context-specific, determined by the urban system's physical characteristics, and determined by an individual's behavior to adapt to heat exposure. Based on this definition, vulnerability is an endogenous characteristic of the urban systems and is determined by its adaptive capacity and susceptibility. The relationship between exposure, susceptibility, and adaptive capacity that determine vulnerability is illustrated in Figure 2-1.
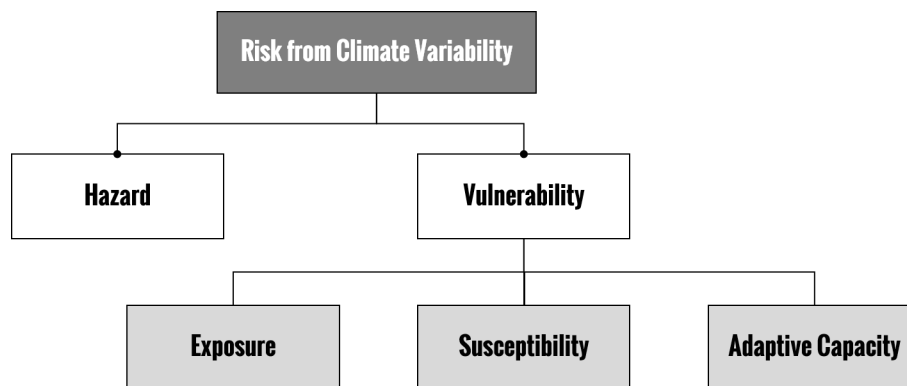
Figure 2-1: Relationship between exposure, susceptibility, and adaptive capacity in the formulation of vulnerability.

The hazard encompasses the potential occurrence of natural or human-induced climate events or trends or impacts that may cause damage to the system, loss of life, loss of property, infrastructure, and provision of essential services (Intergovernmental Panel on Climate Change (IPCC), 2013). In this dissertation context, heatwave event refers to the climate-related hazard affecting the urban system. Exposure represents the presence of urban population, infrastructure, economic activities, or physical assets in settings that can be adversely affected by heat exposure (J. Sharma et al., 2016).

Susceptibility depicts two main components: a) the urban system's physical ability to withstand exposure and related impacts, including access to adaptation means that can influence an individual's ability to cope with heat exposure, and b) physiological and socioeconomic characteristics of the urban population that increase individuals' risk under heat exposure (Kuras et al., 2017). Susceptibility highlights the urban system's specific properties that need to be considered during the development of adaptation strategies.

Adaptive capacity and coping capacity generally include both long-term and short-term capacity to cope and adapt to heat exposure. Coping capacity is defined as " the ability of people, organizations, and systems, using available skills and resources to face and manage adverse conditions, emergencies or disasters which can contribute to the reduction of disaster risks." (UNISDR, 2009). On the other hand, adaptive capacity is "the ability of a system to adjust to climate change to moderate potential damages, to take advantage of opportunities or to cope with the consequences." (Intergovernmental Panel on Climate Change (IPCC), 2013). In this sense, an urban area's adaptive capacity is determined by the ability to adjust to heat exposure in the long term. In contrast, coping capacity is represented by the available urban services (at the building scale or the urban scale) that enable populations to manage and overcome extreme conditions in the short-term range. This implies that after heat exposure brings changes to the urban system in the form of susceptibility, it will try to adjust to such changes to reduce potential damage using available resources represented as the adaptive capacity. Adaptive capacity is similar to susceptibility as it's a characteristic feature of the urban system. For instance, availability of heat-relief amenities, health services, and availability of open space depict the urban system's adaptive capacity.

Risk represents the potential consequences of heat events where human lives, urban physical value is at stake, and the outcomes are uncertain. According to the literature in climate change science, risk is defined as the probability of hazardous events multiplied by impacts if these events occur (Hallegatte & Corfee-Morlot, 2011; J. Sharma et al., 2016). In that sense, risk will result from the interaction between vulnerability and exposure. In the heat vulnerability scope in an urban setting, risk is estimated by summing vulnerability and potential impact considering the probability of heatwave to occur. In this sense, adaptation measures have no control on heatwave hazard since it is linked to the global climate variability; however, they can significantly modify exposure and vulnerability at the local urban scale. Risk to heat vulnerability can be estimated using equation (2) as follows:

$$R = V * \left[\frac{PI}{n}\right] \qquad (2)$$

Where R is a risk, V is vulnerability, E is exposure, and n is the number of exposure indicators used. This chapter reviews components of heat vulnerability and their indicators in an urban setting. The first sections of this chapter will describe the main indicators for susceptibility and adaptive capacity and develop a system dynamics model to estimate heat vulnerability. The second half focuses on developing a general assessment framework for heat vulnerability that will set the basis for the following three chapters. The objective is to identify potential approaches for mapping heat vulnerability in urban settings and related health impacts and limitations to the implementation of adaptation measures.

2.1.1 Components of Heat Vulnerability

Temperature conditions under which heat stress conditions can become risky to human health vary between locations depending on the climate, the physical built environment, and population groups. Defining heat vulnerability requires capturing different conditions and dynamic relationships between climatic conditions, population, and physical urban space to develop and implement an effective heat management strategy (M. Loughnan, Nicholls, & Tapper, 2010).

As discussed above, vulnerability is a function of exposure, susceptibility, and adaptive capacity. These three factors are generally used to identify locations and populations disproportionately at risk from extreme heat events. Numerous studies have identified a set of indicators to quantify the cumulative vulnerability (C.Clark et al., 2000; Lapola, Braga, Di Giulio, Torres, & Vasconcellos, 2019b; Romero-Lankao, Qin, & Dickinson, 2012). This section outlines indicators of susceptibility, exposure, and adaptive capacity under extreme heat exposure in the urban context. Figure 2-2 below describes the three main components of heat vulnerability, namely Exposure (E), Susceptibility (S), and Adaptive Capacity (AC), and list related indicators at the building scale, urban scale, and human scale that will be examined throughout the dissertation context.
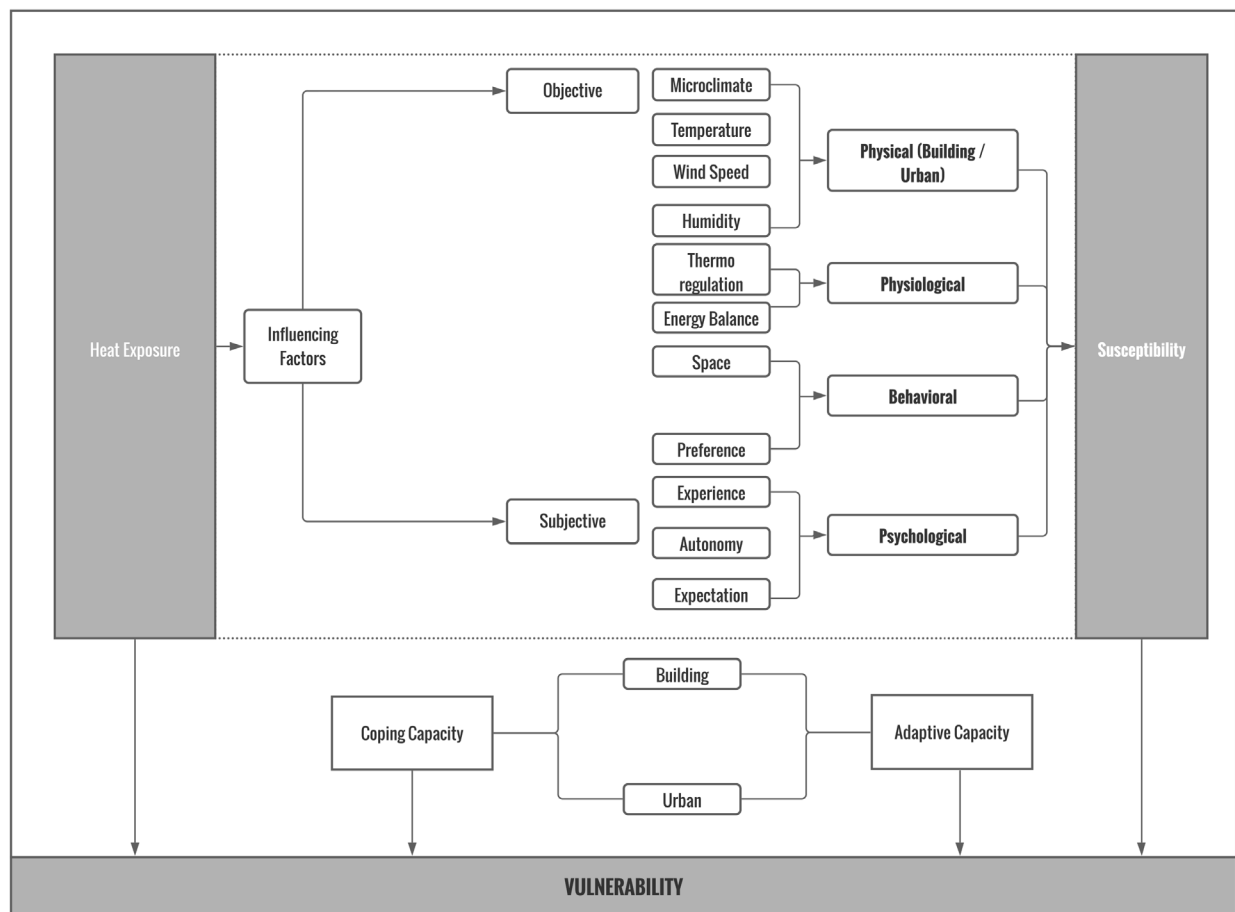
Figure 2-2: Components of heat vulnerability and related indicators addressed in the dissertation.

2.1.1.1 Exposure

Exposure indicators measure the climatic conditions at the building scale and the urban environment to put pressure on the urban population's wellbeing. Environmental conditions that pose threats to human health can occur both at the building level, indoors, and at the urban scale, outdoors (McGregor & Vanos, 2018). In indoor settings, environmental conditions are mainly presented by air temperature, humidity, and thermal radiation. At the outdoor level, other parameters such as wind, direct solar radiation need to be considered. For example, in the absence of ventilation, high temperature and moisture level with direct sunlight can generate heat stress that would limit the body's ability to maintain core temperature within the range of healthy physiological performance (Di Napoli, Pappenberger, & Cloke, 2019). Heat exposure can be associated with different health impacts (Wilhelmi, de Sherbinn, & Hayden, 2012), varying at threshold temperature indoors and outdoors and exposure duration. For example, studies have shown that heat-related mortality can occur at a relatively lower air temperature if the exposure lasted over consecutive days (Bell et al., 2008; Egondi et al., 2012; Harlan et al., 2014). Loughan et al. (2010) found a significant increase in hospital admission by 38% for a 3-day consecutive average temperature of 27°C compared to a daily temperature of 30°C. In this sense, exposure plays a significant role in heat-related health impacts that differ between indoor and outdoor conditions. This section examines exposure indicators representing climate conditions at the urban scale and building scale under which heat stress can occur.

Numerous indices have been developed in the literature to assess heat stress for outdoor environmental factors and the human body (Havenith & Fiala, 2016). One of the most utilized indices is the Universal Thermal Climate Index (UTCI). UTCI is a bioclimatic index that describes heat stress conditions to which the human body is exposed by accounting for a combination of meteorological factors, physiological parameters, and clothing requirements (Jendritzky, de Dear, & Havenith, 2012). It is developed based on the UTCI-Fiala model representing the individual's physiological response to the outdoor environment through an energy balance model coupled with a temperature-adaptive clothing model (Fiala, Havenith, Bröde, Kampmann, & Jendritzky, 2012). It has also been proven that UTCI to be valid in all seasons and climates and on various spatial scales from micro to macro scale (Blazejczyk & Błażejczyk, 2014; Kolendowicz, Półrolniczak, Szyga-Pluta, & Bednorz, 2018; Matzarakis, Muthers, & Rutz, 2014; Urban & Kyselý, 2014).

Thus, it has been used extensively in characterizing heat stress and related health impacts across different locations in Europe (Bleta, Nastos, & Matzarakis, 2014; Di Napoli, Pappenberger, & Cloke, 2018; Nastos & Matzarakis, 2012; Németh, 2011). This research considers UTCI as an indicator of outdoor heat exposure. A study by Pappernberger et al. (2019) has found that UTCI has proven helpful in forecasting and detecting in advance potential heat stress up to 10 days. UTCI is divided into ten different classes ranging from extreme heat stress to extreme cold stress (A. Young, 2021), as shown in Table 2-1 below. Therefore, this research considers the number of consecutive hours spent outdoor where UTCI is above the comfort range (>32°C) as an indicator of outdoor exposure that can limit an individual's ability to perform outdoor activities or go outside when indoor conditions exceed thermal comfort levels.

Table 2-1: Categories of Thermal stress for different ranges of UTCI (A. Young, 2021).

UTCI (°C)	above +46	+38 to +46	+32 to +38	+26 to +32	+9 to +26	+9 to 0	0 to −13	−13 to −27	−27 to −40	below −40
Stress Category	extreme heat stress	very strong heat stress	strong heat stress	moderate heat stress	no thermal stress	slight cold stress	moderate cold stress	strong cold stress	very strong cold stress	extreme cold stress

Studies on heat-related health impacts have shown that housing characteristics have been directly linked to heat stress conditions (Honda, 1995; McGill, Sharpe, Robertson, Gupta, & Mawditt, 2017). High indoor temperature negatively affects an individual's thermal comfort, wellbeing, and health. However, the impacts of indoor conditions on health depend on numerous factors, such as the building's physical characteristics and population group. Heat stress is often related to "overheating". In the adaptive comfort model standard, overheating represents indoor conditions that exceed the "thermal comfort zone." (CIBSE, 2013). Most heat vulnerability and epidemiological studies examined indoor heat exposure based on outdoor climate conditions; only a few research studies have monitored personal exposure and heat stress (AECOM, 2012). Buildings' characteristics such as thermal mass, air sealing, and shading direct affect overheating, especially when air-conditioning is unavailable (Kenny et al., 2019). Table 2-2 outlines findings from the literature for different building characteristics and related-indoor temperatures that exceed thermal comfort standards.

Table 2-2: Indoor heat studies of homes without air-conditioning (Based on (Holmes, Phillips, & Wilson, 2016b)).

Location	No. of homes	Occupant and residential characteristics	Weather scenario	Measured indoor air temperatures	Source
Detroit, Michigan, US	30	Elderly occupants; single-family; wood plus vinyl siding	Two summer days	34.9°C; this was 13.8°C higher than the average outdoor temperature	(White-Newsome et al., 2012)
Athens, Greece	50	Low income; no air-conditioning	Heatwaves over three months	Always exceeded 28°C, and exceeded 30°C for 80-85% of the time	(Sakka et al., 2012)
Montreal, Quebec, Canada	78	Multi-family; no air-conditioning	July analysis	Average of 26.7°C and a maximum of 34.4°C	(Audrey Smargiassi et al., 2008)
Chicago, Illinois, US	1	Fatality from heat stress; single-family home	1995 heatwave	Home thermostat exceeded 32°C	(CDC, 1996, 2013)
Manchester, UK	4	Urban homes	Nine-day heatwave in 2003	Average 24.2-26.3°C, with a maximum of 36°C	(Barclay, Sharples, Kang, & Watkins, 2012)
London, UK	5	Urban homes	Nine-day heatwave in 2003	Average 27.4-29.8°C; outdoor temperature averages 1-3°C higher; maximum 39.2°C	(Barclay et al., 2012)
Seoul, South Korea	20	Elderly occupants; low-income apartments; no air-conditioning	27 July- 6 August 2010 heatwave	Afternoon indoor temperatures averaged 31.9°C, with a maximum of 32.8°C	(Y.-M. Kim, Kim, Cheong, Ahn, & Choi, 2012)

The human body experiences complex thermoregulatory processes when exposed to high temperatures. Such processes are influenced by extrinsic and intrinsic factors like microclimate, behavioral adjustments, and associated heat storage and balance expressed as heat stress or heat strain (Bates & Miller, 2002; Epstein & Moran, 2006). Various heat stress indices have been developed to assess heat stress and thermal comfort. These indices guide both building design and operation to provide comfort. Auliciems and Szokolay (2014) reviewed and evaluated 11 heat indices commonly used to assess heat stress. Over the past couple of decades, various indices have been developed based on environmental factors; others are based on environmental and human factors (Brake & Bates, 2002). A review by Bethea and Parsons (2002) has grouped thermal comfort indices into three main categories: 1) rational indices (heat balance), 2) empirical indices (physiological), and 3) direct indices (environmental). Figure 2-3 summarizes indices included in this study and other studies examined in the literature review to assess heat stress in indoor environments.

Classification of thermal comfort indices based on modelling approach

SIMULATION DEVICE FOR INTEGRAL MEASUREMENT
(WGT, Tg)

SINGLE-SENSOR (SINGLE-PARAMETER) INDEX
(Air Temperature (Ta), Dewpoint Temperature, Physical saturation deficit, saturation deficit, Wet Bulb Temperature (Twb))

ALGEBRAIC OR STATISTICAL MODE
(Apparent temperature, discomfort index, humidex, WBGT, WBDT, Relative Humidity Dry Temperature (RHDT))

PROXY THERMAL STRAIN INDEX
(Cold Strain Index, Physiological Heat Exposure Limit (PHEL), Physiological Index of Strain (PSD, Skin Temperature (SkT))

effects of heat acclimatization (PEHA), Weather Stress Index (WSD, Weather Climate Contrasts (WCC))

SPECIAL PURPOSE INDEX
(Adaptation Strain Index (ASD, Acclimatization Thermal Strain Index (ATSD, Draught Risk Index (DRD, Predicted

PROXY THERMAL STRESS INDEX
(Corrected Effective Temperature (CET), Effective Temperature (ET), Thermal Sensation Index (TSND, Wind Effect Index (WEI))

ENERGY BALANCE STRAIN INDEX
(Heat Stress Index, Predicted Heat Strain (PHS), Reference Index (RD, Relative Heat Strain (RHS), Thermal Discomfort (DISC), Thermal Strain Index (TSD, Required sweat rate (Req SR), Thermal Work Limit (TWL))

ENERGY BALANCE STRESS INDEX
(Apparent Temperature (AT), Heat Index (HD, Clothing Insulation (Ic), Heat Stress Index (HSI_WK), Outdoor Apparent Temperature (OAT), Outdoor Thermal Environment Index (OTED, Perceived Temperature (PT₁), Predicted Mean Vote (PMV), Predicted Mean Vote outdoor (PMV*), Predicted percentage dissatisfied (PPD), Total Thermal Stress (TTS), Thermal insulation of Clothing (TIC_R), Universal Thermal Climate Index (UTCD, Thermal Sensation (TSGIV), Standard Effective Temperature (EST), Standard Operative Temperature (To), Standard Effective Temperature outdoor (SET*))

Classification of thermal comfort indices in overheating assessment in buildings

INDICES BASED ON THE CALCULATION OF THE HEAT BALANCE OF THE HUMAN BODY-INTEGRATES:
Physiological parameters: Skin Wetness, Mean Skin Temperature
Behavioral Parameters: Metabolic rate, clothing insulation
Thermal environment parameters: Dry Bulb air temperature, mean radiant temperature, relative humidity, wind speed.

INDICES BASED ON PHYSIOLOGICAL STRAIN
based on multiple regression equations which correlates between wide range of environmental conditions (Effective Temperature, Corrected Effective Temperature, The Equatorial Comfort Index, Index of Physiological Effect, Predicted Four-Hour Sweat Rate, The Thermal Strain Index)

INDICES BASED ON MEASUREMENT OF PHYSICAL PARAMETERS
derived from direct measurements of physical parameters describing the thermal environmental that are generally related though linear regression analysis. (Equivalent temperature, the Globe Thermometer Temperature, Operative Temperature). ˙

Classification based on long-term evaluation of general thermal discomfort in buildings

COMFORT MODEL-BASED INDICES
Percentage indices (Percentage of time outside the PMV range)
Cumulative indices (PPD weighted Criterion)
Risk Indices (Overheating Risk) – introduced by Nicol et al. [15] which derives from statistical analysis of the measured data and sensation surveys collected in free-running buildings during the SCATs Project [16].
Averaging indices (Average Predicted Percentage of Dissatisfaction (PPD))

CATEGORY-DEPENDENT INDICES
Percentage indices (Percentage of time outside the PMV range)
Cumulative indices (PPD weighted Criterion)

SYMMETRIC AND ASYMMETRIC INDICES
Percentage indices (Percentage of time outside the PMV range)
Cumulative indices (PPD weighted Criterion)
Risk Indices (Overheating Risk)
Averaging indices (Average Predicted Percentage of Dissatisfaction (PPD))

INDICES APPLICABLE ONLY TO SUMMER
Percentage indices (Percentage of time outside the PMV range)
Cumulative indices (PPD weighted Criterion)
Risk Indices (Overheating Risk)
Averaging indices (Average Predicted Percentage of Dissatisfaction (PPD))

INDICES PROVIDED WITH A COMFORT THRESHOLD
Percentage indices (Percentage of time outside the PMV range)
Cumulative indices (PPD weighted Criterion)
Risk Indices (Overheating Risk)

Classification of thermal comfort indices based on their application

INDUSTRIAL AND MILITARY INDICES
(WBGT, Heat Stress Index, Predicted Heat Strain)

HEAT STRESS INDICES USED BY THE WEATHER SERVICES
(Apparent Temperature, Heat Index, Humidex, SET, PET)

HEAT STRESS INDICES USED BY EPIDEMIOLOGIST/PUBLIC HEALTH
(UTCD)

Figure 2-3: Indoor heat studies of homes without air-conditioning (developed by the author based on (Auliciems; & Szokolay, 2014; Blazejczyk, Epstein, Jendritzky, Staiger, & Tinz, 2012; Brake & Bates, 2002; Holmes et al., 2016b; Sen & Nag, 2019; Urban & Kyselý, 2014).

Sen and Nag (2019) have evaluated most heat stress indices developed throughout the literature to identify which indices are most suitable to assess heat stress. The study outlines that rational indices such as Standard Effective Temperature (SET) and Esk (Evaporation Through skin) are useful indicators for heat stress as they account for environmental and behavioral factors. Table 2-3 summarizes the temperature threshold for different heat indices examined in Sen and Nag study and other studies from the literature(Blazejczyk et al., 2012).

Table 2-3: Temperature threshold for different heat indices and their classification (Based on (Holmes et al., 2016b; Jendritzky et al., 2012; Sen & Nag, 2019).

Thermal sensation level	Index								
	HI	Humidex	ET	WBGT	WCT	**SET**	PET	PT	PST
Sweltering (Extreme Danger)	> 54	> 55		> 30				> 38	> 54
Very Hot (Danger)	41 - 54	45 - 55	> 27	28 - 30		**> 37**	> 41	32 - 38	44- 54
Hot (Extreme Caution)	32 - 41	40 - 45	23 - 27	24 - 28		**34 - 37**	35 - 41	26- 32	34-44
Warm (Caution)	27 - 32	30 – 40	21 - 23	18 - 24		**30 - 34**	23 - 35	20 - 26	24- 34
Comfortable		< 30	17 - 21	< 18	> -10	**17 - 30**	18 - 23	0 - 20	14- 24
Cool (Moderate Hazard)			9 - 17		-27: -10	**< 17**	8 - 18	-13: 0	4 -14
Cold			1-9		-39: -28		4-8	-26: -13	-16: -4
Very cold			<1		-54: -40		<4	-39: -26	-36: -16
Frosty (Extreme Hazard)					< -55			< -39	< -36

This research considers SET as an indicator of indoor heat exposure that has been widely used in the ASHRAE standard to evaluate the thermal environment. SET has been developed as a metric to identify livable temperatures in buildings in case of power loss or limited access to the air-conditioning system (Wilson, 2006). SET is also considered a more advanced rational index than the Predicted Mean Vote (PMV), as it was developed for more dynamic conditions than the steady-state comfort response (S. Zhang & Lin, 2020). In addition, SET can predict the thermal physiological response of the human body to heat exposure (B. Li et al., 2018). Given its prominent use as a heat threshold as part of passive survivability assessment in buildings, the research considers hours where SET is above 30°C to be an indicator of heat exposure indoors as part of heat vulnerability assessment.

2.1.1.2 Susceptibility

Susceptibility refers to the characteristics which denote a population's vulnerability to heat exposure. Such factors may vary based on the presence of a population in urban settings or buildings that are highly exposed to extreme temperatures or an individual's medical conditions. The research considers a set of indicators of susceptibility that can be divided into three classes: 1) individual factors, 2) health factors, and 3) socioeconomic factors that would limit an individual's ability to cope with heat exposure. This section presents indicators related to each of the classes mentioned above.

I. Individual Factors

A. Age

The literature on the relationship between heat vulnerability and mortality has consistently shown that elderly populations are at higher risk than their younger counterparts (Engelland, Hemingway, Tomasco, Olivencia-Yurvati, & Romero, 2020; Gover, 1938; Minson, Wladkowski, Cardell, Pawelczyk, & Kenney, 1998; Schlader, Wilson, & Crandall, 2015). Around 84 studies covering the period between 1970 and 2008 have consistently reported increased heat-related mortality with age during extreme heat events (Bark, 1998; Stafoggia et al., 2006). Recent studies have shown that age plays a significant role in human susceptibility to heat exposure (Haines & Ebi, 2019; Mayrhuber et al., 2018; Watts et al., 2019). Early evidence was confirmed during the 2003 European heatwave with a toll of around 70,000 heat-related deaths. In France, heat-related mortality increased by 40-100% in adults older than 65, compared to 20 to 30% in middle-aged adults between 35 and 64 years (Fouillet et al., 2006; Robine et al., 2008). Research by Kenny et al. (2010) and (2014) has identified that increased heat vulnerability with aging is mainly explained by body thermoregulation impairment and failure to maintain stable blood pressure under extreme heat exposure. There are also findings of increased death rates and dehydration risks among infants during extreme heat exposure (Tourneux et al., 2009; World Health Organization (WHO) 2011). This is linked to their immature thermoregulation capacity, small blood volume, and body mass. Children under five years have also been more vulnerable to heat exposure; this is mainly due to their cognitive and immune-system immaturity compared to adults (American Public Health Association (APHA), 2016). In this sense, the research has considered age one of the primary indicators for human susceptibility to heat exposure, especially for populations older than 65 or younger than five years. Age susceptibility is presented as a normalized range between 0 and one, where 0 indicates not susceptible, and one refers to being susceptible based on age.

B. Gender

Numerous studies have reported differences between male and female physiological responses under heat exposure, driven by differences in sweat rate (Foster, Ellis, Doré, Exton-smtth, & Weiner, 1976; Green, Bishop, Muir, & Lomax, 2000). Studies have indicated that females' sweat rates are much larger than males under the same temperature conditions (Mehnert, Bröde, & Griefahn, 2002), which means more heat gain and potentially greater risk under extreme temperatures. One study that examined the relationship between heat vulnerability and gender during the European heatwave found that females of age between 65 to 74 had more significant mortality rates compared to males of the same age with greater risk in females with respiratory conditions and cardiovascular problems (D D'Ippoliti et al., 2007; Glass, Tait, Hanna, & Dear, 2015). Finally, a recent study found that females generally reported a relatively higher incidence of heat-related illnesses than males. Also, males reported higher heatstroke occurrences under the same temperature conditions (Alele, Malau-Aduli, Malau-Aduli, & Crowe, 2020).

C. Social Isolation

In several heat vulnerability studies, social isolation was linked to increased health effects during heatwaves (Klinenberg, 2003b). Literature has reported that individuals living alone, single, unmarried or widowed, mainly were identified at higher risk under extreme temperature exposure (Bouchama et al., 2012; Fouillet et al., 2006; Hansen et al., 2011; Mayrhuber et al., 2018). Klinenberg (2003b) has also reported increased death among residents living alone during the 2005 Chicago heat. Social isolation is

linked to increased heat vulnerability due to the direct effect on cognitive, physical, or mental impairment. Also, it affects the individual ability to modify impacts from heat exposure, such as commuting to a cooling location and losing access to assistance in case of health consequences from increased temperature (Sampson et al., 2013).

D. Race

Ethnic identity and race are often linked to increased heat-related vulnerability and morbidity (Ebi, 2004; Gosling, Lowe, McGregor, Pelling, & Malamud, 2009; Ye et al., 2012; Zanobetti, O'Neill, Gronlund, & Schwartz, 2013). For instance, a study conducted in New York City found that a high concentration of population of color is linked to heat vulnerability (Klein Rosenthal et al., 2014). During the Chicago heatwave in 1995, Klinenberg (2003b) reported that most heat-related deaths were from people of color. Another study has examined the Asian population has found a relatively lower heat vulnerability (Basu et al., 2012). On the contrary, other studies have not found a relationship between ethnicity and heat vulnerability (Anderson & Bell, 2009a). Other related factors in driving the relationship between ethnicity and heat vulnerability, such as community racial composition and neighborhood social structure, are reported in other studies as factors associated with heat-related (Uejio et al., 2011). Several studies in the United States found that racial differences in heat exposure tolerance were attributable to distal characteristics related to income level, poor nutrition, or limited physical health (Hansen, Bi, Saniotis, & Nitschke, 2013; N. A. S. Taylor, 2006; Yardley, Sigal, & Kenny, 2011). Other related parameters are also associated with the surrounding built environment, such as poor building thermal performance, sparse vegetation, or limited access to air conditioning units (Harlan et al. 2006; Ruiz, Steffen, and Smith, 2013). Although numerous studies have identified the strong relationship between ethnicity and increased heat-related vulnerability, race should be considered a proxy for cultural isolation. For example, ethnicity can drive reluctance to commute to a cooling community center due to a lack of standard social norms or cultural background similarities (Sampson et al., 2013; O'Neill, Zanobetti, and Schwartz 2005).

E. Heat Acclimatization

Studies have found a relationship between heat-acclimatization and death rates during extreme heat events. For instance, in Sweden, heat-related deaths were lower than those in Athens and London due to individual acclimatization to heat due to lack of AC (Baccini et al., 2008). Most of the heat-related death events in Europe in 2003 and Russia in 2010 occurred in regions not acclimatized to high temperatures (Barriopedro et al., 2011). Other studies have found a difference in heat acclimatization between people living in naturally ventilated environments than those residing in air-conditioning (de Dear & Brager, 1998). One study examined the relationship between heat acclimatization and human thermal capacity found that the thermal capacity of people who are used to air-conditioning decreases over time with exposure to a stable AC environment (Yu et al., 2012). Such findings correlate with earlier studies on heat-related morbidity that indicate lower thermal adaptability of people living in cold climates than those living in hot environments. Also, people living in warmer climates were found to cope better in extreme heat conditions. The temperature threshold for heat-related morbidity was higher than those living in colder climates (Henderson, Wan, & Kosatsky, 2013; Medina-Ramón & Schwartz, 2007; Sherwood & Huber, 2010). In that sense, heat acclimatization is considered a factor in human susceptibility to heat exposure alongside previously mentioned physiological characteristics that affect the human thermal capacity to extreme heat exposure.

II. Health Factors

A. Medical Condition

Several studies have identified there is an association between heat-related morbidity and medical history for specific diseases besides heatstroke and dehydration (Basu, 2009; Gosling et al., 2009; Kravchenko, Abernethy, Fawzy, & Lyerly, 2013; Oudin Åström, Bertil, & Joacim, 2011; L. R. Turner, Barnett, Connell, & Tong, 2012; Yardley, Stapleton, Carter, Sigal, & Kenny, 2013; Ye et al., 2012). It was found that cardiovascular problems, diabetes, and respiratory disorders have contributed to the increased risk under heat exposure (Bouchama et al., 2012; Nitschke et al., 2013; Tran et al., 2013; Zanobetti et al., 2013; Y. Zhang, Nitschke, & Bi, 2013). This implies that there is a greater susceptibility for a population with these diseases during heat events. Other studies have also confirmed the relationship between pre-existing conditions and hospital visits during extreme heat events (Foroni et al., 2007; Pillai et al., 2014). Laboratory studies have identified that susceptibility due to pre-existing medical conditions is driven by the physiological impairment to a properly functioning cooling mechanism that is mainly affected by health conditions (Crandall & González-Alonso, 2010; Kenney, 2001; Kenny, Yardley, Brown, Sigal, & Jay, 2010). Therefore, pre-existing medical conditions are accounted as one of the primary human susceptibility to heat exposure, including from the literature other different diseases such as renal diseases, respiratory diseases, diabetes, cardiovascular problems, and psychiatric disorders (Gronlund, 2014).

B. Physical Disability

Multiple inequalities increase climate change vulnerability in populations with disabilities (Gaskin et al., 2017). Research findings have shown that people with disabilities experience greater pain and fatigue during extreme temperature events (Field et al., 2012). These people are specifically more vulnerable due to their limited access to adaptation and mitigation responses, which reduces their resilience to extreme heat. Several studies have identified sensory and physical impairment as contributing factors to increase vulnerability to heat exposure (Baker, 2002; Maltais, Wilk, Unnithan, & Bar-Or, 2004). One study found that physical impairment and specific medications mainly affect the thermoregulation process under high temperatures (Kreuzer, Landgrebe, M. Wittmann, M. Schecklmann, Poeppl, & Langguth, 2012). Other studies identified schizophrenia (T. W. H. Chong & Castle, 2004) and spinal cord injuries (Dawson, Bridle, & Lockwood, 1994; Totel, 1974) to contribute to thermoregulation dysfunction significantly. Concerning cognitive disability, studies have shown that people with Alzheimer face additional challenges to adapt to climate change risks such as hurricanes and heatwaves. Finally, limited evidence was found that associates increased vulnerability in populations with sensory impairments or intellectual disability; however, these populations are still considered susceptible compared to healthy individuals in the sense of not comprehending surrounding risks or acting to adapt (Christensen, 2013; Gosling et al., 2009; Lazrus, Morrow, Morss, & Lazo, 2012).

C. Drug or Alcohol abuse

Studies have found a relationship between heat exposure risk and alcohol consumption ((Trang, Rocklöv, Giang, Kullgren, & Nilsson, 2016)). The increased use of alcohol was found to affect thermoregulation under high temperatures and, consequently, increase heat vulnerability. In another study, it was also shown that there is an association between heat-related hospital admissions and drug abuse (Bouchama

et al., 2012). Finally, recent studies have shown increased alcohol consumption and drug abuse during heatwave events, driving higher susceptibility for people with alcoholism or drug abuse history (Cusack, de Crespigny, & Athanasos, 2011; Hansen et al., 2008).

D. Mental Health

Excessive exposure to high temperatures may affect the body's thermoregulation threshold due to acute reactions such as stress hormone release (Simister & Cooper, 2005). According to a study by Sharma et al. (2007), it was found that there is an associated increase in brain temperature following a rise in core temperature after exposure to high temperature. Also, numerous epidemiological studies have reported that elevated temperature may exacerbate psychiatric conditions and consequently affect general mental health (Woodruff, McMichael, Butler, & Hales, 2006). Early studies have found dysfunction in the body's thermoregulation in schizophrenia patients after exposure to high-temperature (Jakovljević et al., 1997). A recent study (Xu et al., 2020) reported a strong relationship between mental health and heat vulnerability, specifically for people suffering from mental diseases such as stress, depression, anxiety, dementia, and schizophrenia. Additionally, people with poor mental health are generally less able to take adaptive or protective measures under high temperatures (S. Lee et al., 2018). Also, evidence from other studies (Hansen et al., 2008; Nitschke et al., 2013) showed that sensory perception of heat is strongly affected by mental conditions, thereby increasing heat vulnerability (Hajat, O'Connor, & Kosatsky, 2010; Hansen et al., 2011; Martin-Latry et al., 2007; Martinez, Devenport, Saussy, & Martinez, 2020; Nordon et al., 2009).

III. Socioeconomic Factors
A. Income level

Studies on heat risk assessment in the United States have found poverty and income level are related to heat-associated risks at the neighborhood level (Madrigano et al., 2013; Klein Rosenthal, Kinney, and Metzger 2014; O'Neill, Zanobetti, and Schwartz 2005). another study in China (Anderson & Bell, 2009a) has also found a correlation between income level and heat-related morbidity, with similar results reported in Japan (E. Y. Y. Chan, Goggins, Kim, & Griffiths, 2012). One study in Italy has also reported a relationship between hospital visits during heatwaves and income levels (Stafoggia et al., 2006). The association between income level and heat vulnerability is primarily driven by the individual ability to pay for high electricity bills due to increased use of AC or transportation cost to go to a cooling shelter (Banwell, Dixon, Bambrick, Edwards, & Kjellström, 2012; Hansen et al., 2011; Sampson et al., 2013; Sheridan, 2007).

B. Access to Health Care

Other related risk drivers can be associated with limited individual access to adequate health care during a heatwave event, strongly tied to income level (Bouchama et al., 2012). Previous studies have found a relationship between hospital visits during heatwaves and lack of access to private health insurance, which would increase vulnerability to heat exposure (Y. Zhang et al., 2013).

C. Access to Community Support

During the Chicago heatwave in 1995, access to a community support system was one of the major drivers for heat adaptation and reduced heat-related morbidity (Klinenberg, 2003b). Community support is critical in promoting coping and adaptation actions such as cooling behaviors, communicating concerns

during heatwaves or supporting socially isolated populations. In the United States, several studies in New York during the 2008 heatwave have identified social support as an indicator for assessing heat vulnerability (Frumkin, McMichael, & Hess, 2008; Metzger, Ito, & Matte, 2010).

D. Education Level

Studies in the United States (O'Neill et al., 2005) and Europe (Borrell et al., 2006; Michelozzi et al., 2005) found a relationship between heat-related morbidity and education. On the contrary, other studies reported no association between education and heat-related mortality (W. Ma et al., 2012; O'Neill, Zanobetti, & Schwartz, 2003; Stafoggia et al., 2006). This is mainly because many emergency departments don't document educational attainment for heat-related hospital visits. During the 2003 heatwave in Europe, it has been found that higher education protected against heat-related risks (Larrieu et al., 2008). Like race and ethnicity, education attainment is relatively linked to other heat-related vulnerability drivers such as income level and occupation. High-educated populations are more likely to understand the types of protective measures needed under extreme heat exposure. In that sense, education level is considered an indicator of heat susceptibility.

2.1.1.3 Coping Capacity

As mentioned previously, coping capacity denotes the population's ability to cope, manage and adapt to heat risk in the short term. In the urban context, coping capacity can be represented by resources at the urban scale and building scale that contribute to an individual's ability to cope with heat exposure and overcome potential risks. Air conditioning and ventilation play a significant role in providing comfortable environmental conditions under heat exposure; thus, this research focuses on access to mechanical cooling and natural ventilation as indicators of urban population coping capacity.

A. Availability of Natural Ventilation

During exposure to high temperatures, heat exposure decreases the human ability to regulate heat (maintain core temperature at 37°C), leading to fatal risks to human health. In addition to high-temperature exposure indoors, there is also the problem of high humidity levels, limiting the body's ability to dissipate heat through sweating and perspiration. The American Society of Heating, Refrigeration, and Air-conditioning Engineers (ASHRAE) has set established an indoor air temperature of 35°C when relative humidity is 50% as a "danger line" for heat stress (ASHRAE, 2017b). Literature studies indicate that cooling with natural ventilation can act as a coping mechanism for extreme heat exposure; however, natural ventilation is only helpful when the outdoor air temperature is cooler than the inside air. However, considering the speed of the wind at the skin and the associated reduction in surface heat transfer coefficient, air movement can promote the removal of metabolic heat if the air temperature is less than skin temperature.

Also, ventilation plays a significant role in determining indoor humidity levels, primarily affecting human thermal comfort (Maragno et al., 2020). However, despite the large role natural ventilation plays as a coping resource for heat exposure, there are several limitations for natural ventilation to act effectively against indoor overheating, such as:
  - Wind speed should be sufficient to act as a driving force for natural ventilation.

- Natural ventilation cooling mechanism is sufficient for indoor heat gains below 40 W/m^2
- Outdoor noise and pollution levels can significantly influence the coping mechanism with natural ventilation (high pollution levels can cause ventilation to affect human health conditions indoors negatively).
- Building depth can affect the complexity of natural ventilation. (In buildings with a depth of more than 15m, natural ventilation becomes more challenging (Allard, Ghiaus, & Szucs, 2009; Ficken, 1978)).
- Surrounding urban density predominantly affects wind speed as studies have identified that mean wind velocity decreases by order of magnitude from the outside urban wind speed (Palme, Carrasco, Ángel Gálvez, & Inostroza, 2017).

The factors above play a significant role in natural ventilation performance as a coping resource for heat exposure. This research considers hours available for natural ventilation as a coping resource when the outdoor air temperature is cooler than indoor and at suitable wind speed levels to drive ventilation.

B. Access to Mechanical cooling Measures

Research on population vulnerability during extreme heat events shows that individuals who lack access to appropriate protective measures such as air conditioning and living in highly exposed urban areas are more vulnerable to heat exposure (Harlan et al., 2014; Semenza et al., 1996b). As a result, populations with limited access to cooling means have increased heat-related morbidity at a lower temperature threshold. Other studies have found heat mortality can be significantly influenced by an individual's physiological adaptation and behavioral adjustments (Anderson & Bell, 2009b; N. A. S. Taylor, 2014).

C. Access to backup power

Electricity is a critical driver in the development and growth of urban communities. Heatwaves significantly threaten the reliability and stability of power supply systems in cities. Increased temperature directly affects electricity demand with the increased use of air conditioners to cope with indoor overheating, leading to generation disruption and blackouts at high costs for human health and economies (Gotanda et al., 2015; Prezant et al., 2005). During heat exposure, vulnerable adults who rely on the power supply are even more challenged beyond just access to air conditioning units. The elderly population is more vulnerable to blackouts, especially those who use power for medical needs or those with limited mobility (Gamble et al., 2013; Behr and Diaz, 2013). Studies have found that backup power availability can positively improve preparedness and coping capacity during extreme weather events such as heatwaves (Lin et al., 2011; D. C. Lee et al., 2016). Also, access to a backup power plan can significantly reduce vulnerability to high-temperature exposure, especially for those at high risk, consequently reducing associated health impacts (Dominianni et al., 2018). In that sense, the research considers access to backup power as one of the coping resources. Access to backup power can help maintain access to mechanical cooling means such as fans or air conditioning units and limit the risks related to medical support for vulnerable elderly residents.

D. Access to Cooling Shelter

Heat vulnerability studies have identified that commuting to cooler places such as cooling shelters during high-temperature exposure can act as a cooling resource, especially during heatwaves (Bouchama et al., 2012; Sampson et al. 2013). However, other studies have found that the main limitation with cooling

centers is the lack of sustainable funding for these shelters. Thus, cooling shelters can act as a coping resource for individuals who lack the means to stay cool indoors, especially for those who can't afford to use air conditioning or for the homeless who don't have anywhere to go during extreme heat events (Gronlund, 2014; Sampson et al., 2013). This research identifies proximity and accessibility to the cooling shelter as a coping resource during heat exposure. The research also accounts for the proximity between the building and a cooling shelter within walking distance of 500 m that the elderly population can easily approach during high-temperature exposure.

2.1.2.4 Adaptive Capacity

Adaptation capacity characterizes the population's ability to extreme heat as a function of available resources, access to urban services, and other amenities associated with heat risk reduction and management in the long term (Wilhelmi & Hayden, 2016). Understanding existing access to resources to cope with heat exposure is vital in heat vulnerability assessment and identification of heat adaptation strategies. This research considers the availability and access to heat adaptation resources as indicators of a population's adaptive capacity.

A. Access to Health Services

Studies on heat vulnerability in the United States reported that the geographical location of health services and travel distance of served populations play a significant role in increased heat-related morbidity (Anggraini & Oliver, 2019). Other studies found that most emergency room visits during heat events were from people living within 12 miles (Loughnan ME, Phan, Lynch, & McInnes, 2013). The accessibility of health care services with a suitable travel distance can significantly reduce heat-related health risks, especially for vulnerable populations. In this research, proximity to a health care service with a distance of 12 miles (1.6 km) is considered as an adaptive capacity indicator.

B. Access to open space/park

Green spaces are considered necessary amenities in heat vulnerability assessment. In an urban context, vegetation can help reduce heat-related risks by providing shading and reducing temperature through evapotranspiration. Also, green spaces can help people adapt during extreme heat due to their ability to reduce the surrounding temperature and provide access to drinking fountains (Maragno et al., 2020; Önder & Akay, 2014).

C. Access to community support

Community support plays a significant role in promoting cooling behaviors and support socially isolated individuals during extreme heat exposure. Klingenberg's study on Chicago heatwave 1995 (Klinenberg, 2003b) identified that a social support system is crucial during extreme heat events. Other studies also confirmed that social support, whether from family or community groups, could significantly influence vulnerable populations' risk levels during heat exposure (Sampson et al., 2013).

2.2. Dynamics of Heat Vulnerability

Exposure to extreme heat poses significant threats to human health and quality of life in cities globally. As discussed previously, the urbanization process is strongly linked to extreme temperature exposure in cities through the Urban Heat Island (UHI) and other local effects that will intensify with the global

increase in mean temperature (Tomlinson et al., 2011). This section addresses the interplay between the physical built environment and heat vulnerability as a dynamic feature of the built environment's physical characteristics and the human system's socioeconomic factors that differentially place population and urban stock at risk from heat exposure. The dynamic relationship between exposure components in the built environment and associated vulnerability has received only modest attention in the existing literature (Dilling, Daly, Travis, Wilhelmi, & Klein, 2015; Hallegatte & Corfee-Morlot, 2011; Slobodan & Simonović, 2012). The relationship between heat vulnerability and urban development manifests feedback relationships between heat exposure, available urban resources for adaptation, characteristics of the social system, and the surrounding built environment. Heat exposure is considered a shock affecting both the urban and the human systems. When these two systems are under shock, it may trigger risks such as heatstroke and morbidity in the human dimension and can immediately put pressure on the urban service capacity such as health services and power supply.
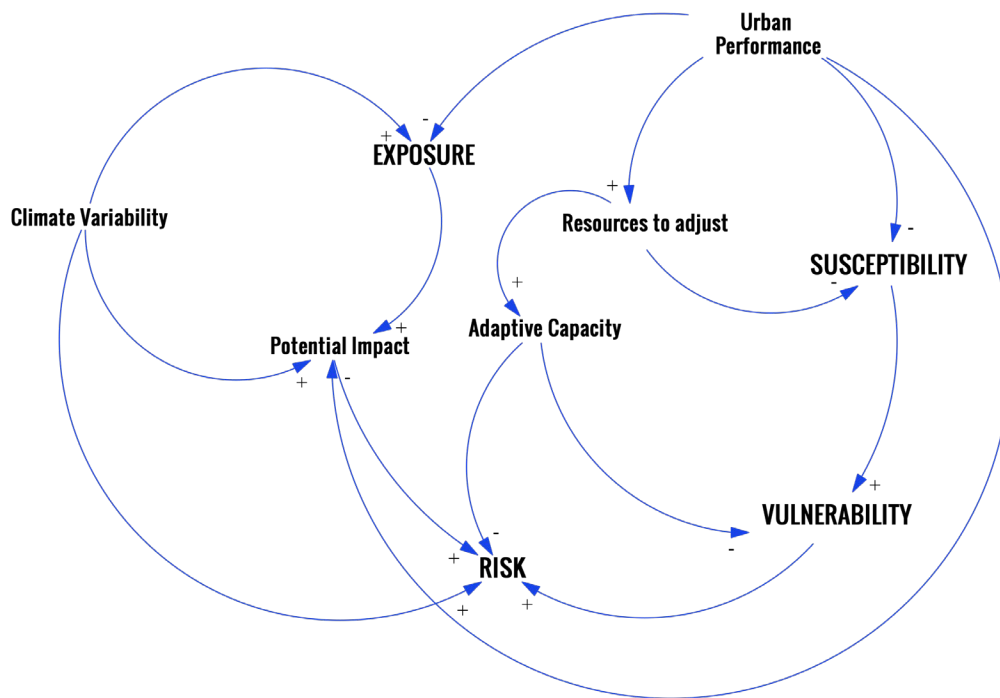
Figure 2-4: Causal loop diagram between heat exposure, susceptibility, and adaptive capacity in heat vulnerability assessment.

The mechanism between heat vulnerability, exposure, and adaptive capacity is presented through a causal loop diagram shown in Figure 2-4. The causal loop diagram's left side indicates the impact of global climate variability on increased heat exposure. The right part represents impacts on the urban system vulnerability defined in susceptibility and adaptive capacity. Thus, the upper right part of the diagram represents the urban response to heat exposure (urban performance) as the ability of an urban system to adapt to extreme heat through the provision of health services, heat-relief amenities, and quality of housing stock. The lower right side depicts the human system response to heat exposure as a function of population characteristics that drive susceptibility. The urban performance also affects susceptibility, as poor infrastructure and an old building stock can increase susceptibility.

In contrast, susceptibility can be reduced by improving the urban adaptive capacity through improving urban performance. This dynamic relationship between susceptibility and adaptive capacity is governing the vulnerability level. Risk arises from the potential impact of future climate hazards, a future heatwave in this context.

2.3 System Dynamics as an approach for Heat Vulnerability Quantification

Despite the vast literature on heat vulnerability in urban areas, the complexity and interaction between different vulnerability components described above are not fully explored. The purpose of this section is to discuss the dynamic relationship of heat vulnerability components and associated indicators in heat vulnerability assessment. System dynamics is used as a modeling approach to examine and outline the structure of these governing relationships. System dynamics (SD) is an operative approach utilized primarily to reveal relationships of complex systems with respect to their non-linearity, time delay, and structure (Bala, Arshad, & Noh, 2018). Forrester (1961, 1990) first developed this approach to investigate the structure of industrial processes to improve their organizational form. Since then, SD has been widely used as an effective tool for modeling intersectional dynamics and interactions between variables in the system to simulate its dynamic evolution and organizational boundaries (Forrester, 1961). SD describes both quantitive and qualitative causal relationships between the variables of the system. These relationships can either be positive when variables proportionally change or negative when they change inversely (Slobodan & Simonović, 2012). SD is used to assess the relationship between exposure, susceptibility, and adaptive capacity presented above.

The evaluation of urban community vulnerability to heat is a multidimensional dynamic problem. The model examines this problem by capturing the environmental, social, and behavioral dimensions subject to vulnerability induced by heat exposure. The model expands the feedback system between exposure, susceptibility, adaptive capacity, and associated vulnerability within the neighborhood as the system's boundary. The purpose of the developed model is to: a) extend the field of system dynamic analysis to explore urban and building performance and heat vulnerability by examining the interactions between the physical urban system and human behavior in response to heat exposure, and b) demonstrate the structural relationship between heat exposure sub-components and their influences on different factors of susceptibility in driving or reducing vulnerability within the urban boundary.

The proposed SD model identifies heat-related vulnerability as the primary variable of interest, developed around two main feedback loops: reinforcing loop (+) from susceptibility and exposure, balancing (-) from adaptive capacity. As heat exposure increases, pre-existing health conditions can exacerbate due to heat stress, leading to increased susceptibility in reinforcing pattering. This relationship is balanced through the provision of cooling options represented by the adaptive capacity. The model development is comprised of three main phases:

1- Structuring phase: aims to identify main variables and their sub-components. The objective is to understand the vulnerability of who and caused by what;

2- Scenario analysis: the purpose of scenario analysis is first to examine the validity of the hypothesized feedback loops and to identify any critical factors shaping the development of the model;

3- System perspective: offers a representation of the system dynamic behavior and feedback mechanisms exhibited in the scenario analysis. The system perspective phase addresses simulation outputs and outlines feedback loops driving the results to clarify knowledge and understanding of the system and outline policies that will improve system behavior.

2.3.1 Model Structure

As outlined above, there are primary factors that shape the role of exposure, susceptibility, and adaptive capacity under the scope of heat vulnerability assessment. This section presents the key variables and flow structure that determine the driving relationship between exposure, susceptibility, adaptive capacity, and resulting vulnerability. The heat vulnerability SD model will help identify the impacts of vulnerability on social and physical factors at the neighborhood level. The proposed model consists of various dimensions of vulnerability aggregated under exposure, susceptibility, coping capacity, and adaptive capacity. Exposure includes the characteristic profile of the surrounding urban space (building and urban block) that can drive heat-related health impacts under high temperatures. Susceptibility includes socio-economic profiles of the urban population that can exacerbate health risks under heat exposure. Coping capacity and adaptive capacity deal with services or measures to improve the population's ability to cope and adapt to high-temperature exposure. Each component is divided into subcomponents that are based on the specificity of vulnerability assessment in urban contexts. The multidimensionality of heat vulnerability is quantified using sets of indicators as proxies combined into a composite index reflecting the overall vulnerability score. Table 2-4 outlines the main components of vulnerability and related sub-components used as inputs for the heat vulnerability model.

Table 2-4: System variables and their indicators.

Variable		Indicator
Exposure	Indoor exposure	No. of consecutive hours where SET is above 30°C
	Outdoor Exposure	No. of consecutive hours where UTCI is above 32°C
Susceptibility	Building Susceptibility	Limited access to mechanical cooling/backup power
	Urban Susceptibility	Availability of Cooling shelters / Open spaces/ parks
	Human Susceptibility	Medical Condition – Access to health Insurance – Drug or alcohol Abuse- Age- Income level – Social Isolation- Access to Community Support
Coping Capacity	Building Coping Capacity	Availability of active cooling/availability of backup power
Adaptive Capacity	Cooling shelters	Cooling shelter available from a walking distance of 200 m
	Outdoor cooling potential	Hours where the outdoor air temperature is cooler than the indoor temperature
	Health service	Health amenity available from a distance of 1 km
Potential Impact	Increase in indoor heat exposure under future climate scenario	
	Increase in outdoor exposure under future climate scenario	

The model's structure is based on integrating two types of data sets as model inputs: 1) primary data from households to construct susceptibility and associated sub-components, and 2) hourly simulation for indoor and outdoor climatic conditions using energy simulation models. By using energy simulation models, the model accounts for the impacts of the physical characteristics of the surrounding urban environment that can either increase or lessen the magnitude of potential heat exposure and refrain the depending only on climate models that don't account for exposure at the micro-scale. Vulnerability

assessment revolves around four primary dimensions, namely, Exposure (E), Susceptibility (S), Coping Capacity (CC), and Adaptive Capacity (AC). These are dynamically interconnected and system-specific as follows:

Vulnerability = ƒ(Exposure; Susceptibility; Coping Capacity; Adaptive capacity)

The relationship between all four vulnerability components is governed by the local characteristics represented in the urban system (surrounding built environment and urban population) at the neighborhood level. Thus, vulnerability is a positive function of the urban system's exposure and susceptibility and a negative function of the system's coping and adaptive capacity. The indicators of each of the four vulnerability components have been identified based on the literature findings on heat vulnerability assessment, as presented in section 2.1 above. The details of each element and its direct and indirect relationship to overall vulnerability are outlined in Table 2-5.

Table 2-5: Description of major and sub-components of heat vulnerability Assessment model.

Category		Proxy Variable	Proxy For	Functional Relationship
Exposure/Urban Susceptibility	*Building Level*	Indoor exposure (SET > 30 C)	Building Thermal Performance	No. of consecutive hours > 30C+⟶indoor heat exposure
		Renovation Date		Recent Renovation date - ⟶ indoor heat exposure - ⟶ Building Susceptibility
		Construction Date		Old Construction - ⟶ Building Quality +⟶ Building susceptibility
		Construction Materials		Poor construction material - ⟶Building insulation Performance
		Window-to-wall Ratio	Heat Gain from Envelope	Window-to-wall Ratio+⟶Heat Gain indoors+ ⟶Building exposure
		Orientation		Building area in alignment to the sun +⟶Heat Gain indoors+⟶Building exposure
		Housing Type (Attached/Detached)		Attached Housing +⟶Heat Gain indoors+⟶ Building susceptibility
	Urban Level	Outdoor Exposure (UTCI > 32 C)	Potential for outdoor heat stress exposure	No. of consecutive hours > 32C+⟶Exposure increases+⟶Urban Susceptibility
		Vegetation coverage	Potential for outdoor heat relief	Vegetation coverage- ⟶Urban Susceptibility
Susceptibility	*Human Susceptibility*	Age	Physiological capacity	Age+⟶Susceptibility
		Gender	Response to heat exposure	Females are more susceptible to heatstroke than males
		Social Isolation		Social Isolation +⟶Susceptibility
		Medical Condition		Medical Condition +⟶Susceptibility
		Drug / Alcohol Abuse		Drug / Alcohol Abuse+⟶Susceptibility
		Mental Health		Mental Health+⟶Susceptibility
		Income Level		Low Income +⟶Susceptibility
		Access to Health Care		Access to Health Care - ⟶Susceptibility
		Access to Community Support		Access to Community Support- ⟶Social Isolation - ⟶Susceptibility
		Education Level		Low Education Level +⟶Susceptibility
Coping Capacity		Hours for Natural Ventilation	Short-term response to heat exposure	Hours for Natural Ventilation+⟶ Building Coping Capacity
		Access to Back up Power		Access to Back up Power +⟶Building Coping Capacity
		Access to AC/mechanical Cooling		Access to AC/mechanical Cooling+⟶Building Coping Capacity

Adaptive Capacity	Proximity to Cooling Shelter	Long-term response to heat exposure	Proximity to Cooling Shelter+⟶Urban Adaptive Capacity
	Proximity to Park- Open Space		Proximity to Park+⟶Urban Adaptive Capacity
	Proximity to Hospital		Proximity to Hospital+⟶Urban Adaptive Capacity

Heat exposure is considered in the model as a function of indoor and outdoor exposure when people go outside for a cooling outlet if it gets too warm inside. In assessing exposure, the number of consecutive hours is considered based on findings in the literature on how prolonged exposure can drive heat-related health impacts (Pyrgou et al., 2017; Kenny et al., 2019). Susceptibility consists of three main components: a) building susceptibility, b) urban susceptibility, and c) human susceptibility. Building susceptibility represents a building's physical characteristics impacts on potential heat risks such as limited availability of natural ventilation can exacerbate health impacts during heat exposure. To examine how building and surrounding urban amenities can influence the individual capacity to mitigate heat risks, vulnerability is estimated as a function of susceptibility minus the sum of coping capacity and adaptive capacity to capture both long- and short-term impacts. A critical factor in the interrelationship between heat exposure and potential health impacts is the individuals' adaptation response to heat. These actions are classified into three main categories, as follows (Kwok & Rajkovich, 2010):

Physiological Adaptation: linked to the body's ability to adapt to heat through physiological changes like sweating

Psychological Adaptation: based on the individuals' perception of thermal comfort and conditions that offer a thermally comfortable environment using building control systems.

Behavioral Adaptation: refers to the individuals' response to adapt to heat through a series of adjustments. These adjustments include personal adjustments like changing clothing level and contextual adjustments like opening windows, using air conditioning, and closing window blinds to reduce heat stress.

In the model development, physiological adaptation is included as part of human susceptibility as a function of age and gender. Psychological adaptation is represented in indoor exposure based on hours when thermal comfort levels are exceeded. Finally, behavioral adaptation is modeled as part of coping capacity and adaptive capacity to heat exposure, whether at the building or urban scale. Coping capacity indicates the available resources for short-term adaptation to heat. It usually occurs at the building level, such as opening windows for ventilation or access to backup power in case of power loss to maintain livable conditions indoors through mechanical cooling. Adaptive capacity reflects the available urban services that will help individuals adjust to heat exposure, like access to cooling shelters, parks, and proximity of health amenities.

After determining all components and sub-components of heat vulnerability, all the values are normalized to a relative position between 0 and 1. It is also assumed that all of the heat vulnerability components have equal importance, and thus all indicators are weighted equally. This approach has been extensively used in heat vulnerability assessment in the literature, and it has been recommended to help avoid any subjectivity in the overall heat analysis (Aubrecht & Özceylan, 2013; Di Napoli et al., 2018; Wolf, McGregor, & Analitis, 2014).

The vulnerability dimension was assessed on a scale of 0 to 1 with equal weights to all main and sub-components. Thus, the index of exposure containing both indoor and outdoor exposure is calculated as follows:

$$Exposure\ (E) = \frac{W_{ind}*\ Ind_{exp}+W_{out}*\ Out_{exp}}{W_{ind}+\ W_{out}} \quad (3)$$

Where W_{ind} is the weight of indoor exposure, W_{out} is the weight of outdoor exposure, Ind_{Exp} is the number of consecutive hours where SET is above 30°C, and Out_{exp} is the number of hours where UTCI is above 32°C. Susceptibility is calculated using the following equation:

$$Susceptibility\ (S) = \frac{Ws_1*\ Indic_1+Ws_2*\ Indic_2+Ws_3*\ Indic_3+Ws_n*\ Indic_n}{Ws_1+\ Ws_2+Ws_3+\ Ws_n} \quad (4)$$

Where W_s is the weight of each indicator, $Indic_n$ is the indicator value, and n is the total number of susceptibility indicators. Coping capacity and adaptive capacity are calculated following the same approach, where coping capacity was calculated using the following equation:

$$Coping\ Capacity\ (CC) = \frac{Wcc_1*\ Indic_1+Wcc_2*\ Indic_2+Wcc_3*\ Indic_3+Wcc_n*\ Indic_n}{Wcc_1+\ Wcc_2+Wcc_3+\ Wcc_n} \quad (5)$$

W_{cc} is the weight of each indicator and $Indic_n$ is the indicator value, and n is the total number of coping capacity indicators. Adaptive capacity is calculated as follows:

$$Adaptive\ Capacity\ (AC) = \frac{Wac_1*\ Indic_1+Wac_2*\ Indic_2+Wac_3*\ Indic_3+Wac_n*\ Indic_n}{Wac_1+\ Wac_2+Wac_3+\ Wac_n} \quad (6)$$

Where W_{ac} is the weight of each indicator, and $Indic_n$ is the indicator value, and n is the total number of adaptive capacity indicators. The structure of model formulation, description of each indicator, and quantification approach are described in Table 2-6.

Table 2-6: Formulation of model variables and their units.

A. Exposure		
Indoor Exposure Range	Hourly simulation of SET for an extreme hot week	Hours
Consecutive Hours above Comfort Range	Number of consecutive hours where SET is above 30°C	Hours
Hours available for natural ventilation	Hourly representation of times where the outdoor air temperature is cooler than the indoor temperature	Hours
Indoor Cooling Potential	Number of consecutive hours where natural ventilation can be utilized	Hours
Indoor Occupation	Hourly representation of times when people stay indoors during the week	Hours
Indoor Occupation Hours	Net hours spent indoors	Hours
Indoor Exposure	IF THEN ELSE ((Consecutive Hours above Comfort Range-(Indoor Cooling Potential +Hours Available for Active Cooling))>=Indoor Occupation Hours, Indoor Occupation Hours,(Consecutive Hours above Comfort Range-(Hours Available for Active Cooling +Indoor Cooling Potential)))	Hours
Outdoor Occupation	Hourly representation of times when people go outside during the week	Hours
Outdoor Occupation hours	Net hours spent indoors	Hours
Outdoor Exposure Range	Hourly simulation of UTCI for an extreme hot week	Hours
Outdoor Discomfort Hours	Number of consecutive hours where UTCI is above 32°C	Hours
Outdoor cooling potential	Hourly representation of times where the outdoor air temperature is cooler than the indoor temperature	Hours

Hours available for outdoor activities	Number of consecutive hours where the outdoor air temperature is cooler	Hours
Outdoor Exposure	IF THEN ELSE (Outdoor Discomfort Hours-Outdoor Cooling Potential>=Outdoor Occupation Hours, Outdoor Occupation Hours, (Outdoor Discomfort Hours-Outdoor Cooling Potential))	Hours
B. Susceptibility		
Indoor Susceptibility	(((((Indoor Exposure-1) *(1-0))/ (24-1))+(((Indoor Exposure-1)*(1-0))/(24-1)))/2	Dimensionless
Outdoor Susceptibility	(((((Outdoor Exposure-1) *(1-0))/ (24-1)) +(((Outdoor Exposure-1) *(1-0))/ (24-1)))/2)	Dimensionless
Urban Susceptibility	Indoor Susceptibility + Outdoor Susceptibility	Dimensionless
Drug or Alcohol Abuse	A value between 0 -1 representing if occupants are susceptible due to drug and alcohol abuse	Dimensionless
Medical Condition	A value between 0 -1 representing if occupants are susceptible due to pre-existing medical condition	Dimensionless
Access to Health Insurance	A value between 0 -1 representing if occupants are susceptible due to access to health services	Dimensionless
Access to Community Support	A value between 0 -1 representing if occupants are susceptible due to access to social support network	Dimensionless
Family Size	Family size per apartment	Persons
Social Isolation	Represented by family size and lack of access to community support IF THEN ELSE ((Family Size<2:AND: Access to Community Support=0), 1, 0)	Dimensionless
Household Monthly income	Income level per household	$/month
Minimum income Threshold	The lowest monthly household income per neighborhood	$/month
Maximum Income Threshold	The highest monthly household income per neighborhood	$/month
Income level	1-(((Occupants' Monthly Income-Minimum Income Threshold) *(1-0))/(Maximum Income Threshold-Minimum Income Threshold))	Dimensionless
Male life span	Life expectancy in males for the examined population	Year
Female life span	Life expectancy in females for the examined population	Year
Minimum risk Threshold	Age under which is considered risky for heat exposure (Infants)	Years
Age Level	Represents susceptibility due to age (((("F.Occupant 1"-Minimum Risk threshold)*(1-0))/(Female Lifespan Threshold-Minimum Risk threshold))+((("F.Occupant 2"-Minimum Risk threshold)*(1-0))/(Female Lifespan Threshold-Minimum Risk threshold))+((("M.Occupant 1"-Minimum Risk threshold)*(1-0))/(Male Lifespan Threshold-Minimum Risk threshold)))/family size	Dimensionless
Human Susceptibility	((0.143*(1-Access to Community Support))+(0.143*(1-Access to health Insurance))+(0.143*Age Level)+(0.143*Drug or Alchohol Abuse)+(0.143*Income Level)+(0.143*Medical Condition)+(0.143*Social Isolation))	Dimensionless
C. Coping Capacity		
Hours available for Active Cooling	Hourly schedule for mechanical cooling (AC/Fans)	Hours
Availability of backup Power	Number of hours that a backup power can support in case of power loss	Hours
Coping with Backup Power	IF THEN ELSE((((((Hours Available for Active Cooling-1)*(1-0))/(24-1))+(((Hours Available for Active Cooling-1)*(1-0))/(24-1)))/2)<0, 0, ((((Hours Available for Active Cooling-1)*(1-0))/(24-1))+(((Hours Available for Active Cooling-1)*(1-0))/(24-1)))/2)	Hours

Coping with Natural Ventilation	IF THEN ELSE((((((Hours Available for Natural Ventilation-1)*(1-0))/(24-1))+(((Hours Available for Natural Ventilation-1)*(1-0))/(24-1)))/2)<0, 0, ((((Hours Available for Natural Ventilation-1)*(1-0))/(24-1))+(((Hours Available for Natural Ventilation-1)*(1-0))/(24-1)))/2)	Hours
Coping Capacity	0.33*Coping with Natural Ventilation+0.33*Coping with Backup Power+0.33*Outdoor Cooling Capacity	Dimensionless
D. Adaptive Capacity		
Cooling Shelter	A value between 0 -1 representing adaptive capacity with access to cooling shelter	Dimensionless
Nearby Park	A value between 0 -1 representing adaptive capacity with access to a nearby park	Dimensionless
Outdoor Cooling Capacity	IF THEN ELSE((((((Outdoor Cooling Potential-1)*(1-0))/(24-1))+(((Outdoor Cooling Potential-1)*(1-0))/(24-1)))/2)<0, 0, ((((Outdoor Cooling Potential-1)*(1-0))/(24-1))+(((Outdoor Cooling Potential-1)*(1-0))/(24-1)))/2)	Dimensionless
Adaptive Capacity	0.33*Cooling Shelter+0.33*Nearby Park or Shaded outdoor Area+0.33*Outdoor Cooling Capacity	Dimensionless
E. Susceptibility		
Susceptibility	0.5*Human Susceptibility+0.5*Urban Susceptibility	Dimensionless
F. Vulnerability		
Vulnerability	0.33*SUSCEPTIBILITY+(0.33*(1-Adaptive Capacity))+(0.33*(1-Coping Capacity))	Dimensionless
G. Risk		
Risk	Potential impact*Vulnerability	Dimensionless

Figure 2-5 describes the cause-effect relationship and the system structure between the various elements of heat vulnerability and related sub-components. The model hypothesis is that an increase in susceptibility and exposure will cause an increased vulnerability that can be balanced with improved coping capacity at the building scale and adaptive capacity at the urban scale. Through simulation, it is examined whether the complementarity among different indicators of coping capacity and adaptive capacity could help address increased vulnerability from heat exposure in populations who are highly susceptible due to their socio-economic characteristics. Three main scenarios are examined: 1) extreme vulnerability (E.V) assuming no access to any of coping and adaptive capacity measure, 2) improvement in coping capacity only (C.C), 3) improving in both coping and adaptive capacity (A.C/C.C). These scenarios are designed to assess how changes in urban services can influence the magnitude of vulnerability in populations that are considered highly susceptible.

The dynamic hypothesis is that when exposure increases, both urban susceptibility (as a function of its physical characteristics) and human susceptibility (as a function of the population's socio-economic factors) will increase vulnerability. These effects can only be balanced by improving coping capacity (either reducing exposure from changes in the physical urban space or increasing access to behavioral adaptation measures) at the building scale and the urban scale. The proposed SD model will provide a unique advantage to assess vulnerability by extending the model boundary to address any additional questions or problems as they arise. The model is based on the following assumptions:

1- For simplicity, access to backup power has no restrictions;
2- The relevant time horizon is the typical extreme hot week;

3- Changes in coping and adaptive capacity are immediate with no impact from policy delay or availability of funding resources.
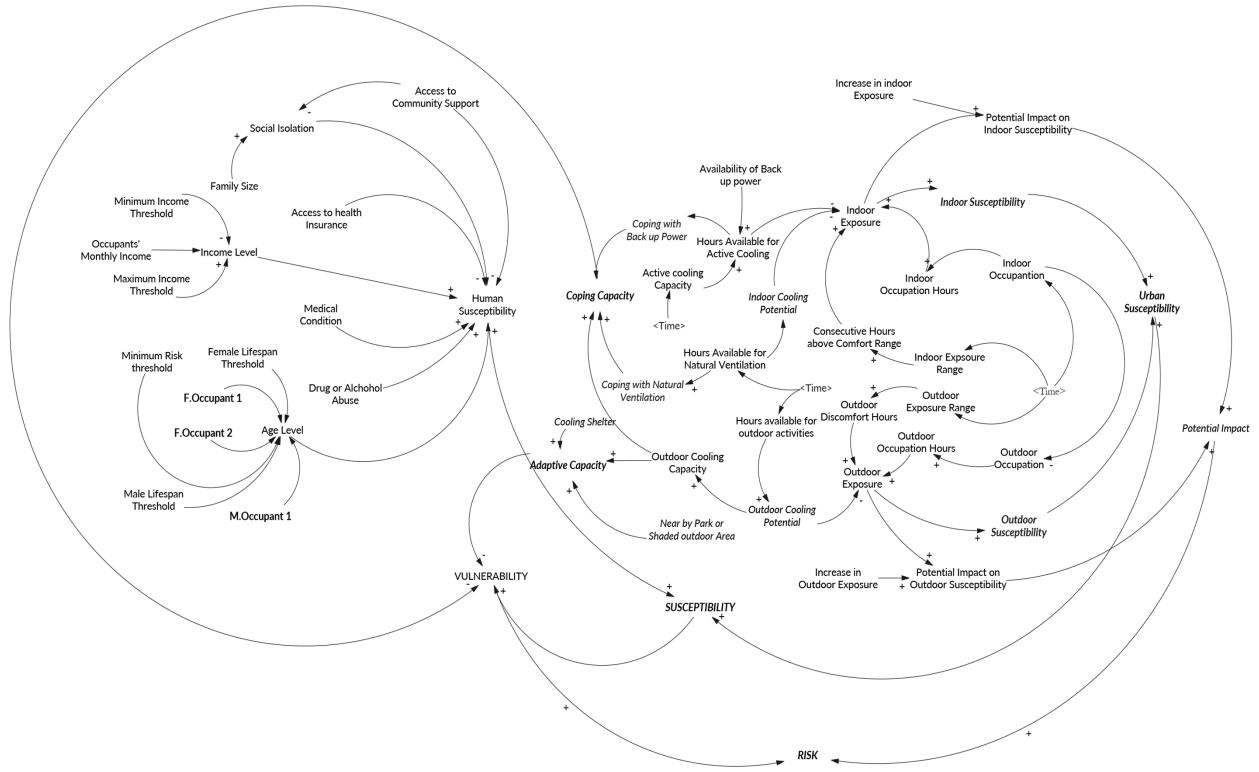
Figure 2-5: Structure of heat vulnerability SD model.

2.3.2 Case Study

A multi-family building in a low-income neighborhood in Cairo, Egypt, is examined in the SD model described above; AlDarb AlAhmar is a low-income neighborhood in Cairo, Egypt. The area has a mix of historical buildings from the 1700s through the late 20th century and buildings from 2010 and 2014. The total studied area is 2.8 acres, and it was specifically selected for its unique architectural character and diversity of building types, and economic challenges. Living standards are primarily considered for low-income, where air conditioning units are not typical and rarely installed. Ceiling fans and portable fans are the most common apparatus used for ventilation. There are three main archetypes identified from the site survey. The characteristics of envelopes' thermal properties vary with construction methods; historical buildings from the 1700s to 1800s, modern apartment buildings from the 20th century, and informal buildings built after 2010. Historical buildings represent around 72% of the existing building stock in Al Darb AlAhmar. Therefore, a multi-family historical building of three floors is chosen as a representative model of the building stock in the study area. Characteristics of building envelopes in archetype were identified from an on-site survey and summarized in Table 2-7.

Table 2-7: Construction material characteristics for historical archetypes in Al Darb AlAhmar.

Building Type	Historical		
Number of floors	2F	3F	4F
Average Built-up area	150 m2		
WWR	15% - 20%		
Glazing U-Value	6.25		
Wall U-Value (W/m2 K)	0.5	0.5	0.6
Internal Heat Capacity	75	73	72
External Heat Capacity	62	60	59
Roof U-Value (W/m2 K)	1.39		
Solar Heat Gain Coefficient (SHGC)	0.5		

The floor area of the residence examined in the study has an average area of 80 m^2. Onset Hobo data loggers were installed in three representative archetypes from July 6th to July 12th and August 8th through August 15th, 2018. Indoor temperature and relative humidity readings are used to analyze indoor climatic conditions and validate simulation results. The accuracy of the temperature loggers used was ± 0.21°C. All loggers were placed in the zones with sufficient air movement and away from internal heat sources and solar radiation. The outdoor air temperature was collected from the nearest weather station located 4.9 km from the analysis area. Outdoor temperature readings indicate high temperatures from July 7th until July 12[th,] 2018. Two simulations were executed for the representative archetype: hourly simulation for SET for an extreme hot week in Cairo, Egypt (from August 15th to August 22nd), and UTCI simulation with respect to the surrounding urban block within a diameter of 500 meters. The outputs of the simulations were then implemented as indicators of exposure in the SD model.

2.4 Results

In this section, the simulation model results and outputs of the three scenarios examined in the SD model are presented. Figure 2-6 illustrates the simulated indoor air temperature and recorded air measurements. Data from buildings' surveys and questionnaires were used to calibrate the simulation model with actual conditions. Simulation's mean square root error decreased substantially after adding questionnaire data. The questionnaire was tailored to address occupancy times, the number of equipment owned, adjustments residents use to regulate temperature and ventilation times. All these data were arranged by archetype and added to the simulation model explained in detail in chapter 3.

SD model simulations were performed using a daily time step. The heat vulnerability model presented in Figure 2-5 above is implemented in the Vensim software package, allowing for easy modification in the system structure and simulations of different scenarios. Information related to human susceptibility was collected through in-person interviews of a representative family of three members (female 55 years old, female 75 years old, and male 62 years old) and used as input to SD simulations. To validate the model's performance, the model formulation was tested under two scenarios: i) extreme scenario where there is no access to coping and adaptation resources, and ii) adaptation scenario that encompasses full access to adaptation amenities, cooling shelters and parks, and complete availability of backup power and

ventilation at the building level. Figure 2-6 compares results between the two examined scenarios. It can be noted that under the extreme scenario, vulnerability is at a maximum value of 1.0, while under the full adaptation scenario, vulnerability approached 0.
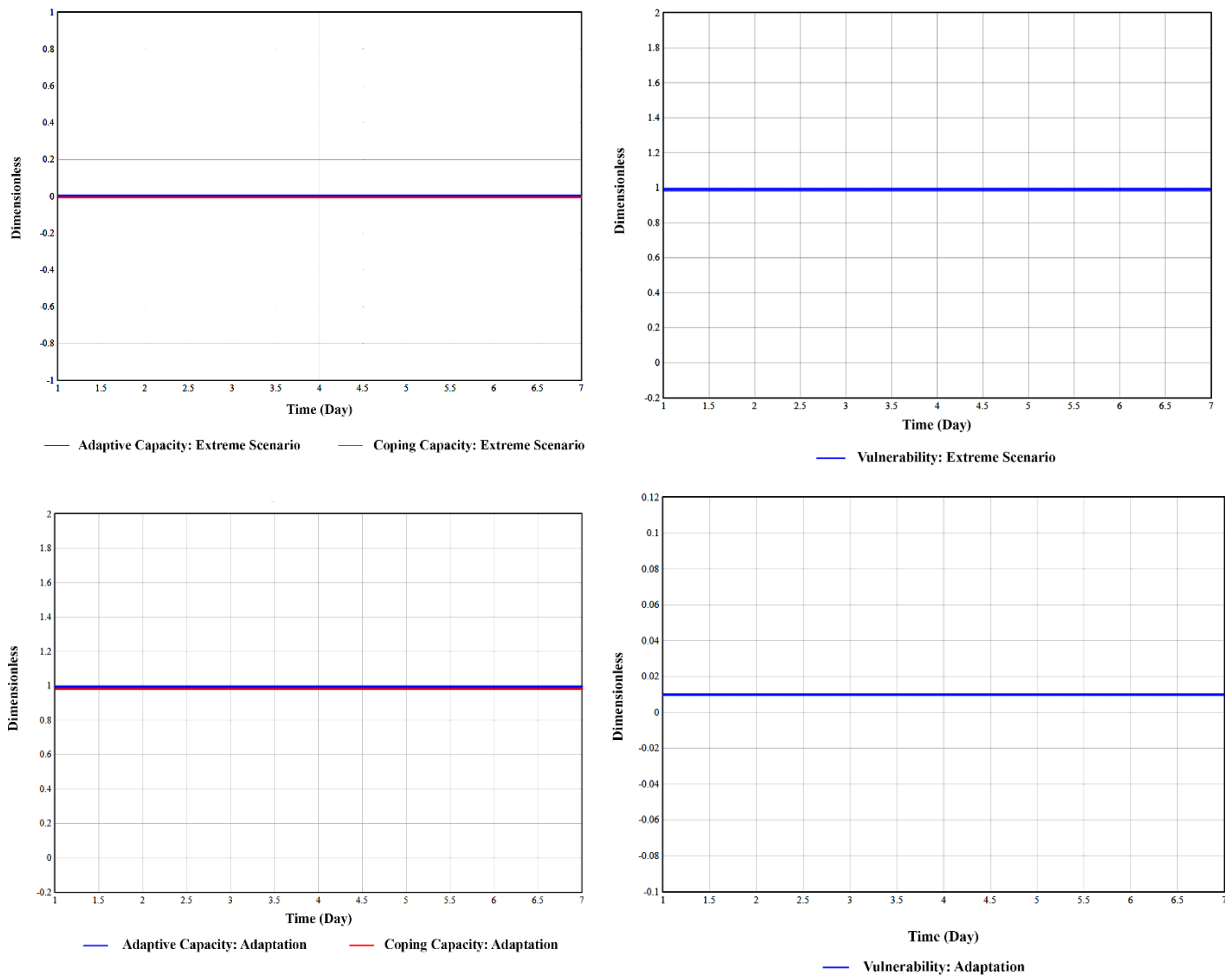
Figure 2-6: Top, coping and adaptive capacity and related vulnerability under the extreme scenario. Bottom, results of full adaptation scenario.

Next, the model is tested under the extreme vulnerability scenario, where all factors contributing to social vulnerability are assumed to equal 1 to imply an extreme condition of high susceptibility. The extreme vulnerability scenario shows that although indoor and outdoor exposure aren't high throughout the day, vulnerability is high due to a lack of access to coping and adaptation measures and socio-economic factors. These results imply that even under moderate exposure, a population can still be considered vulnerable due to other related socio-economic factors such as age, disability, low income, or medical condition and living in an urban setting that is highly susceptible due to lack of coping and adaptation services such as cooling spaces, secured power supply and proximity to health service that can drive their vulnerability to heat exposure. Figure 2-7 illustrates model output for extreme for the extreme hot week in the examined archetype and values for susceptibility, coping capacity, adaptive capacity, and associated vulnerability.
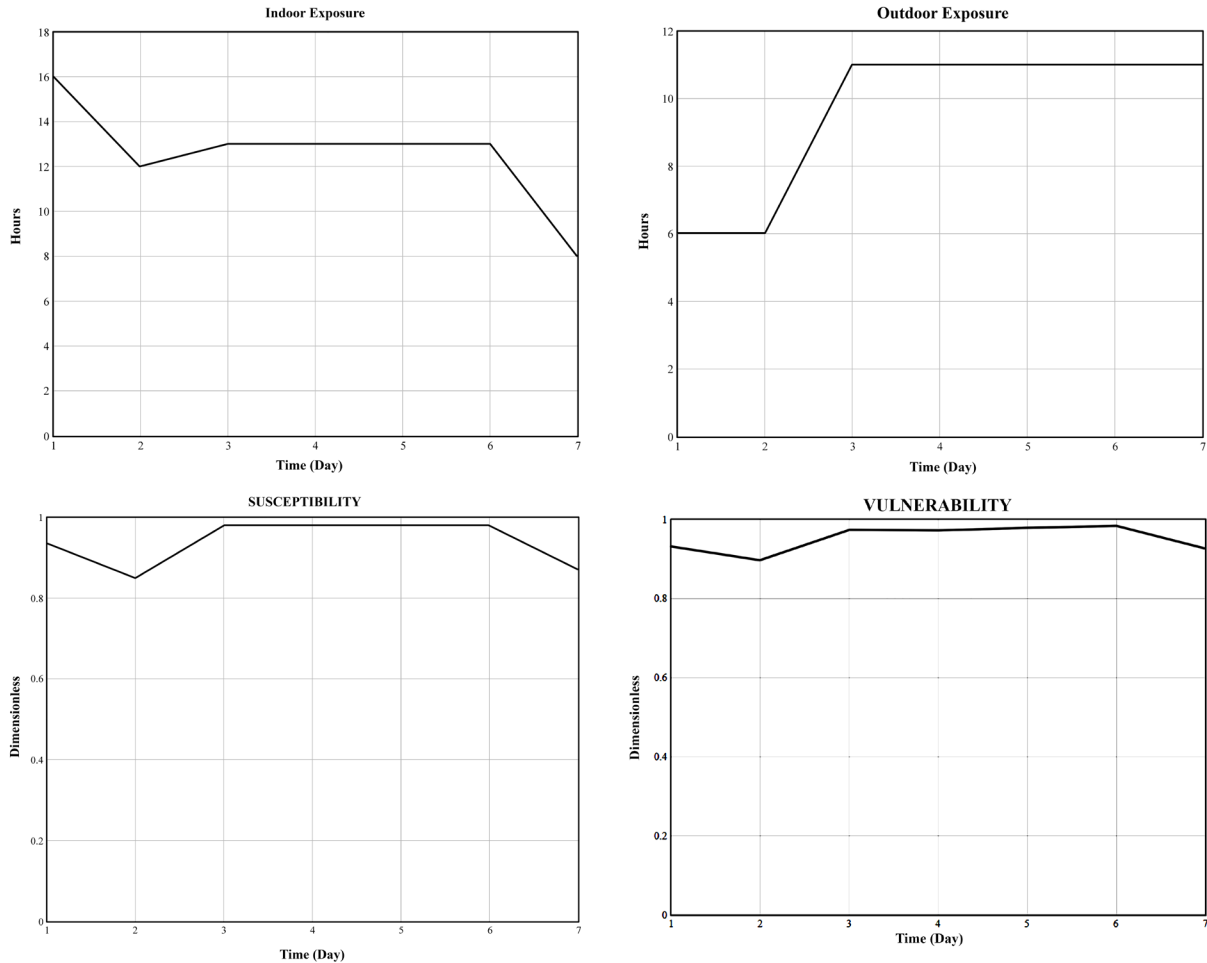
Figure 2-7: Results for the extreme vulnerability scenario and indoor and outdoor exposure (no. of consecutive hours where exposure is above comfort threshold) from the simulation model.

Next, simulations were developed for the coping capacity (cc) scenario to examine the effect of improved coping mechanisms at the building scale. Here, backup power is introduced for three consecutive hours every day as a measure of coping capacity. In the summertime for the past five years, Cairo has been experiencing a series of blackouts that can last up to seven consecutive hours during the daytime from increased demand for air conditioning. Figure 2-8 graphically visualizes the coping capacity results in the reference scenario (extreme vulnerability) and coping capacity scenario (access to backup power). As expected, the examined scenario shows lower values for vulnerability under the same socio-economic characteristics. Also, improvement in the urban susceptibility profile as a result of reduced susceptibility at the building scale. The total susceptibility is considered relatively close due to impacts from socioeconomic factors of the population. Results from the CC scenario underline that during heat exposure, the magnitude of vulnerability can vary significantly from one household that can substantially affect policy planning through understanding which area to prioritize and what sectors of the population.
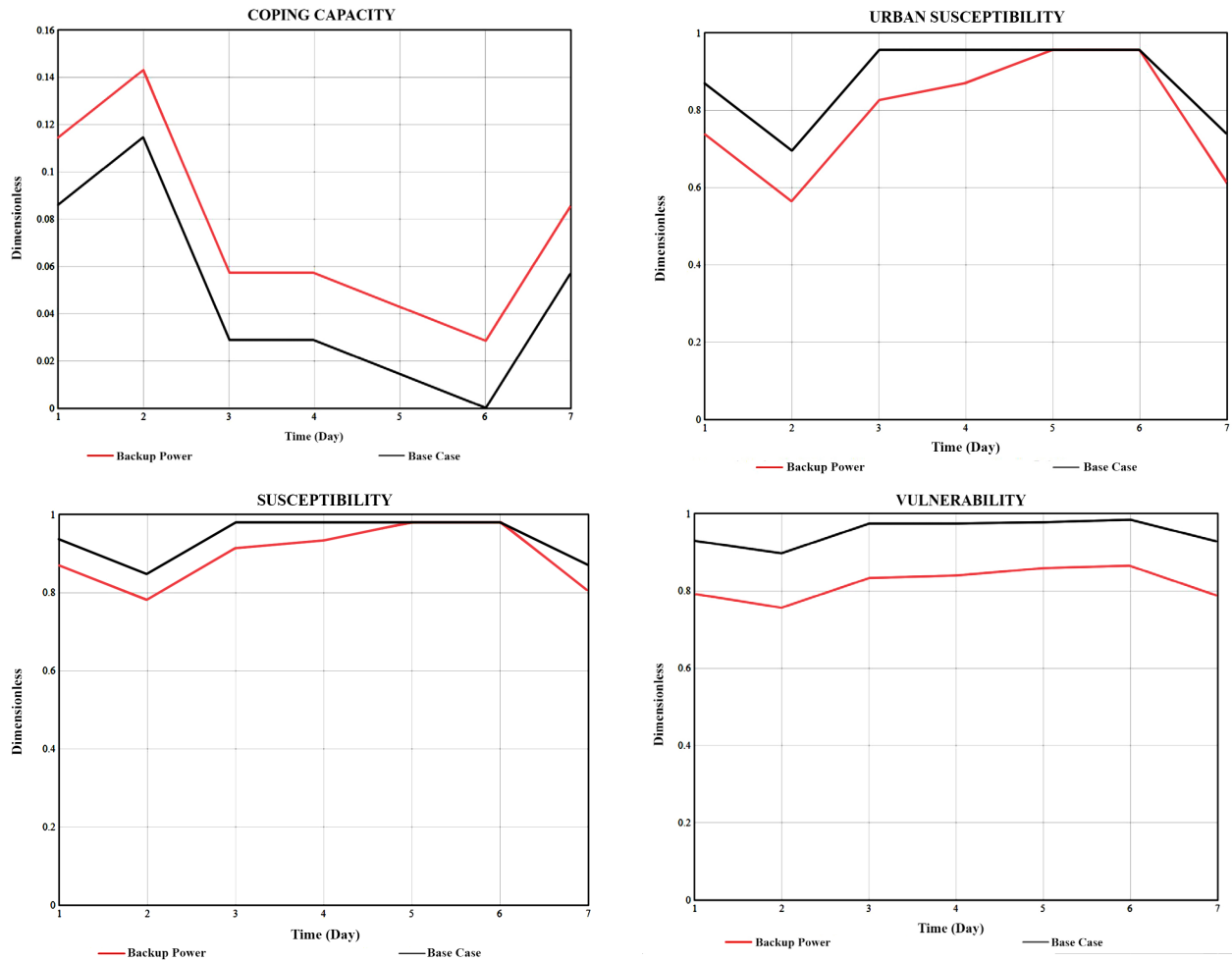
Figure 2-8: Results of Coping Capacity Scenario (access to backup power) compared to reference scenario (Extreme Vulnerability).

For the AC/CC scenario, access to backup power at the building scale and access to a nearby cooling shelter are evaluated. Also, access to community groups was changed in human susceptibility to examine how eliminating social isolation can influence vulnerability. Results show a significant reduction in vulnerability compared to the other two scenarios, as illustrated in Figure 2-9. Also, potential impacts are modeled as an increase in indoor and outdoor exposure by 30% to assess risk levels. There is a reduction in overall susceptibility (urban and human) and significant adaptive capacity and coping capacity improvement. Finally, the simulated risk profile indicates that risk has been reduced significantly under improved coping and adaptive capacity for risk level. This is because the population can be considered vulnerable to heat exposure, but the risk can be significantly mitigated with access to coping and adaptation measures. This ties back to the dynamic hypotheses of coping and adaptative capacity and reducing vulnerability and risk levels. Suppose a population is considered highly vulnerable, but the potential impact in future heat exposure is relatively lower. In that case, risk levels will not be as high as vulnerability, as shown in Figure 2-9 below. These results indicate that the surrounding built environment's physical characteristics play a significant role in driving exposure magnitude and the potential impact that defines risk levels. These relationships are often not fully explored in heat vulnerability assessment. Most of the focus is on the

socioeconomic characteristics alone or large urban scale risk assessment that doesn't fully capture these micro dynamics occurring at the building scale and surrounding urban amenities.
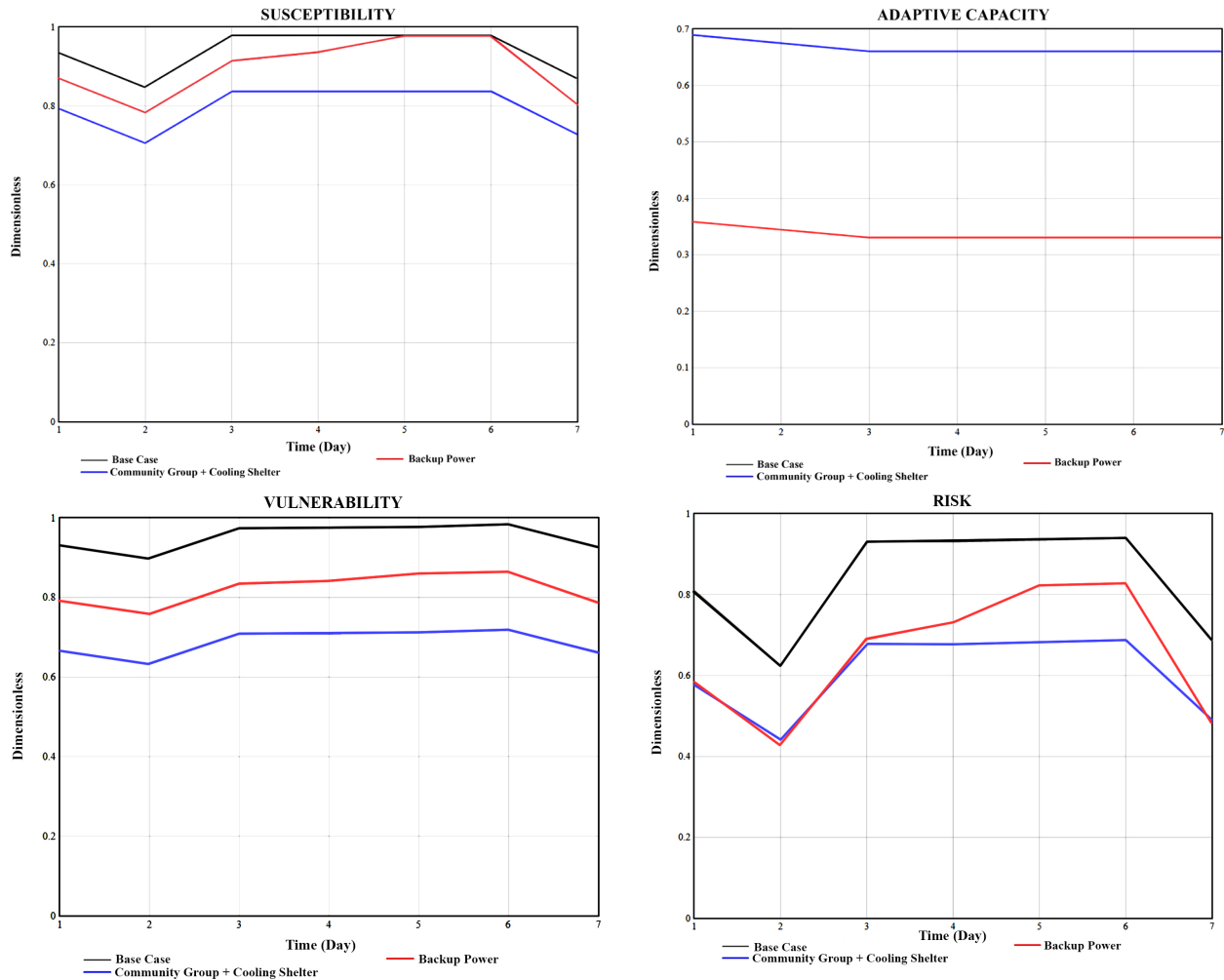
Figure 2-9: Results of the three examined scenarios for susceptibility, adaptive capacity, vulnerability, and related risks.

Results from the proposed SD model confirm the underlying hypothesis that vulnerability and risk from heat exposure are dynamically linked to the coping and adaptive capacity of the surrounding built environment with the urban population's socioeconomic characteristics. Findings from the model indicate that exposure occurring at both the building and urban levels can significantly influence the project risk due to the potential impacts of future overheating. Also, vulnerability assessment requires a more in-depth examination of socioeconomic characteristics alongside surrounding urban amenities to improve or exacerbate potential heat exposure risks. These findings imply that large-scale assessment would need to be coupled with a detailed evaluation of heat exposure dynamics at the building scale and how individuals interact with the surrounding urban services to assess which areas need to be prioritized in adaptation policies.

2.5 Discussion

The first section of this chapter develops a quantification approach for heat vulnerability assessment in urban settings using SD modeling. The representative case study results in Cairo, Egypt, show that in highly dense urban areas with no air conditioning access, the indoor heat exposure represented around 90% of the day was above the thermal comfort range (SET> 30°C). Building simulation results showed daily indoor maximum temperature is generally more than 30°C, which is large enough to drive potential health impacts, specifically for highly susceptible populations such as elderly residents and infants. These results indicate potential health risks from prolonged exposure, such as an increase in blood pressure (M. Kim, Chun, & Han, 2010; Y.-M. Kim et al., 2012), sleeping quality (Muzet, Ehrhart, Candas, Libert, & Vogt, 1983), and cognitive behavior (Cedeño Laurent et al., 2018a).

The urban population's socioeconomic factors are still vital in heat vulnerability assessment; however, they need to be coupled with information on the built environment's impacts. Such data can provide a more comprehensive evaluation of highly exposed areas, highly vulnerable areas, or areas at risk. Besides, social susceptibility indices can provide a sense of which sectors of the population can assist in an extreme heatwave. Incorporating building and urban characteristics of the areas that accommodate susceptible populations will help facilitate adaptation strategies and preparedness to future heatwaves. The proposed analysis of heat vulnerability in low-income urban communities to respond to potential climate risks reveals the relative importance of the surrounding built environment in heat risk management. The possibility of enhancing social-urban resilience to heat exposure and improving urban capacity is vital to understand when thinking about heat adaptation strategies. The study results in the following issues to assess heat exposure impacts and adaptation mechanisms of low-income urban communities.

1- Strategies to address coping capacity impacts: The SD model results suggest that building physical characteristics significantly beget exposure and causes the increased vulnerability. Therefore, building retrofit can significantly mitigate impacts heat exposure and promote coping capacity at the building level. In addition to building retrofit measures, improving coping capacity such as access to a backup power supply in the case of blackouts and access to clean water for hydration will enhance the individual's ability to cope with heat exposure, especially in low-income urban areas.

2- Improved urban services to strengthen adaptive capacity: The physical specification of the surrounding urban space act as a catalyst and can make communities more vulnerable to heat exposure, as was denoted in the extreme vulnerability scenario. Therefore, strategies must be evolved to reduce susceptibility created by low urban services. Thus, urban amenities in terms of adaptation resources (cooling shelters, parks, health services) may facilitate adequate adaptation in highly vulnerable communities in the long term.

2.6 Urban Heat Vulnerability Assessment Framework

Most of the existing heat vulnerability assessment is mainly based on socio-economic factors that rarely consider the built environment's spatial and physical parameters, which can exacerbate or lessen heat exposure impacts (Jänicke et al., 2019). This chapter aims to fill this gap by developing a framework to perform heat vulnerability assessment at the neighborhood scale, taking into account the physical properties of the surrounding built environment, human adaptive capacity, and policymakers' role in the success of adaptation measures. The framework intends to support the heat adaptation planning process by better understanding the local dimension of heat vulnerability distribution that can increase risks during extreme heat events. The proposed framework for vulnerability assessment involves analyzing the physical parameters of the urban space, indoor exposure at the building level, and occupants' adaptive capacity using spatial information, building performance simulations, and in-person surveys. This mix of spatial data, simulation models, and occupants' assessment is designed to support policymakers in developing adaptation strategies informed by the distribution of high-risk urban areas that accommodate highly exposed building stock and vulnerable populations. This framework's intended audience includes researchers, policymakers, community planning, concerned and interested citizens in heat risks, and stakeholders who wish to understand spatially-based assessment of heat vulnerability. The structure of the framework is divided into three primary levels of assessment that each supports the four phases of climate adaptation planning, as illustrated in Figure 2-10 below:

1. Preliminary assessment of heat vulnerability: which supports the primary analysis phase in the adaptation planning process
2. Detailed assessment of indoor heat exposure: results from this assessment can assist in the definition of adaptation strategies and prioritization of high-risk urban areas;
3. Urban intervention and policy development for heat adaptation: supports policymakers in implementing and monitoring adaptation measures.
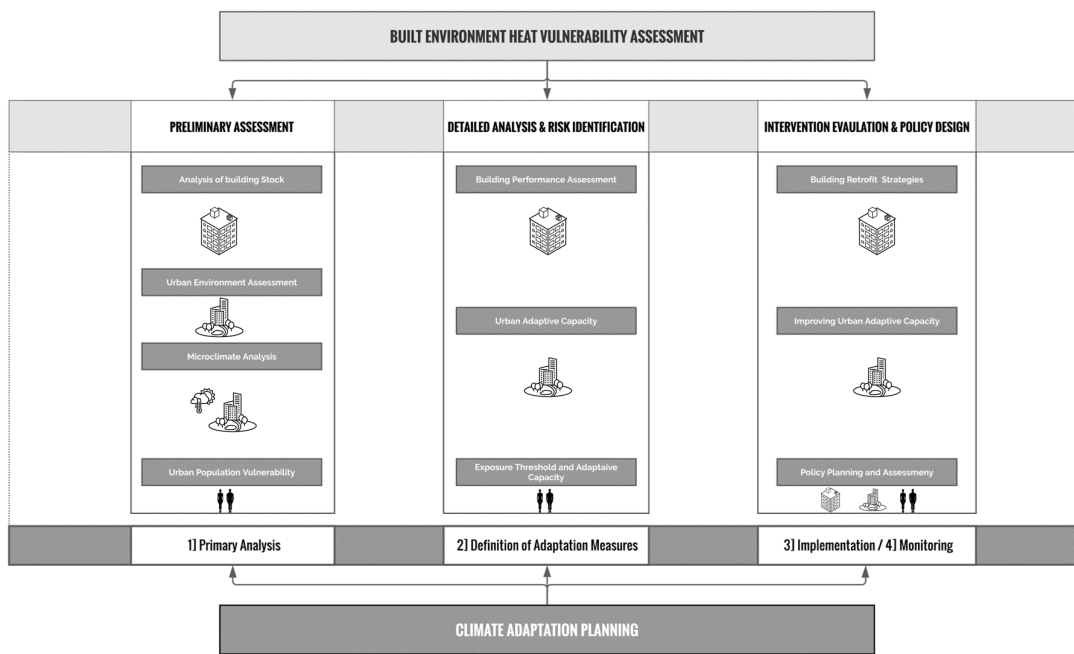

Figure 2-10: The three levels of heat vulnerability assessment framework and their relationship to climate adaptation planning.

2.6.1 Preliminary Assessment of Heat Vulnerability

This section describes the methodology and data types related to each level of the proposed framework to carry out the heat vulnerability assessment. Exposure to extreme heat is primarily due to urban physical conditions. The urban configuration can significantly exacerbate the range and magnitude of heat exposure, and by contrast, can mitigate exposure through vegetation and other urban cooling strategies. The purpose of the preliminary assessment level is to provide an overview of the general urban condition and identification of existing stresses with heat exposure and associated health impacts by examining three main components: local climate variability governed by the physical characteristics of the urban space, indoor exposure moderated by the building thermal properties, socio-economic susceptibility, and individual and household capacity to cope with heat threats. In this sense, a set of vulnerability indicators representing exposure, susceptibility, and adaptive capacity are used to identify the spatial distribution of the population who are considered at risk from heat-related impacts. Here, a range of indicators, analytical techniques, and spatial scales are presented to assess what denotes a cumulative vulnerability for a given urban area, as shown in Figure 2-11.
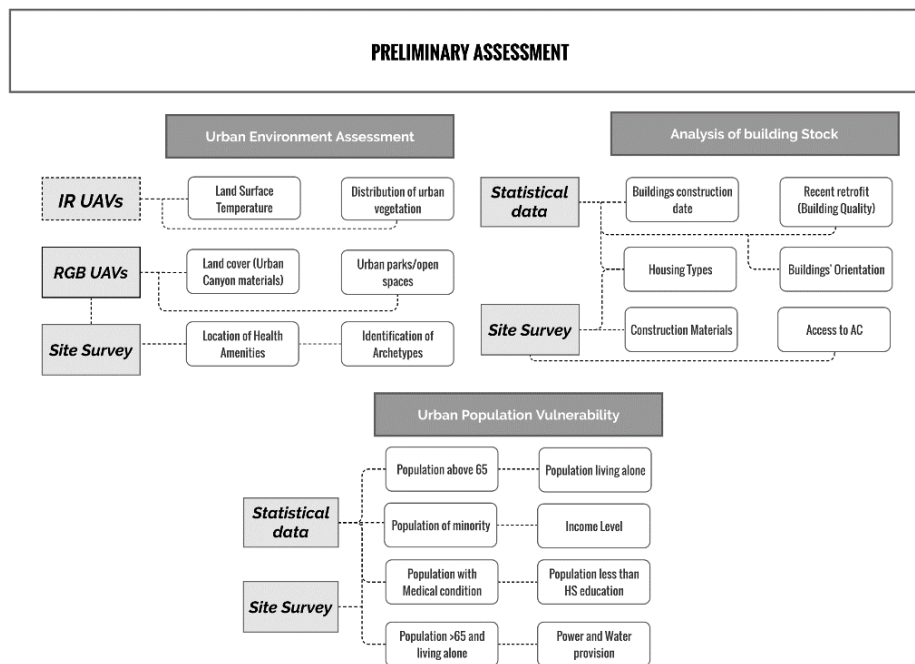
Figure 2-11: Preliminary assessment of heat vulnerability and associated indicators.

In the proposed methods set, Unmanned Aerial Vehicles (UAVs) equipped with infrared sensors and RGB cameras are introduced in the data collection and analytics for heat vulnerability assessment. UAVs have been recently explored in the literature as a reliable technology in the overall evaluation of the built environment due to the improved accessibility to data, cost reduction, and time efficiency (Jordan et al., 2018). In the field of climate change assessment, UAVs' application has expanded rapidly as the technology experienced a surge in availability and reliability (Villa et al., 2016). Recent findings from the literature indicate a rapid development in UAVs technology (Grosso et al. 2020) with several promising innovations that could provide numerous advances in data accessibility and time efficiency in assessing neighborhoods' conditions. The application of UAVs in heat vulnerability assessment is discussed and presented through two applied case studies in chapter 4.

The first layer includes building stock assessment; depending on the housing condition, quality of construction, and building envelope's thermal properties, a building can either exacerbate or lessen exposure during extreme heat events (Kenny et al., 2019; Maller & Strengers, 2011; Wright et al., 2005). Thus, construction date, recent retrofit, housing type, and construction materials are proposed as indicators of housing susceptibility to heat exposure. Also, such characteristics can be used as an indicator of potential indoor exposure. Since air-conditioning and other mechanical cooling means are the preferred approaches to coping with the heat (Palmer et al., 2014; D'Ippoliti et al., 2010), access to mechanical cooling is used as an indicator of buildings' adaptive capacity.

At the urban scale, heat exposure magnitude has been extensively studied in the literature (Romero-Lankao et al., 2012). Some studies in the literature defined the hazard magnitude of heat in an urban area using land surface temperature (LST) to reflect temperature conditions (Johnson, Wilson, & Luber, 2009; Rinner et al., 2010; Streutker, 2003). In addition to LST, the reflected solar radiation ratio depends significantly on the surface albedo and urban geometry, driving heat exposure from UHI (J. Yang, Wang, & Kaloush, 2015). Several studies have examined the impacts of road reflectivity on outdoor heat stress due to the consequent increase in mean radiant temperature (Salata et al., 2017; Santamouris et al., 2018; Wang & Akbari, 2016). Therefore, urban canyon albedo is considered as an indicator of outdoor heat exposure. Since LST is mainly tied to geographic location and related climate seasonality, coupling it with urban albedo will provide a better understanding of exposure magnitude. These two parameters, LST and urban albedo are used to assess an urban area's susceptibility to heat exposure. For instance, an urban area with high LST and high albedo is considered highly susceptible to heat exposure and vice versa. Vegetation coverage plays a role in regulating high temperature by providing shading and heat absorption (F. Li, Chen, Zeng, Zhao, & Wu, 2014). Here, the level of vegetation coverage (vegetation ratio) and the availability of heat relief amenities such as cooling shelters and health services are considered indicators of the urban adaptive capacity.

The third component of the preliminary assessment is concerned with urban populations. As outlined previously, the socio-economic aspect of heat vulnerability has been extensively discussed in the literature. Based on the findings from the literature, five key indicators for human susceptibility are identified: age, socioeconomic status, pre-existing health condition, ethnicity, and social isolation (Anderson & Bell, 2009a; Baldwin et al., 2019; Curriero et al., 2002). A detailed discussion on the structure and description of each of these indicators is presented and discussed thoroughly in the second half of this chapter. The urban population's adaptive capacity is defined as responding successfully to heat exposure through behavioral and technological adjustment (Chow et al., 2012; Intergovernmental Panel on Climate Change (IPCC), 2013). It is well established in the literature that under heat exposure, individuals tend to rely mostly on water and power to cope with heat stress, whether through mechanical cooling or water for hydration (Costello et al., 2009; IEA, 2018; Maller & Strengers, 2011). Since access to mechanical cooling and heat-relief amenities were included as indicators of adaptive capacity, here, stable access to power and water supply is considered as an indicator of behavioral adjustments representing the household's adaptive capacity.

2.6.2 Detailed Assessment of Indoor Heat Exposure

Studies on health risks during extreme heat events have reported that most heat-related mortality was reported while people were indoors in their own homes (CDC, 2013; Fouillet et al., 2006). It was also found that low-income households and socially isolated individuals are at greater risks from heat exposure (Fouillet et al., 2006; Kaiser et al., 2007; Semenza; et al., 1996). These findings denote indoor heat exposure can impose high risks to human health during extreme heat events. However, most heat-related risk studies don't fully account for indoor temperature and associated health impacts and typically examine vulnerability and risk impact among populations as a whole (Kenny et al., 2019). Given that the urban population, mainly the elderly, spend between 80 to 90% of their time indoors (Neil E. Klepeis et al., 2001), existing heat-vulnerability analyses that don't account for indoor exposure tend to underestimate health impacts resulting in misinformed adaptation policies and intervention measures (Kuras et al., 2017).
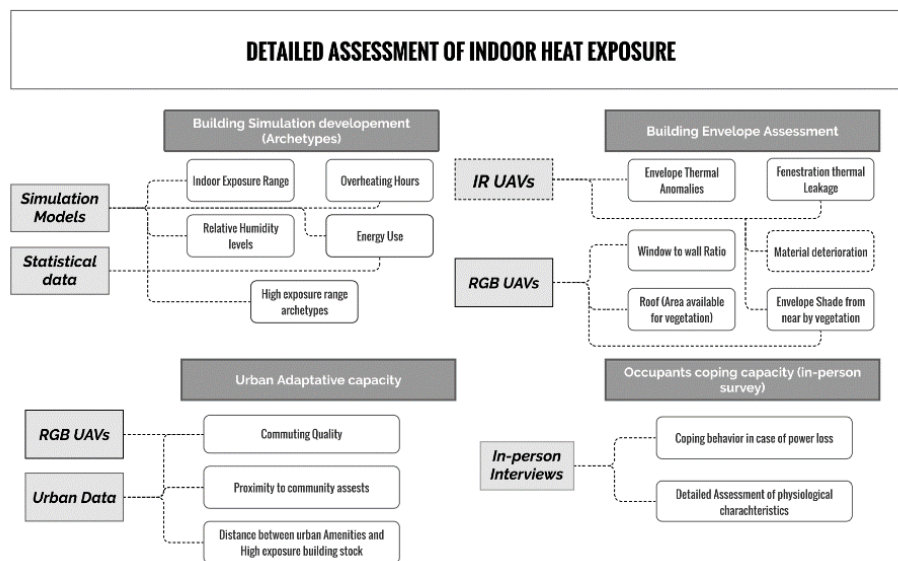
Figure 2-12: Detailed assessment of indoor heat exposure, indicators, and proposed research methods.

Since indoor exposure primarily depends on the built environment's properties, outdoor conditions, occupant's behavior, and building's physical characteristics, heat vulnerability assessment needs to account for the association between indoor heat exposure and human health. Also, individual or household adaptive behavior to use climate control under extreme heat exposure is dominantly influenced by the indoor thermal comfort levels (Frey, Destaillats, Cohn, Ahrentzen, & Fraser, 2014; Neil E. Klepeis et al., 2017; Kuras et al., 2017). Thus, assessing heat vulnerability from an indoor exposure perspective would require a direct assessment of buildings' thermal performance to understand how temperature is moderated, alongside information on occupants' behavior under extreme temperature. Thus, the purpose of level 2 is to address these gaps by introducing an indoor heat exposure assessment workflow as outlined in Figure 2-12 above. The indoor heat exposure uses building energy simulation models to assess indoor exposure combined with in-person interviews to account for human adaptive capacity and behavioral measures under high temperatures. Also, community support and proximity to

heat-relief amenities are included as indicators of the household's adaptive capacity and representation of how individuals interact with the available urban services during heat exposure.

2.6.3 Urban Intervention and Policy Development for Heat Adaptation

As outlined previously, the vulnerability of an urban population to heat is represented by exposure to high temperature, population susceptibility, and adaptive capacity to cope or respond to heat events. Characterization of the spatial variability of heat vulnerability and related impacts, factoring in exposure, susceptibility, and adaptive capacity, can help policymakers and city planners identify agglomeration of highly vulnerable populations and develop adaptation scenarios to enhance their resilience (Borden, Schmidtlein, Emrich, Piegorsch, & Cutter, 2007; Laska & Morrow, 2006; Reckien, Wildenberg, & Bachhofer, 2013). Findings from the literature show that even with adequate heat warning systems and access to air conditioning, extreme heat will still represent a significant concern to human health in the next 20 years without the proper understanding of how to design and implement suitable adaptation measures (Aubrecht & Özceylan, 2013; Wilhelmi et al., 2012).
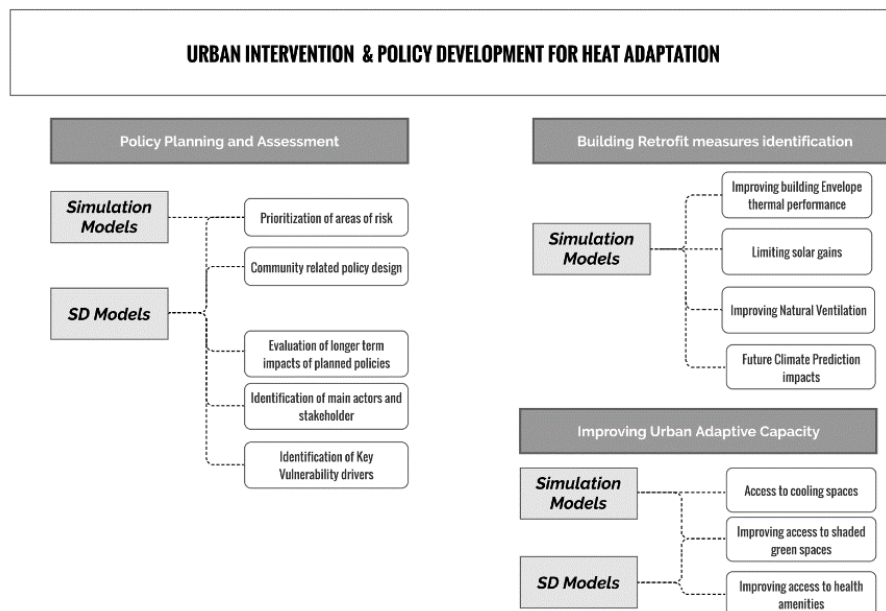
Figure 2-13: Urban intervention and policy development for heat adaptation and related indicators.

The impacts of heat vulnerability at the neighborhood level on population health are critical to analyze and integrate with adaptation strategies (Romero Lankao & Qin, 2011). The primary purpose of level 3 of the framework is to connect adaptation policy development to vulnerability assessment. This will help decision-makers frame adaptation measures that can effectively target specific urban locations and populations considered high risk from heat exposure. Also, level 3 addresses adaptation strategies at both the building scale and the urban scale with a continuous evaluation of the decision-making process as drivers for planned strategies' success or failure, as illustrated in Figure 2-13. The three main components of this level constitute 1) identification of adaptation measures at the building scale to lessen the impacts from indoor heat exposure, 2) improving urban adaptive capacity by increasing population's access to adaption amenities, and 3) the assessment of planned policies with respect to where the areas of high risk are located, available funding to support adaptation measures, and time needed to executed planned

strategies effectively. Policy assessment will guide policymakers on how planned policies can effectively reduce heat vulnerability and detect early on any potential delays that can occur throughout the decision-making process that can directly affect the success of heat adaptation policies.

2.7 Summary

Planning for heat risk management is challenging, especially in areas where the population is susceptible to socioeconomic factors or living in deteriorated urban areas. Meanwhile, analysis results show that these characteristics can substantially determine the overall vulnerability to heat exposure. Past research has implicated an individual's socioeconomic factors as a determinant of heat-related health impacts during extreme heat events. This chapter has outlined the importance of the physical characteristics of the surrounding built environment in vulnerability assessment. From the literature review, numerous gaps of existing heat vulnerability frameworks have been identified to account for indoor and outdoor exposure coupled with individual behavioral adaptation. This chapter discussed existing gaps in the literature in implementing urban-related variables as indicators for vulnerability assessment. A heat vulnerability quantification approach using SD modeling is introduced using a set of already established indicators for potential health-related impact under heat exposure. The analysis was coupled with an energy simulation model to represent the effects of the building's physical characteristics in exacerbating or mitigating indoor exposure and outdoor exposure.

Heat events present a complicated exposure pathway that is compounded by the presence of context-independent urban and social factors. A literature review of heat vulnerability assessment outlined an apparent disconnect between vulnerability assessment and building science. On the other hand, urban and building science has the same disconnect of not accounting for socioeconomic and behavioral implications of heat exposure. Therefore, this research developed a heat vulnerability framework that accounts for the gap between social vulnerability assessment and building and urban science. The framework core structure is based on an interdisciplinary overlap between urban, social, and building-based evaluation that can offer an opportunity to capture missing impacts in heat risk assessment. The proposed framework may help integrate social and urban science coupled with policy-related strategies into heat vulnerability assessment.

Based on our findings in the analysis presented in this chapter, the heat vulnerability framework should account for indoor and outdoor exposure to heat, meaning the impacts of the surrounding built environment need to be incorporated with population social vulnerability. The following three chapters provide an application of each assessment level outlined in the vulnerability assessment framework. Chapter three will examine the detailed assessment level in heat quantification, emphasizing heat-related health impacts from prolonged exposure in urban areas with limited access to air conditioning. Chapter four will outline the application of UAVs technology in the assessment of the built environment. Finally, chapter five will conclude with policy implications and guidelines for heat adaptation planning.

III. DETAILED ASSESSMENT OF HEAT VULNERABILITY

Climate change risks are considered one of the major global concerns that face humankind in the 21st century. Climate change effects are expected to exacerbate drastically over the next two decades, including increased intensity of weather events, frequent drought periods, and prolonged periods of extreme heat events. Scientific evidence indicates that climate change will significantly impact the built environment over the next decades (Crump, 2011; Spengler, 2012). Such findings underline that the urban population will be challenged with high exposure to climate events that will require cities to be more equipped to combat their effect. With rising global temperature, the consequence of climate change is now recognized as one of the significant issues facing humans in this century. While there is an extensive body of literature on the effect of extreme outdoor air temperature on mortality, there is a significant limitation of our understanding of the implications of excessive indoor conditions and human health. Furthermore, it is estimated that heat vulnerability is more significant for urban populations as they spend around 80% to 90% of their time indoors (N E Klepeis et al., 2001; Leech, Nelson, Burnett, Aaron, & Raizenne, 2002b). This infers the need to establish a threshold for indoor temperature above which heat stress can occur at a dangerous level to human life. However, numerous factors affect individual thermal comfort, depending on environmental and physiological factors. Therefore, it is challenging to establish a threshold for indoor conditions that are considered comfortable for everyone. This chapter examines and identifies indoor condition thresholds that can cause high health risks under extreme heat exposure—specifically, urban populations living in an arid climate in low-income neighborhoods. The analysis pays attention to the impacts of archetypes' physical characteristics (historical buildings) with no access to air conditioning on heat-related health risks and implications from climate change projections. The chapter is divided into two main sections. The first section presents an overview of overheating risks indoors and the impacts of excessive heat on human health. A case study in AlDarb AlAhmar in Cairo, Egypt, is developed to examine potential heat-related health impacts from indoor exposure and associated indoor climatic conditions threshold and the role of human's adaptive capacity under extreme heat exposure. Section two presents a computational approach using machine learning to quantify indoor heat exposure at the district level using AlDarb AlAhmar district in Cairo as a case study.

3.1 Indoor Overheating Assessment

Recent research findings highlight the growing vulnerability of the urban communities in developing regions to heat exposure. Such populations usually reside in building with poor ventilation and limited air-conditioning access, which increases the risks from extreme heat exposure (Lomas & Porritt, 2017). On the other hand, in developed regions or territories where air-conditioning is available, there is a growing concern to examine the impacts of heat exposure on human survivability and thermal comfort during power supply failure. Currently, around 30% of the global population experiences not less than 20 days of excessive heat annually that is considered threatening to human life, and it is projected that by 2100 three out of four people will be subject to deadly heat stress (Kenny, Flouris, Yagouti, & Notley, 2018; Mora et al., 2017b). Evidence from the 2003 European heatwave underlines the risks associated with prolonged exposure to excess heat fatalities that can occur indoors (Valleron & Boumendil, 2004). At least 35,000 people died due to the 2003 heatwave, with 14,802 deaths recorded in France alone (United Nations Environment Programme (UNEP), 2004). In 2015, around 110 people died in Egypt from rising temperatures, while 580 people were hospitalized due to heat exhaustion after the temperature reached 47 °C (AlAhram, 2015; BBC, 2015b).

The relationship between indoor overheating exposure and health-related risks is examined in this chapter through three driving mechanisms. First, building physical characteristics modify indoor temperature and consequently affect potential indoor exposure. This includes the role of materials' thermal capacity to modulate heat exposure and regulate indoor temperature levels during extreme heat events (Kenny et al., 2018; Mavrogianni, Davies, Wilkinson, & Pathan, 2010a; Phil, 2005; White-Newsomea et al., 2012). Other parameters such as building orientation, geometry, number of windows, and occupancy density are also considered crucial determinants of building capacity to regulate the relationship between indoor-outdoor temperature. Surrounding urban context; also plays a role in how buildings absorb solar radiation and adjust heat throughout the day (K. J. Lomas & Kane, 2013; Kevin J. Lomas & Porritt, 2017). A study by White-Newsome et al. (2012) examined how building-specific characteristics can impact indoor microclimate by analyzing three primary parameters: 1) material of exterior walls, 2) construction date of the building, and 3) housing type as a metric for occupancy density. The study found that older dwellings were built with a relatively lower insulation level that has influenced indoor thermal comfort levels and are therefore considered more vulnerable to heat exposure. The study has also shown that surrounding vegetation cover plays a critical role in regulating indoor air temperature.

The second mechanism is occupants' response to heat exposure. While buildings are exposed to the same environmental conditions, occupants' coping action to compact heat exposure differs significantly. The interrelationship between surrounding climatic conditions and the human physiological sensation of heat stress is the individuals' adaptation response to heat exposure, referred to as "Coping Capacity" (Hayden, Brenkert-Smith, & Wilhelmi, 2011). Coping capacity refers to the human ability to lessen the impact of exposure to extreme heat using a range of actions to reduce heat stress (Hayden et al., 2017b). As discussed in Chapter 2, this behavior is a function of the availability of active adjustments such as mechanical cooling, whether it's an air conditioning system, ceiling fans, or passive adjustments by opening the windows, changing clothing level, taking a shower, or hydrating.

Third, the threshold of indoor microclimate, where the high indoor temperature may increase health-related risks. While there has been a vast body of literature assessing the indoor condition and thermal comfort, there has been a gap in examining the indoor climatic conditions threshold that can help indicate potential health risks associated with heat exposure. This raises the question about defining a temperature threshold for vulnerable populations living in deteriorated urban settings with limited coping capacity. Numerous studies have identified different heat stress indices to examine the impact of heat exposure on human health (Epstein & Moran, 2006). Predicted Heat Strain (PHS) and Wet Bulb Globe Temperature (WBGT) are the most internationally utilized indices for heat stress and related health impacts (Holmes et al., 2016b). However, the duration of heat stress conditions and their effects on human health are not thoroughly examined in the literature. Thus, indoor conditions are assessed with respect to the duration of exposure to identify overheating thresholds that can be associated with potential health risks. Also, the relationship between outdoor conditions (such as solar radiation, humidity, and air temperature) and indoor conditions can directly influence indoor threshold, especially in buildings without air conditioning. Lee et al. (2015) have found a strong correlation with a seasonal pattern between outdoor air temperature and indoor air temperature in Seoul, Korea, that is high during the summer and low during the winter months. The study has also found that dwellings with no AC had a higher slope of regression than those with AC, as shown in Figure 3-1.
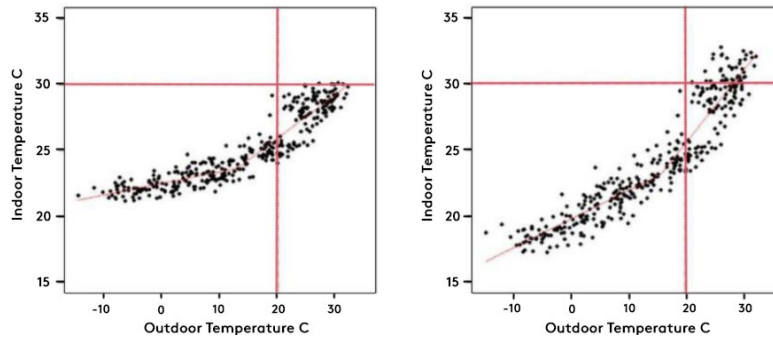
Figure 3-1: Scatterplot and regression results for the indoor and outdoor relations detached houses with AC (left) and no AC (right) (K. Lee & Lee, 2015).

3.2 Human Health and Heat Exposure

In this section, the relationship between indoor heat exposure and related health impacts is examined. Through the literature, the research outlines factors driving heat-related health risks to identify indoor conditions linked to higher risks on human health. The chapter reviews relevant studies globally that examined heat exposure and temperature ranges related to risk to investigate the indoor overheating threshold that drives risks. Exposure to extreme heat situations often results in heat stress, which is also associated with overheating. Heat stress is a physiological state when the human body is exposed to intense thermal conditions and consequently affects essential body functions (Seth H. Holmes, 2016). Human thermal comfort is a function of two main components: i) parameters related to surrounding environmental conditions such as air temperature (AT), relative humidity (RH), mean radiant temperature (MRT), and wind speed, and ii) factors related to human physiological characteristics such as metabolic rate, clothing level, age, and gender (Abdel-Ghany, Al-Helal, & Shady, 2013; Macpherson, 1973). However, heat stress is strongly dependent on the human body's thermoregulation resulting from exposure to the

aforementioned environmental parameters (Enander & Hygge, 1990). The steady range in which the human body maintains constant core temperature is identified as the homeothermy zone, as illustrated in Figure 3-2 below. This range includes the thermal comfort range and the threshold of more extreme hot and cold conditions (N. Lacetera, U. Bernabucci, H.H. Khalifa, 2003). The human body's steady thermal state is within a core temperature of 37°C (Ramsey, 1995; Ramsey & Chai, 1983), and above this temperature, risk levels start to exacerbate.
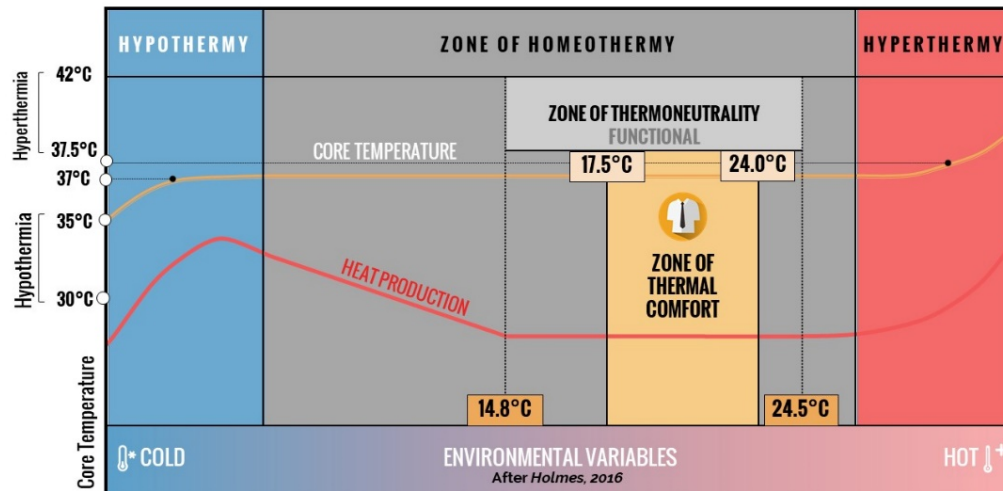
Figure 3-2: Homeothermy (adapted from (N. Lacetera, U. Bernabucci, H.H. Khalifa, 2003; Seth H. Holmes, 2016).

Heat stress occurs when the body fails to maintain heat balance. The three risk ranges presented in Figure 3-2 above show that by reaching a core temperature of 38°C, physical activity's capacity starts to decrease; at 39°C, the potentials of heatstroke and heat exhaustion are expected. When the core temperature reaches 40°C, it is considered a life-threatening stage (A. I. Barreca, 2012). Prolonged exposure to high temperatures indoors has significant adverse health effects due to the human body's extreme demand to regulate temperature, known as the body's thermoregulatory mechanism. Even though this process is highly efficient in regulating body temperature, the human body has difficulty disposing excess heat, causing heatstroke under extreme conditions. Most of the literature has concluded that the best approach to overcome indoor overheating is deploying air conditioning systems or other mechanical cooling systems. The optimum conditions for thermal comfort in hot weather have received less attention when it comes to dwellings with no access to air conditioning systems in the context of developing regions. In such areas, the provision of suitable indoor conditions is considered public health (M. S. Goromosov, Solomonovic, & World Health Organization, 1968; Kenny et al., 2017).

According to the IPCC report on climate change consequences (Edenhofer et al., 2014), around 30% of the global population is exposed to extreme heat for at least 20 days each year. And 2100 projections indicate that three out of four people every year will be under the risk of extreme temperatures considered deadly, including the most vulnerable populations. With growing risks from heat exposure, there is a need to explore how physiological responses to heat exposure can help identify different health risk levels. The following section focuses on the relationship between indoor heat exposure, thermal stress, and human health.

3.2.1 Indoor Microclimate, Thermal comfort, and Human Health

Climate is a catalyst that drives indoor thermal conditions and the climate-building interplay. Housing characteristics play a significant role in mitigating or exacerbating indoor heat exposure levels. Studies from the literature have identified building age, floor plan, roof albedo, insulation level, number of floors, and material thermal characteristics among the governing factors that drastically affect how buildings moderate heat exchange between outdoor and indoor environments (Alam, Sanjayan, Zou, Stewart, & Wilson, 2016; Keller, 2013). Also, numerous factors govern the relationship between heat exposure and human health in buildings. These factors can be divided into climatic factors (outdoor temperature, wind speed, solar radiation), building-related factors (material thermal properties, heat gain, and losses, availability of air-conditioning), and individual factors (clothing level, metabolic rate, and medical history) (Nicol & Humphreys, 2002). Also, heat stress is significantly affected by the individual preference of the surrounding environmental conditions such as humidity, air temperature, and air velocity (Kenny et al., 2018).

Another vital factor to consider is human acclimatization to heat, as people who were born and raised in regions with high temperature and humidity tend to have a higher tolerance to heat exposure compared to those living in colder climates (Tham, Thompson, Landeg, Murray, & Waite, 2020). The American Society of Heating, Refrigeration, and Conditioning Engineers (ASHRAE) standard 55 (2017) has defined thermal comfort as "The state of mind that expresses satisfaction with the thermal environment" with a thermal comfort range between **23°C to 28°C**. Given this global definition of comfort with the assumption of specific, a growing number of studies have developed various models to assess the range of thermal conditions indoors within which occupants will feel most comfortable (Luo et al., 2016). These studies revealed that building characteristics, including construction materials' thermal capacity, orientation, window properties, and surrounding urban context, play a crucial role in moderating indoor thermal conditions. However, fewer studies examined the threshold of indoor thermal conditions above which health risks can happen depending on body physiological response.

One of the early studies that examined the impact of various temperature thresholds on human health was conducted between 1951 and 1963 to establish optimum health standards for microclimates in dwellings in hot regions (Gromosov, 1963). The study examined the indoor temperature of 2834 air-conditioned apartments in 13 towns in Kazakhstan, Uzbekistan, and Turkmenistan, recording the physiological response of 6000 adults. The study's findings identified a threshold for room temperature corresponding to physiological risk levels, summarized in Table 3-1 below. Although this study's results are interesting to understand the impact of different temperature ranges on human health, it doesn't capture the relationship between exposure duration to different temperatures and physiological reactions.

Table 3-1: Human physiological response to various temperatures in an air-conditioned dwelling. (Adapted from (M. Goromosov & WHO, 1968)).

Physiological Response	Initial Levels [a]	Indoor temperature range (°C) [b]			
		24-25	26-28	30-31	33-34
Heart Rate (Beats per minute)	64	64-66	68	72	74
Mean Skin Temperature (C)	33	33.3	33.6	34.7	35.6
Respiration Rate (Breaths per minute)	16	18	18	20	22
Thermal Sensation	Comfortable	Comfortable	Warm	Hot	Hot & Oppressive

a. Initial levels indicate average physiological response in optimum indoor summer conditions early morning with a resting activity level.

b. Average recorded temperature from 106 observations on 27 adults. Average relative humidity 50%, mean outdoor temperature 35°C, and air movement ranges between 0.10 – 0.15 m/sec.

In Europe, Basu and Samet's study (2002) is one of the few that examines indoor temperature and physiological response for elderly residents. The study analyzed skin temperature and heart rate for 42 elderly adults simultaneously with ambient temperature in Baltimore, Maryland, in the USA, over a 48hour period. Results from the study revealed that there is a positive correlation between indoor ambient temperature and skin temperature. For every 0.56°C increase in ambient temperature, skin temperature increased by 0.08°C. In 2012, Kim et al. (2012) examined the impact of indoor conditions for low-income housing in South Korea. They concluded that increased air temperature negatively correlated with blood pressure in elderly residents and positively linked to increased body temperature. A recent study by Kenny et al. (2017) showed that elderly adults store 1.8 times more heat than younger counterparts at a temperature of 44°C.

The World Health Organization (WHO) has defined groups of populations that are more vulnerable to high and low temperatures than others (Ormandy & Ezratty, 2012). With such a definition, it has recommended an indoor temperature range between 18°C to 24°C that is associated with minimum health risks (M. Goromosov & WHO, 1968). However, the extent to which this range applies to the vulnerable population with no access to air conditioning systems remains in question. Another study in the Netherlands that examined the impact of high indoor temperature and sleep disturbance found an increase of 1°C of indoor air temperature in a range between 20.8°C to 29.4°C raised the risk of sleep disturbance at night by 24% (Loenhout et al., 2016). Concerning relative humidity, a case-controlled study in New York City in the United States reported a significant impact from humidity exposure and indoor air temperature above 26°C and increased cardiovascular emergency calls (C. K. Uejio et al., 2016). These studies presented a wide range of temperature thresholds and their potential impacts; however, the effect of exposure duration on human health remains limited.

3.3. Methods

Previous research on heat-health impacts was mainly founded around using ambient meteorological measurements to classify heat exposure. Recent studies have declared that this approach has resulted in a misidentification of potential health impacts from heat exposure (Wolkoff, 2018). For instance, dependence on meteorological measurements disregards the building's microclimate, varying significantly from municipal measurements. Also, a wide range of human adaptive measures can substantially influence the level of heat exposure indoors. As a result, it can either alleviate or exacerbate any potential health consequences. A recent study in Detroit, Michigan, has found that human adaptive behavior under heat exposure frequently occurs within a temperature range of (23.8 C–26.6 C) and is least common when the temperature exceeds 32.2C (White-Newsome et al., 2011). This implies the urgency to examine how high temperatures can influence the human body's thermoregulation process during heat stress. Also, these issues are crucial for the elderly population who may experience health problems like low blood pressure, high core temperature that is detrimentally impacted by dehydration as they usually tend to have increased sensitivity to heat exposure (A. A. Williams, Spengler, Catalano, Allen, & Cedeno-laurent, 2019).

High indoor temperature negatively affects human thermal comfort and wellbeing. The introduction section showed a gap in examining the relationship between indoor conditions and human health, especially for vulnerable population groups with limited mechanical cooling access. This section outlines the methodology framework for assessing indoor overheating and associated health-related impacts from heat exposure. A representative low-income urban area in Cairo, Egypt, is analyzed under current climatic conditions and the 2050 future climate scenario. The methodology framework is divided into four main components, as presented in Figure 3-3, and carried out through the following steps:

1. **Building Archetypes Classification**

Classification of different building types based on construction methods and envelope thermal properties: a series of site surveys were carried out between July and August 2018 to collect information on the building stock's physical characteristics, including information on construction methods, building age, and average population density. Also, findings from a study by The Aga Khan Trust for Culture rehabilitation project were used that covered the period between 2009-2013 (Aga Khan Trust for Culture (AKTC), 2005, 2013). There are three main archetypes identified in the study area from the site survey: a) historical buildings that date back from the 1700s and early 20th century, b) buildings from the late 20th century, and c) new construction.

2. **Indoor Monitoring and Calibration**

Quantification of the impact of increased air temperature on overheating hours indoors: fifteen subclasses of the historical buildings' archetypes, one building from the late 20 century, and one representative type from new construction are modeled with respect to the surrounding urban context and calibrated for annual overheating simulation. Onset Hobo data loggers were installed in the developed archetypes from July 6th to July 12th and August 8th to August 15th. Indoor temperature and relative humidity readings are used to analyze indoor climatic conditions and validate simulation results. The accuracy of the temperature loggers used was ±0.21°C from 0° to 50°C, Relative Humidity accuracy: ±2% from 20% to 80% typical to a maximum of ±4.5%; below 20% and above 80% ±6% typical). All loggers were placed in the

zones with sufficient air movement and away from internal heat sources and solar radiation. The outdoor air temperature was collected from the nearest weather station, located 4.9 km away from the analysis area. Outdoor temperature readings indicated high temperatures from July 7th until July 12[th,] 2018. Indoor wind speed samples were measured in 20 representative buildings without ceiling fans, indicating a low indoor air movement with an average indoor wind speed across the 20 samples of 0.2 m/s and between ~0.2 – 0.5 m/s at the urban canyon level. Samples were taken at 8 pm to examine if natural ventilation would impact indoor cooling potentials. The calibrated archetypes were then used to develop a building template inside UMI to quantify the study area's overall indoor overheating. Simulations are carried out in Grasshopper Honeybee and EnergyPlus using the Egyptian Typical Meteorological Year weather file (ETMY) covering 12 to 21 years and ending in 2003. The temperature threshold is presented as the operative temperature above the ASHRAE comfort range of 26.9°C (American Society of Heating & Conditioning Engineers (ASHRAE), 2017). All buildings were examined solely on natural ventilation (average Hourly Air Change Rate (ACH) 0.5) and no mechanical ventilation system access.

3. Indoor Overheating Assessment

Quantification of overheating impacts across different archetypes: a simulation model of the study area was developed in the Urban Modelling Interface Rhino plugin (UMI) using the building template developed in step 2. UMI is an urban performance simulation model developed by the Sustainable Design Lab at the Massachusetts Institute of Technology (Reinhart, Dogan, Jakubiec, Rakha, & Sang, 2013). UMI is urban energy modeling and simulation engine using Rhinoceros (McNeel, 2021) as the modeling interface and EnergyPlus for building by building simulations. It is also linked to Urban Weather Generator (UWG) developed by Bueno, Norford, Hidalgo & Pigeon (2013) to account for the hourly urban heat island effect. UMI offers an integrated urban simulation capability, including operational energy use, overheating, daylighting, embodied carbon emission, and walkability over neighborhood scale. The simulation module integrates the EnergyPlus engine and Radiance. A building template containing information on construction material thermal properties, glazing ratio, occupancy schedule, equipment loads, ventilation schedule, and occupancy density was developed inside UMI for AlDarb Al Ahmar. A total area of 2.8 acres was modeled and simulated for hourly indoor operative temperature from January 1st to December 31st.

Examination of Future climate Scenarios: 2050 IPCC A2 scenarios (IPCC, 2014b). Climate Change Weather generator tool developed by the sustainable energy research group at Southampton University (Jentsch, James, Bourikas, & Bahaj, 2013) is used for morphing 2050 weather files under the A2 scenario.

4. Exposure Threshold Assessment

Identification of current users' adaptation strategies under extreme heat exposure: 300 personal interviews were carried out to collect information on types of behavioral adaptation adjustments, typical clothing levels, ventilation times, equipment types, income level, health conditions, and types of environmental control systems. The interviews' data was also used to calibrate the simulation model by incorporating a suitable occupancy schedule and equipment load estimation.

Analyzing the effect of prolonged heat exposure on health risks: To assess potential health impacts, Heart Rate (HR) was considered as a physiological indicator for potential risk associated with heat

exposure (Zamanian et al., 2017). Other indices that reflect physiological response under heat exposure include skin temperature, core temperature, sweat rate, and dehydration risks (Holmes, Phillips, & Wilson, 2016a; Parsons & Kenneth, 2011). Ren et al. (2011) examined the effect of apparent temperature and HR variability across the elderly population. The study's findings suggested a strong association between high temperature and HR variability that may affect cardiovascular function. Williams et al. (2019) have recently examined the impact of high indoor temperature on human health in dwelling in the U.S. through examining HR variability with air temperature. The study showed that indoor air temperature above the 24°C threshold caused significant decrements in the HR of examined occupants. The study also concluded that monitoring maximum hourly indoor climate can be a strong predictor of mean hourly heart variability, indicating potential heat-health impacts. This research examines the relationship between indoor air temperature and HR through personal monitoring for 12 participants living in AlDarb AlAhmar between the 15th and 18th of July. The age structure of the population in AlDarb AlAhmar consists of 19% between the age range of 50 to 60 years, 23% > 60 years, 23% 40 to 50 years, 23% 30 to 40 years, 16% 20 to 30 years, and 3% less than 20 years (Aga Khan Foundation, 2013). The personal monitoring group's age distribution represents the population average age in AlDarb AlAhmar, with 50% of the sample between 40 to > 60 years old.
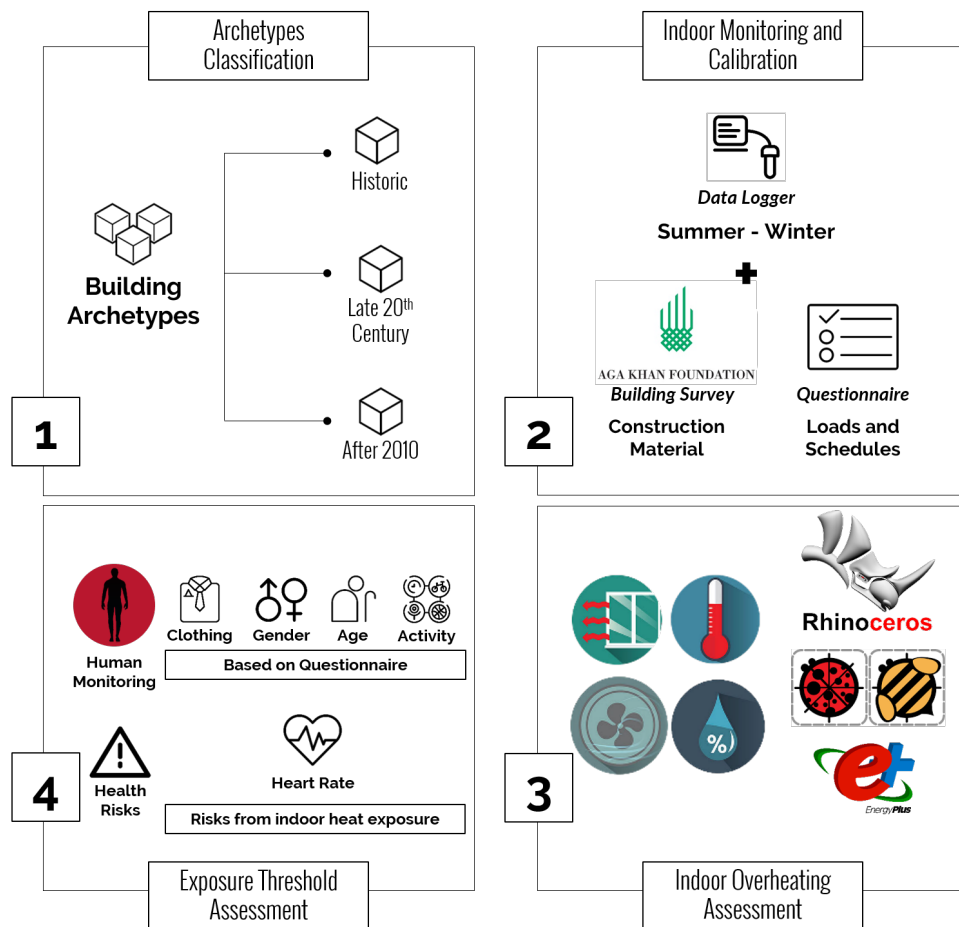

Figure 3-3: Analysis framework and methods used.

3.3.1 The case of Al Darb Al Ahmar in Cairo

Cairo is the most populated city (metro area population: 9,533,040) in Egypt, with an overall climate characterized as hot arid (Köppen classification: BWh) with high solar radiation most of the year (SODA SRD, 2020). The mean maximum temperature in Cairo ranges between 25°C to 30°C over the summer (from June to August), with a maximum relative humidity of 57% (Robaa, 2013). Over the past decade, Cairo has witnessed a series of heatwave events. The most extreme incidents were reported back in 2015 when air temperature reached 47°C causing a total death toll of 106 across Egypt (AP, 2015; The Guardian, 2015b). Most of the heat-related deaths reported were from the elderly population living in low-income neighborhoods or informal settlements (BBC, 2015a; The Guardian, 2015a). These populations are most affected by extreme heat exposure due to low-income levels and limited access to air-conditioning units. An additional factor contributing to increased thermal risk during heat exposure is the loss of power supply, especially during summer months, as people may experience power loss for some cases that could go above five consecutive hours (Fahim & Thomas, 2014; Reuters, 2014).

Under these conditions, Al Darb AlAhmar, a low-income neighborhood in Cairo, was chosen to conduct the assessment. Al Darb Al Ahmar is a district in Islamic Old Cairo with a total area of 315 acres (1.3 km2) that contains more than 114 historical Islamic monuments (Aga Khan Foundation, 2013). The area accommodates low-income families living in deteriorating housing conditions with limited access to community facilities and urban services. The area has a mix of unique historical buildings from the 1700s and early 20th century (Aga Khan Foundation, 2013). The rich historical context of Al Darb AlAhmar has been threatened by the continuous demolition of the historic buildings and the construction of new high-rise buildings that were recently built between 2010-2014 (Figure 3-4).
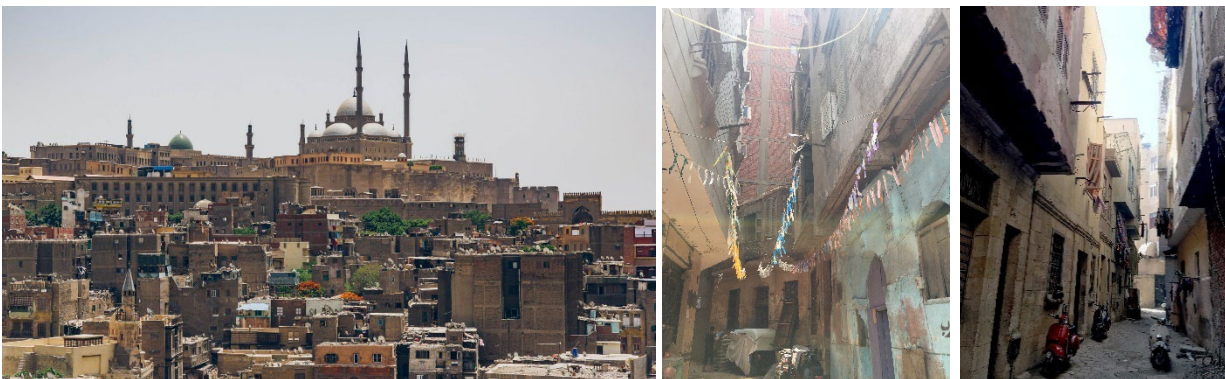
Figure 3-4: Left, Aerial view of Al Darb AlAhmar neighborhood, Right, street view for Atfet Assad (Author, 2019).

The total studied area is 2.8 acres, and it was specially selected for its unique architectural character and diversity of building types, and economic challenges. Living standards are primarily considered for low-income, where air conditioning units are not typical and rarely installed. Ceiling fans and portable fans are the most common apparatus used for ventilation.

3.3.2 Building Archetypes

There are eight main archetypes identified from the site survey. The characteristics of envelopes' thermal properties vary with construction methods into three main categories: historic, late 20th century, and new construction built after 2010. Historical buildings represent 73% of the existing stock in the study area, the late 20 century archetypes account for 11%, and new construction represents 16%, with a floor average area floor area ratio (F.A.R) is 1.0. Figure 3-5 illustrates the study area with the distribution of the three main archetypes identified from the survey and literature.
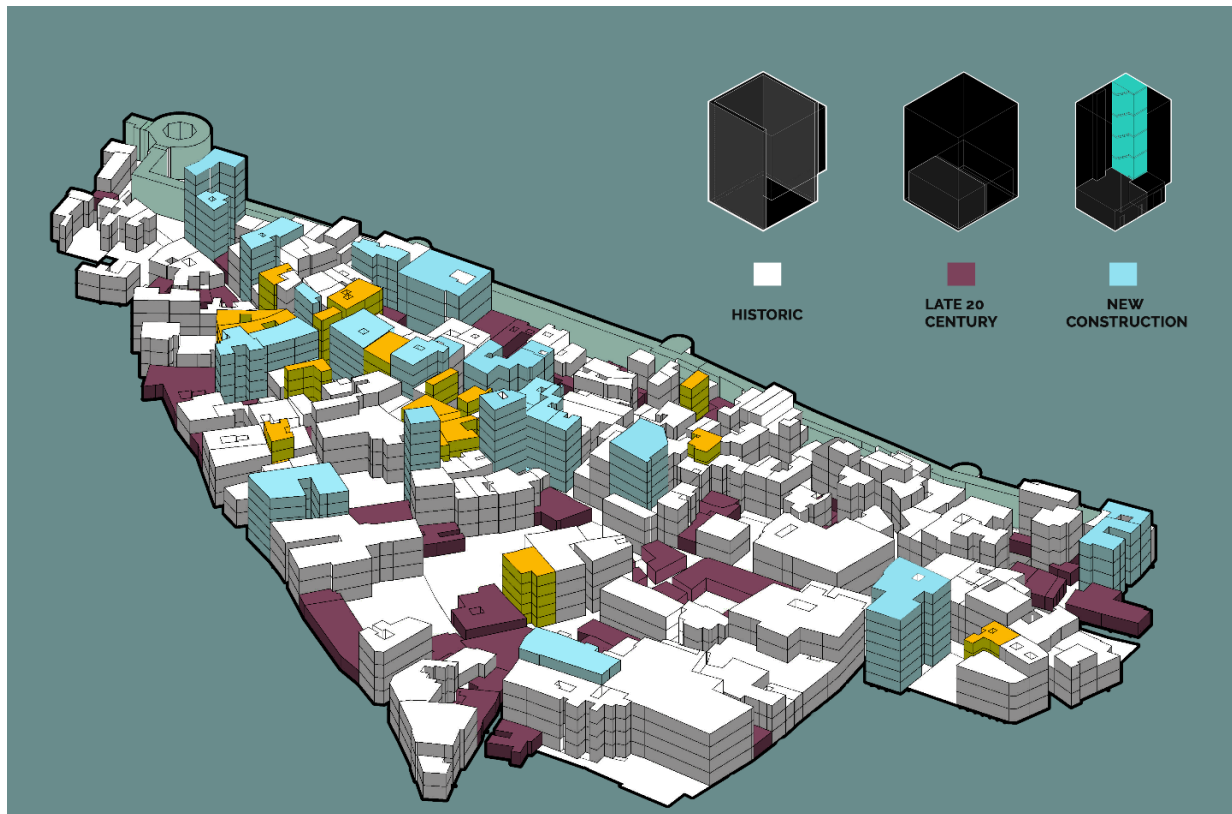
Figure 3-5: Archetypes distribution in the study area.

The main construction in a historic building is a mix of buildings that date back to the 17th century to the late 19th century. The original structure is a load-bearing stone wall, with the ground floor built of 60 cm walls consisting of 20X40 cm limestone and one layer of 6x20 cm red brick. The added story is constructed of 25 cm of red brick for the 2-floor building, and the third and fourth floors are recessed from the façade usually and built of 20 cm red brick and a wooden roof. Archetypes from the late 20th century and informal are mainly reinforced concrete and beam structures, with the external wall of thick red brick without insulation with a thickness of 25 cm. In comparison, new construction has a wall thickness of 12.5 cm of red brick with no wall insulation (Figure 3-6).

| Historic | Late 20 Century | New Construction |

Figure 3-6: Archetypes classification in the study area based on construction method and number of floors. (Source: Author).

The characteristics of building envelopes in each archetype were identified based on-site survey and Attia's database for Egypt's construction materials (Attia & Wanas, 2012). Table 3-2 below summarizes the building envelope's characteristics in each archetype.

Table 3-2: Envelope thermal properties for the different archetypes.

Archetype		Opaque Wall	Wall Thickness (cm)	Specific Heat (J/kg-k)	Thermal Conductivity (W/m-k)
Historic	One floor	Limestone	40	720	1.5
	Two floors		60		
	Three floors		80		
	Four floors		120		
Late 20th Century (5 floors)		Brick wall	25	921	1.31
New Construction (6-10 floors)			12.5		

The residence's floor area examined in the study ranged between 30 m^2 and 100 m^2, with an average area of 80 m^2. Onset Hobo data loggers were installed in 15 representative archetypes from July 6th to July 12th and August 8th to August 15th. Indoor temperature and relative humidity readings are used to analyze indoor climatic conditions and validate simulation results. The accuracy of the temperature loggers used was ± 0.21°C. All loggers were placed in the zones with sufficient air movement and away from internal heat sources and solar radiation. The outdoor air temperature readings were collected from the nearest weather station, located 4.9 km away from the analysis area. Outdoor temperature readings indicate high temperatures from July 7th until July 12th, 2018. The three archetypes presented above are used as representative models for residential buildings in the study area. The study was limited with accurate information on the historic archetypes due to various modifications over the years for glazing. Therefore, using findings from the site survey, most windows are single-glazed and assumed to be 0.003 m thickness glass pane. The glazing ratio varied across the three types, but the overall window-to-wall rate ranged between 15% to 45% of the total wall area. The details of each archetypes' material characteristics are summarized in Table 3-3 below.

Table 3-3: Building material characteristics.

	Historical			Late 20th Century	Informal (after 2010)
	2F	*3F*	*4F*		
Average Built-up area	150 m2			*250*	*350*
WWR	15%			45%	46%
Glazing U-Value	6.25			6.25	6.25
Wall U-Value (W/m2 K)	0.5	0.5	0.6	1.7	2.8
Thermal Admittance (W/m2 K)	4.2	4.2	4.2	7.5	9.5
Internal Heat Capacity	75	73	72	81	82
External Heat Capacity	62	60	59	113	144
Roof U-Value (W/m2 K)	1.39			1.5	1.5
Solar Heat Gain Coefficient (SHGC)	0.5			0.5	0.5

3.3.3 Urban Typologies

AlDarb AlAhmar is part of the old Islamic Cairo urban fabric bounded by multiple historical gates dating back to the Ayubid and Fatimid eras. However, the district has been maimed by inappropriate development practices, causing irreversible large tracts that lack the original urban fabric definition (UNESCO, 2012). The urban fabric in Al Darb AlAhmar exemplifies some original features from the Islamic city's hierarchy of open spaces, yet, the continuous demolition of historic buildings and new construction have interrupted the actual urban fabric's unity. However, the unique feature of the urban fabric in Al Darb AlAhmar is the small scale of the street spaces and their hierarchy that have maintained their toponymy since the late 19th century.

There are four types of street patterns that exemplify the hierarchy and the physical urban characteristics of Al Darb AlAhmar: Darb (pathway which usually has a width between 5-4 m), Hara (Alley with an average width of 4-3 m), Atfa (Side alley with an average width of 3-2.5 m), and Zuqaq (dead-end alley with width between 2-1.5 m) (Arnaud & Depaule, 2020; UNESCO, 2012). The area is characterized by a very dense, compact urban fabric with irregular streets consisting of two- to four-story buildings mostly built on small plots (UNESCO, 2012; C. Williams, 2002). Other residential buildings that are not considered monumental or traditional buildings from the old Islamic city are five- to ten-story buildings scattered around the area and mostly built on large land plots (Elkatsha, 2000).

The urban development over time in Al Darb AlAhmar has influenced the urban morphology, the texture of the built-up fabric, and the compactness level. Three main patterns were identified (Figure 3-7) that represent the structure of the urban typology in the study area: i) original historic fabric, which is characterized by a high level of compactness and continuity in the urban fabric with building heights around two- to four-story buildings and the presence of empty plots and old buildings' ruins, ii) mixed urban fabric between traditional historic buildings and buildings that date back to the early 20th century built on large plots with inconsistent architectural style ranging between four- to five-story buildings, and iii) new urban fabric dominated with new constructions that have significantly increased since the January 25th revolution due to lack of limited governmental capacity to monitor property ownership and construction guidelines. These buildings are characterized by inadequate construction patterns, poor

architectural style ranging from five- to ten-story buildings built on large square plots. Despite the variation between the three urban types discussed previously, the urban fabric preserves its original character but with widespread physical degradation and inconsistent redevelopment interventions.

| Original historic fabric (Atfa) | Mixed/ modified urban fabric (Darb) | New urban fabric (Hara) |
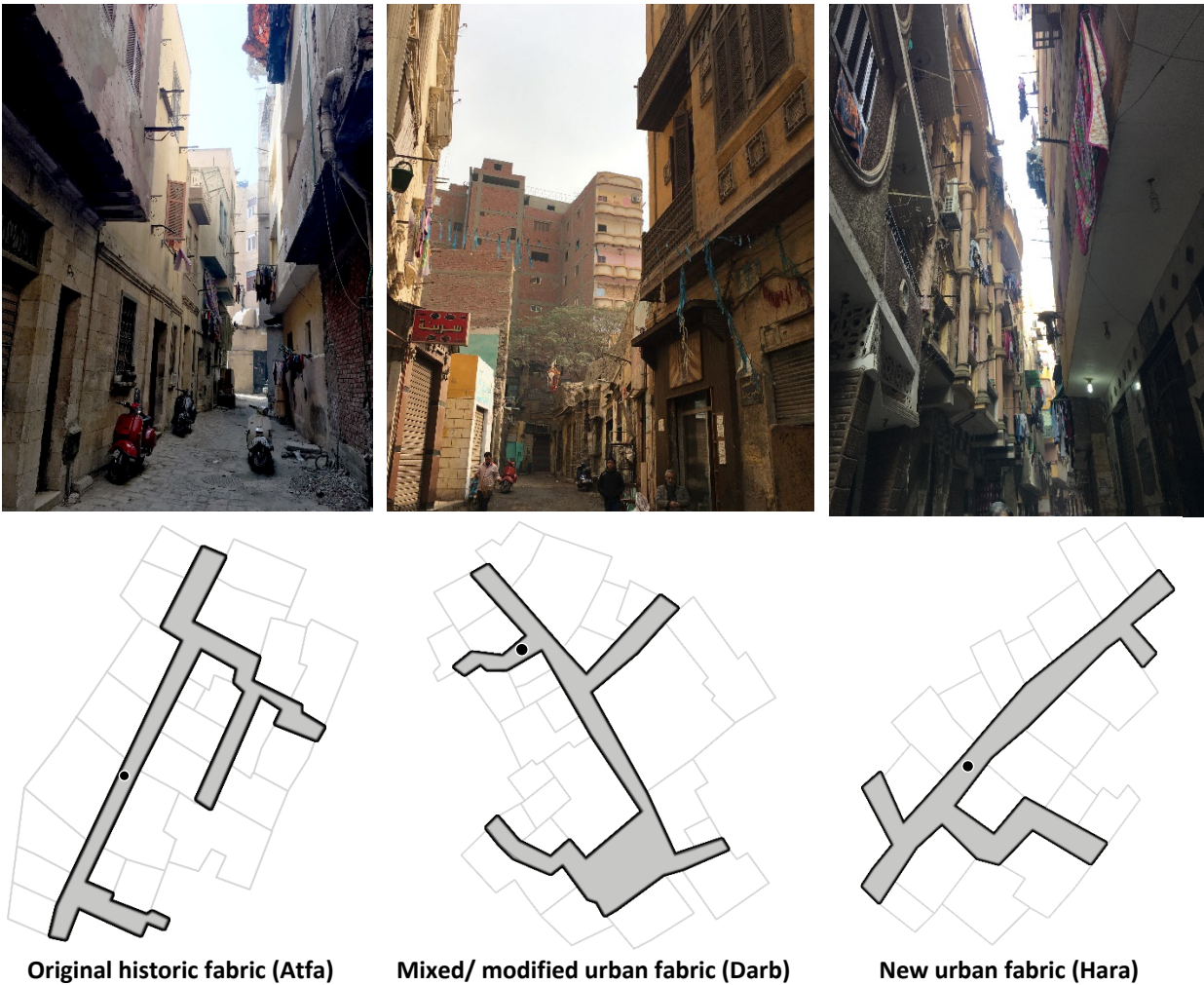
Figure 3-7: Three urban typologies identified in Al Darb AlAhmar and associated street type. (Source: Author).

From the general assessment using studies from the literature and site surveys, 12 urban block typologies were identified under the three main urban fabric patterns discussed above in Al Darb AlAhmar. The research considered building type, height, and street width as the primary identifying parameters of each typology and an area of 500 meters as the boundary for the urban block typology. Figure 3-8 summarizes the urban typologies identified in Al Darb AlAhmar district and associated building type, urban density, street width, and urban patterns.

Historic Zuqaq

Urban Fabric: Historic
Street type: Zuqaq
Building Type: Historical (2-4F)
Plot Size: 60-80 m

Historic Atfa

Urban Fabric: Historic
Street type: Atfa
Building Type: Historical (2-4F)
Plot Size: 50-100 m

Historic Hara

Urban Fabric: Historic
Street type: Hara
Building Type: Historical (3-4F)
Plot Size: 50-100 m

Historic Darb

Urban Fabric: Historic
Street type: Darb
Building Type: Historical (3-4F)
Plot Size: 80-100 m

Mixed Zuqaq

Urban Fabric: Mixed
Street type: Zuqaq
Building Type: Mixed (3-5F)
Plot Size: 80-120 m

Mixed Atfa

Urban Fabric: Mixed
Street type: Atfa
Building Type: Mixed (4-5F)
Plot Size: 60-120 m

Mixed Hara

Urban Fabric: Mixed
Street type: Hara
Building Type: Mixed (4-5F)
Plot Size: 80-150 m
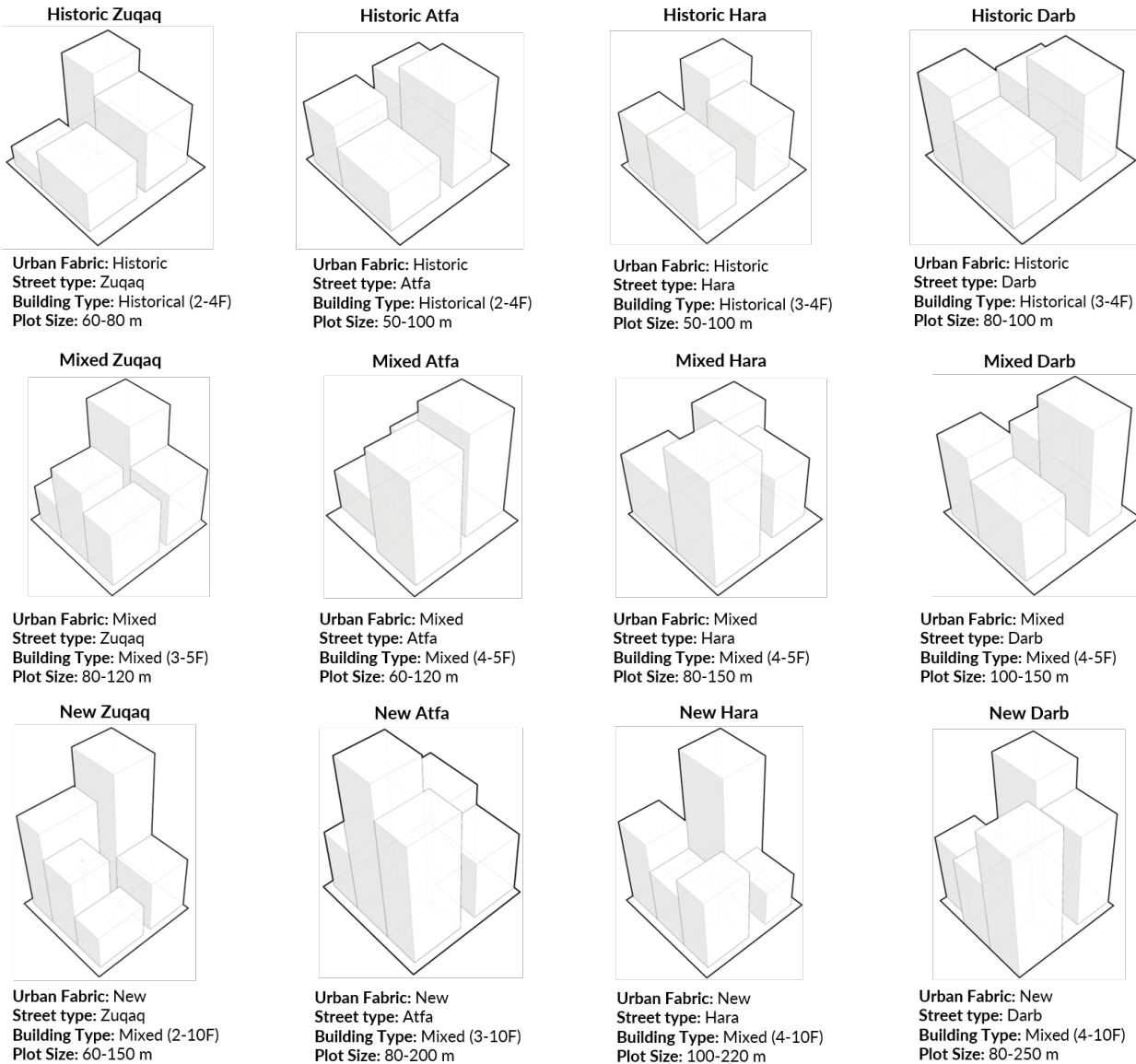
Mixed Darb

Urban Fabric: Mixed
Street type: Darb
Building Type: Mixed (4-5F)
Plot Size: 100-150 m

New Zuqaq

Urban Fabric: New
Street type: Zuqaq
Building Type: Mixed (2-10F)
Plot Size: 60-150 m

New Atfa

Urban Fabric: New
Street type: Atfa
Building Type: Mixed (3-10F)
Plot Size: 80-200 m

New Hara

Urban Fabric: New
Street type: Hara
Building Type: Mixed (4-10F)
Plot Size: 100-220 m

New Darb

Urban Fabric: New
Street type: Darb
Building Type: Mixed (4-10F)
Plot Size: 80-250 m

Figure 3-8: Urban typologies in Al Darb AlAhmar. (Source: Author).

In addition to the urban fabric changes, available open space has been reduced significantly, as illustrated in Figure 3-9 below. The map from 1930 shows the distribution of historical buildings with courtyards and open spaces that have either disappeared or been modified until 2019. The most significant difference is Al Azhar Park's addition, which was introduced in 2005 to provide the residents with outdoor cooling opportunities to counterbalance the changes in the open space network's original structure. Although Al Azhar park can provide Al Darb AlAhmar residents with a significant cooling outlet, the park is only accessible for free between 12 pm to 4 pm, limiting the residents' ability to use it as an adaptive capacity resource during extreme heat exposure.
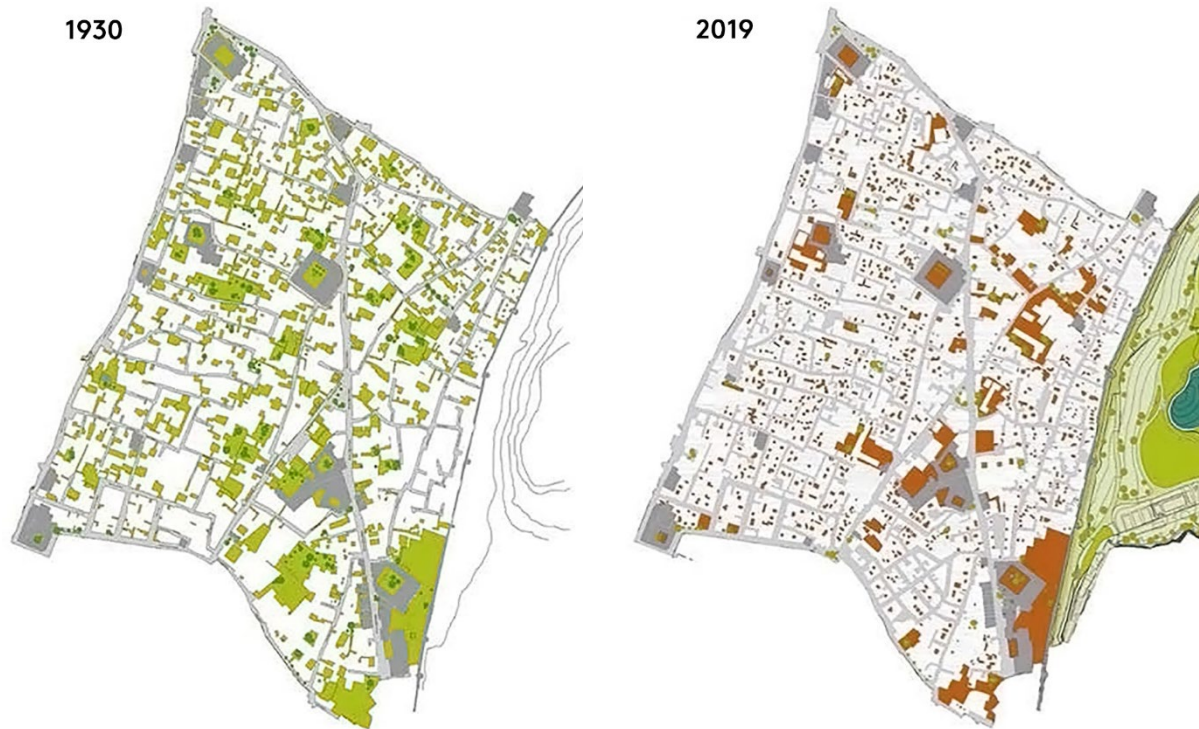
Figure 3-9: Urban fabric and open spaces development in Al Darb AlAhmar between 1930 and 2019. (Ramírez & El Habashi, 2020).

3.3.4 Human Adaptive Capacity

To define how do the occupants react to heat exposure, a survey for 300 residents was developed to understand types of heat adaption behaviors, both indoor (using ceiling fans, opening windows, or using window blinds) and outdoor (going to Al Azhar park, sitting in front of the house, or sitting on top of the roof) derived from site observations. Also, demographic information (age, sex), socioeconomic (average monthly income), and years living in AlDarb Al Ahmar (Table 3-4). The survey included information about average occupancy rates, type of equipment, and occupancy and ventilation schedule.

Table 3-4: Summary of the survey subjects of residential occupants in the study area.

Sample size	300
Gender (% of the sample)	
Male	(132) – 44%
Female	(168) - 56%
Mean Age	**48**
Minimum age – Maximum age	(21 – 93)
Average years living in the neighborhood	**15 years**
Minimum year lived – Maximum year lived	Two years – 60 years
Average monthly income	**50$/month**
Minimum income – Maximum income	5$ - 150$

The site survey indicated an average occupancy density between 4-6 persons per apartment. Therefore, the average occupancy density per apartment was assumed to be five people per apartment. Also, it has

been found that 20% of the survey are between 60 and 80 years old, with 42% living alone. In addition, most low-income residents for income ranging between 5$ - 50$/m had a high percentage of elderly and infants compared to relatively higher income (> 50$/m). The survey also covered indoor thermal comfort response at different periods of the day; early morning 8:00 am to 10:00 am, afternoon 12:00 pm to 2:00 pm, and evening 6:00 pm to 8:00 pm. Thermal comfort questions were developed using ASHRAE thermal sensation vote (TSV) (American Society of Heating & Conditioning Engineers (ASHRAE), 2017) scale of +3 for (hot) to -3 for (cold) for the total 300 residents, made up of 168 females (56%) and 132 males (44%). The sample was chosen to represent the actual population structure in AlDarb Al Ahmar. The survey indicated a significant dependence on fans and ceiling fans for cooling, implying a low airspeed in this dense urban fabric, limiting natural ventilation's potentials. Occupancy, ventilation, and lighting load information from the survey were used to develop simulation models. Equipment loads and lighting density were assumed based on a local study (Attia, Evrard, & Gratia, 2012) that developed a representative energy simulation database for building stocks in Egypt. Infiltration rates were equal to 0.5 air changes per hour (ACH), assuming that most buildings have relatively low airtightness.

3.3.5 Heat Exposure Threshold

The research focuses on the potential health impacts of increased temperature to understand the expected increase in overheating hours across different archetypes. A group of 18 low-income residents who participated in the survey, living in the study area, specifically in three different historic buildings with no access to AC units, participated in a personal monitoring assessment experiment to examine the impact of elevated indoor air temperature on human health. The first building (Building A) was a three-story historic building, a four-story historic (B) both from the late 18th century, and 8-floor new construction (C). All residents live in a top-floor apartment, and buildings are situated in a historic urban fabric with hara as the street type. The assessment took place between July 15 to July 18th, utilizing Onset Hobo data loggers to record indoor air temperature and relative humidity levels during the personal monitoring. Participants were asked to report times where they went outside to exclude these datasets from the analysis. Participants were also asked to record their thermal experience at three times of the day: early morning 8:00 am to 10:00 am, afternoon 12:00 pm to 2:00 pm, and evening 6:00 pm to 8:00 pm using the ASHRAE thermal comfort scale of +3 for (hot) to -3 for (cold). Participants were asked to wear a Fitbit Wireless activity tracker watch to monitor HR in beats per minute (bpm) with indoor air temperature. Participants were also instructed to wear it at all times except during bathing. Before conducting the assessment, a summary of the study scope and protocol was verbally explained to all consented participants through a series of personal meetings at each building. The participant group consisted of a balanced mix of age and gender. To examine the effect of limited access to mechanical cooling, the selection criteria were based on elderly participants living alone above 55 years old or residents and younger residents in the lowest income category. One participant had a pre-health condition of a heart problem across the selected sample and was younger than 55 years old. Table 3-5 summarizes the characteristics of the selected group of participants, including demographic information, medical history, and environmental conditions.

Table 3-5: Characteristics of the participants and environmental conditions.

	Building (A)	Building (B)	Building (C)
Number of participants	*6*	*6*	*6*
Sex, n (%) male	*(3) 50%*	*(3) 50%*	*(3) 50%*
Sex, n (%) female	*(3) 50%*	*(3) 50%*	*(3) 50%*
Age, n (%) < 55 years old	*(4) 75%*	*(2) 25%*	*(3) 50%*
Age, n (%) > 55 years old	*(2) 25%*	*(4) 75%*	*(3) 50%*
Ever smoker, n (%)	*0*	*(2) 25%*	*0%*
Pre-existing medical diagnosis Heart disease	*0*	*0*	*25%*
Temperature, mean (SD)	*32.18 (0.50)*	*32.0 (1.51)*	*32.72 (0.73)*
Relative Humidity (SD)	*52.65 (2.90)*	*51.5 (9.29)*	*47.14 (6.92)*

A statistical model was developed in Python to examine the relationship between indoor air temperature and HR. HR data and indoor air temperature were statistically analyzed through the following steps:

1- To assess the frequency in which the HR value changes with air temperature, data was cleaned and organized by the mean number of readings per hour. Mean hourly readings are calculated by splitting the data into subsets; each subset represents an hour. For instance, if one hour has n readings, this means that there will be multiple subsets in the form: {0:n}, {1,n+1},…,{i,n+i} where i is an integer ranging from 0 to the number of readings. Next, the mean of heart rate and the indoor air temperature of each subset is computed, and each subgroup will represent a coordinate point (temperature, HR). To reduce noise in data, a savgol filter (Gallagher, 2013) is applied in Python as part of the analysis algorithm.

2- The relationship between indoor air temperature and HR was modeled in Python as a Poisson model, where mean hourly HR is viewed as a dependent variable and maximum hourly air temperature as an independent variable. The analysis revealed a positive correlation between maximum hourly indoor air temperature and mean hourly HR per minute (R^2= 0.85, p < 0.001).

3- To identify the indoor air temperature threshold that can potentially pose a risk to human health, a threshold of 93 bpm for males and 95 bpm for women was determined as the risk limit (Palatini & Julius, 1999; Peer, Lombard, Steyn, & Levitt, 2020). The model objective function was set to output the indoor air temperature at which HR exceeds the risk limit referred to as "**Risk Threshold**" and the number of ascending sequences of hourly readings that preceded the risk limit, referred to as "**Exposure range**."

3.4 Results

This section presents the simulation model results for different archetypes described above; indoor overheating, human adaptive capacity during under heat exposure, and potential impacts on human health are presented.

3.4.1 Indoor Overheating Assessment

Figure 3-10 shows the simulated indoor air temperature and recorded air measurements. Information from the site's surveys was used to calibrate the simulation model with actual conditions. The mean square root error decreased substantially after adding survey data. All these data were arranged by archetype and added to the simulation model.
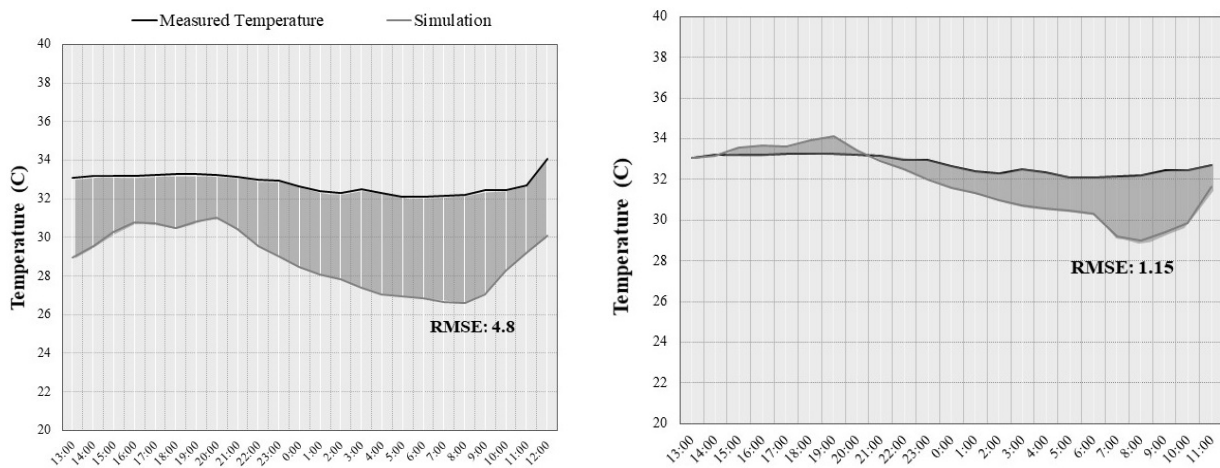

a. Initial simulation results before integrating data on occupancy schedules and lighting and equipment loads

b. Simulation results after calibration with site data and personal occupancy survey

Figure 3-10: Simulation results for indoor air temperature and recorded summer measurements.

Overheating simulation results indicate that most overheating hours occur between June and October, with a higher frequency between July and August, as presented in Figure 3-11-a below. The daily distribution shows that during the summer months from May to September, most of the overheating hours occur in the nighttime from 11 pm to 6 am (Figure 3-11-b). The large concentration of overheating hours in nighttime poses threats related to potential disruptive sleep from increased temperature. It can also be noted that indoor thermal conditions far exceed the overheating criteria set by the Chartered Institute of Building Service Engineers (CIBSE), which is no more than 5% of the occupied time (CIBSE, 2017). This section examines the differences between the three main archetypes presented above and the impact of the surrounding urban fabric by comparing different urban typologies and street types. Simulations were developed for the extreme hot week to represent potential high indoor temperature under which occupants are exposed, between August 19th to August 25th.
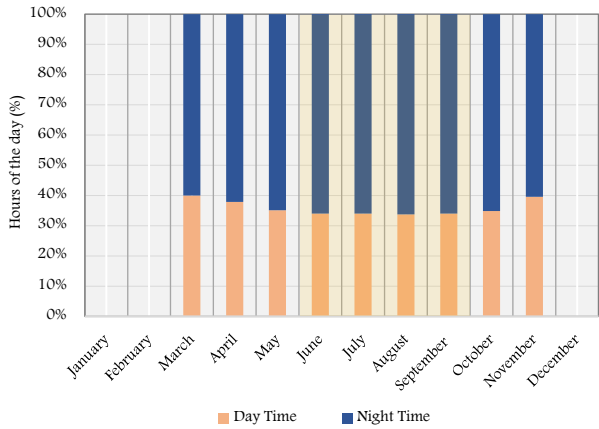
a. Annual overheating simulation and monthly distribution
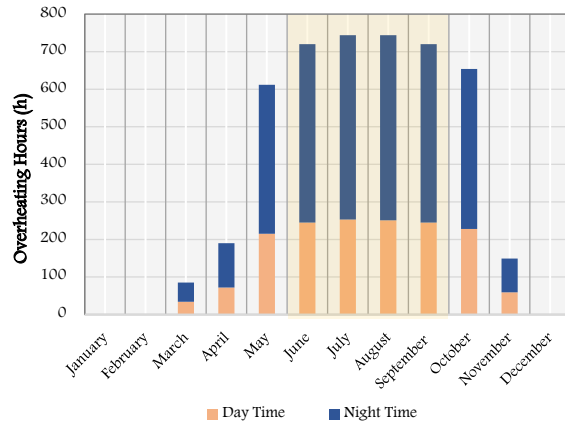
b. Daily distribution of overheating hours. Daytime represents the time from 6 am to 11 pm, and Nightime represents 11 pm to 6 am.

Figure 3-11: Overheating monthly and daily simulation results for a representative historic building.

Operative temperature simulations for a typical summer week and an extreme hot week shows that higher floors have higher average operative temperature than lower floors. Hourly operative temperature simulation for July revealed that during the first three days of the month, temperature exceeds a monthly average of 32.8°C, as presented in Figure 3-12-a.
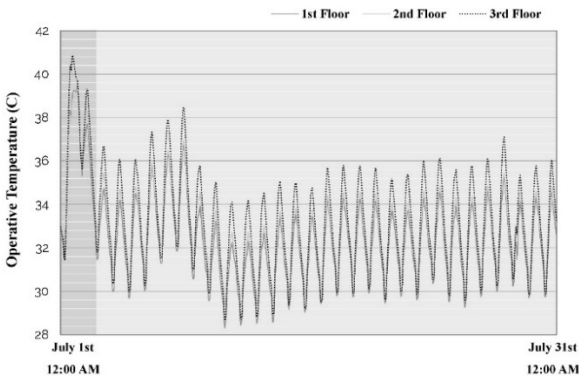
a. Hourly Operative temperature for July. The highlighted region represents the highest observed operative temperature above the monthly average from July 1st to July 3rd.
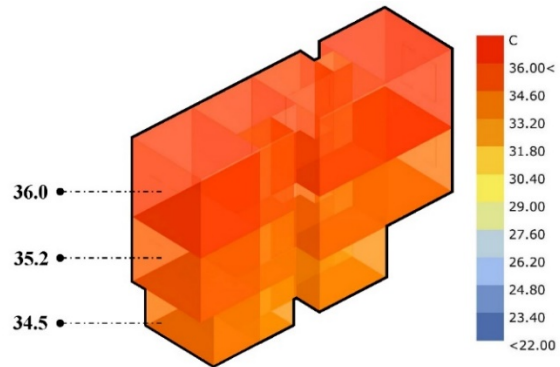
b. Average hourly operative temperature for an extreme hot week (19th to 25th of August).

Figure 3-12: a. Hourly operative temperature for each floor in July, b. Operative temperature for the extreme hot week.

The three main archetypes discussed above were examined against each other to understand the differences in indoor conditions. Figure 3-13 shows indoor air temperature in a roof floor apartment for a historical building of four floors, a 20th-century building of four floors, and new construction of eight floors located in the historic urban fabric typology with Hara street type during an extreme hot week. Each boxplot in this Figure contains each archetype's hourly indoor air temperature (168 points for each), indicating a lower range of indoor air temperature in the historical archetype located in the historic fabric compared to 20th century and new construction. The survey provided additional insights on indoor

conditions range where participants reported thermal discomfort. Around 87% of the participants reported an indoor air temperature of 31°C as the threshold where they started to feel thermal discomfort. As shown in Figure 3-13 below, the thermal discomfort threshold reported by the participants is at the 10th percentile of the hourly simulation in all three archetypes.
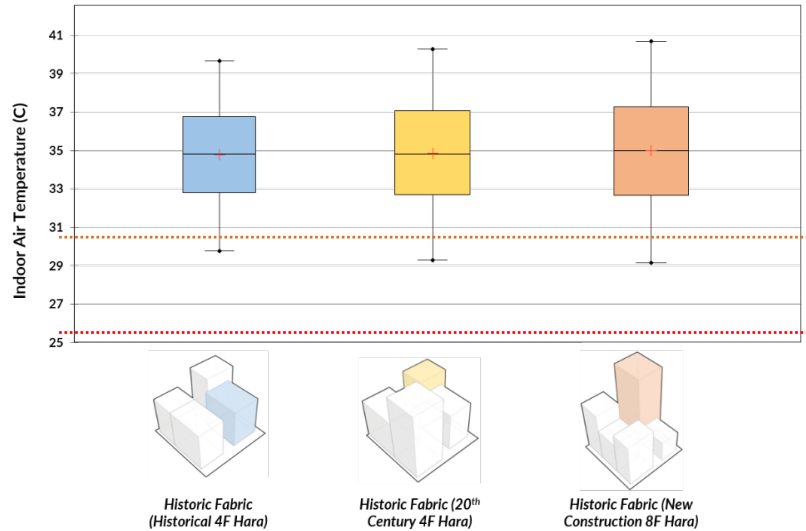

Figure 3-13: Indoor air temperature for an extreme hot week. Each boxplot in this figure contains hourly operative temperature data for the three archetypes historical building of four floors, 20th century of four floors, and new construction of eight floors in historic fabric urban block type and Hara as a street type. The dashed red line represents the operative temperature threshold of 26.9°C according to ASHRAE Standards, and the dashed orange line represents the reported threshold when they felt thermal discomfort from the survey at 31°C.

Figure 3-14 shows the cumulative distribution of indoor air temperature in a roof floor apartment for the three main archetypes in the same urban block typology (historical urban fabric with Hara type) for an extreme hot week. The vertical axis represents the cumulative fraction of hours at or below specific indoor air temperature. For instance, the dashed vertical black line represents the thermal discomfort threshold reported by the participants from the survey; in the new construction archetype (Figure 3-14-c), the curve shows 0.1 at an indoor air temperature of 31°C means that indoor air temperature for this archetype that is below 31°C represents 10% of the time.

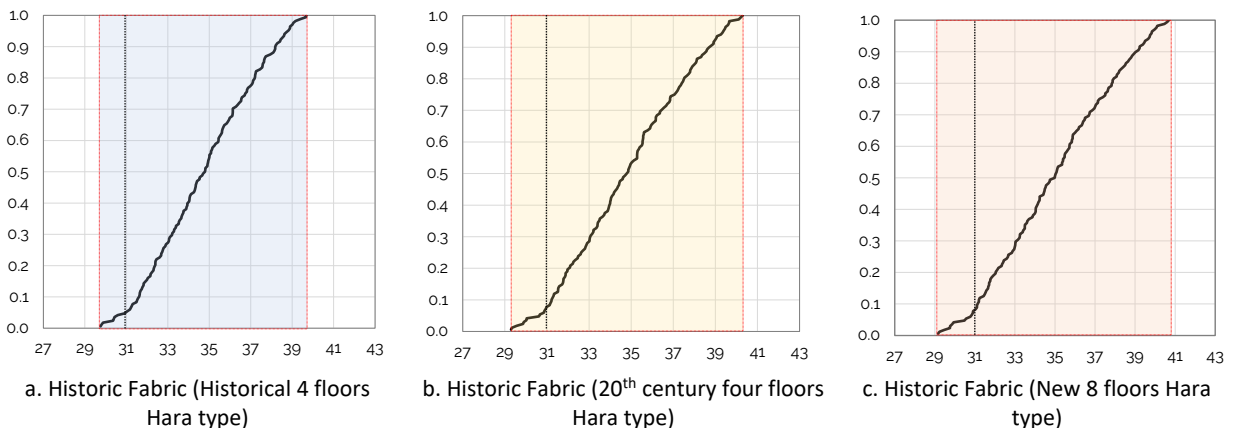| a. Historic Fabric (Historical 4 floors Hara type) | b. Historic Fabric (20th century four floors Hara type) | c. Historic Fabric (New 8 floors Hara type) |

Figure 3-14: Distribution of hourly indoor air temperature in three archetypes: Historical four floors, 20th century four floors, and new construction eight floors. The dashed vertical black line shows the threshold temperature when occupants reported thermal discomfort at 31°C.

Next, the impacts of surrounding urban typology are examined. The research compares the indoor operative temperature for a historical building of four floors in three different urban typologies: historic fabric, mixed fabric, and new urban fabric with Zuqaq as the street type. Figure 3-15 shows that mixed and new urban fabric has a slightly higher indoor operative temperature range for a roof floor apartment than a historic urban fabric. The average operative temperature is 35°C for the historic fabric, 36°C for the new urban fabric with a difference by one degree, and the average maximum operative temperature is around 40°C. This can be explained by the characteristics of the surrounding buildings as new construction buildings' height range from 6 to10 floors that may influence wind speed at the urban canyon level, temperature change, and heat loss from low-rise historical buildings. The clustering of tall buildings in a dense urban fabric with narrow streets can also induce heat-trapping and reduce the potential for indoor heat to dissipate.
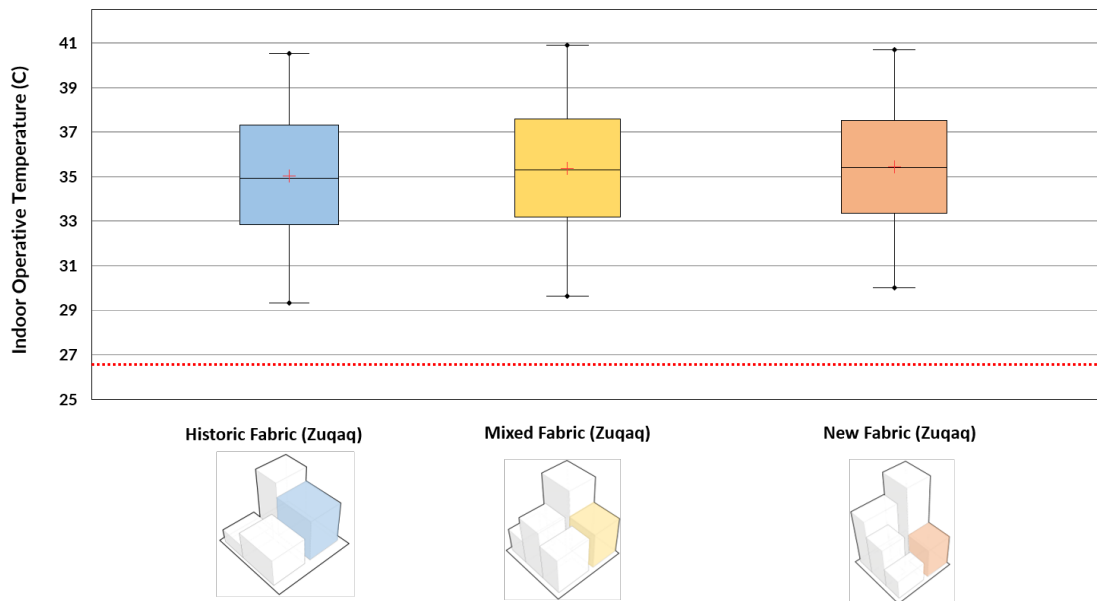

Figure 3-15: Indoor operative temperature for an extreme hot week. Each boxplot in this figure contains hourly operative temperature data for a historical building of 4 floors in three different urban typologies. The dashed red line represents the operative temperature threshold of 26.9°C.

To understand the impact of different street widths on indoor conditions, hourly simulations were carried out for historical buildings of four floors located in the historic urban block type. The surrounding buildings are the same height of four floors based on what was identified from the site survey to represent the original historic fabric. The simulation results show that increased street width influences indoor conditions, as noted in the increased operative temperature between the Zuqaq type and Hara type (Figure 3-16). On the other hand, Darb, a street type with a width between four and five meters, is significantly higher than Atfa. These results imply that street width can influence indoor conditions, as illustrated in Figure 3-16 below. In Atfa and Hara type, average indoor air temperature increased by 1.0°C than Zuqaq type, while Darb showed an indoor air temperature lower by 2.0°C than in Hara and Atfa. This is due to urban canyons with wider streets and lower buildings tend to be cooler as it enhances wind speed at the canyon level allowing indoor heat to dissipate, similar to findings from other studies found in the literature (Chatzidimitriou & Axarli, 2017; Matthews, 2017).
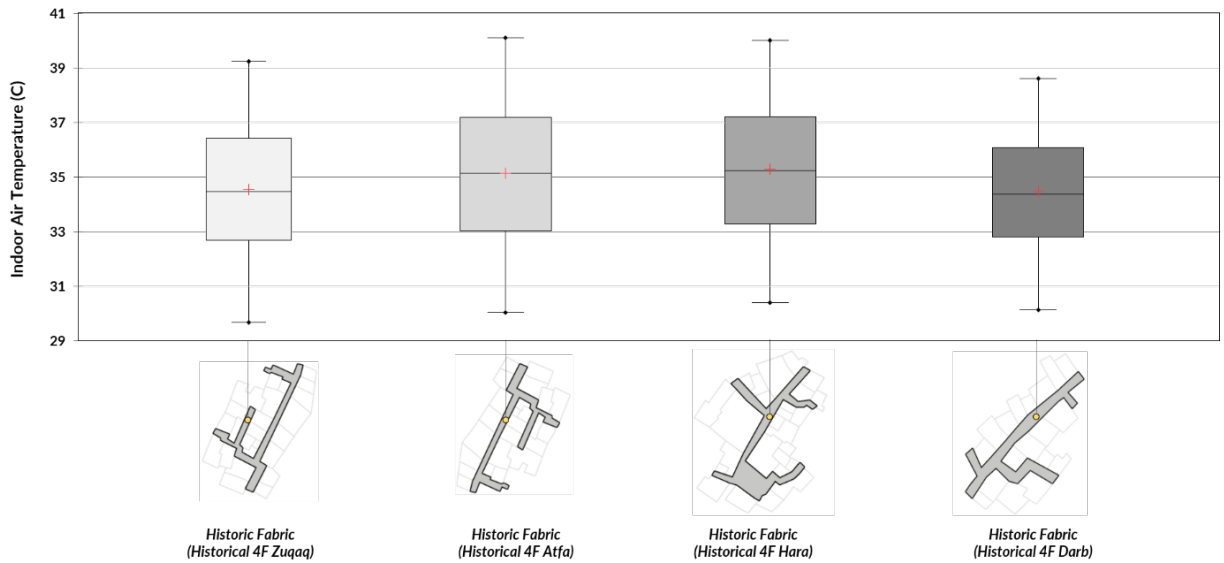
Figure 3-16: Indoor air temperature for roof floor apartment in the historical building of four floors across different street types.

The subsequent stage was to use validation for individual archetypes to develop an urban template for UMI inputs. An urban area of 1.2 acres is simulated for annual overheating hours above 26.9°C. Simulation results highlight that historical buildings have relatively higher overheating hours than archetypes from the late 20th century and new construction. The roof floor across all archetypes had higher annual overheating hours than other floors in the same building. The average annual overheating in historical buildings ranged from 4800 hours to 6300 hours, as shown in Figure 3-17-a. Archetypes from the late 20th century and new construction had average annual overheating hours ranging between 3000 and 3500 hours annually, as presented in Figure 3-17-b. Urban-level simulation results confirm the finding from the individual archetype analysis discussed above.
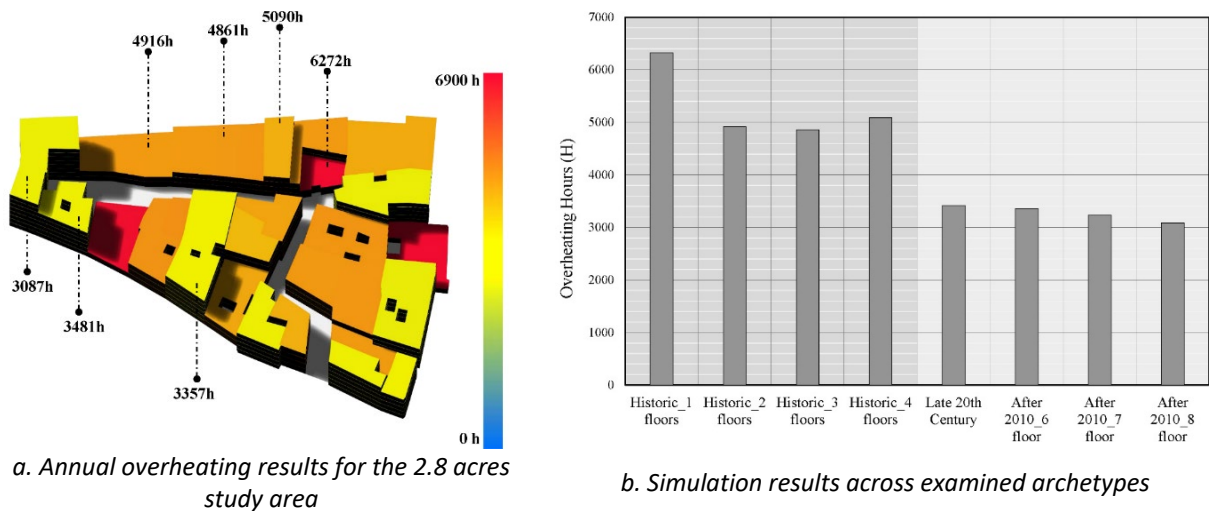

a. Annual overheating results for the 2.8 acres study area

b. Simulation results across examined archetypes

Figure 3-17: Overheating simulation for three Archetypes.

3.4.2 Heatwave Impacts and Future Climate Scenarios

Examining building thermal performance under extreme heat events or climate change scenarios has been an active research area over the past decade. This research serves as another incentive for previous efforts to highlight the impacts of heatwaves on indoor overheating in low-income neighborhoods with limited access to adaptation measures such as AC or power supply. This section examines the performance of different archetypes during extreme heat exposure to prioritize building types of higher risks. Among the efforts to develop a metric for heat vulnerability of buildings during extreme heat exposure, Nahlik et al. (2017) simulated buildings under steady-state Dry Bulb Temperature of 44°C and relative humidity 2% for one week to assess temperature differences between indoor and outdoor as a representative of a heatwave impact on buildings without power supply. The study showed that the indoor air temperature of buildings without air conditioning approaches outdoor temperature but never reaches it. Results from Nahlik's research don't accurately represent indoor conditions of an extreme heatwave, as it assumes internal loads to be only coming from envelope conduction.

Thus, the same approach was applied to the three main archetypes (four floors historical, four floors from late 20ᵗʰ century, and eight floors new construction) located in the same urban typology (historic fabric with hara as the street type) to examine how indoor air temperature changes. The simulations were carried out using a steady outdoor temperature of 44°C and relative humidity of 2%. Figure 3-18 shows a similar daily pattern in indoor air temperature in roof floor apartments across the three main archetypes. In the absence of AC, the indoor air temperature across the three archetypes doesn't fall below outdoor temperature, as it becomes challenging to lose internal gains to warmer external conditions through conductions. The new construction archetype showed the highest increase in indoor air temperature, with maximum indoor air temperature reaching around 49.5°C compared to 48.5°C in the historical archetype.
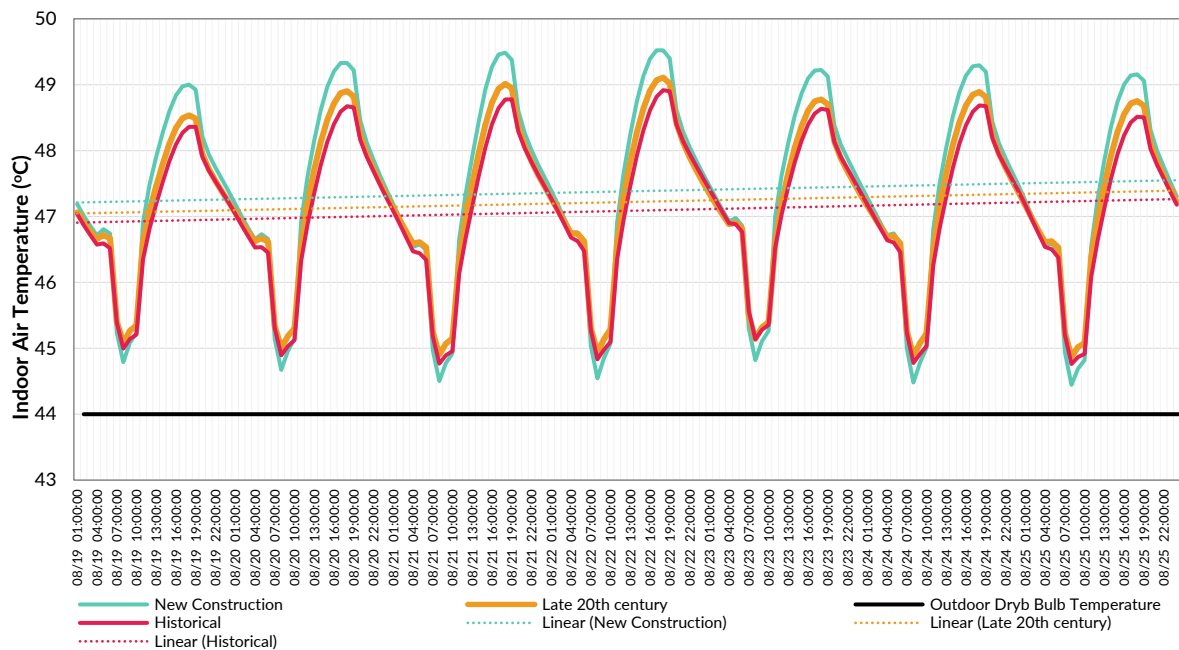

Figure 3-18: Changes in indoor air temperature of the three main archetypes during a constant outdoor temperature of 44°C.

Next, using the simulation workflow discussed in the methods section, changes in indoor air temperature are assessed using the climate records of an actual heatwave that happened in Egypt in 2015. The differences in indoor air temperature between the three main archetypes examined above and located in historic urban fabric urban typology are compared. The 2015 heatwave happened between the 6th and 9th of August, so the meteorological records between August 4th and 12th were used. Figure 3-19 shows simulation results with a significant increase in indoor air temperature throughout the heatwave that is always higher than the outdoor air temperature with a decline in the difference in all archetypes between indoor and outdoor temperature.
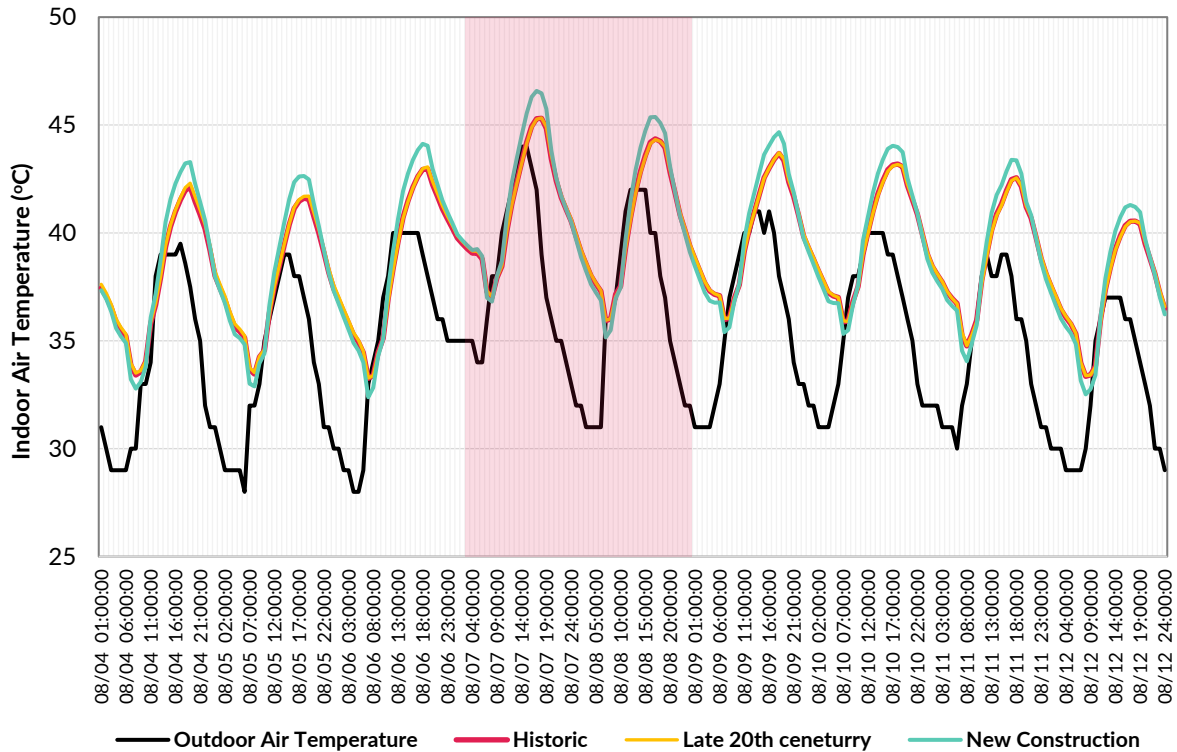

Figure 3-19: Changes in indoor air temperature for the three main archetypes in historic fabric typology during the 2015 heatwave. Indoor air temperature is always warmer than outdoor.

The diurnal variation of outdoor air temperature during the peak of the 2015 heatwave (between August 7th and 8th) is 35°C at predawn to warmest around midday, where outdoor air temperature reached 44°C. The indoor air temperature with no AC scenario follows the varying outdoor dry bulb temperature with a minor time lag from the thermal mass, as illustrated in Figure 3-18. There is a significant heat gain from occupancy, equipment loads, and solar gain throughout the three main archetypes that cause the indoor air temperature to remain above the outdoor air temperature. In all three archetypes, the largest delta T (ΔT) occurs during the nighttime when the outdoor temperature cools down, as shown in Figure 3-20. In contrast, the indoor air temperature stays high, causing an increased heat exposure and lower capacity to absorb heat the next day. Delta T (ΔT) reduces through envelope conduction; consequently, as the outdoor temperature increases with the severity of heatwave, indoor air temperature increases significantly, creating uninhabitable indoor conditions for occupants, especially in the absence of mechanical cooling means. Across the three archetypes, indoor air temperature starts to cool down and

becomes lower than the outdoor air temperature during the early hours of the day between 6 am and 7 am and starts to increase again till it reaches the outdoor air temperature by midday (between 1 pm and 2 pm). The 2015 heatwave simulation results indicate potential high risks from overheating due to high temperatures, especially at night, that can potentially disrupt sleeping and pose elevated risks to the vulnerable populations. It can also be noted that wind speed during the heatwave peak specifically was relatively lower, especially at nighttime (12 am to 4 am), as shown in Figure 3-20-b. Findings from the nearest hospital records during 2015 indicated that around 158 emergency visits between August 9th and 10th (Ahmed Maher Teaching Hospital, 2015) could be relatively tied to high indoor heat exposure from the previous two days.
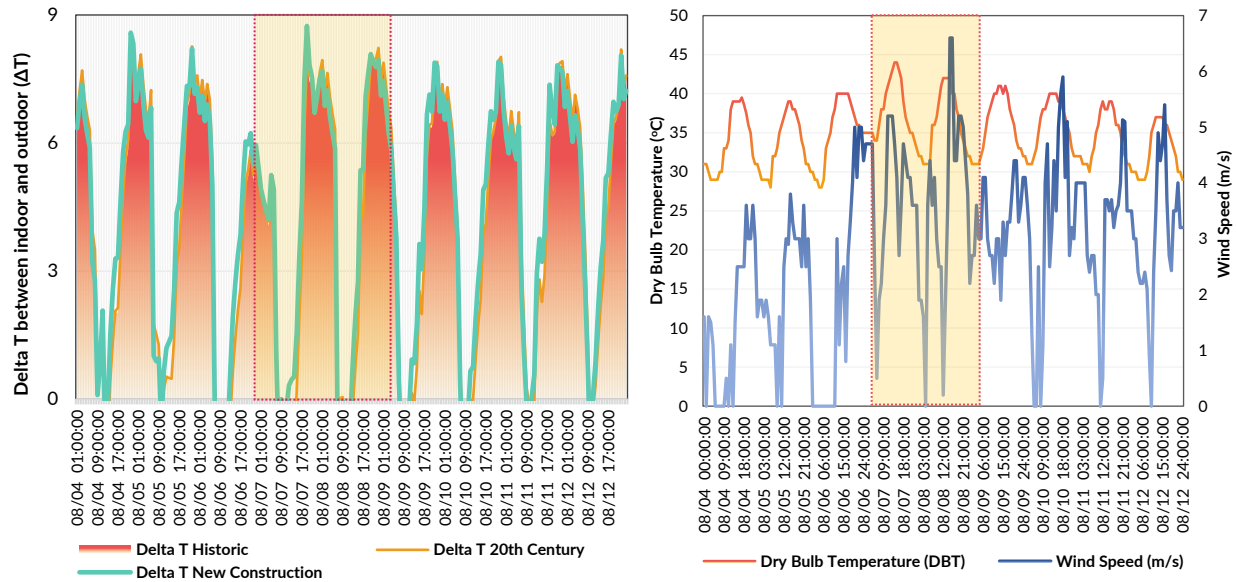
a. Delta T between indoor and outdoor temperature

b. Dry Bulb temperature and wind speed during 2015 heatwave

Figure 3-20: a. Delta-T between interior and outdoor air temperature, b. Wind speed and dry bulb temperature during the 2015 heatwave. Indoor air temperature is cooler than outdoor historical and late 20th century at the early hours of the day between 7 am, and 11 am and starts to increase until it reaches the outdoor air temperature around midday and stays above the outdoor air temperature till the early hours of the morning of the next day.

Next, the research examines the projected increase in overheating hours across different archetypes under the 2050 A2 climate scenarios. The A2 scenario is based on high growth in population to reach 15 billion by 2100 and slower technological change resulting in a continuous increase in GHG emissions (Ogunlade Davidson, 2014). Figure 3-21 shows outdoor dry bulb temperature and relative humidity for the 2050 scenario, current weather file, and meteorological data for the 2015 heatwave. The 2050 scenario doesn't include heatwave events, and temperature and humidity are relatively lower compared to meteorological records from the 2015 heatwave, where dry bulb temperature is higher by an average magnitude of 5°C.
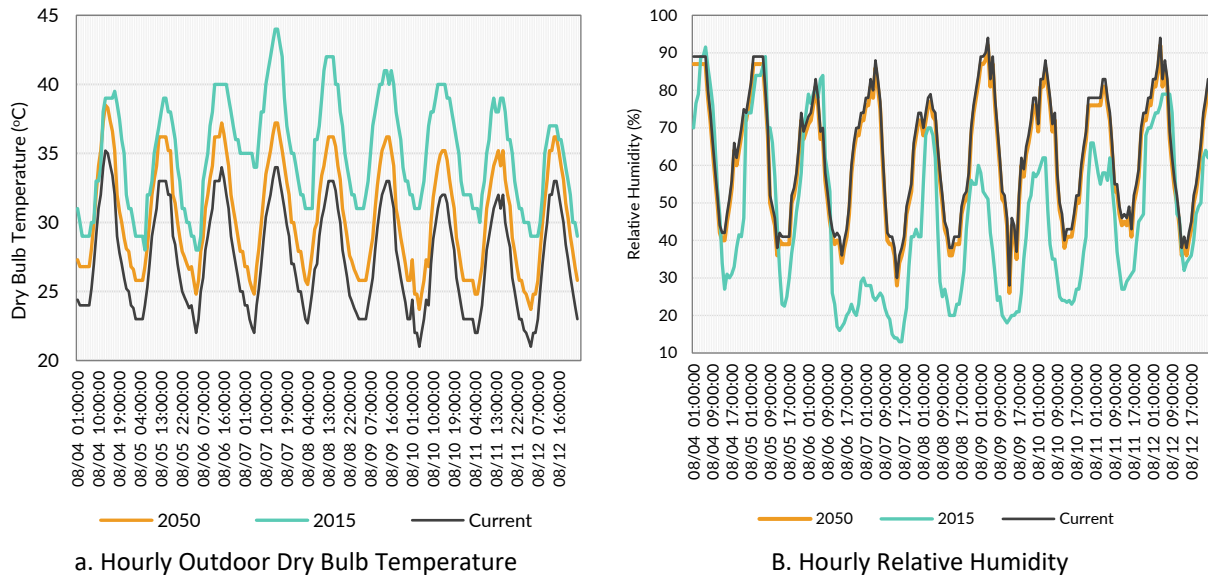
a. Hourly Outdoor Dry Bulb Temperature   B. Hourly Relative Humidity

Figure 3-21: Outdoor Dry Bulb Temperature (Left) and Relative Humidity (Right) for A2 scenario in 2050, current climate file, and meteorological data of 2015 heatwave for the same week.

By simulating the 2050 scenario, several trends have been identified. Generally, there is a significant increase in overheating hours, especially for archetypes from the late 20th century and new construction archetypes. Figure 3-22 below presents the increase in overheating hours across all eight archetypes for current conditions and 2050 scenarios. Results show that archetypes from the late 20th century and new construction had an average increase in overheating by 18% by 2050. Notably, historic buildings had an average increase of 6% by 2050. Although historical archetypes have a higher number of overheating hours, future scenario simulations how that new construction buildings have a faster increase in the indoor operative temperature range in comparison. Also, 2015 heatwave simulation results indicated a potential for high indoor heat exposure that may pose significant risks to vulnerable populations under future climate projection given the projected increase in overheating potentials from urban simulation results.
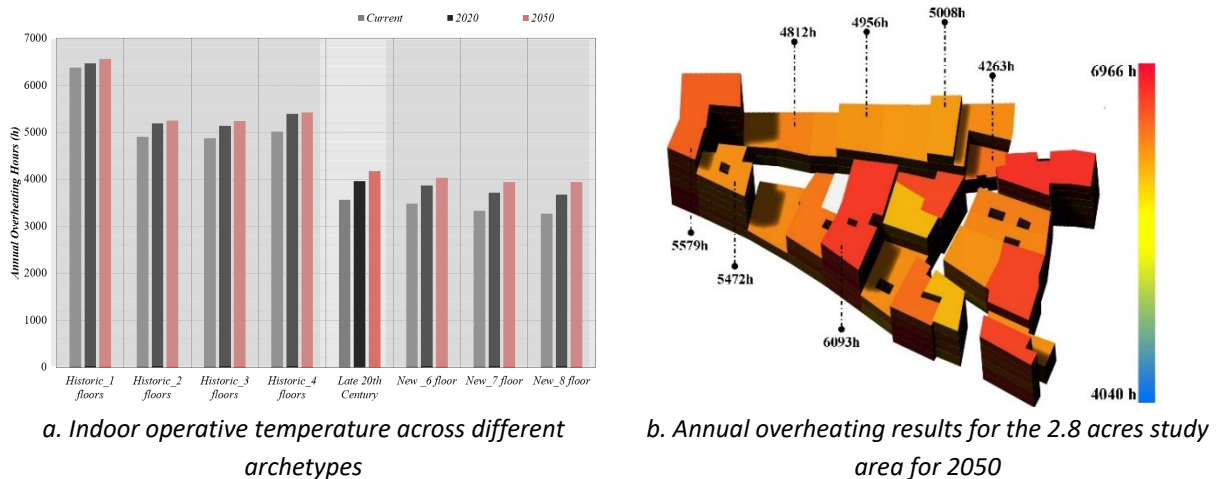

a. Indoor operative temperature across different archetypes

b. Annual overheating results for the 2.8 acres study area for 2050

Figure 3-22: Annual overheating simulation results for current conditions, 2020 and 2050 scenarios.

3.4.3 Human Adaptive Capacity

Current and future heat risks call for a better understanding of human adaptive capacity under heat exposure, and what types of measures are being used to cope with current and potential extreme heat events in the future. In this research, a survey was conducted to understand residents' adaptive capacity to heat exposure, including social practices, attitudes, and access to adaptation resources at the urban level, and understand the available resources for heat stress adaptation. The survey consisted of a mix of closed-ended questions utilized to quantify and identify types of heat adaptation measures and occupants' behavioral adjustments during heat exposure; open-ended questions that were used contextualize adaptive capacity from occupants' individual experiences at a greater depth. The survey was presented in Arabic and conducted over the two weeks of August 8th to August 22nd. The time was chosen to get the actual occupants' thermal experience during a typical summer week and was mainly conducted between 10 am to 4 pm. The survey sampled were divided into 25 sections for data collection to cover the entire 12 administrative sectors (Sheiakha) of AlDarb Al Ahmar district, as presented in Figure 3-23.
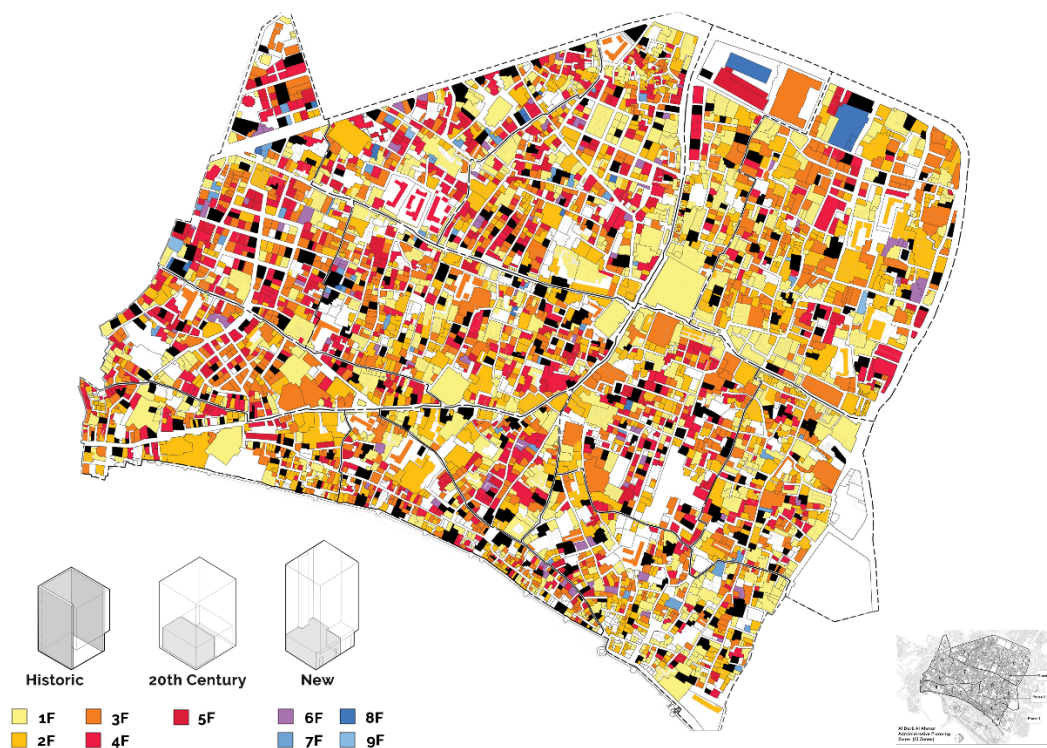
Figure 3-23: Distribution of surveyed samples (highlighted in black) in AlDarb Al Ahmar District in August 2019.

a. Demographics

More than half of the 300 surveyed residents were female (56.6%), most of the respondents reported they have lived in AlDarb Al Ahmar for more than 15 years (51.6%), and around 30% had a monthly income of less than 30$, while 12% reported having a monthly income more than 50$. The surveyed sample was relatively uneducated. Around 45% of the respondents were illiterate, 5% had primary education, 18% high school, 24% completed high school, and 8% had a university degree. For employment, 65.4% of the respondents were unemployed, and 34.6% were employed. Most of the unemployed sample (males) depended on daily jobs that can leave them for weeks without any form of income. The survey included

questions about the distribution of the vulnerable population (elderly above 60 years old and infants below five years). Around 53% of the surveyed sample had at least one elderly (older than 60 years old) in the apartment, and 78% had one infant per apartment, as illustrated in Figure 3-24 below.
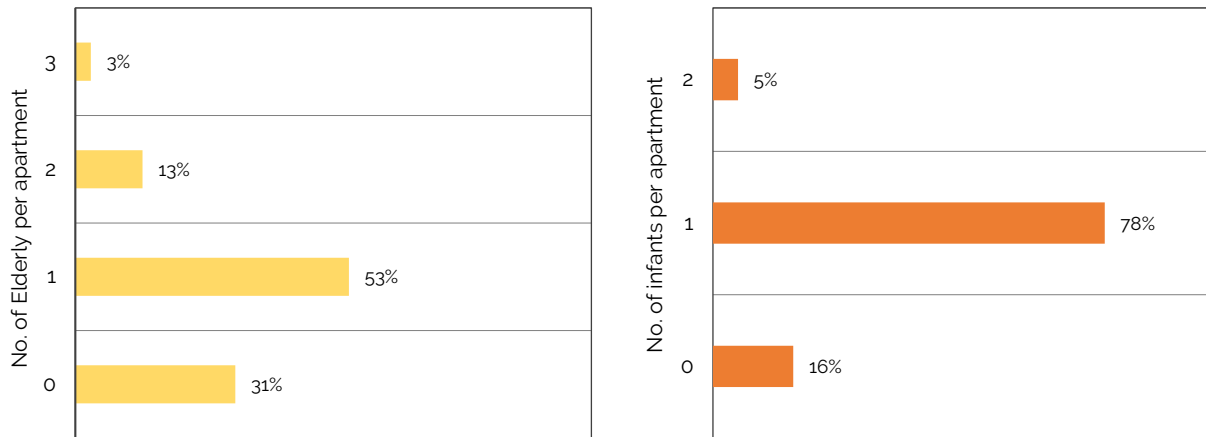
a. Number of the elderly per apartment in the surveyed sample

b. number of infants per apartment in the surveyed sample

Figure 3-24: distribution of vulnerable population in the surveyed samples.

b. Experience with heat

The survey included questions related to heat sources and time of the day to examine their thermal experiences. Around 44.5% of the respondents lived in historical archetypes, 23% lived in late 20th century buildings, and 32.5% lived in new construction. Approximately 81% of the respondents who lived in historical buildings reported experiencing thermal discomfort (indoor conditions are warmer than usual) between 7 pm to 11 pm. In comparison, 84.3% of the respondents who lived in new construction reported experiencing thermal discomfort between 12 pm to 3 pm. In the survey, thermal discomfort levels were also examined, and around 55% of the surveyed sample who lived on the top floor reported a thermal sensation vote of 3 (hot).

In contrast, 50% of the respondents who lived in intermediate floors reported a 1 (slightly warm) thermal sensation vote. Also, the research identified that there is a relationship between floor location and discomfort response. When respondents reported hot surroundings as the primary source of discomfort, they are mainly the top floor residents. On the other hand, people on the ground level reported that high humidity level was the primary source of thermal discomfort (Figure 3-25).
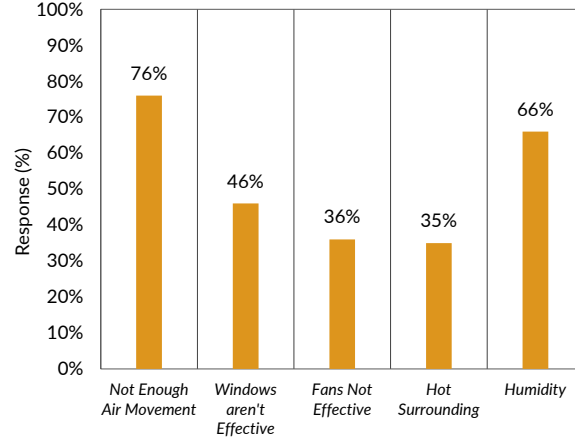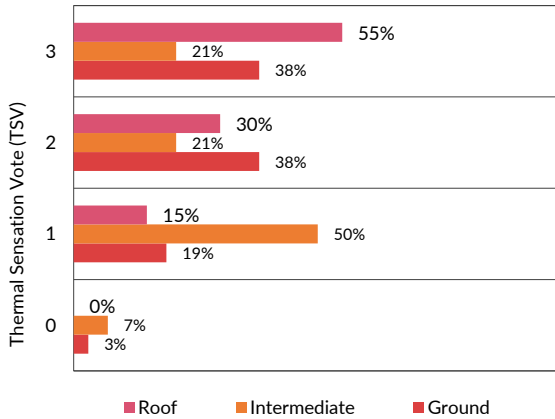
a. Reported thermal sensation vote by floor location   b. Sources of heat based on the surveyed sample

Figure 3-25: Reported thermal sensation votes by floor location (left), sources of thermal discomfort based on the survey.

c. Adaptive capacity

From the survey, the research has identified that 86% of occupants who work are away from the apartment between 11 am - 6 pm, and 43% of the surveyed residents stay at home during the weekend (Friday and Saturday). Also, the research found two patterns of coping mechanisms that residents rely on during heat exposure; passive such as opening windows, opening the apartment door, using window blinds, and active through either using ceiling and portable fans. Table 3-6 below summarizes the main coping capacity patterns identified from personal interviews and site surveys for 300 residents.

Table 3-6: Occupants' coping mechanisms based on personal interviews.

	Income A (5-20$/m)	Income B (20-50$/m)	Income C (50-150$/m)
Distribution	30%	58%	12%
Passive Coping Capacity	15%	4%	1%
Active Coping capacity	85%	96%	99%
Elderly Percentage	18%	17%	1%
Infants Percentage	21%	28%	15%
Access to AC unit	0	4%	50%

The research identified two types of coping habits that occur during high indoor temperatures; at the building level (sleeping on the roof, sitting in balconies, taking a shower), and at the urban level (sitting in front of the house, going to the nearest open space, going Al Azhar park). Only 3% of the surveyed sample reported going to Al Azhar Park (Figure 3-26). This small fraction is mainly due to: i) some buildings are not within walking distance to the park, and ii) access to AlDarb Al Ahmar residents is only free from 12 pm to 4 pm, which is the time where most of the residents are either doing households chores or working. Therefore, this limits the park's capacity to serve as a cooling space for the district's residents, as previously highlighted. Several open spaces called "Midan" are open areas neighboring some of the oldest mosques. Around 20% of the surveyed residents reported spending time at the closest Midan when it gets warm inside.
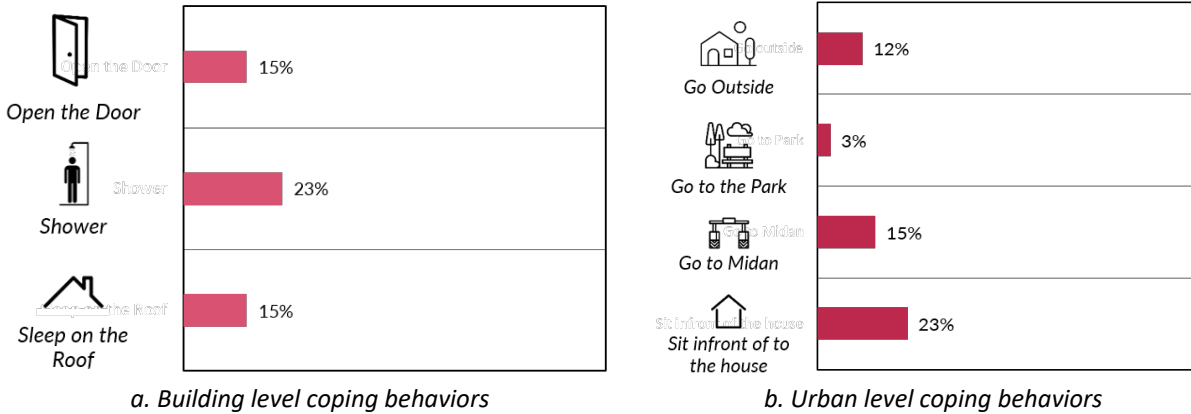
a. Building level coping behaviors	*b. Urban level coping behaviors*

Figure 3-26: Reported coping behaviors at the building and the urban level based on residents' responses.

d. Awareness of heat risks

The survey included questions related to how aware are the residents of heat exposure risks. The majority of surveyed residents (87.6%) reported not being aware of the severe risks of continuous heat exposure without proper hydration or ventilation. Of the participants who recalled hearing about heat-related risks, the primary source was information from the local tv news (6.8%), internet (4.4%), and newspaper (1.2%). When asked if they had received information about heat-related illness prevention, 2.4% mentioned the local tv news as the primary source. Around 98.6% didn't know what measures to be followed during a heat event. These results indicate a lack of knowledge in AlDarb Al Ahmar residents on heat-related risks and a lack of information/resources on coping with heat exposure.

3.4.4 Heat Exposure Range and Human Risk Threshold

Health-related risks from prolonged exposure to high temperatures arise from multiple factors such as social isolation, age, income level, and medical condition (Palmer et al., 2014). To examine the effect of prolonged exposure to high temperatures, the research monitored a cohort of residents in AlDarb Al Ahmar. The target population included people living in historical building archetypes mainly situated in historic fabric, representing the study area's most common building and urban pattern. Also, targeted residents lived on the top floor apartment, with 25% of the sample lived alone (socially isolated) and 25% had an existing medical condition to evaluate impacts of prolonged heat exposure on human health. The research assessed the study group's thermal experience during personal monitoring to understand the level of thermal stress with respect to indoor air temperature. Statistical analysis showed a relationship between indoor air temperature and HR; the physiological indicator measured by heart rate indicated that maximum indoor air temperature was a good predictor of mean heart rate ($p < 0.001$), as illustrated in Figure 3-27. Examining the threshold range where the heart rate risk limit is exceeded, it was found that across the 18 participants, HR increases above 90 bpm under a **Risk Threshold** ranged between 31-34 and an average **Exposure Range** of 2.5-3 hours. This threshold was found to vary between elderly residents: in female elderly participants, the average exposure range was 2.5 hours, while in males, it was 3 hours. Previous studies have identified an indoor air temperature of 26°C as a threshold that can influence cognitive performance (Cedeño Laurent et al., 2018b). Also, a recent study (A. A. Williams et al., 2019) has identified a threshold of 24°C of indoor air temperature to impact HR and sleep disruption.
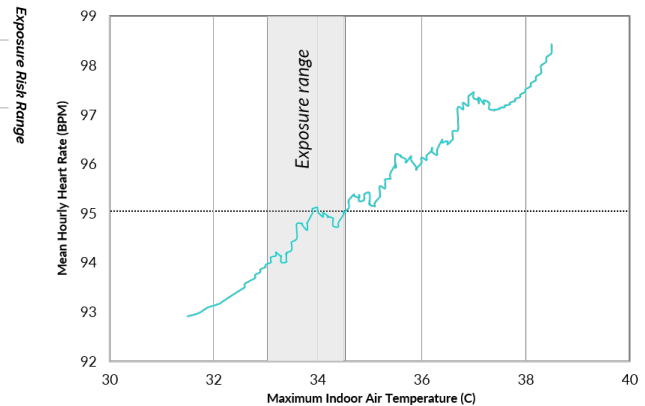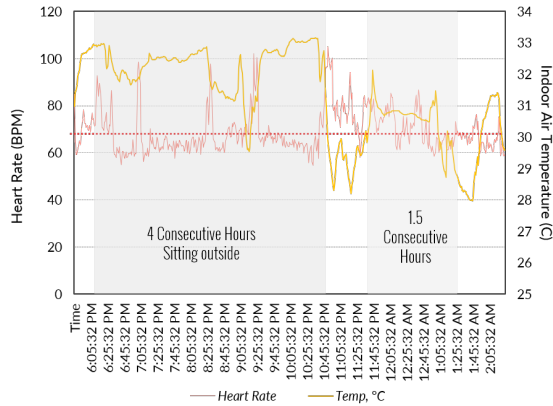
a. Heart rate and indoor air temperature for one of the monitored samples with a heart problem (age 31)

b. Relationship between maximum indoor air temperature and mean hourly heart rate

Figure 3-27: left- heart rate and indoor air temperature for one of the samples, right- the relationship between maximum indoor air temperature and mean hourly heart rate.

Participants were also asked to report thermal stress levels using TSV and compared their answers to average and maximum indoor air temperature and heat index values during these times. Results show that around 80% of the monitored samples who lived in historical buildings reported a TSV of 3 between 6 pm and 12 am at an average indoor air temperature between 33 and 34°C and a heat index of 37°C. For the new construction archetype, around 66% of the sample reported a TSV of 3 between 6 pm and 12 am, while 50% of the participants reported a TSV of 3 between 12 pm to 2 pm, as shown in Figure 3-28. As expected, the number of participants who reported TSV of 3 reported that their apartment was getting too hot at these times, which followed an increase in indoor air temperature between 31-33 in historical buildings and 32-34 in new construction.

Also, there is a relationship between reported TSV and heat index. The research found that relative humidity levels in historical buildings were relatively higher than in new construction, which corresponds with the results from the survey that most of the residents mentioned humidity to be the source of discomfort lived in historical buildings. Examining survey results with personal monitoring findings, most residents who reported high humidity levels lived in historical buildings with Hara and Zuqaq as a street type facing new construction archetype (height ranges from 6 to 8 floors). Also, the majority of historical buildings had smaller floor areas (50-100 m²) with high occupancy density per apartment (5-6 people/ apartment) compared to new construction (150-250 m²) with an occupancy density of 4-5 people/apartment.
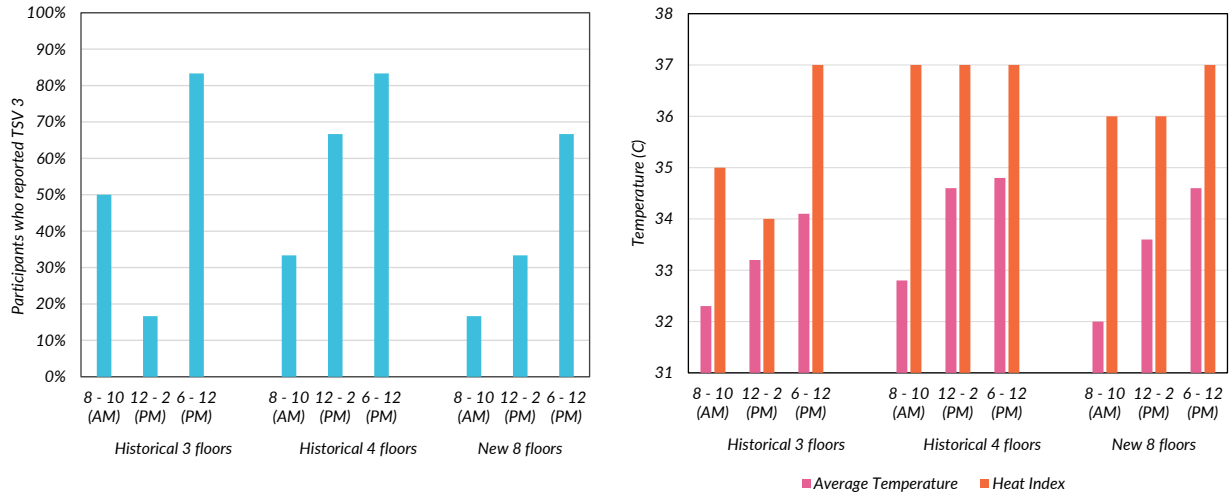
a. Thermal sensation vote for the 18 participants *b. Average indoor air temperature & heat index*

Figure 3-28: left- thermal sensation vote (TSV) reported by the participants during the experiment, right- corresponding average indoor air temperature and heat index.

3.5 Discussion

This section reports an in-depth investigation of potential health risks associated with increased indoor overheating for vulnerable populations with limited mechanical ventilation access. The goal was to investigate the threshold for indoor conditions that could result in health risks, specifically for elderly residents. A quantitative analysis using residents' surveys was designed to develop a representative simulation model. Results from the simulation highlighted strong evidence of overheating across examined archetypes. Generally, the upper floors showed a higher number of overheating hours, especially for historical archetypes. These results can be explained by the wall bearing structure system commonly used in a historic building, with a wall thickness of 12.5 cm for a three-story building compared to a lower floor of 40 cm thickness. The second phase of the analysis focused on developing an urban simulation model to investigate the potential increase in overheating over a large urban scale. This analysis was carried out in UMI using an actual occupancy scenario from the residents' survey. The simulation results revealed a significant increase in overheating across all archetypes, especially in historic buildings. This can be directly linked to a small floor area with a high population density per m^2 compared to newer buildings. As historic archetypes were initially designed to accommodate one family, a change of use resulted in higher population density than newer archetypes. On the other hand, the 2050 climate scenario results revealed a faster increase in archetypes from the late 20th century and new construction.

In general, the AlDarb Al Ahmar study results show a significant discrepancy in living conditions, specifically between historic buildings and new construction. The change in building use from a small building footprint initially designed to accommodate a single-family to a low-rise apartment building to accommodate multiple families has altered these buildings' thermal experience. This change in building use has created a thermally stressed indoor environment that may pose higher risks in extreme heat events. Results from individual archetype simulation and urban typologies have reflected that changes in the urban fabric have altered the outdoor environment from how it was initially designed. Changes in open spaces network with the population density have also limited residents' adaptive capacity when it

gets warm indoors. These results highlight the urgency to develop policies, information resources, and residents' support programs for these areas to underline types of behavioral measures and resources in case of an extreme heat event.

Numerous studies have examined the relationship between heat exposure and human health in laboratory settings. This research has characterized the individual temperature exposure at low income-housing with no access to AC using wearable devices. Simultaneously, environmental monitoring and behavioral factors were incorporated in the analysis using the survey to identify factors that influence individuals' adaptive capacity during high-temperature exposure and potentially affect individual's susceptibility during extreme heat events. Health implications associated with increased overheating showed that for historic buildings, there is a threshold of exposure under an indoor air temperature range between $31-34\,°C$ for an Exposure range between 2 to 3 consecutive hours. The analysis's main limitation is focusing on a single building type and the size of the monitored sample with the assumption of consistent ventilation scenarios. The monitored sample in AlDarb Al Ahmar showed that indoor air temperature could alter physiology, increasing the heart rate with range markers between $31\text{-}24\,°C$. Simultaneously, these temperature ranges have not impacted participants' daily activities. Still, they reported some disturbance in their sleep as most of the participants reported night time between 6-10 pm to be the warmest time of the day. Further research should investigate the effects of changing ventilation and occupancy schedules alongside a larger sample's monitoring.

Future work can also examine the impact of passive strategies with other thermal comfort indices such as Wet Bulb Global Temperature (WBGT), Predicted Heat Strain (PHS), and Sweat Rate (SR) across varying activity levels and occupants' types. Findings from this research are limited to the examined sample. Still, it can be used as a starting point for how the duration of exposure can impact heat-related health impacts. Also, the temperature threshold identified in this study is relatively higher than what has been reported in previous work in the literature. Therefore, occupants' acclimatization to these high temperatures should be considered a factor when assessing heat-related health risks (D. Chong, Zhu, Luo, & Zhang, 2019). Results from this research highlight the complexities of heat vulnerability. Residents that were examined in AlDarb Al Ahmar were exposed to similar ambient conditions. Still, their buildings and surrounding resources have played a role in exacerbating or mitigating heat exposure risks.

3.6. District Level Heat Vulnerability Assessment

The first section of the chapter illustrated the potential risks of indoor overheating and high-temperature exposure at the building level. This section focuses on assessing the vulnerability at the district level under potential heatwaves to provide suitable mitigation and adaptation strategies. Previous studies that have examined heat vulnerability at the urban level (district, community, sub-district) depended on the spatial distribution of vulnerable populations to identify areas of high risk independently from indoor overheating at the building level (Dong et al., 2014; Walton, Poudyal, Hepinstall-Cymerman, Johnson Gaither, & Boley, 2016). In most of these studies, the unit of analysis comprises multiple factors (building densities, open spaces, distribution of susceptible population) that are different at the spatial level, and each has a significant difference in their spatial distribution that contributes to the overall vulnerability assessment. The current gap in large-scale assessment is the limited understanding of which factors form the most significant impact on heat vulnerability, whether it is from exposure to heat at the building scale or limited accessibility to heat mitigation and adaptation measures at the district level. The main limitation of a large-scale vulnerability assessment is that it's a computationally expensive process to model and simulate indoor conditions at the district level. This section provides an approach to district-level vulnerability assessment considering indoor thermal conditions at the building level using machine learning models.

Machine learning (ML) is a powerful technology that stemmed from exploring artificial intelligence science (H. Li et al., 2016). Based on the literature, machine learning methods can learn nonlinear relationships between independent and target variables and conduct predictions through computational statistics (Y. Zhao, Genovese, & Li, 2020). The application of machine learning in building science has focused on modeling and predicting commercial building energy consumption (Robinson et al., 2017) and predicting indoor thermal conditions (Mateo et al., 2013). Yet, in the domain of indoor environment and overheating prediction, machine learning has not been widely utilized. Therefore, this section presents a machine learning approach for modeling and predicting overheating risks at the building scale to assess heat vulnerability and related risks at the district level. An overview of different machine learning models and their application in the built environment are presented to outline models or algorithms used in the building science field. Then the research presents the proposed model structure, input variables, and accuracy assessment. Finally, the district-level indoor overheating analysis is used to identify exposure range, areas of high risks, and potential interventions to improve adaptive capacity under heat exposure. AlDarb Al Ahmar district is used as the primary case study expanding on the analysis presented in section one of this chapter.

3.7 Machine Learning and Building Science

Machine learning (ML) is an expression used to describe computer algorithms that learn from data to conduct predictions. The adaptive learning capability of ML models has enabled ML models to handle complex problems effectively, as ML models can improve from subsequent training and pattern identification (Arulmozhi et al., 2021). The learning process for these algorithms involves using a significant amount of data with a small number of inputs. Various ML methods have been used in building performance fields to estimate energy use in buildings and cooling and heat loads under multiple scenarios (Seyedzadeh, Rahimian, Glesk, & Roper, 2018). In modeling and predicting building energy use, machine learning models operate as a black box with limited information on building systems. Then, algorithms discover the relationship between various input variables and output targets through learning from large data sets.

The accuracy of ML models depends on the amount of training data used to predict targets, though the relationship between inputs and outputs is undefined. This approach is known as supervised learning in the ML field (Azuatalam, Lee, de Nijs, & Liebman, 2020). In building energy modeling, input/training variables are measured or calculated using simulation to estimate target outputs (Figure 3-29). There are three widely used supervised learning techniques in the building science field: Artificial Neural Networks (ANN), Support Vector Machine (SVM), and Gaussian distribution regression (Chaudhuri, Soh, Li, & Xie, 2019). The second approach in ML is unsupervised learning, where it is mainly applied to unlabeled data to cluster them based on hidden similarities in their underlying features (Robinson et al., 2017). The most commonly used methods in unsupervised learning are K-means and hierarchical clustering. This approach has been widely used to determine building energy benchmarks and performance; hence, unsupervised algorithms provide more precise classification by grouping various buildings with similar baseline than traditional methods that mainly depend on building energy use type (Seyedzadeh et al., 2018). In unsupervised learning, all input data are used as training samples for classification, and generated clusters are considered the learning targets (Figure 3-29).
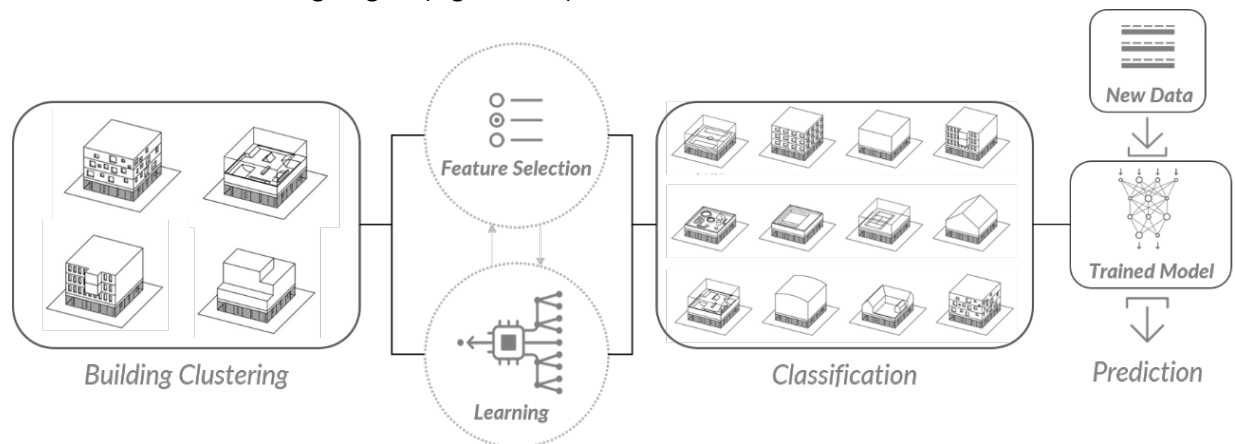

Figure 3-29: Left- General schematic diagram of supervised learning, Right- Diagram of clustering buildings for energy benchmarking. (Based on (Robinson et al., 2017).

3.7.1 Motivation: ML and Indoor Environment Prediction

Early studies in the application of ML to forecast indoor conditions have combined linear models with Artificial Neural Networks (ANN) to model and predict indoor daily temperature profiles in buildings (Hippert & Pedreira, 2004; Mechaqrane & Zouak, 2004; Thomas & Soleimani-Mohseni, 2007). These studies varied in the type of buildings, training data sets, and analysis methods used. These research efforts have shown that neural network models outperform linear models in predicting temperature profiles and forecasting indoor air temperature. In recent studies, new techniques have emerged in the field of building science and indoor climate forecasts, such as Extreme Learning Machines (ELMs), general regression neural networks (GRNN), ANNs with non-linear autoregressive techniques (NARX), and Multilayer perception (Seyedzadeh et al., 2018). Cosma and Simha (2019) used a non-invasive ML approach to predict indoor thermal comfort for real-time feedback. Wu et al. (2018) examined the applicability of using ML models in predicting thermal perception using ANN and SVM over conventional statistical indicators.

Another study by Chaudhuri et al. (2019) developed a framework to predict thermal comfort in buildings using two components: a feed-forward neural network model and an optimization algorithm for the optimal indoor air temperature to reduce the discrepancy between energy efficiency and indoor comfort. As discussed above, ML models have been used to conduct solutions to complex problems such as prediction, clustering, and classification. However, there is a knowledge gap in using ML techniques in modeling and predicting building microclimate (Mateo et al., 2013). The research tries to evaluate the performance of ML models to predict indoor conditions to guide the development of district-level indoor heat vulnerability assessment. Research on ML application in indoor overheating assessment and heat vulnerability is scarce, and this section aims to fulfill this gap. The proposed model seeks to utilize building simulation as inputs to a machine learning model to predict large-scale district indoor overheating, a process that is both computationally expensive and time-intensive to conduct using simulation models.

3.7.2 Artificial Neural Networks (A.N.N.)

Artificial Neural Networks are a nonlinear machine learning method inspired by how the human brain neural network proceeds and processes information, where it copies information propagation in a simplified manner (Walker, 1990). Data flow from one neuron (processing element) with weight and is sent through a link (axon) to the next neuron. This process is combined with other weighted information from other neurons using an activation function (Bourdeau, Zhai, Nefzaoui, Guo, & Chatellier, 2019) and repeated until the accuracy error converges to fit the data when the number of iteration is reached. The structure of ANN consists of multiple neurons divided into three main layers: an input layer either used to train the model or execute the final predictions, a hidden layer that links the input and output layer, an output layer to give the final results, and an activation function that forms the relationship between the three layers (Figure 3-30).

ANN are usually designed based on three criteria: i) learning method that is related to final error propagation and how this process affects the weights, ii) the connection between different neurons, how many layers and how many neurons are communicating, and iii) the activation function between the different layers (Magoulès & Zhao, 2016). The accuracy of ANN prediction significantly depends on the training data and the structure of the model, which can also influence the model's performance with respect to overfitting and underfitting.
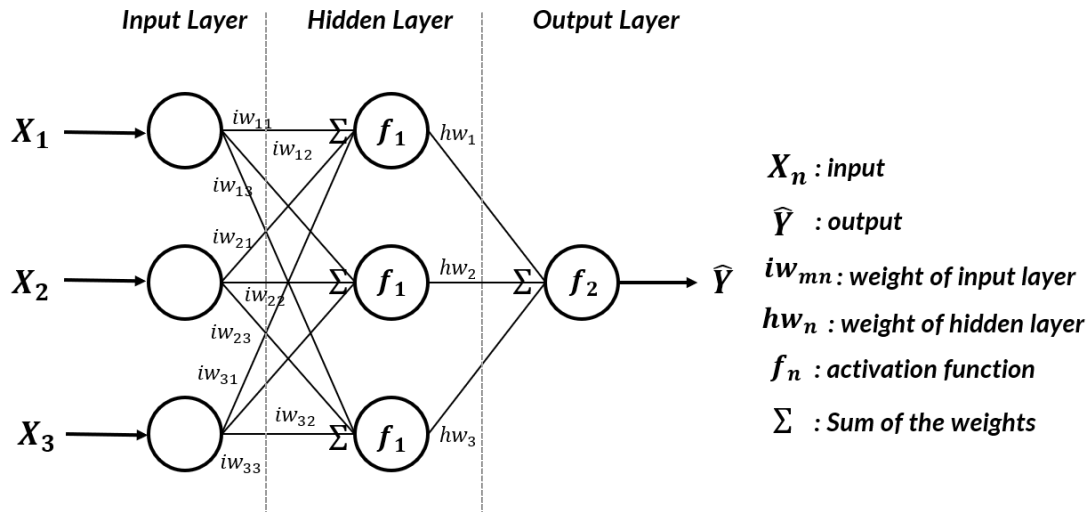
Figure 3-30: Schematic of a classical three-layer ANN. (Magoulès & Zhao, 2016).

The ANN application has expanded significantly in the past couple of years due to its capability to capture the non-linear relationship between variable inputs and outputs. Most ANN applications in the building science field have focused on energy use prediction, commonly known as the chief ML technique, to learn key patterns in building systems (Mateo et al., 2013; Tso & Yau, 2007). Kalogirou et al. (1997) used ANN to predict heating demands in buildings using training data of 225 buildings that varied from small to large spaces. ANNs were also used to optimize occupants' behavior for HVAC systems usage. Aydinalp et al. (2002) used neural network models to estimate cooling energy demand. The study showed that ANN models could be a good estimator of the effects of socioeconomic factors on energy consumption in the residential sector.

Moreover, the recent ANN application in the building science field has proven to be a feasible approach for modeling multivariable problems related to a building's thermal comfort. Mustafaraj et al. (2010) used a multilayer neural network to predict indoor air temperature in a building in London. Also, Afroz et al. (2018) used ANN as a modeling approach to estimate indoor air temperature for a library building in Australia. Qi et al. compared indoor temperature predictions for buildings in China using two methods: Back Propagation Neural Network (BPNN) and support vector machine (SVM). Although numerous studies have used ANN techniques in thermal comfort and temperature prediction, the application of ANN in estimating indoor overheating for heat vulnerability assessment is still limited.

3.8 Methods

This section describes data used in model development and training and machine learning methods used in the study. The research expands on AlDarb Al Ahmar case study presented in the first half of this chapter using simulation outputs as input data for the proposed ANN model. Next, results from the ANN model were incorporated into district-level heat vulnerability assessment using an image augmentation technique. Finally, results from the model are compared and evaluated for performance and accuracy.

3.8.1 Modelling Parameters

The simulation process investigates various parameters related to archetype physical characteristics identified from the site survey discussed in section 3, such as archetype geometry, window-to-wall ratio (WWR), envelope construction, and building orientation. Two different plan shapes were modeled to represent archetypes' floor plans in AlDarb Al Ahmar. They included a rectangular floor plan (1 to1.5 width to length ratio) and a square (1 to 1.1 width to length ratio). The floor area of each floor plan varied according to the archetype and was determined based on the site survey and previous urban analysis conducted by Aga Khan Foundation (Aga Khan Foundation, 2013) as follows: historical (60 to 100 m^2), late 20th century (80 to150 m^2), and new construction (100 to 250 m^2). Each floor plan was divided into thermal zones by perimeter and core and orientation, as illustrated in Figure 3-31 below.
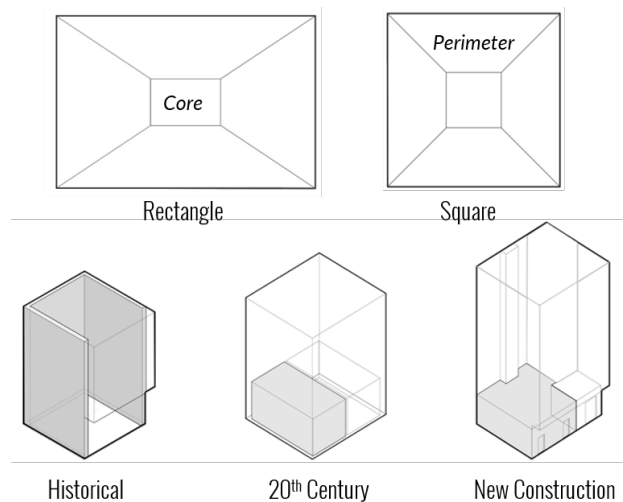
Figure 3-31: Plan geometry with thermal zoning for the three main archetypes.

For the urban context, representative urban typologies identified from the site survey of 500 m^2 are modeled. The presence of neighboring buildings plays a role in indoor climatic conditions; thus, the research models eight cases of all the possible adjacent buildings, including: historical (2 to 4 floors), late 20th century (4 to 5 floors), and new construction (5 to 8 floors). The research developed 800 urban typology base cases for the three main representative archetypes in AlDarb AlAhmar, including all the possible scenarios for neighboring buildings type, street width, and urban density, as illustrated in Figure 3-32. Since the area is considered highly dense, urban density was modeled based on the surrounding urban context. A fixed plot area and Floor Area Ratio (F.A.R) of 1.0 and height limits were kept constant and changing the number of building's sides exposed to the street; ranging from low density (three sides overlooking the street), medium density (two sides), and high density (one side).

*New Urban Typology
Low Density*

*New Urban Typology
Medium Density*

*Mixed Urban Typology
High Density*

*Fatma Al Nabweya Street,
AlDarb Al Ahmar District*
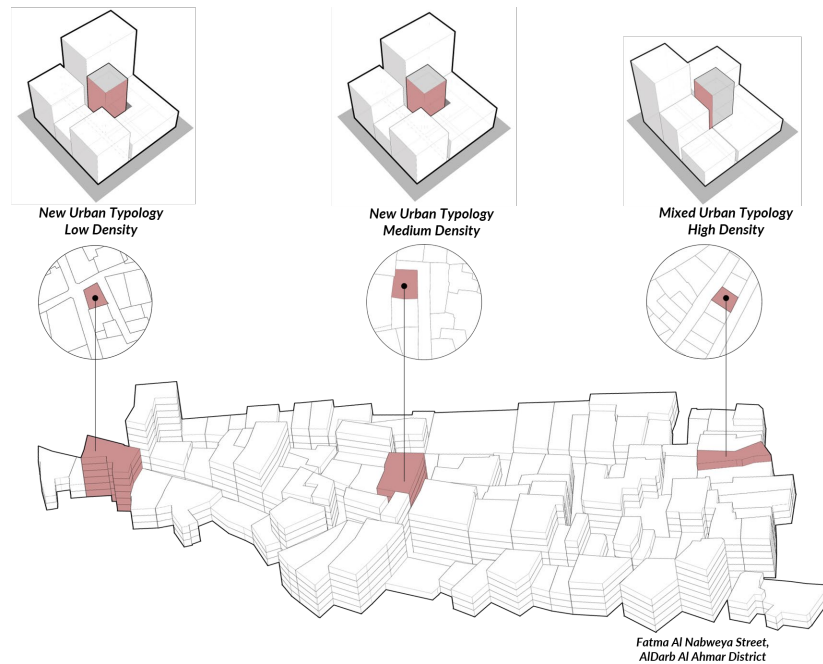
Figure 3-32: Example of different urban typologies and density types in AlDarb Al Ahmar.

The key model parameters used in the simulation are listed in Table 3-7 below. Equipment load and occupancy schedule were based on the site survey discussed in section 4 of this chapter. Since AC units are scarce in AlDarb AlAhmar, all the representative cases were modeled with no access to AC to assess the health risk impacts from heat exposure independently from AC usage. Simulations were carried out for an extreme hot week (August 18th to August 25th) using the Egyptian Typical Meteorological Year weather file (ETMY) covering 12 to 21 years and ending in 2003. Next, an IDF is generated for every permutation of archetype parameter for a total number of 200 IDF as listed in Table 3-7.

Table 3-7: Parameters values used for IDFs' development.

Parameter	Permutation Values
	Building Geometry: Square and Rectangle.
	Window-to-Wall Ratio: 20%, 40%, 60%.
	Orientation: N,S,E,W.
	Wall Insulation **Historical:** Limestone wall: 40 cm to 120 cm, sand fill 5 cm, 2.5 cm mortar, 2.2 cm plaster. U-Value: (0.5-0.6) **20th Century:** Red Brick wall: 25 cm, 2.5 cm mortar, 2.2 cm plaster. U-Value: (4.1) **New Construction:** Red Brick wall: 12.5 cm, 2.5 cm mortar. U-Value: (8.3)
	Street Types: Zuqaq (2.5 m), Atfa (3.0 m), Hara (4.0 m), Darb (5.0 m).
	Density: Low, medium, and high.
	Urban Block Typology: Historic, Mixed, New.

3.8.2 Simulation Workflow

The proposed framework for district-level indoor overheating assessment combines building simulation output with ML techniques by integrating simulation automation using python scripting language with ANN to conduct large-scale overheating predictions. The overheating assessment workflow starts with generating a simulation dataset for four main parameters: indoor air temperature, relative humidity, standard effective temperature (SET), and operative temperature. Next, simulations were conducted using EnergyPlus and Python's Eppy library for the three main archetypes and urban typology configurations. An investigation of building geometry representation, orientation, and the window-to-wall ratio is explored by manipulating EnergyPlus IDF using Python's Geomeppy library. The structure of the simulation workflow consists of four main steps: representative cases 3D modeling, IDFs manipulation, changing building parameters, and model testing, as presented in Figure 3-33 below.
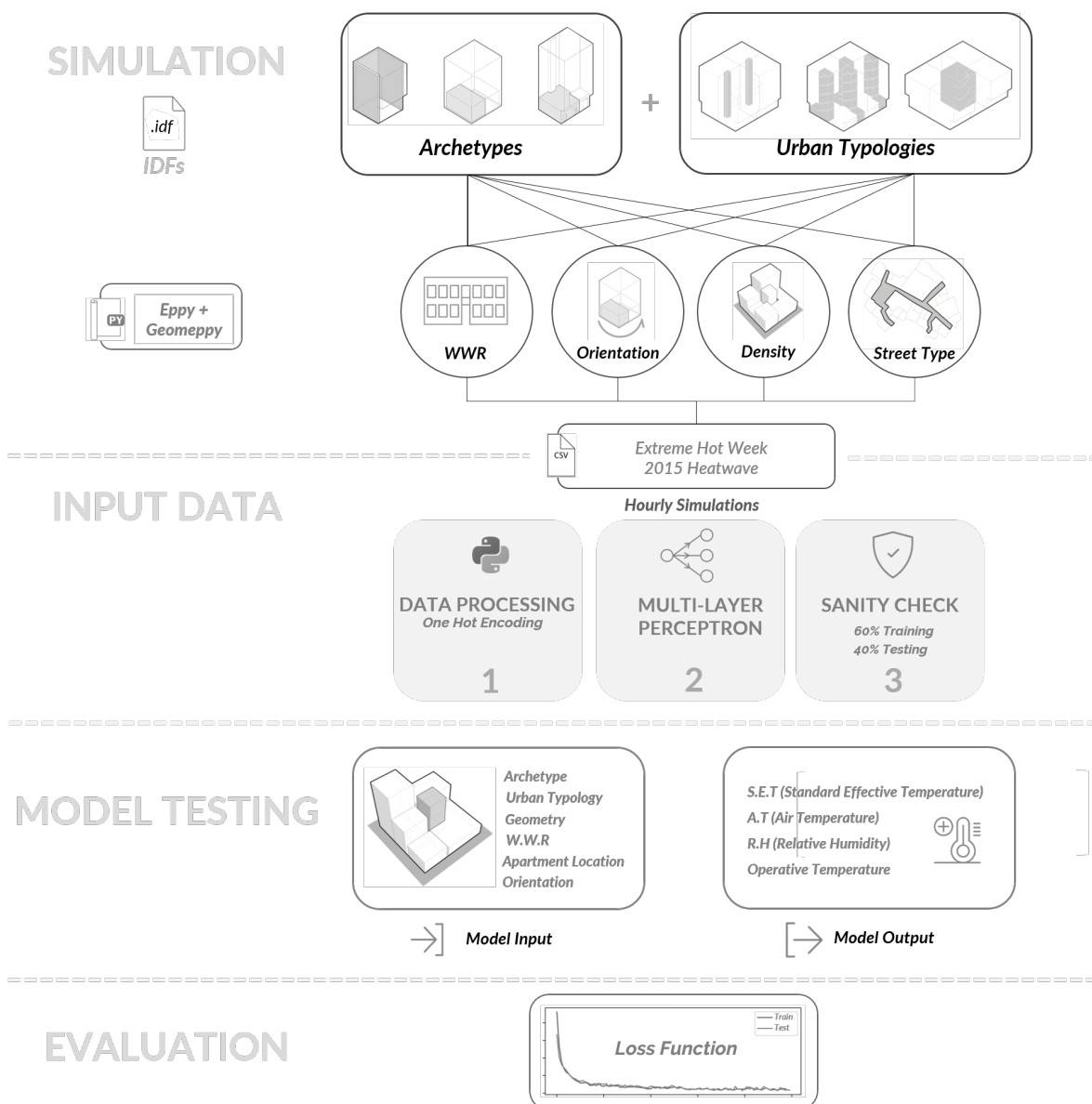
Figure 3-33: Simulation Workflow Diagram.

3.8.3 ANN Model Architecture

Multilayer perceptron (MLP) is one of the most widely used neural network models in the building science field (Fadare, 2009; Guresen, Kayakutlu, & Daim, 2011). MLP models are composed of several layers linking inputs to specific outputs (Thomas & Soleimani-Mohseni, 2007). The procedure of MLP is based on non-linear mapping for a set of input data to multiple outputs in an adaptive manner which is achieved through learning from examples using backpropagation algorithms (Magoulès & Zhao, 2016). In MLP, error-correction learning is used to train the ANN, where errors are propagated through the network and modified in the hidden layer (Chae, Horesh, Hwang, & Lee, 2016). MLP has also been applied in various scientific fields such as medical research (Nasser & Abu-Naser, 2019), environment (Banerjee, Singh, Chatttopadhyay, Chandra, & Singh, 2011; Iglesias et al., 2014), and building energy (Chae et al., 2016; Neto & Fiorelli, 2008). From the literature, it has been found that MLP can provide the desired accuracy in prediction with only a single hidden layer and a sufficient number of neurons. Therefore, in this work, MLP can be used to predict indoor thermal conditions for urban stock in AlDarb Al Ahmar district. The structure of MLP is fully connected and consists of three layers: input layer to gather model's input vectors (x), a hidden layer (h) that is characterized by non-linear neurons, and output layer to yield output vectors (y) (Moradzadeh & Pourhossein, 2019; Seo & Eo, 2019). Figure 3-34 illustrate the schematic non-linear mapping between input and output vectors. Each layer contains 64 neurons where each neuron is connected through weights, and output is activated with non-linear ReLU Function (rectified linear unit: max (0,x)) to help the neural network to stack deeper (Eckle & Schmidt-Hieber, 2019). The MLP is formalized using the following equation:

$$Y = \left(b + \sum_{i=1}^{N} w_i x_i\right) \qquad (1)$$

Where: Y is the output signal, f is the nonlinear transfer function, b is the bias, x is the input signal, and w is weight vectors a for N (number of inputs). The reasoning behind using MLP is due to their ability to learn through training (Thimm & Fiesler, 1997) from a dataset with known input and output vectors. Thus, simulation data will be used as input vectors to train the MLP model to forecast indoor conditions.
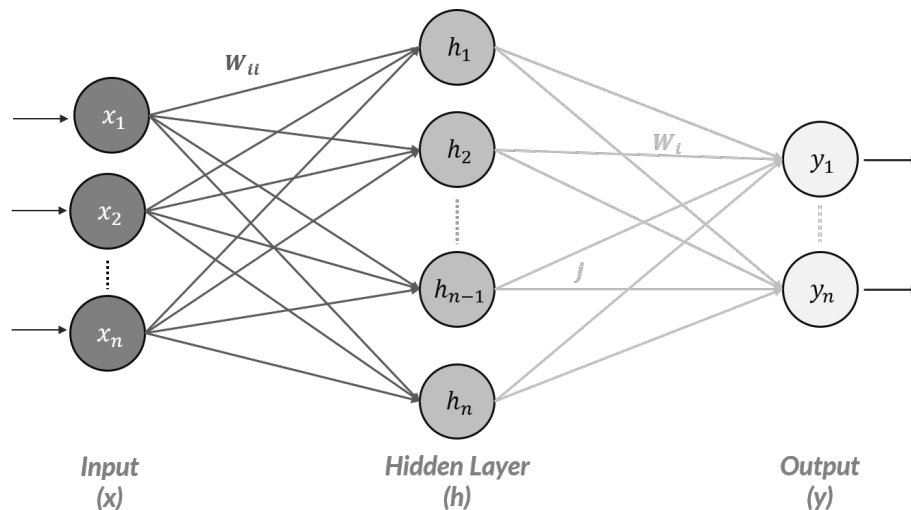
Figure 3-34: Schematic structure of Multilayer Perceptron (MLP). Based on (Thimm & Fiesler, 1997).

3.8.4 Model Learning, Testing, and Evaluation

There are three primary phases to improve the MLP model's accuracy in prediction; learning, testing, and generalization (Mba, Meukam, & Kemajou, 2016). The learning step involves using a training dataset (hourly simulations output) of N inputs and outputs paired in the form of D= $\{x_i, t_i\}_{i=1}^{N}$. The variable x represents the samples of each of the input vectors (n_y+n_u+1), t is the target input variable which corresponds to the simulation outputs for indoor air temperature, relative humidity, mean radiant temperature, operative temperature, and standard effective temperature. In the learning phase, the weight of each input vector (w) is adjusted to minimize an error function J, which represents the sum of squares of errors between simulation output t_i and model prediction $y_i= y (x_i; w)$ using the following equation:

$$J(w) = \frac{1}{2} \sum_{i=1}^{N}\{y_i - t_i\}^2 = \frac{1}{2} \sum_{i=1}^{N} e^2 \qquad (2)$$

Backpropagation was used as the learning algorithm as it is considered the best convergence to a minimum of mean square error (MSE) (Haykin, 1999). Testing and generalization phases involve evaluating the MLP model to produce accurate output when tested with data examples not used in the learning phase. In this model, there are 12 feature vectors used as inputs and four-vectors as outputs representing indoor air temperature, relative humidity, operative temperature, and SET (Figure 3-35).
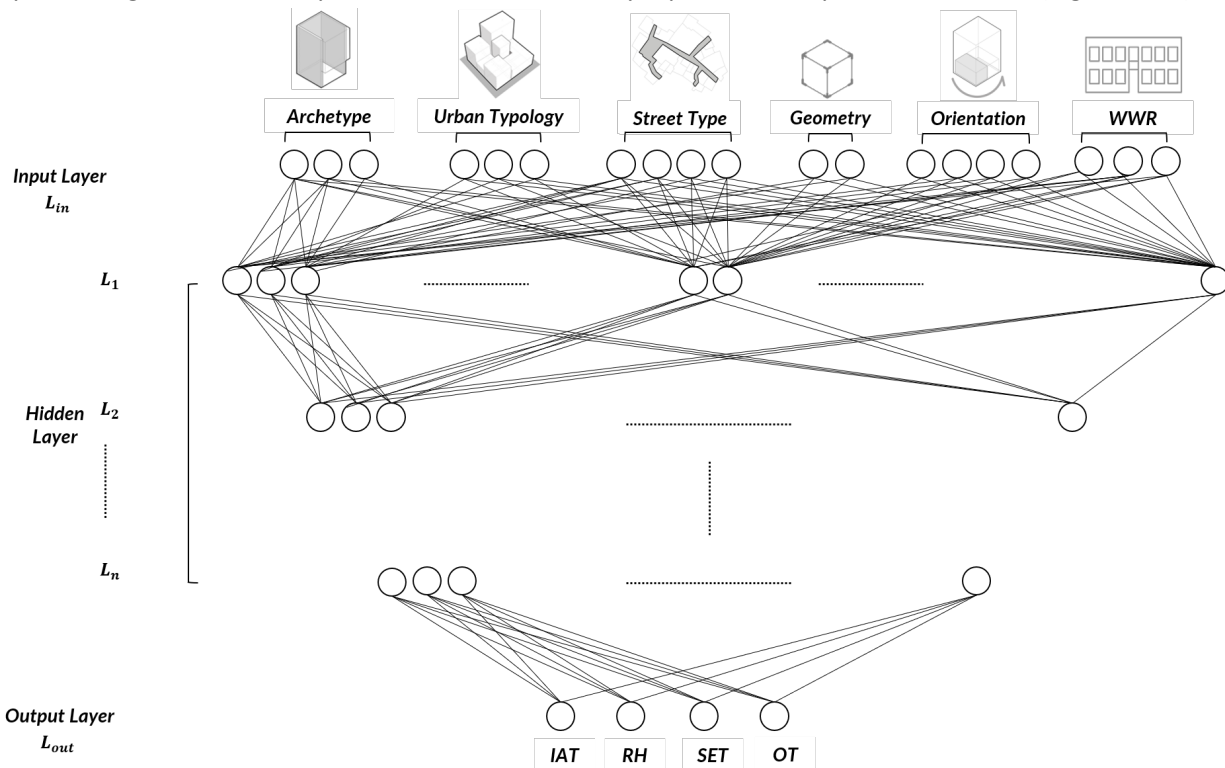
Figure 3-35: MLP structure with inputs and output vectors.

The data set consisted of 720,000 simulation points divided into 60% as training/learning data and 40% as testing data to validate and evaluate the accuracy of the prediction of each network. The cost function MSE (Mean Square Error) was used to assess the prediction error between actual and predicted values in

the training process. The primary purpose of the training process is to minimize the cost function that is implemented by adjusting the weights iteratively using the following equation:

$$\omega - \eta \; \frac{\partial c(\omega,b)}{\partial \omega} \rightarrow \; \omega', b - \eta \; \frac{\partial c(\omega,b)}{\partial b} \rightarrow \; b' \quad (3)$$

Where η is the learning rate that determines how quickly or slowly to update the weights and parameters based on the model's ability to predict actual value. The model training process was relatively fast as it took around 620 seconds to train the model using 1,038,240 data points and the prediction time for 692,160 points took about 242 seconds.

Numerous statistical indices are used in the literature to evaluate ANN predictive performance (Banerjee et al., 2011; Seo & Eo, 2019). These indices include Coefficient of Variation (CV), Root Mean Squared Error (RMSE), Mean Squared Percentage error (MSPE), and Mean Absolute Error (MAE), Mean Square Error (MSE), and the coefficient of correlation (R). After training and testing each neural network in the MLP model, MSE was used to assess the model's accuracy and performance. The specific definition of all the performance indices is provided in equations (3-7) below.

$$Root \; Mean \; Square \; Error \; (RMSE) = \; \sqrt{\frac{1}{N}\sum_{i=1}^{N}(x_i - y_i)^2} \qquad (4)$$

$$Mean \; Absolute \; Errot \; (MAE) = \frac{1}{N}\sum_{i=1}^{N}|x_i - y_i| \qquad (5)$$

$$Coefficient \; of \; Determination \; (R) = \; \pm\sqrt{\frac{\sum_{i=1}^{N}(y_i-x_i)^2}{\sum_{i=1}^{N}(x_i-x^-)^2}} \qquad (6)$$

$$Coefficient \; of \; Variation \; (CV) \; = \; \sqrt{\frac{\frac{1}{N}\sum_{i=1}^{N}(x_i-y_i)^2}{y_i}} \qquad (7)$$

$$Mean \; Square \; Error \; (MSE) = \; \frac{1}{N}\sum_{i=1}^{N}(x_i - y_i)^2 \qquad (8)$$

Where:
x_i is the actual value and y_i is the predicted value, and N is the total data in the dataset used for prediction evaluation. All prediction values are rounded off, and the final prediction value was used to calculate Mean Square Error (MSE) and the model's total accuracy, as discussed above. The MLP model architecture and structure were developed in a Python environment using the following libraries: Pytorch, Pandas, Numpy, Skilearn, pandas, Keras, and TensorFlow.

3.8.5 Model Performance and Validation

After training the model using the data described above, the results presented in Figure 3-36 shows the variation trend of the error convergence throughout the learning process over training epochs for indoor air temperature (IAT). The training data set was divided into 30 epochs, with each epoch contained 34,600 points. It can be noted that the initial training period and error curve decreased significantly and very quickly. Also, the minimum error was reached after nine training epochs and reached a stable value. It can be indicated from Figure 3-36 (left) the model achieves 0.25 temperature difference after training on 1100 data point only, which implies that the model can learn efficiently from a small data sample that covers all archetype cases.
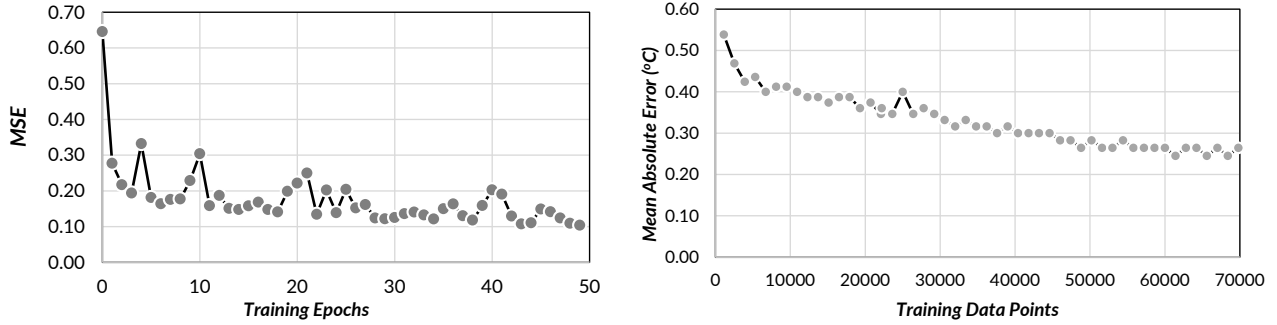
Figure 3-36: Left, Error Convergence Curve for each training cycle (epoch), Right, MAE during training in °C.

Figure 3-37 compares model outputs and actual simulation results for SET. The model's prediction accuracy improved significantly after five training epochs. Next, a validation test was conducted for 20 simulation points for the four predicted parameters to calculate the Mean Square Error (MSE) to make the results independent of the selected initial parameters.

| Before training | After 5 epochs | After 9 epochs |
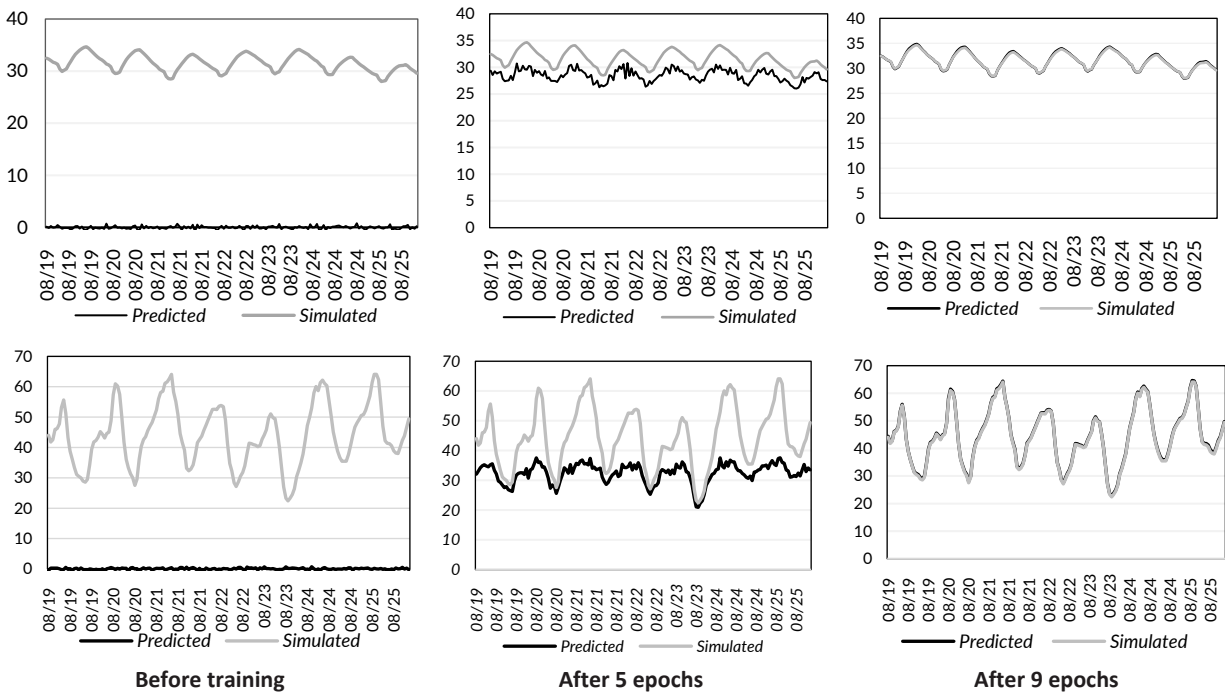
Figure 3-37: Predicted SET and Relative Humidity from MLP and actual values for different training epochs.

Four different testing sets were created to calculate the model's performance through the training. Set A for indoor air temperature, set B for SET, set C for relative humidity, and set D for operative temperature. The MSE for set A is 0.42 at the beginning of training for 1000 datapoint and 0.12 for set D, while the average mean absolute error for the model is 0.12 after training for 420,000 points. Table 3-8 summarizes MAE for training sets for the 4 examined parameters at the beginning of the training at 1000 data points and the end of the training at 420,000 data points.

Table 3-8: MAE for the four testing sets at the beginning and the end of the training.

	Set A	Set B	Set C	Set D
MAE (1000 point)	0.42	0.36	0.85	0.13
MAE (420,000 point)	0.09	0.098	0.197	0.12

3.9 District Level Prediction

As discussed above, an MLP model was developed to help predict indoor exposure and heat vulnerability assessment at the district level. As illustrated above, the model has shown a decent accuracy in predicting indoor conditions represented in the four tested parameters, namely, indoor air temperature, SET, relative humidity, and operative temperature. Next, MLP model prediction outputs are combined with classical computer vision methods to model heat vulnerability for AlDarb Al Ahmar district. Here, a building stock map for AlDarab Al Ahmar district was used to assist in spatially visualizing the distribution of blocks or buildings with higher vulnerability levels and prioritize areas of intervention. The research develops an assessment profile as input data to perform district-level prediction for indoor exposure and heat vulnerability. The assessment profile carries eight sources of primary information: archetype, building orientation, number of floors, building geometry, apartment location, street type, WWR, and urban block typology. These input data are then detected and translated from a 2D image and fed into the MLP model to predict indoor conditions at the district level. The district-level assessment workflow is based on pixel analysis techniques to detect archetypes class, urban typology, orientation, building geometry, and street type from 2D image data.

a. Detecting Archetype: to differentiate between different archetypes, the research used pixel analysis to detect building archetypes based on a survey map that contained color-coded information for all archetypes (Figure3-38). Most of the pixel analysis methods are sensitive to any changes in pixel data; thus, color distribution was unified for the survey map to analyze the pixel properties in the color space and characterized each pixel according to its three trichromatic components, red (R), green (G), and blue (B), where all red color derivates in the image have the same value, so the information in all pixels of the same color is unified. For this purpose, the research used the KNN algorithm (K-Nearest Neighbor). KNN algorithm is an unsupervised algorithm used to classify all pixels' values by assigning them to the same color class (Z. Zhang, 2016). The KNN function uses Euclidean distance to classify pixels of the same color using the following equation:

$$D(p,q) = \sqrt{(p_1 - q_1)^2 + (p_2 - q_2)^2 + \cdots + (p_n - q_n)^2} \quad (9)$$

Where p and q are pixel values compared with n characteristics which is here a tuple of (Red, Green, and Blue). Next, graph theory methods are applied to detect all pixels of the same color to detect each archetype within the 2D map. Here the research uses Breadth-First Search (BFS) algorithm to detect all pixels of the same color value and output them into an archetype class (Figure 3-38). The BFS algorithm is a graph search algorithm applied to find all vertices/pixels from a given vertex or pixel (Silvela & Portillo, 2001). The BFS workflow starts with an arbitrary pixel, visits all neighboring pixels outwards and in all directions level by level, and outputs all pixels of the same value in a queue or boundary, as shown in Figure 3-38 below.
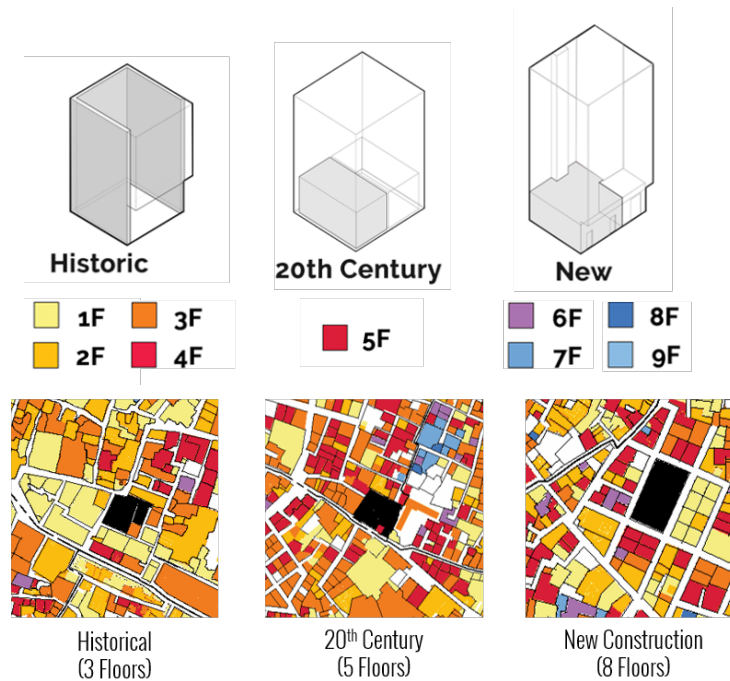
Figure 3-38: Top, Archetypes and their color classes, Bottom detected archetypes from the BFS algorithm.

ii. Detecting Building Orientation: Next, pixel analysis methods are applied to detect building orientation from the 2D image. For a given archetype detected, the center pixel is calculated using the following equation:

$$(x, y) = \left[\left(\frac{x_{min} + x_{max}}{2} \right), \left(\frac{y_{min} + y_{max}}{2} \right) \right] \quad (10)$$

Where, (x,y) represents the coordinate of the center pixel, x_{min} is the leftmost pixel located the building boundary, x_{max} is the rightmost pixel, y_{min} is the bottommost pixel, and y_{max} is the upmost pixel. After calculating the center pixel, arrows are expanded in all possible directions (Figure 3-39) to identify the orientation. This is determined by how many arrows' paths will be disconnected with another archetype and how many will be disconnected by a street. The building orientation is detected and represented by overlooking a street; thus, for those arrows disconnected by streets, the median value is estimated at the y axis angle to define the building orientation. The orientation angle is calculated assuming the main north orientation on the map is facing upwards.

b. Urban Typology: using the following pixel analysis approach in orientation detection, the research applies the same approach to detect urban typology where the archetype of interest is located. Here the typology type is estimated based on the density of the urban block (number of surrounding buildings). After calculating the center pixel following the above approach, the percentage of arrows disconnected by a neighboring archetype is calculated. For example, if ~25% of the arrows were disconnected by an adjacent building, it denotes a low-density urban block, ~ 50% represents medium density, and high density if ~75% of the arrows were disconnected by a neighboring archetype. Since archetypes are detected at the pixel level described above, the urban block typology can then be identified. For instance, if the results represented a low-density urban block and surrounding pixels are historical archetype classes, this building is located in historic urban block typology.

c. Building Geometry: next, archetype geometry is determined, whether its square plan or rectangular. This process is carried out by estimating the detected archetype pixels ratio using the following equation:

$$G_a = \frac{x_{max} - x_{min}}{y_{max} - y_{min}} \quad (11)$$

Where, G_a is the detected archetype geometry, x_{max} & x_{min} are the maximum and minimum pixel values in the x-direction, and y_{max} & y_{min} are the maximum and minimum pixel values at the y-direction. If the ratio between pixels' value at the x and y direction is close to 1, the archetype's geometry is a square; otherwise, it will be rectangular. Therefore, the ratio threshold for a square geometry is set between 0.9 and 1.1 and rectangular to be less than 0.9.

d. Street Width: a pixel analysis algorithm is developed to detect street type (width) that is based on two primary steps: 1) identification of border pixels and 2) calculating street width based on vector length. In the first step, the pixels group that represents the street boundary is identified. These pixels represent a street-side if not located within the boundary of the detected archetype or another adjacent archetype. After detecting the pixels group that doesn't belong to the detected archetype and lies within a street, the average vector for every pixel located on the detected street-side is calculated.

In the second step, the length of every vector passing through the street until an opposite archetype disconnects it is calculated, where the average length of all vectors passing through the street will denote the total street width.

After detecting the assessment profile with eight primary inputs for a given archetype in the 2D image, the trained MLP model described above is applied to run district-level prediction for the four key parameters.

The MLP will produce 168 hourly simulation values representing each hour of the day for an extreme hot week. Thus, each apartment in each of the different archetypes will have a matrix of values (4, 168) where four rows correspond to the key examined parameters and their hourly simulations. For optimization and fast performance, the model exploits a parallelization technique to compute the values of multiple parameters at the same time instead of computing one parameter for each apartment in a sequential process using the TensorFlow Python library to compute outputs simultaneously. This parallelization allows the model to perform simulations in a time-efficient manner compared to regular simulation workflow. The model takes two seconds to compute each of the four parameters for 5000 buildings.

3.9.1 Heat Vulnerability & Adaptive Capacity

Adaptive capacity at the district level has been widely explored using large-scale data on population socio-economic characteristics. However, adaptive capacity at the district level, considering household level exposure and surrounding urban amenities, is an understudied area in heat vulnerability assessment (Cai et al., 2019). Here, the output from district-level heat vulnerability assessment and distribution of surrounding urban amenities is used to examine the overall adaptive capacity that can guide short-term interventions against potential extreme heat exposure and long-term adaptation strategies. For heat vulnerability assessment, as it was discussed in chapter 2 of this dissertation, vulnerability is a function of Susceptibility (S), Exposure (E), and adaptive capacity (AC). vulnerability is considered a function of an

urban area's susceptibility to heat exposure and its adaptive capacity, where vulnerability is calculated using equation (12) as follows:

$$V = (E + S) - AC \qquad (12)$$

V represents vulnerability, E is the exposure of an urban area or building, S is the susceptibility, and AC is the adaptative capacity. There are many existing methods for heat vulnerability at the district-level, such as using GIS data to perform spatial assessment (Inostroza, Palme, & De La Barrera, 2016), principal component (Zhu et al., 2014), multi-criteria analysis (Rinner et al., 2010), and equal weight method (Weber, Sadoff, Zell, & de Sherbinin, 2015). The research chooses the equal weight method for this work as it has been proven to be simple to use and more effective in realizing multi-level evaluation in large-scale heat vulnerability assessment studies. Using equation 12, heat vulnerability at the district level is assessed. The process of district-level heat vulnerability assessment is carried out using the following steps:

Step 1: Calculate exposure at the building level and output buildings where indoor air temperature exceeds 34°C based on human monitoring results conducted at the first half of this chapter and SET is above 30 °C following LEED passive survivability guidelines (LEED, 2021) for more than four consecutive hours of the day during the extreme hot week.

Step 2: Calculate Susceptibility at the building level based on building age. Here historic buildings with no retrofit are considered more susceptible to heat exposure than the new construction archetype. The algorithm used to detect archetypes was also utilized to output the distribution of older buildings in AlDarb Al Ahmar district.

Step 3: Calculate adaptive capacity at the urban block level. The research considers 500 meters of walking distance proximity to cooling shelters and al Azhar park as an indicator for adaptive capacity at the urban block level using the graph search algorithm BFS described in detail in chapter 4. The BFS algorithm was used to compute the distance of each pixel or group of pixels from a specific amenity class and identify the shortest path from the source (heat adaptation amenity). The reasoning behind this approach is to examine heat vulnerability distribution in scenarios where power supply is not available, which is a typical case in Cairo during the summertime. Thus, adaptive capacity outside the building level was evaluated to account for surrounding urban amenities that can improve occupants' adaptive capacity mechanism during extreme heat exposure, using the graph search algorithm described above to calculate the distance of each building to Al Azhar Park. Finally, the three vulnerability indicators described above, exposure, susceptibility, adaptive capacity, were normalized using an equal weight approach to calculate heat vulnerability at the district level (Figure 3-39).
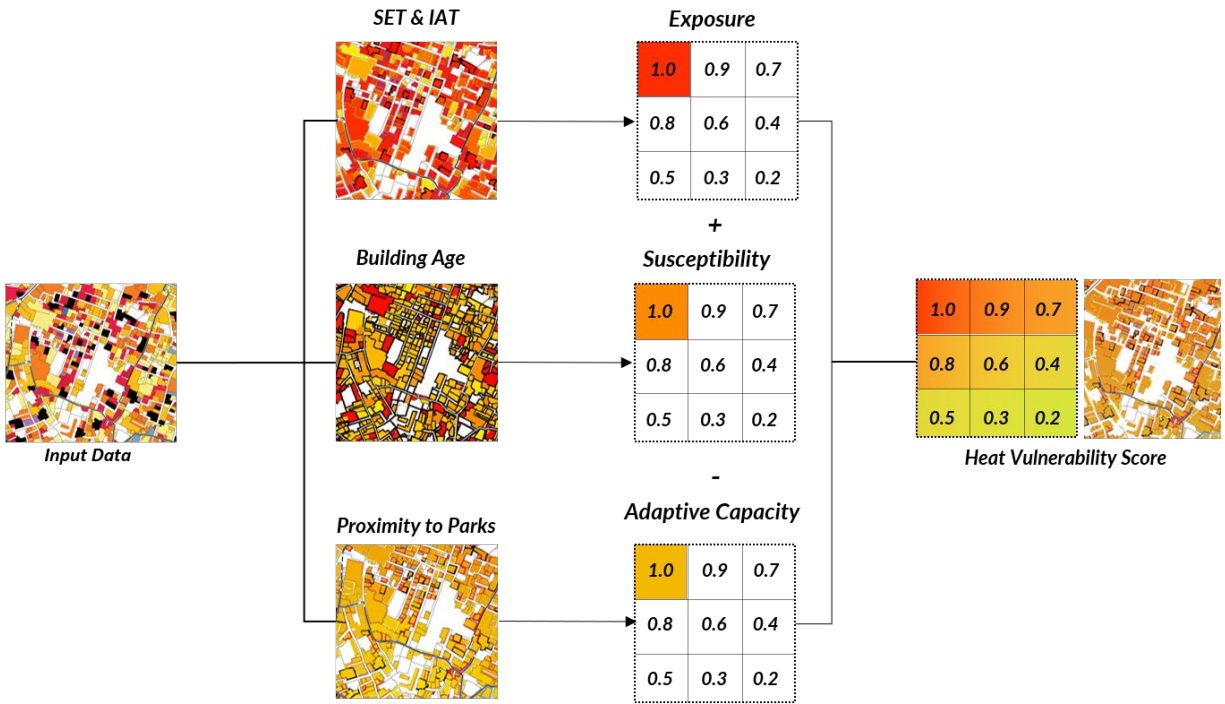
Figure 3-39: The three steps used for district-level heat vulnerability assessment.

3.10 Results

Figure 3-40 presents the average extreme hot week output at the district level for indoor air temperature and SET, where each color represents the weekly average per building. It can be noted that these results confirm with results presented in individual archetype simulations where indoor air temperature and SET are higher for new construction archetypes that are primarily located in new urban fabric urban typology. Results from the model were translated into a web visualization tool (mena-cc.com/heatwaves) where the python model runs online and produce hourly simulation results per building and per apartment by floor location based on user interaction for the four examined parameters in this research, namely, indoor air temperature, relative humidity, SET, and operative temperature. The purpose of the MENA heatwave platform is to act as a medium to present these results for interested policymakers at the district level on locations with high indoor exposure and strategies to improve district adaptive capacity.
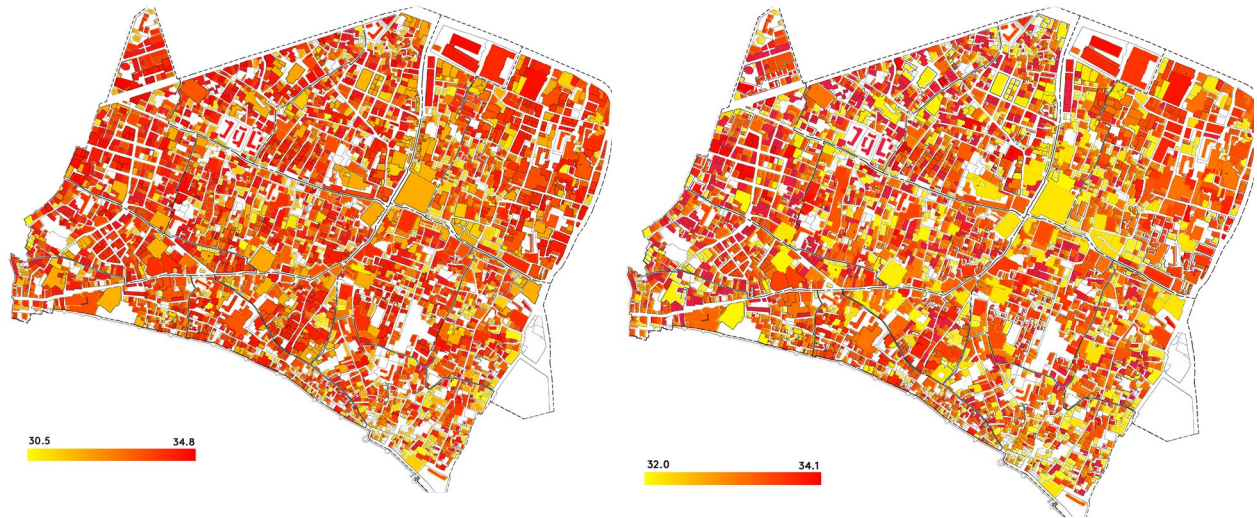
Figure 3-40: Left, Average indoor air temperature and Right SET for an extreme hot week at the district level.

Next, a district-level exposure assessment was used to estimate overall vulnerability following equation 11. Since the ML-based approach outputs four main indoor climatic parameters, the BFS algorithm was used to detect at the pixel level buildings, roads, and available open space to evaluate adaptive capacity at the district level. Here the research considers proximity to open spaces/parks as an indicator for adaptive capacity. As highlighted earlier, Al Azhar Park is the central open space in AlDarb Al Ahmar district that residents use as an outlet when indoor temperature increases, which was also identified from the questionnaire. Figure 3-41 represents adaptive capacity at the district level considering proximity for Al Azhar Park within walking distance of 200 meters. The assessment of adaptive capacity is then normalized and used to calculate vulnerability at the district level.
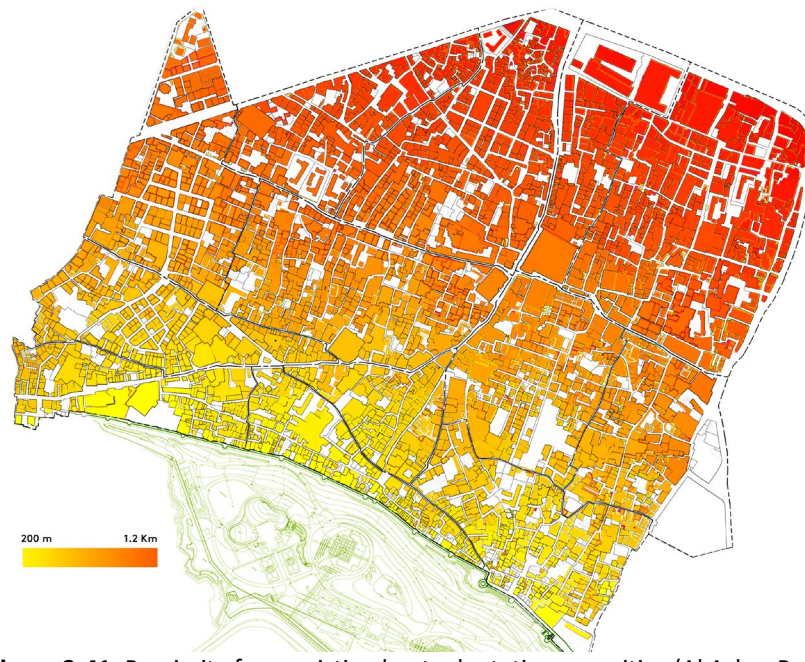
Figure 3-41: Proximity from existing heat adaptation amenities (Al Azhar Park).

Following the methodology described in section 3.8.5, heat vulnerability at the district level is calculated, as illustrated in Figure 3-42. It can be noted that although historic archetypes had higher indoor

conditions, buildings that are within proximity to Al Azhar park had lower vulnerability due to their high adaptive capacity. This level of capability to compute heat vulnerability at the district level would assist policymakers in identifying areas with limited adaptive capacity and building stocks/archetypes at high risk due to either high indoor exposure or limited access to adaptation resources and prioritizing sets of adaptation intervention based on vulnerability assessment.
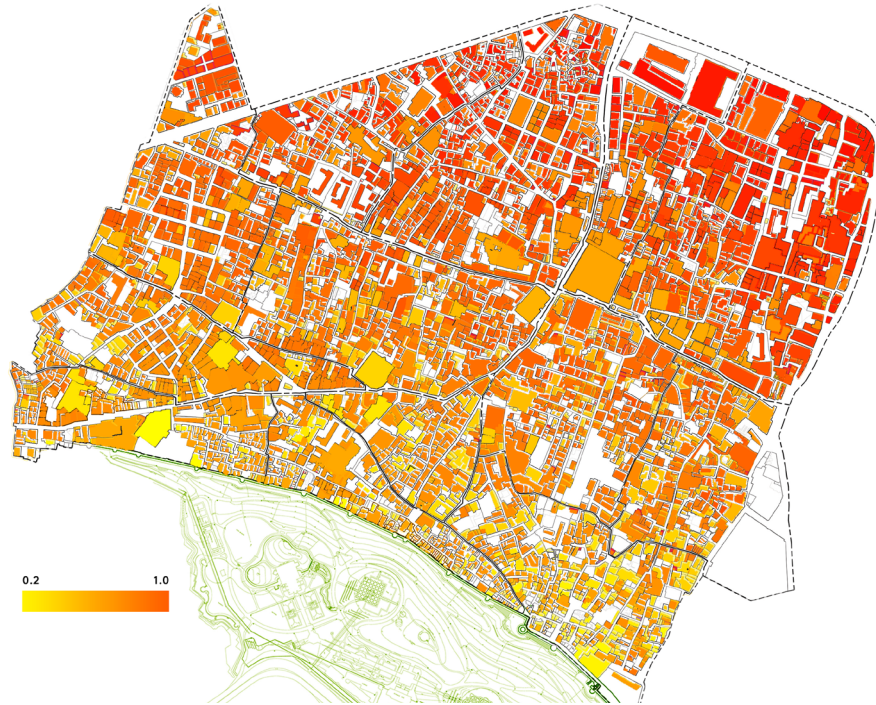
Figure 3-42: Heat Vulnerability at the District level based on existing conditions and adaptive capacity amenities.

Next, the output from the vulnerability assessment at the district level was used to identify possible interventions to reduce vulnerability against potential heat exposure in the face of climate change. As discussed above, most residents who don't have direct access to Al Azhar park go to Midan or use the building roof when indoor temperature increases. The research examines changes in heat vulnerability through two main urban intervention scenarios; i) increasing access to open spaces/urban parks and ii) adding cooling shelter. The research considers available unutilized vacant plots in AlDarb Al Ahmar to be transformed into open spaces to provide equitable access to adaptation resources especially given the limited time frame to Al Azhar Park. From the site survey and Aga Khan site plan for vacant buildings, around 65 unutilized buildings can be retrofit and used as a community center all year round to serve the local community and be used as a cooling shelter during the summer months. This will improve residents' adaptive capacity against future heatwaves, mainly because around 89% of the surveyed sample didn't have access to AC. Figure 3-43 illustrates heat vulnerability after adding open spaces to improve total adaptive capacity.
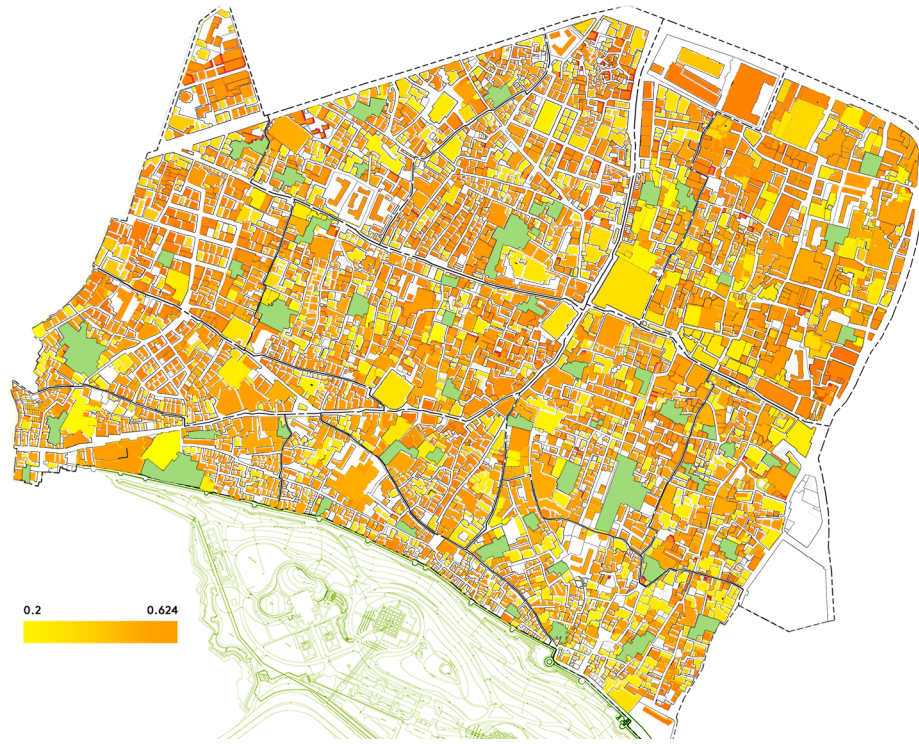
Figure 3-43: Heat Vulnerability after improving adaptive capacity by reutilizing vacant plots as open spaces.

Figure 3-44 presents heat vulnerability after adding cooling shelters. It can be noted that the average vulnerability was reduced by 97% after adding open spaces compared to the base case presented in Figure 3-42 and by around 93% after adding cooling shelters. These two interventions can significantly reduce potential heat risks at AlDarb Al Ahmar district during future heatwaves. Yet, the cost of these interventions is a critical parameter while determining the most suitable strategies. Thus, the cost of an average park with 300 m^2 was compared to retrofitting an existing building with the same area in Cairo. It was found that utilizing vacant plots into open spaces would cost around 150,000 L.E (9500$) compared to 450,000 (29,000$) to retrofit an existing building of the same area (AECOM, 2019; Gleeds, 2020). Findings from the analysis presented in this section show that adaptive capacity is an important measure when conducting a heat vulnerability assessment. The workflow presented here for district-level vulnerability assessment will be helpful to identify drivers of vulnerability, whether from indoor heat exposure at the building level or limited access to heat adaptation amenities at the urban block level. This will be helpful to identify which strategies can be most effective and urban areas that more attention while planning these strategies. Also, occupants' behavior during extreme heat exposure can be used as an indicator to identify what set of urban interventions can be utilized to improve adaptive capacity.
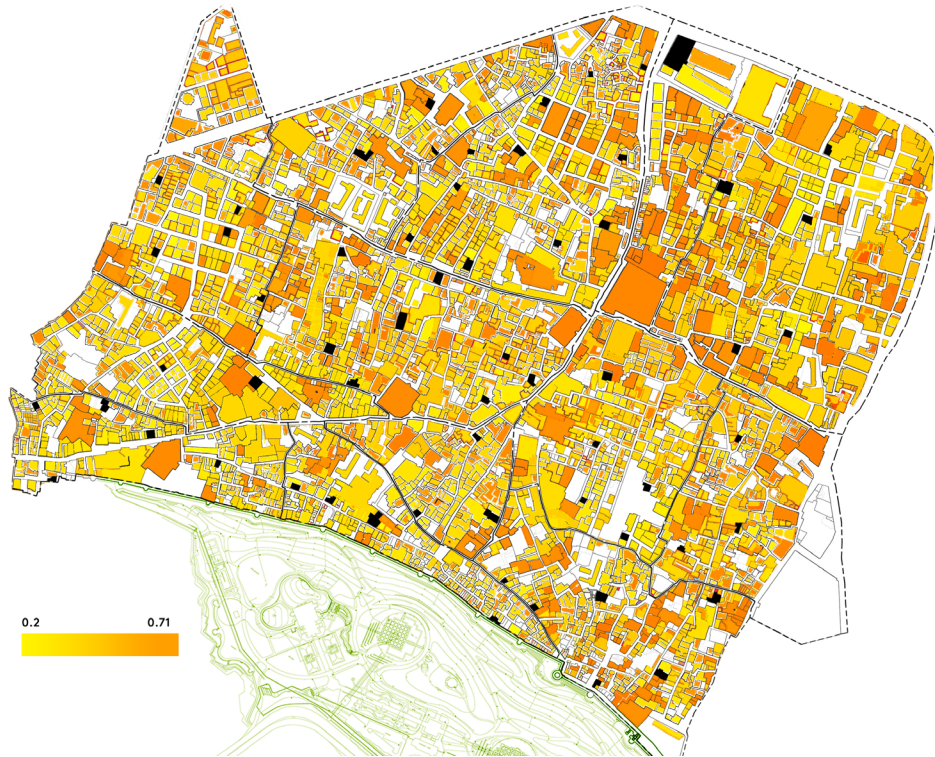
Figure 3-44: Heat Vulnerability after utilizing vacant houses as cooling shelters.

3.11 Discussion

The section presented ML model as an approach for large-scale urban assessment of heat vulnerability and indoor exposure at the building scale. Although ML has the advantage of providing valuable information for large-scale evaluation in a time-efficient manner, there are some limitations. First, since ML models are all data-driven models, they tend not to perform outside the training data, limiting the applicability of the developed model to other cases. For instance, the proposed model was trained on data for building stock representation in Cairo, and extreme hot week simulation, will not perform outside that data set, annual indoor heat exposure. However, this problem can be addressed by extending the training dataset to include more extensive data ranges with retraining techniques to ensure that ML models can accommodate new datasets effectively. The second limitation was overfitting when the model learned too much from training datasets and reduced prediction accuracy. Yet, this problem can be addressed using existing methods with outside training to increase forecasting generality. Also, early stopping throughout the training can help reduce overfitting and maintain the model's accuracy and increase generalization in prediction (Singaravel, Suykens, & Geyer, 2018).

Another limitation is that ML models are black-box models; thus, they cannot understand the underlying structure of the parameters' behavior. To overcome this problem, ML models can be combined with physics-based and mathematical models, such as combining simulation models or measured data with ML models. Finally, previous research has identified that inadequate parameter selection during model development can lead to poor forecasting and affect the overall model's performance (Wei et al., 2018). Numerous methods can assist in selecting model parameters, such as expert knowledge in ANN early development and automated architecture selection methods.

The proposed workflow described in the second half of this chapter offers an opportunity to replicate this framework to other districts with different training datasets to carry out heat vulnerability assessment that considers building-building indoor exposure at the district level. The ML model was developed from simulation-generated data and later used to estimate district-level exposure and associated heat vulnerability. Using simulation data was proven to help highlight the effects of different parameters related to building physical characteristics rather than depending only on measured data sets of indoor conditions to train the model as explored in other studies. The main findings in this work's scope indicate that the ML-based approach is very accurate in assessing indoor heat exposure at the district level with minimum computational needs and in a time-efficient manner compared to traditional methods. The proposed ML framework will also be helpful for a neighborhood with vulnerable population characteristics that need to perform assessment rapidly and effectively to identify the types of necessary interventions to help adapt to future climate conditions.

3.12 Summary

Planning for district-level heat vulnerability assessment that accounts for the physical characteristics of individual buildings is a challenging task. While it's a necessary process for policymakers, planners, and stakeholders involved in the heat adaptation planning process to identify what types of urban interventions are required, developing a district-level simulation model is a computationally expensive process. The framework proposed in this chapter overcomes some of these challenges by incorporating ML and image processing techniques as a new way to examine heat vulnerability and related risks at the district level. The chapter presented an assessment workflow that combines whole building energy simulation models and machine learning methods to carry out large-scale heat vulnerability assessments. Then the chapter briefly explored how outputs from the assessment can be used to explore simple strategies to improve the overall district-level adaptive capacity against future heat risks.

The framework of detailed heat vulnerability assessment at the building level coupled with occupants' behaviors and their psychological and physiological characteristics is critical to identify areas of high risks and estimate the percentage of the population at high risk and distribution of building stocks that are more susceptible to increase in temperature in the future. Finally, the hybrid model of simulation-based and ML-based methods presented in this chapter provide a replicable framework to identify the impacts of urban intervention strategies on the overall heat vulnerability at the district level to assist in the decision-making process.

IV. AERIAL THERMOGRAPHY FOR RAPID VULNERABILITY ASSESSMENT

The building envelope holds substantial energy efficiency and heat risk mitigation opportunities, especially in the residential sector. Around 25% of buildings' total energy use results from heat gains and losses of the building envelopes ((DOE), 2015). As discussed in the previous chapters, building physical characteristics play an essential role in mitigating potential health-related risks from heat exposure. The lack of sufficient information on the performance of existing buildings makes it difficult to assess the impact of retrofit strategies to face heat exposure risks and, as a result, makes tackling building envelope improvements quite challenging. For example, excessive heat gain and associated energy use issues that result from damaged or missing insulation are challenging to detect until after the damage cost becomes expensive (National Renewable Energy Laboratory (NREL), 2012). Also, problems can occur from improper verification of the thermal performance of façade materials of existing buildings under extreme weather conditions. In addition, the thermal envelope assembly may deteriorate over time with a resultant decrease in performance. This chapter examines the use of Unmanned Aerial Vehicles (UAVs) to assess existing building envelope thermal performance as an approach to be utilized for rapid heat vulnerability assessment. The first section of this chapter presents a case study using aerial thermography for building envelope assessment in the Boston metropolitan area, Massachusetts. The study examines the applicability of using UAVs equipped with an infrared camera to estimate existing building thermal transmittance (U-Value) and its implication on detecting an envelope's thermal anomalies and enhancing the accuracy of Building Energy Modelling (BEM). The second half of this chapter expands the use of aerial thermography coupled with the evaluation of urban adaptive capacity to rapidly estimate potential areas of high vulnerability under extreme heat exposure, using a neighborhood in the Bronx, NYC as the case study.

4.1 Introduction

Over the past decade, automated calibration for BEM has been at the forefront of building science research. The majority of these techniques use optimization functions by iteratively adjusting the value of different parameters to reduce the discrepancy between simulated and measured data. Previous work (Nagpal, Mueller, Aijazi, & Reinhart, 2019) found that data-driven methods could deliver sufficiently reliable estimates of internal loads when auto-calibrating BEMs. However, these models presented discrepancies in estimating climate-dependent characteristics, mostly when envelope parameters were unknown. Therefore, it is vital to accurately determine the existing condition of building envelopes for the models to estimate retrofit savings reasonably using such methods. Building and site audits are two of the most commonly used techniques to reduce envelope-related uncertainty errors in simulation models (Coakley, Raftery, & Keane, 2014). The main goal of building inspections is to measure and evaluate energy consumption data, examine energy use patterns, and detect energy losses. Generally, there are three typical levels for building and site audits (Thumann, P.E., C.E.M. & Younger, C.E.M., 2017):

1- **Walkthrough:** energy use data are examined and quantified through a visual inspection of building energy systems to evaluate average energy use and establish benchmarks.
2- **Energy Audit:** this includes a detailed analysis of building energy losses and the characteristics of energy systems using site measurements. Also, at this level, the efficiency of building systems and energy conservation measures are evaluated.
3- **Investment Grade:** energy simulation models are developed and employed to predict annual energy use, considering weather conditions, building systems, and occupancy schedules.

Although building audit provides energy simulation models with vital information on the performance of building systems, it sometimes can be imprecise (Shapiro, 2009). Also, it can lead to inexact energy use evaluation and misrepresentation of energy savings potential. In addition, building audit is considered a time and labor-intensive process that can sometimes be coupled with situations where safety and accessibility are challenging (Rakha, Liberty, Gorodetsky, Kakillioglu, & Velipasalar, 2018; Shapiro, 2009). This chapter aims at addressing one of the most challenging, labor-intensive, and prone to error aspects of energy audits by using Unmanned Aerial Vehicle (UAV) platforms equipped with infrared cameras as a method to calibrate energy simulation models and rapid heat vulnerability assessment by estimating existing envelope's thermal transmittance. The first section of this chapter consists of three main parts: 1) background, which provides an overview of thermography applications in the evaluation of buildings' envelope; 2) methodology section, which describes main data collection procedures, and the developed simulation model for a case study; 3) results, which summarizes findings from the simulation model calibration and provides a conclusion of the study.

4.2 Background

In 1800, Sir William Herschel first discovered the infrared range in the electromagnetic spectrum (M. Vollmer, 2002). Later in 1840, John Herschel was the first person to record a "thermograph" image using evaporation differences of a thin-film directly exposed to a heat source (Kylili, Fokaides, Christou, & Kalogirou, 2014). After the 1940s, infrared imaging was mainly for night vision imaging in military applications (Barreira, de, Delgado, & Ramos, 2012). By the 1960s, infrared imaging was first commercialized and opened up for different applications, including building inspection and agriculture

applications (Barreira et al., 2012). Since the late 1970s, Infrared Thermography (IRT) has been widely utilized in building inspection, HVAC documentation, and energy audits (FLIR Systems, 2011). With IRT technology, it has become possible to quantify radiation emitted from objects' surfaces and convert them into thermographic images (Buzug, Schumann, Pfaffmann, Reinhold, & Ruhlmann, 2006). IRT also captures real-time thermal data on the building envelope that provides more accountable data than using standard thermometers that are profoundly affected by external weather conditions (Kirimtat & Krejcar, 2018). Over the past 25 years, IRT has been successfully implemented in the inspection and deterioration assessment for historic buildings and sites (Avdelidis & Moropoulou, 2003).

As mentioned previously, the most suitable retrofit strategies for a building's envelope can significantly affect the identification of appropriate retrofitting strategies to improve buildings' adaptive capacity under heat exposure. Thus, a comprehensive assessment of the envelope's performance is vital to improve energy efficiency. IRT is considered a suitable method for safer and more efficient evaluation of the whole building envelope thermal performance than the typical energy audit process as it enables access to building areas that can be considered risky to human lives such as roofs (Kirimtat & Krejcar, 2018; Tejedor, Casals, & Gangolells, 2018). However, prior to assessing the buildings' envelope, it is crucial to identify the appropriate assessment methods. This section provides an overview of the different measurement approaches using IRT as well as several analysis methods.

4.2.1 Infrared Thermography: Measurement and Analysis Schemes

The process of envelope evaluation using thermography can be classified into three steps: measurement, analysis, and documentation, as presented in Figure 4-1. First, the measurement step includes data collection and primary assessment of the envelope's existing condition. Second, the quantification of data uses numerical analysis to identify types of thermal abnormalities and their severity. Finally, documentation to summarize thermal anomalies detection, class, location, and overall assessment of the envelope.

Generally, most of the envelopes' thermal defects happen in three forms: moisture, air leakage, and conduction heat loss (Kirimtat & Krejcar, 2018). Each one has different visual and thermal characteristics that are important to identify. Additionally, the envelope's thermal defects are greatly affected by external weather conditions such as wind, air temperature, and precipitation (Kirimtat & Krejcar, 2018). There are two main approaches to examine thermal anomalies: qualitative and quantitative IRT (Schwoegler, 2006). The difference between the two methods is the regulation of measurement procedures, which need to be established before launching the analysis. Qualitative IRT is utilized to determine the presence of thermal abnormalities using visual evaluation of temperature differences in the measured radiation spectrum.
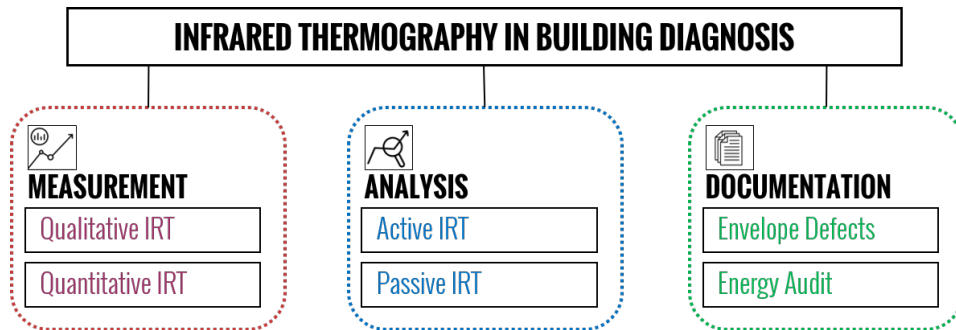
Figure 4-1: Classification of IRT in building performance diagnosis. Based on (Fox, Coley, Goodhew, & De Wilde, 2014; Kirimtat & Krejcar, 2018).

It should be noted that qualitative measurements only distinguish potential thermal anomalies, and do not estimate the severity of defects. Thus, this approach is mainly used when thermal anomalies are easily detectable (Fox et al., 2014). Also, thermographers need to have a sufficient level of knowledge to decide whether thermal differences imply potential defects or not. Additionally, qualitative IRT is suitable for damage identification in historic buildings' structures and envelopes' deterioration. Quantitative IRT is based on numerical analysis to quantify thermal anomalies (Pearson, 2011). This method is used for envelope thermal diagnosis, such as the determination of thermal transmittance. However, the main challenge in this method is that external weather conditions may influence the results' accuracy. According to the International Organization of Standardization (ISO), EN 13187:1998 (International Standards Organization, 1983), thermal irregularities caused by high thermal transmittance are commonly examined using qualitative thermography. In contrast, thermal bridges are mainly detected using quantitative thermography (Francesco, Giorgio, & Francesco, 2011).

In the building energy audit field, qualitative and quantitative methods are used at different process levels. At the walk-through level, qualitative IRT is used to collect information for the following parameters: a) performance of buildings' envelope; b) identification of air leakage and heat losses; c) evaluation of thermal insulation; d) characterization of building energy systems; and e) indoor climatic conditions for thermal comfort assessment. Quantitative IRT is used for the development of simulation models and quantification of thermal anomalies through the evaluation of the following parameters: a) thermal transmittance measurement; b) severity and percentage of thermal defects; c) examination of insulation quality; and d) moisture and air leakage determination (Kirimtat & Krejcar, 2018; Kylili et al., 2014). Figure 4-2 below summarizes levels of energy audit and types of IRT measurement used in each level.
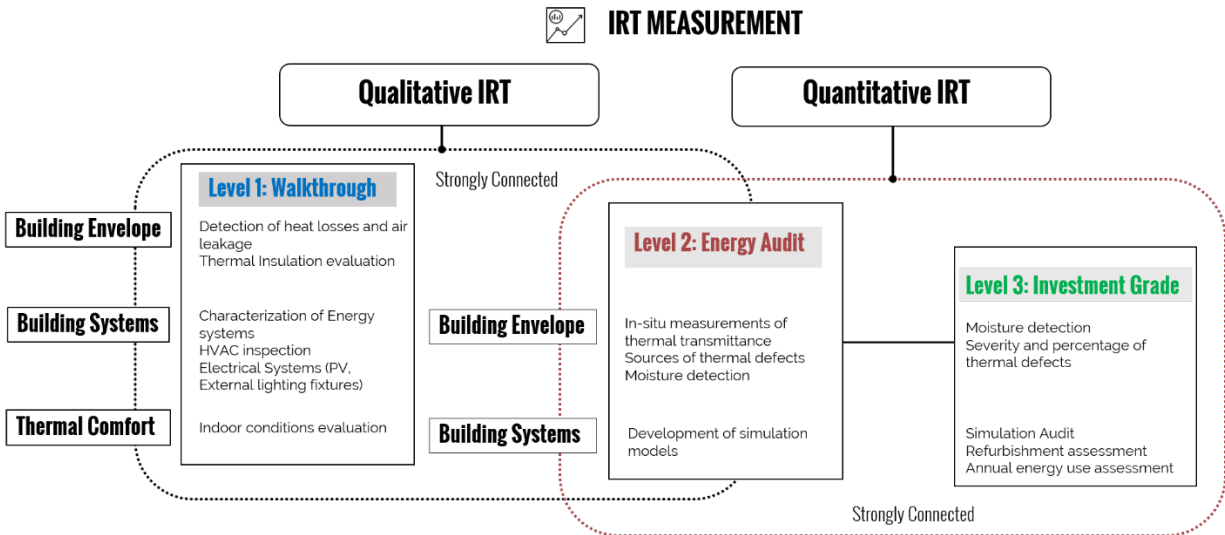
Figure 4-2: Measurements methods of IRT and their application in building energy audit. Based on (Kirimtat & Krejcar, 2018; Lucchi, 2018).

Thermography analysis techniques in the literature are classified into two approaches: active thermography and passive thermography (Fox et al., 2014; Lucchi, 2018). In the field of envelopes' thermal evaluation, both methods are used to detect the existing condition of façade materials. Passive thermography focuses on the whole building envelope to identify energy loss problems by measuring temperature differences under normal solar radiation conditions. Fox, Goodhew, and De Wilde (Fox et al., 2014) proposed eight different applications for passive thermography; 1) walkthrough survey (internal and external); 2) aerial thermography; 3) time-lapse; 4) perimeter walk around survey (exterior only); 5) automated fly-past survey; 6) street pass-by thermography; 7) repeat survey; and 8) mock target. They provided a detailed review and analysis of the potentials and limitations of different thermography applications. Aerial thermography was found to be most effective in identifying leakage problems for large scale buildings, but it is rarely used, while the automated fly-past survey is considered the most efficient in heat leakage from windows and moisture detection in roofs (Lucchi, 2018).

Walk-through and walk-around surveys are the most frequently used approaches in an energy audit, yet they are prone to changing weather conditions (Dall'O', Sarto, & Panza, 2013; Mateo-Garcia, Ahmed, & McGough, 2017). Active thermography concentrates on particular building envelope areas, where they are thoroughly examined to identify thermal defects. In this approach, an external energy source generates a temperature variation between the outdoor environment and the building's envelope. This approach is classified into a) Pulsed Thermography (PT), b) Lock-in Thermography, and c) Laser Spot Thermography (LST) (Lucchi, 2018). The drawback of this approach is that it requires prior knowledge of the existence of thermal defects before executing the survey (Haralambopoulos & Paparsenos, 1998; Sun, 2006). Lucchi et al. (2018) have found that passive thermography is the most common method in thermal anomaly detection. Figure 4-3 summarizes the application of thermography analysis methods in building audits.

IRT ANALYSIS
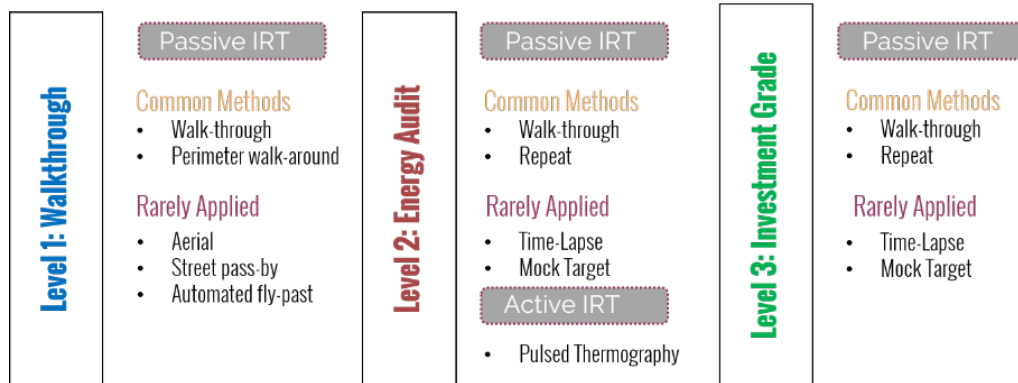
Figure 4-3: IRT methods and their application in building energy audit process.

Given the review presented above, it is essential to identify the primary purpose of the thermography survey before deciding what measurement and analysis methods are to be used. Fox et al. (Fox et al., 2014) have developed a decision-making process for thermography surveys that identifies measurement methods and analysis schemes for different building survey applications, as presented in Figure 4-4 below.
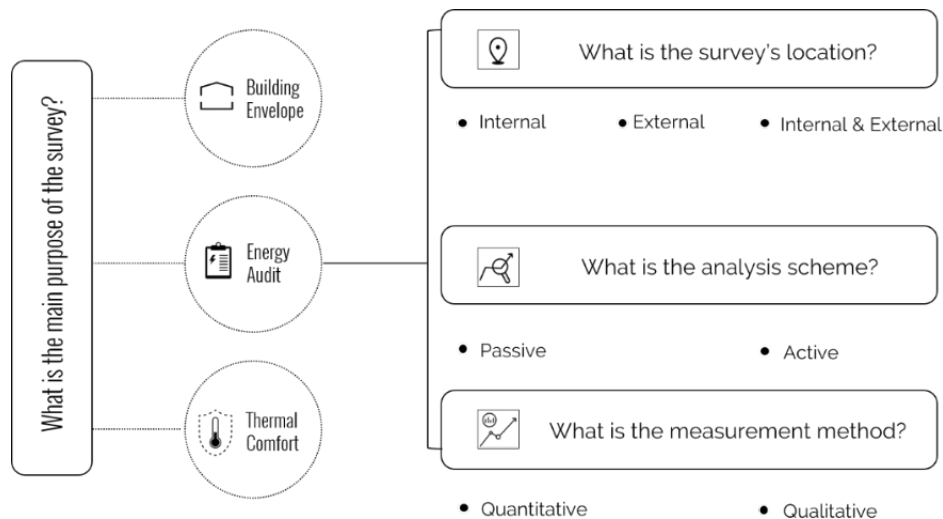
Figure 4-4: The decision-making process for infrared thermography surveys in building diagnosis. Based on (Fox et al., 2014).

4.2.2 Aerial Thermography

Advancements in remote inspection using UAV have provided professionals with valuable data to examine and assess built environments accurately and rapidly, at minimum costs and safety risks. The use of drones in monitoring construction sites has been investigated (Irizarry, Gheisari, & Walker, 2012), and its advancements include integration with Building Information Modeling (BIM) and mixed-reality frameworks (Hg et al., 2019). This approach's efficacy increases significantly when coupled with IR imaging, multispectral imaging, or time-lapse videography, as UAVs can contribute to a wide variety of building surveys (Kylili et al., 2014). The aerial approach provides a safe outlook into remote or inaccessible building components (Rakha et al., 2018). And as these improvements continue to grow, a

broad spectrum of industry fields will use its application (Corsi, 2010). A comprehensive overview of aerial thermography applications in the built environment has been presented in (Rakha & Gorodetsky, 2018a). This approach's primary benefit is the non-destructive testing capabilities provided by thermography (Stepanić & Lesičar, 2019), which could be extended using possible innovations in the use of manipulators for an assessment of inaccessible envelope conditions (Stepanić & Lesičar, 2019). These tools can provide valuable insights to energy auditors. Previously surveyed auditors concurred that UAV use combined with thermal imaging would improve workflow in their investigations. They believed that IR imaging would also aid in client communications (Mauriello, Norooz, & Froehlich, 2015). It should be noted that pre-flight planning considerations should be part of the audit procedures to produce reliable results. Firstly, some weather conditions should be avoided for stable UAS flights. These include rain, snow, and heavy wind. Secondly, solar loading, sunlight exposure, shadows, and self-shading may affect thermal imaging outcomes. Therefore, it is recommended to inspect envelopes at close temporal intervals and to collect RGB images in tandem to clarify each inspected situation. Thirdly, external surface temperatures may be affected by high humidity, wind speed, and precipitation. Therefore, it is recommended to avoid data collection during or in an immediate time period following a sudden change in these conditions.

The main limitation of UAV technology is battery performance, especially on long flights. However, battery technology is advancing every day as new companies push the boundaries with drone technologies for new alternatives such as solar-powered UAVs. Also, thermal transmittance calculation using UAVs requires detailed information on building construction materials and their thermal properties, indoor temperature conditions, and history of any previous retrofitting intervention. Other limitations for the aerial thermography process include possibly compromising IR and RGB images due to angular deflection. When capturing light deflection in reflective materials, such as glass and metal, camera angles are a challenge to be addressed. In this research, images are collected at a perpendicular angle to the envelope, which is only problematic with highly reflective surfaces, and should be addressed in future work. Also, inspection distance calculations rely on the drone operator's expertise and may be fixed for each inspection procedure. Distances are a function of the size and geometry of buildings and the camera's Field of Vision (FOV) and should be designed to fit the specifications of each camera accordingly.

There are three main procedures that need meticulous planning when using UAV combined with IR imaging (Rakha & Gorodetsky, 2018a): 1) Site Acquisition, which includes individual building audits, building cluster (or neighborhood) surveying, and planning for data obscuring through obstacles (such as trees, street furniture, etc.). 2: Flight Path Planning, entailing the identification of survey locations (interiors and exteriors), the audit focus, and envelope components (such as windows, doors, etc.), as well as considerations for flight path design which focus on distances from targets, bearing angles and drone altitudes. 3) Post-Flight Data Analysis Techniques, including data formatting, quantitative and quantitative methods, and image processing techniques, with possible 3D photogrammetry integration.

4.2.3 U-Value Assessment

One of the main properties directly linked to the envelope's thermal performance is thermal transmittance (U-value) (O'Grady, Lechowska, & Harte, 2017; Seghier, Lim, Ahmad, & Samuel, 2017). The value of thermal transmittance is considered an important metric to quantify the heat transfer of building envelopes. However, the envelope's U-value is not consistent, as it is significantly influenced over time by surrounding climatic conditions, level of maintenance post-occupancy, and the façade's material condition. Previous research indicates that U-values are generally reduced over time by 50% post-occupancy (Foam-Tech, 2015). Thus, this underlines the need for more accuracy in modeling energy use for post-occupancy conditions. IRT has been widely applied in assessing the envelope's thermal performance over the past three decades. The IRT application was first deployed to quantify heat flow fluxes through a wall, referred to q value (Francesco et al., 2011). Vavilov et al. (E.Grinzatoa, V.Vavilov, & T.Kauppinenc, 1998) developed an approach using Heat Flow Meters (HFM) to measure a reference point's temperature on the wall. In this approach, the wall's thermal resistance is assumed to be constant but unknown. The first pilot study to use thermography to quantify facade thermal transmittance dates back to 2008 when Madding (Madding, 2008) proposed a numerical approach to assess heat balance in buildings' walls and estimate U-value using equation (1):

$$U = \frac{4\varepsilon\sigma T_m^3 (T_S - T_{refl}) + h_c (T_S - T_{in})}{T_{in} - T_{out}} \quad [\frac{W}{m^2.K}] \quad (1)$$

where
$$T_m = \frac{T_s + T_{refl}}{2} \quad (2)$$

The numerator represents the sum of radiative energy for a given wall, expressed as Stephan-Boltzmann law and the convection input. ε is the emissivity value of the wall surface, T_m is the temperature difference between the apparent measured temperature T_{refl} and wall surface temperature T_S, and σ is Stefan-Boltzmann constant. Convection is calculated as the product of the temperature difference between internal and external walls and h_c (the convection coefficient). The denominator represents the difference between outdoor and indoor air temperature. Later, Tanner et al. (C. Tanner, B. Lehmann, T. Frank, 2011) developed a standardized method for measuring wall U-values with thermography using a convective heat coefficient value of 8.7 W/m².K. Another study by Grinzaton et al. (E., P., G., & Peron, 2010) developed an IR camera approach to assess existing buildings' conditions by estimating radiative flows across the wall. The convective flows were determined using a standard value of 7.69 W/m².K (F. Altmayer, Bauman, Gadgil, & C. Kammerud, 1982). Results showed that this approach effectively calculated values close to designed U-values but different from the ones calculated using the traditional method of the HFM. Dall'O' et al. (Dall'O' et al., 2013) applied IRT in estimating a walls' thermal transmittance using a different heat balance approach. In this study, they assumed that convection heat exchange with outdoor air is equivalent to the heat transfer through the wall excluding radiation at the outer surface, as presented in equation (3) as follows:

$$U = \frac{h_{out}(T_S - T_{out})}{T_{in} - T_{out}} \quad [\frac{W}{m^2.K}] \quad (3)$$

T_{out} is the outdoor air temperature, T_s represents the surface temperature of the exterior wall, and T_{in} is the indoor air temperature. In this equation, heat transfer through convection is calculated as a function of wind speed, as provided in equation (4).

$$h_{out} = 5.8 + 3.8054v \qquad (4)$$

In 2015, a study by Albatici et al. (Albatici, Tonelli, & Chiogna, 2015) extended previous work in the field of IRT and thermal transmittance assessment and proposed the following equation (5):

$$U = \frac{\varepsilon_v \sigma (T_s^4 - T_{out}^4) + 3.8054v(T_s - T_{out})}{(T_{in} - T_{out})} \qquad \left[\frac{W}{m^2.K}\right] \; (5)$$

where ε_v represents the wall's emissivity, T_s is the surface temperature of external walls, T_{out} is the outdoor air temperature, v is wind speed, and T_{in} is the indoor air temperature.

Although IRT is a useful method to evaluate envelopes' performance, several factors affect the accuracy of the assessment. Such factors can be found at (Rakha et al., 2018) and include temperature difference (ΔT), humidity, ambient air temperature, wind speed, camera angle, the distance between the IR camera and the building façade, external optics temperature, and thermal reflection, among others.

4.3 Methods

Over the past decade, UAVs' role in surveillance and building inspection has been gaining tremendous interest (Rakha & Gorodetsky, 2018a). Their efficiency stems from their capacity to capture high-resolution data with significant time efficiency with minimum dependence on human labor (L. Ma, Li, Tong, Wang, & Cheng, 2014). The most common application of UAVs in building inspection is through the utilization of aerial thermography. This method provides a comprehensive assessment of building envelope performance by collecting a series of infrared images over the same timeframe in a fast manner that has a considerable advantage compared to walkthrough inspection.

This chapter proposes a framework to estimate the envelope's thermal transmittance from aerial thermography data to be incorporated in rapid heat vulnerability assessment following four main steps, as illustrated in Figure 4-5 below. First, the deployment of UAVs equipped with an IR camera for data collection. Information captured from this data will highlight issues such as material deterioration, heat losses, and overall performance of building envelope. Next, thermal anomalies identification through examining temperature gradient and variation across building envelope. Third, estimating thermal transmittance using air temperature difference between outdoor and indoor conditions numerically. The final step integrates estimated U-value into A BEM model to better model and calculate heating energy use for the winter month.
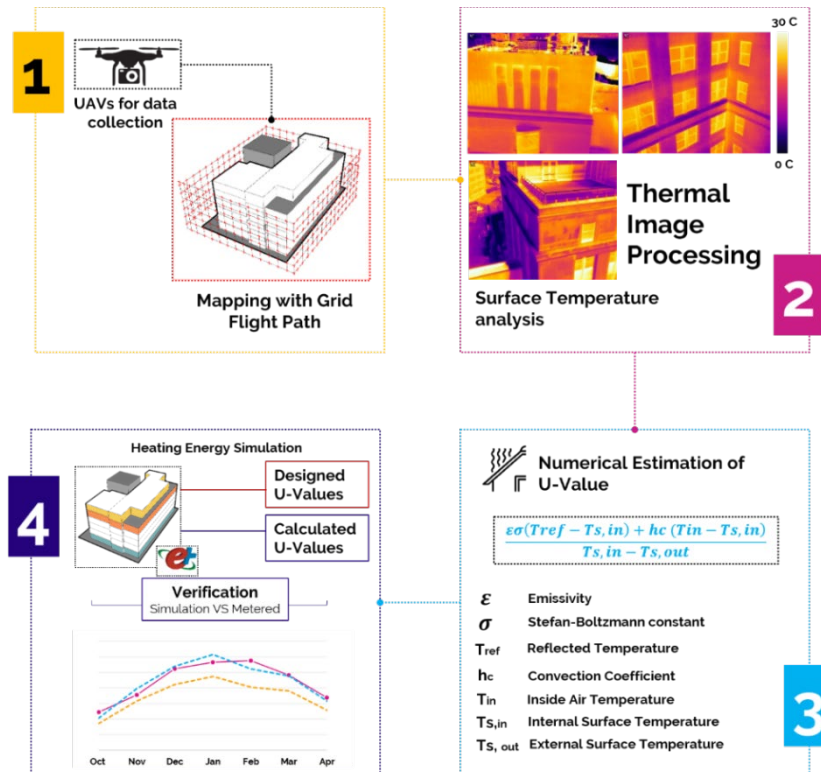
Figure 4-5: Proposed framework and analysis methods.

4.3.1 Case Study

A campus building in Boston, MA, was identified to test the proposed analysis framework's efficacy. The selected building recently underwent a major renovation. As part of the renovation process, the design team developed a detailed energy simulation model to evaluate the energy impact of various envelope upgrades. The final recommendations were implemented, and the building envelope was renovated to incorporate additional insulation to significantly reduce the envelope's thermal transmittance and improve overall energy efficiency (Figure 4-6).
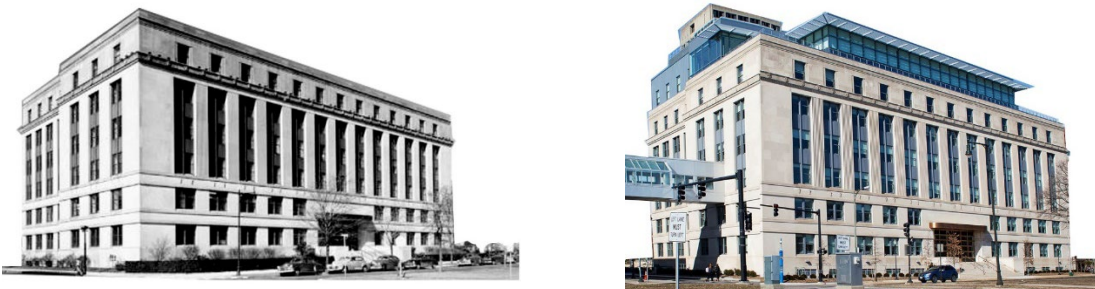
Figure 4-6: Building images before (left) and after (right) retrofitting (Massachusetts Institute of Technology, 2019).

Measured heating energy use post-renovation during the wintertime is significantly higher than the predicted energy use from the simulation model based on the envelope properties derived from design drawings and specifications (Figure 4-7). With internal load and occupant usage parameters relatively well known and reasonably accounted for in the model, this discrepancy makes this building an ideal case study to assess whether "as-designed" envelope model inputs reasonably represent "as-built" performance;

and whether an energy model that incorporates "as-built" instead of "as-designed" inputs predicts the post-retrofit energy use more accurately.
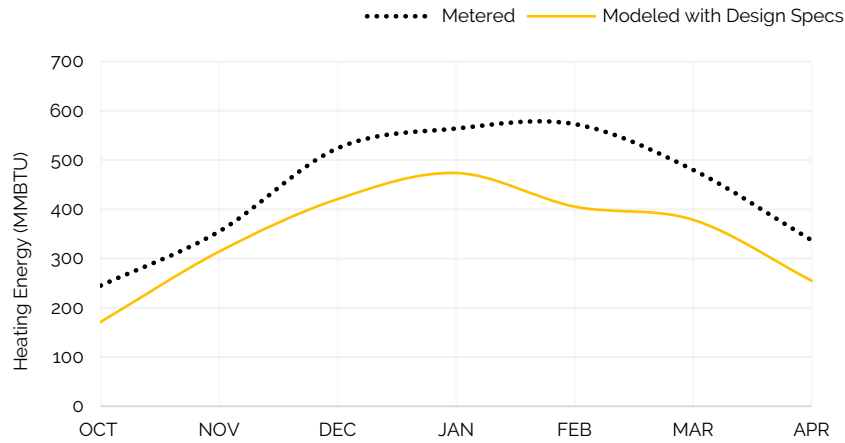
Figure 4-7: Comparative assessment of post-renovation metered and modeled wintertime heating energy use.

4.3.2 Aerial Thermography Workflow

To determine the "as-built" envelope performance for this study, a DJI Inspire 1 drone equipped with a FLIR Zenmuse XT thermal camera (DJI, n.d.) was used for data collection. Two main factors affect the accuracy of the data collection: climatic conditions (such as solar radiation, wind speed, rainfall, cloud coverage) and the flying method. In this study, the data was collected on March 31st, 2018, during the early hours of the morning (between 6:00 to 8:00 am) before sunrise to avoid any potential distortion from sun solar radiation. The outdoor air temperature was eight ºC to ensure temperature differences between indoor and outdoor of 10 ºC, according to Snell & Spring's recommendation (2008). A strip method is used for flying procedures where the UAV is constantly flying horizontal and vertical perpendicular to the façade (Rakha & Gorodetsky, 2018a), as illustrated in Figure 4-8 below. Distance between UAV and façade is calculated according to the camera's focus angle and resolution to achieve a 90% overlap between each image.
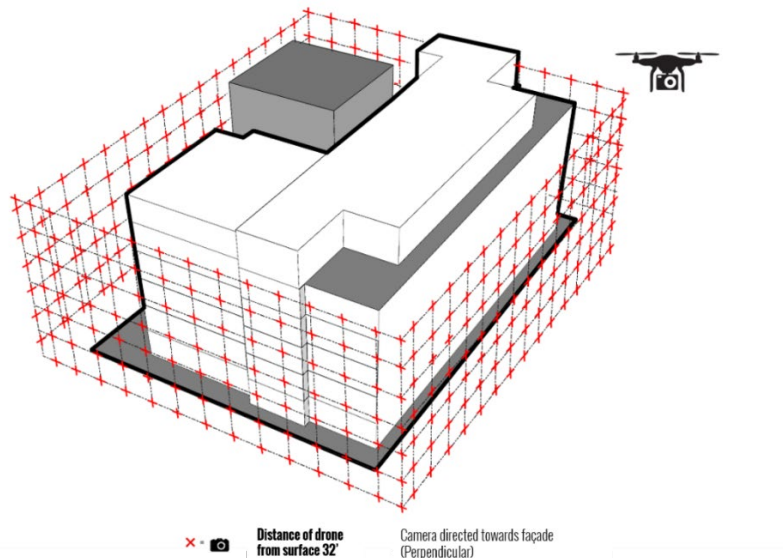
Figure 4-8: Flying procedures used in data collection (grid pattern with 90% overlap).

4.3.3 U-Value Calculation and Validation

A standardized convection coefficient (h_c) of 8.7 W/m^{2}K derived from Tanner et al. was used to estimate U-value from IR data(C. Tanner, B. Lehmann, T. Frank, 2011). The overall heat transfer coefficient is calculated using a modified version of equation (1) as follows:

$$\frac{\varepsilon\sigma(T_{refl} - T_{s,in}) + h_c\left(T_{in} - T_{s,in}\right)}{T_{s,in} - T_{s,out}} \quad (6)$$

Where:

ε	Emissivity	1
σ	Stefan-Boltzmann constant	W·m^{-2}·K^{-4}
T_m	temperature difference between T_{refl} and T_S	Kelvin (K)
T_{refl}	the apparent measured temperature	Kelvin (K)
T_S	Exterior wall surface temperature	Kelvin (K)
$T_{s,in}$	Interior wall surface temperature	Kelvin (K)
h_c	Convection Coefficient	W/(m^2•K)
T_{in}	The indoor air temperature	Kelvin (K)
T_{out}	The outdoor air temperature	Kelvin (K)

To verify dimensional consistency:

$$U = \frac{W.m^{-2}.K^{-4}.K^3.(K-K) + W.m^{-2}.K^{-1}.K}{K-K}$$
$$= \frac{W.m^{-2}.K^{-4}.K^4 + W.m^{-2}}{K}$$
$$= \frac{W.m^{-2} + W.m^{-2}}{K}$$
$$\frac{W}{m^{-2}.K}$$

Following ASHRAE standards, the convective coefficient used in the study is based on standard wind conditions (ASHRAE, 2017a). To estimate the emissivity of the exterior wall, the research followed the FLIR user manual (FLIR Systems, 2016, 2019) to estimate an emissivity value using black tape with an emissivity value of 0.95. The reflected temperature was calculated following the procedure of ASTM E1862-97 (ASTM International, 2018) by using an aluminum foil method at an emissivity value of 1. The same procedures were used in a handheld thermal FLIR camera which was used to measure $T_{s,in}$ simultaneously with outdoor surface temperature from the UAVs IR camera for each façade. To calculate U-Value, the thermal transmittance is calculated for each façade separately by averaging temperature differences from IR data. For areas with different U-values, the average value is estimated using the following equation:

$$U_{avg} = U_1 * \frac{A_1}{A_1+A_2} + U_2 * \frac{A_2}{A_1+A_2} \quad (7)$$

Where:

U$_{avg}$: Average U-value of a facade

U$_1$: U-value for areas with thermal anomalies

U$_2$: Total façade area U-value simultaneously

A$_1$: The area of the thermal anomaly

A$_2$: The area of non-thermal anomaly

To examine the usability of aerial thermography in calibrating energy simulation models, the calculated U-value was used in an energy simulation model to compare two different scenarios. First, modeling heating energy using design specification and modeling heating energy based on estimated U-value from aerial thermography flight. Next, simulation output is compared to metered energy use to examine accuracy improvement in heating energy simulation.

To assess the accuracy of the two simulation scenarios, a goodness of fit (GOF) error was calculated for each model. GOF is a statistical index defined by ASHRAE Research Procedure 1051 (Reddy & Maor., 2006) as a ranking metric for simulation results accuracy. This metric is a weighted combination of the coefficient of variation (CV) of Root Mean Square Error (RMSE) and normalized mean bias error (NMBE). CVRMSE quantifies the variability between measured and simulated results monthly, while NMBE measures the error percentage between simulated and measured energy use over the year. ASHRAE Guideline 14 (Gillespie et al., 2002) recommends a 3:1 weight allocated for NMBE compared to CV. The overall GOF is calculated using the following equations:

$$GOF = \sqrt{\frac{w_{CV}^2 \cdot GOF_{CV}^2 + w_{NMBE}^2 \cdot GOF_{NMBE}^2}{w_{CV}^2 + w_{NMBE}^2}} \quad (8)$$

and,

$$GOF_{CV} = \sqrt{\frac{\sum_{i=1}^{n}(y_i - \hat{y}_i)^2}{(n-1) \times \bar{y}^2}} \times 100 \quad (9)$$

$$GOF_{NMBE} = \frac{\sum_{i=1}^{n}(y_i - \hat{y}_i)}{n \times \bar{y}} \times 100 \quad (10)$$

where,

w:	weighting factor 3 for NMBE; 1 for CV
i:	month of the year
n:	number of months in consideration
y_i:	measured energy use for a given month
$\hat{y}_i$:	predicted energy use for a given month based on simulation output
$\bar{y}$:	the average value of measured monthly energy use

4.4 Results

Temperature readings from around 500 images were analyzed using the FLIR analysis tool (FLIR Systems, n.d.), as presented in Figure 4-9. The analysis examined temperature differences and variations across each façade and output potential areas of thermal anomalies. Next, temperature differences between indoors and outdoors are used in the estimation of existing thermal transmittance. For indoor air temperature, typical setpoints for different spaces were used as a measure for indoor conditions. The indoor surface temperature was determined using a hand-held thermal camera where values were recorded simultaneously with outdoor surface temperature from the UAVs IR camera for each facade.
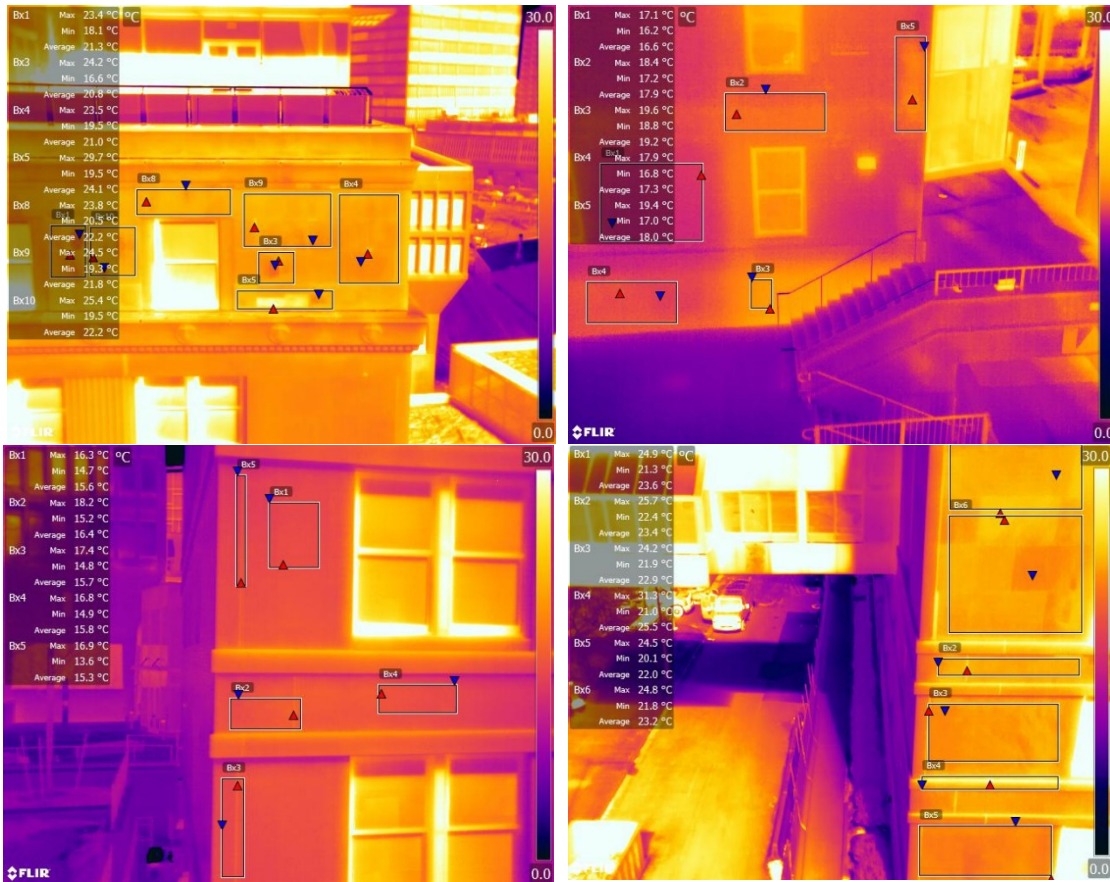
Figure 4-9: Sample of thermal imaging analysis.

The thermal imaging analysis indicated three types of thermal anomalies in the building examined, namely, thermal bridge, degradation of façade's material, and insulation failure. The distinction between the three anomaly types was based on two main criteria: the shape of the anomaly and location. For thermal bridge was identified as liner vertical or horizontal anomalies mainly located around a building corner and between floors. Material deterioration implies a degradation of cladding materials or cracks, which was identified as a bulk shape anomaly; finally, the insulation failure represents thermal leakages around doors and windows and insulation degradation across the building envelope. This anomaly was detected as vertical or horizontal anomalies located around doors and windows or bulk irregularities with a temperature difference of three degrees compared to the surrounding envelope.

Material degradation was common across all facades, specifically in the newly added floors. The southern façade had the most significant insulation failure occurrence with a temperature difference range of 8-9 degrees in the affected areas compared to the rest of the façade. Thermal bridges mainly occurred in the building corners, primarily southern and eastern corners and between floors. Around 65% of the windows indicated a potential for thermal leakage that needs to be further investigated. Figure 4-10 below outlines the types and percentage of occurrences for each class across the four facades.
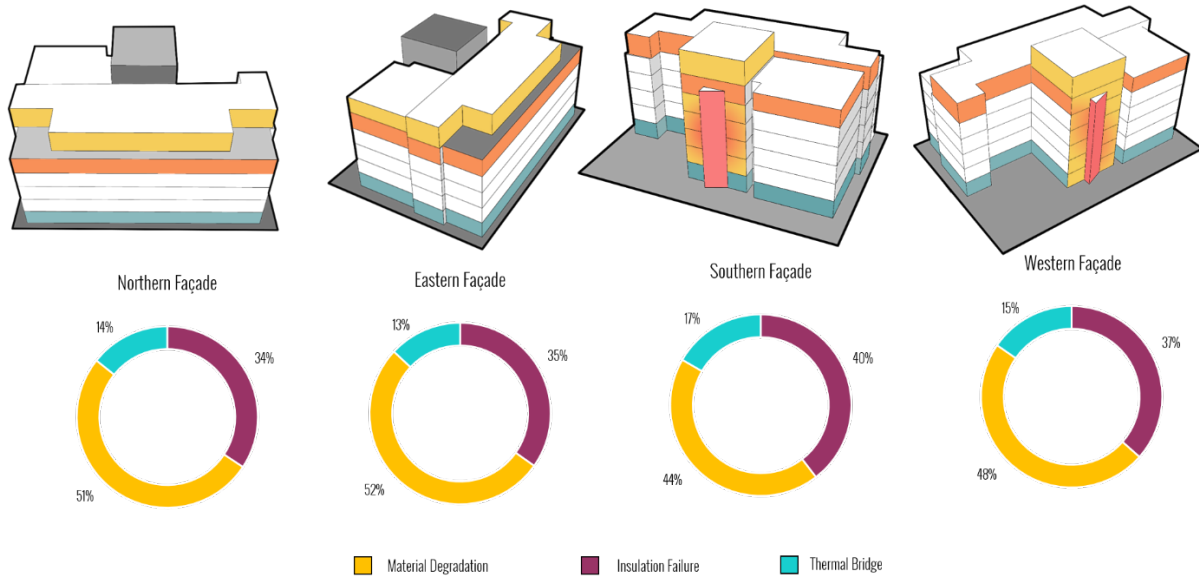
Figure 4-10: Types of thermal anomalies and their distribution across the examined facades.

As discussed earlier, a whole BEM was developed for the examined building to be used for this analysis. Figure 4-11 represents the model generated during the renovation process. Model inputs such as the envelope's thermal properties, internal loads, lighting power, operating schedules, and building systems were determined according to the design specifications.

Figure 4-11: Left, rendering of the developed energy model; Right, a photograph of the building post-renovation.

U-values of building facades were calculated using information from the aerial thermography flight following the methodology described above. Table 4-1 compares the U-values of exterior walls based on design specifications and calculated thermal flight values. Results from the IR flight and U-value estimation were validated against the observations of maintenance personnel. The energy model incorporates detailed zone-by-zone definitions of lighting and equipment power densities, usage profiles, and HVAC parameters. Table 1 also broadly summarizes these other energy model inputs.

Table 4-1: As-designed and calculated U-Values from the UAV flight.

Exterior Wall U-Value (Btu/hr-ft²-°F)				
Orientation	Designed Opaque	Calculated Opaque	Designed Fenestration	WWR
SE, SW	8" Limestone + 8" Brick + 3" Spray Foam Insulation U: 0.053	0.282	0.361	30%
W		0.203		97%
N, NE		0.142		21%
Building Average lighting Power Density		W/ft2 0.67		
Building Average Equipment Power Density		W/ft2 0.84		
General HVAC Configuration		*Dedicated outside air system supply ventilation air to thermal zones with chilled beams and fan coil units. Chilled water and steam and supplied by the central campus plant*		

Figure 4-12 compares heating energy use for three cases: simulation-based on design specifications, calculated U-value from the UAVs flight, and measured heating energy use. Results indicate that model error is significantly reduced after incorporating calculated U-values (blue line) compared to previous simulations based on design specification (yellow line).
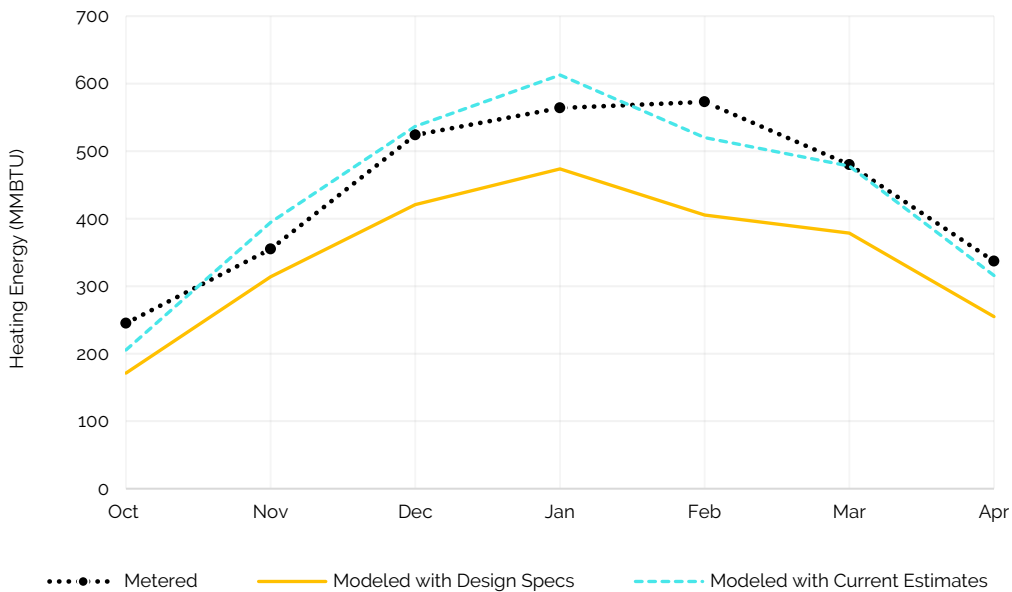
Figure 4-12: Comparison between measured and simulated heating energy use.

The comparison between the two models is presented in Table 4-2. Results show that the simulation models' output with as-built envelope properties is considerably better calibrated, with CVRMSE under 10% and NMBE lower than 1%, and an overall GOF of about 1%. These results represent a significant improvement over the NMBE of 21%, CVRMSE of 25%, and overall GOF error as high as 22% in the previous model. ASHRAE Guideline 14 (Gillespie et al., 2002) specifies that for simulation models to be considered calibrated, uncertainty criteria of 15% for CVRMSE and 5% for NMBE need to be achieved. Results indicate that the previous simulation model failed to meet these criteria; the model results with as-built envelope properties fall well within these uncertainty limits.

Table 4-2: Goodness of fit results between simulated and modeled with current estimate U-Values.

Goodness of Fit Errors			
Modeled Envelope Case	GOF_{CV}	GOF_{NMBE}	GOF
Design Specs	24.8%	21.4%	21.8%
Current Estimates	8.8%	0.5%	0.9%

U-value is calculated based on four independent inputs; emissivity, reflected temperature, indoor temperature, and convective heat coefficient. Thus, the sensitivity of each input is tested by varying their values ± 15% to test how calculated thermal transmittance would vary. Results from the sensitivity analysis are summarized in Table 4-3 below. From the sensitivity analysis, the research identified that emissivity and reflected temperature didn't significantly impact the final calculated U-value compared to indoor temperature and convective heat coefficient.

Table 4-3: Sensitivity of calculated U-value for different independent inputs.

Orientation	Calculated Opaque	ε	ε	T_{refl}	T_{refl}	T_{in}	T_{in}	h_c	h_c
		0.8	*0.99*	*17*	*23*	*19*	*25*	*7.4*	*10*
SE, SW	0.282	0.283	0.280	0.285	0.279	0.384	0.196	0.209	0.355
W	0.203	0.202	0.203	0.207	0.200	0.305	0.203	0.203	0.203
N, NE	0.142	0.144	0.140	0.148	0.140	0.244	0.142	0.140	0.142

4.5 Discussion

This section presents a framework by which building retrofitting strategies can be better identified and informed by improving the assessment process of existing building envelopes. The innovation aims to present UAVs to enhance evaluator experience significantly by overcoming physical barriers encountered in typical building audit procedures and incorporating this method in heat vulnerability assessment. This approach is specifically useful when evaluating various buildings without relying on a single-image approach for auditing. This approach's efficacy stems from providing a whole building infrared imager data by which designers can better engage with and identify targeted building performance issues. The proposed framework has demonstrated a significant reduction in simulation errors, and future work would address its applicability to other climates and more complex built environment conditions.

The proposed framework addresses multiple challenges that are limiting current building energy audits processes, such as 1) physical inaccessibility for building components such as roofs that are typically challenging to monitor in the typical energy audit procedures, 2) time-efficient compared to regular audit activities that are usually prone to human error, 3) overcoming safety and life-threatening settings that are common in a detailed inspection by reducing dependency on human labor. Such difficulties in building energy audits can significantly affect Whole Building Energy Modelling (BEM) practices and, as a result, misinform retrofitting design decisions. Also, manual modeling processes in current retrofit BEM are challenged with time-intensive and labor-intensive activities requiring better means to examine buildings with more safety, accuracy, and time-efficient manner.

The future of integrating such remote sensing techniques as innovative technologies in the built environment industry relies on coalescing integrative approaches between such robots and practices (Pan, Linner, Pan, Cheng, & Bock, 2020; Y. Yang, Pan, & Pan, 2019). Data collection automation and translation into energy models continue to evolve using computer vision as a Machine Learning-based approach for BEM (Dino et al., 2020; Rakha et al., 2018). As such techniques evolve, so will the efforts to integrate them seamlessly. And that is why there is a need to automate the audit missions beyond data collections and analysis. This posits challenges include navigating UAS in various dense and congested environments (Goudarzi, Hine, & Richards, 2019) and managing data, possibly through Geographic Integration Systems (GIS) (CHO., Leite, Behzadan, & Wang, 2019). The practical use of such approaches may face issues such as having an unskilled or aging workforce. This industry is averse to change or having the technology perceived as too complex with subpar infrastructures to support it (Davila Delgado et al., 2019).

The proposed approach can expand to examine different thermal anomalies and measure heat transfer across other components such as roofs, windows, etc. Future work may focus on testing the developed framework for various building types (such as residential and office buildings) and different climatic conditions to assess its applicability to other settings and various building types. In conclusion, the work discussed in this section presents an opportunity to incorporate aerial thermography in heat vulnerability assessment and BEM workflow. The framework can be useful specifically during the development of simulation models targeted towards representing existing built environment conditions to assess potential heat risks in existing building stocks and quickly identify types of buildings more susceptible to heat exposure. Also, aerial thermography can be utilized for neighborhood-level assessment to examine and identify the most effective retrofitting scenarios, where time-saving and cost-reduction potentials can be achieved when assessing multiple buildings compared to traditional building inspection processes. The following section develops and illustrates the applicability of using aerial thermography in urban heat vulnerability assessment using a neighborhood in the Bronx, NYC, as the primary case study.

4.6   Rapid Heat Vulnerability Analytics Using UAVs

Unmanned Aerial Vehicles (UAVs) have revolutionized numerous industries and sectors of human life by providing a wide range of applications and services that were limited before. Over the past decade, there has been a growing interest in utilizing UAVs as a fundamental technology in various applications in the built environment. Recently, the wide availability of wireless technology has made the deployment of UAVs more accessible. The application of UAVs in climate change research has been rapidly expanding to become an integral technology for environmental monitoring and climate change risk mapping (Tmušić et al., 2020). This section presents a framework for the integration of UAVs technology in heat vulnerability assessment. The framework offers a methodology for using UAVs equipped with RGB and IR cameras to provide a comprehensive assessment of the building envelope's thermal performance critical to evaluate heat vulnerability potentials at the building level. Figure 4-13 illustrates a detailed workflow for building envelope assessment using UAVs to provide accurate data on building thermal performance and implications from heat exposure. Existing studies on heat vulnerability underline the need for a citywide approach for buildings' envelope thermal envelope that can be examined rapidly for various archetypes (Nahlik et al., 2017). The purpose of the framework is to provide a rapid evaluation of

buildings' susceptibility under heat exposure based on the identification of thermal envelope performance by detecting envelope deterioration, thermal anomalies, and physical defects that can influence indoor conditions without using detailed simulation models. The framework is designed to answer three main questions: i) How to characterize buildings' thermal performance at the neighborhood level rapidly and efficiently? ii) what is the relationship between buildings with low thermal performance and areas with high-temperature forecasts? iii) Where can building envelope improvements be most effective for heat adaptation.
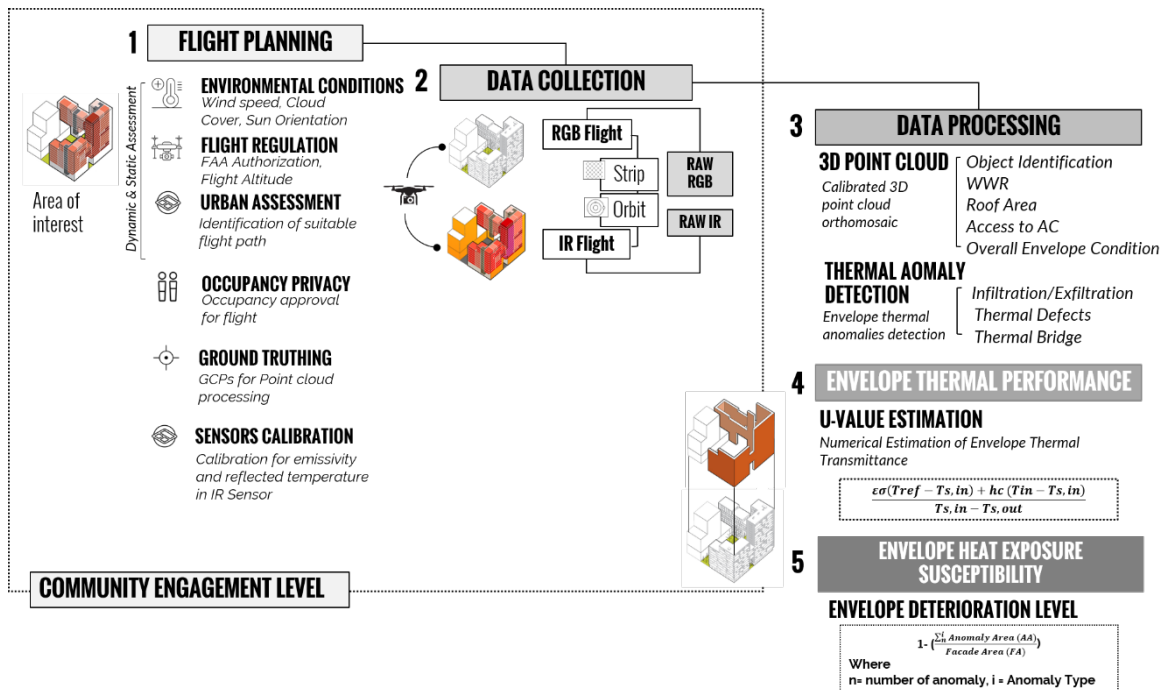
Figure 4-13: Framework for Rapid Heat Vulnerability Assessment using UAVs.

4.6.1 Flight Planning

The first step of the proposed framework is related to UAVs flight planning to ensure suitable data collection of hyperspectral (RGB) and infrared information. The flight planning process entails 4 main components, as illustrated in Figure 4-13 above. The first component relates to the assessment process and consists of 1) static flight assessment; and 2) dynamic flight assessment (Besada, Campana, Bergesio, Bernardos, & De Miguel, 2019). The static flight process includes gathering information related to compliance with Federal Aviation Administration (FAA) Regulations (flight altitude, air rules, speed), identifying surrounding obstacles, conditions of the surrounding urban traffic, or potential network interruption from nearby infrastructure (electricity towers), and surrounding static geofences. Gathering this information will be critical for flight path design in step 2.

Dynamic flight assessment includes assessing environmental conditions (air temperature, wind speed, cloud coverage), temperature differences between indoor and outdoor that may significantly influence the quality of collected IR data (Rakha et al., 2018), navigation system availability, and urban traffic. Gathering information on surrounding climatic conditions can significantly influence the quality of data collection. For example, high wind speed can cause images to be blurry, which is an important factor to

consider during flight planning. The second component is related to occupancy privacy during the data collection process. It usually involves providing a detailed description of the purpose of the flight and the type of data collected to request inspection authorization for the premise to be inspected. This process should be prepared in an accurate space-time description of the flight and be operationally consistent with the UAV's operator needs. The third component consists of the design and geo-location of ground control points (GCPs) to assist in processing the 3D point cloud in step 3. Lastly, the fourth component relates to the calibration of UAVs' radiometric sensors following the procedures discussed in the first section of this chapter to ensure the quality of the collected data.

4.6.2 Data Collection

UAV-based data acquisition entails collecting successive waypoints (2D such as RGB and IR or 3D like LiDAR). In building inspection missions, the UAV's operator (pilot) designs a flight plan to acquire both hyperspectral and IR data. This process requires knowledge of multiple factors such as distance from the building, altitude, and speed. Numerous studies in the literature have examined the optimal offset distance from the building during envelope inspection. Rakha et al. (2018b) offered some recommended distances (varying between 3m to 25m) during envelope inspections. However, the optimal distance from the façade relies heavily on the data needs, camera resolution, image overlap target to generate 3D point cloud models, and building height. Before the data collection process, a pre-established flight path is developed, considering the distance from each façade side and the ideal route for time efficiency and safety. From the literature, there are two main flight paths for building inspection based on geometric approaches: vertical or horizontal strip pattern and orbital pattern (Rakha et al., 2018). Based on previous studies, the vertical and horizontal strip has been proven to be the most suitable for building envelope anomaly detection using both RGB and IR cameras (Falorca & Lanzinha, 2020; Rakha & Gorodetsky, 2018b). Another critical parameter in the data collection phase is image overlap to collect sufficient data to generate accurate 3D models. From the literature, the recommended overlap should be at least 75%-80% for frontal overlap and at least 60%- 70% side overlap (between flying strips) (PIX4D, 2020; Rakha et al., 2018). The UAV'S gimble angle should be maintained at 90 degrees during data collection and flying at a constant height for each strip (Figure 4-14). Image resolution can significantly affect the accuracy of thermal anomaly detection in the IR data and the quality of processing 3d point cloud models from RGB images. Since image resolution and target image overlap can influence the quality of image processing, the optimal distance from the building façade for vertical strip flights can be calculated using the camera's field of view (FOV) and required overlap as input using the following equations:

$$\text{Distance from the façade } D = \frac{I_h}{\tan F_v} \qquad (10)$$

$$\text{Image height } I_h = \frac{\frac{I_d}{(1 - Target\ Overlap)}}{2} \qquad (11)$$

where I_h is the image height, F_v is the camera's vertical field of view, and I_d is the image distance calculated in the flight software. Also, camera resolution is a critical determinant of the offset distance between the UAV and the building to achieve the required overlap criteria. Current UAV technology comes with a high-resolution RGB camera ranging from 12 megapixels to 20 megapixels (Messina, Peña, Vizzari, & Modica, 2020). On the other hand, IR cameras generally come with lower resolution ranging from 320 × 240 to 640 x 512 (Ortiz-Sanz, Gil-Docampo, Arza-García, & Cañas-Guerrero, 2019).
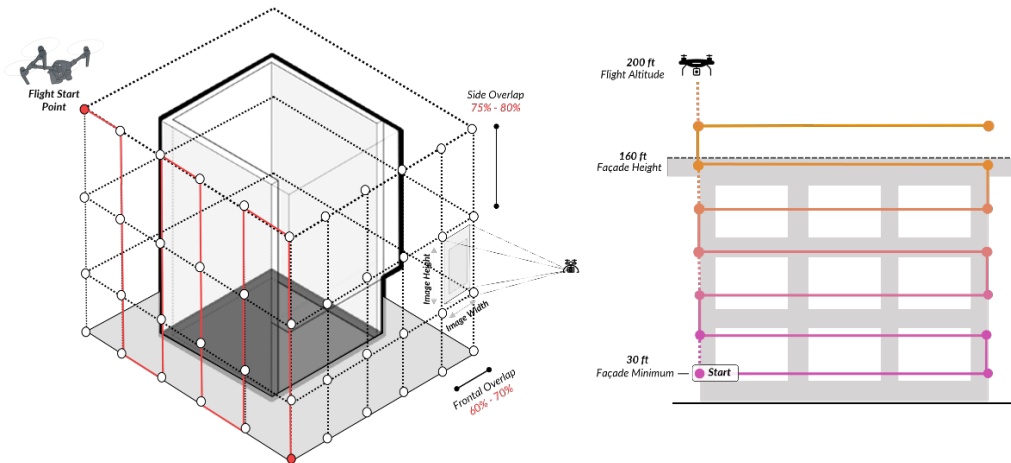
Figure 4-14: Left, Flight vertical strip pattern type with schematic measurement/distance reached by the UAV's camera lens. Right, schematic visualization of UAV's flight horizontal strip path with start point and endpoint and maximum allowable altitude.

4.6.3 Data Processing

In the proposed framework, there are two types of data processing; each involves a specific output to inform heat vulnerability assessment: 3D point cloud from RGB data and thermal anomaly detection using IR data. The generation of the 3D point cloud is based on image segmentation, which is carried out based on feature similarity between spatially connected pixels in each image captured from the UAV. RGB image processing starts with importing all captured images into commercial photogrammetric software commonly used for UAV's data/aerial data. PIX4D is considered one of the most widely used photogrammetry software that is based on image segmentation to stitch and connect geospatially overlapped images.

The processing phase consists of six main steps (Burdziakowski et al., 2020): photo alignment, ground control points (GCPs) localization, 3D point cloud generation, 3D mesh, and texture generation, which can be exported in standard format (.obj) and visualized in other modeling platforms such as Revit and Rhino, Digital Elevation Model (DEM) production, that carry information of different object heights, and Orthomosaic generation (Figure 4-15). GCPs are points with known coordinates used to improve the accuracy of the 3D point cloud generation. Literature suggests a minimum of three GCPs is required for UAVs data (in UAV with Real-Time Kinematic (RTK) payload), yet, increasing the number of GCPs will result in better accuracy in the final output (Oniga, Breaban, & Statescu, 2018).

DATA **PROCESS** **OUTPUT**

RGB Data

Ground Control Points

Check Points

Photo Alignment

Ground Control Localization

Dense Point Cloud

Mesh & Texture Building

Digital Surface Model

Orthomosaic Generation
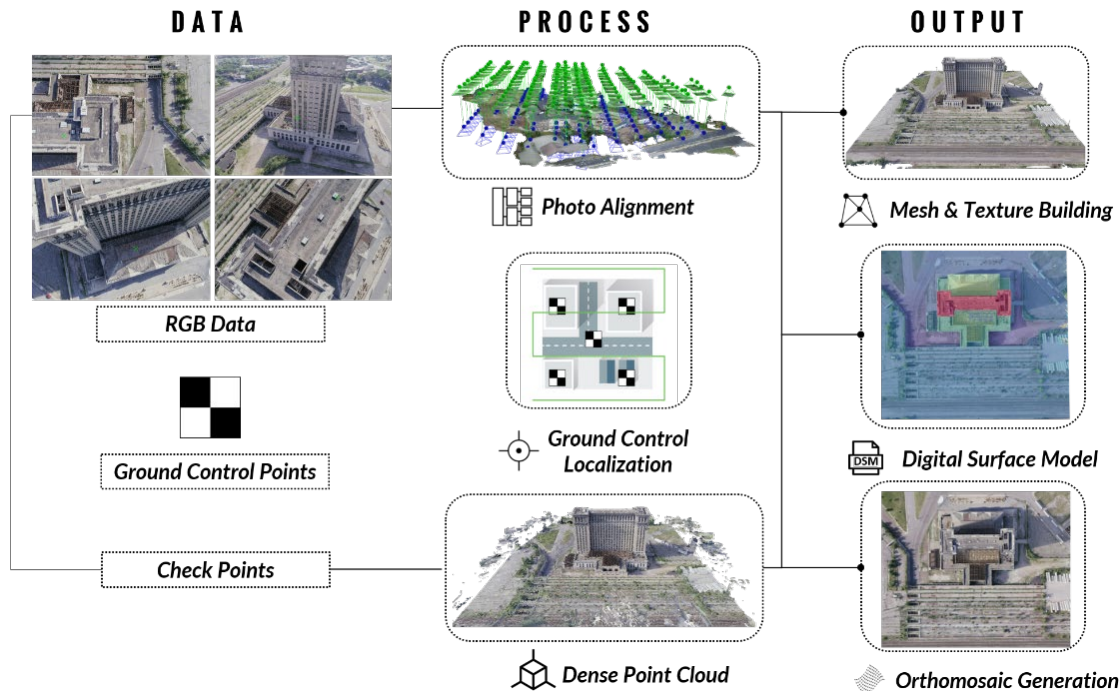
Figure 4-15: Photogrammetric process using UAV RGB data.

Generating 3D pointcloud and orthomosaic images helps in gathering information related to the envelope conditions and its physical characteristics rapidly, such as roof area, façade's deterioration condition, and window-to-wall ratio (WWR). In the proposed heat vulnerability assessment framework, orthomosaic and digital surface model (DSM) are used to calculate façade height and roof area by combining 2D information from orthomosaic with 3D information from DSM.

The second data type is IR data, mainly used for a more in-depth evaluation of building thermal envelope performance. In the heat vulnerability framework, IR data are collected to examine how the outdoor environment interacts and influences indoor conditions. This relationship is governed by the temperature difference between the internal wall and the external wall through conduction. In order to detect thermal anomalies accurately using aerial thermography, it is recommended to conduct the flight during the winter with a minimum temperature difference of 10°C, at night or early hours of the day, or during a cloudy day with low wind speed to minimize any false detection from convective heat losses (Balaras & Argiriou, 2002; Ortiz-Sanz et al., 2019). During the IR data collection, there are two types of thermal anomalies that are detected: infiltration/exfiltration, and thermal bridge /missing insulation (Figure 4-16). Infiltration and exfiltration are detected in IR thermography as a vertical or horizontal area with temperature difference around the frame of doors and windows due to air leaking from inside to outside or vice versa (Balaras & Argiriou, 2002). A thermal bridge is usually caused by a structural element that cuts out the thermal insulation barrier creating a short circuit path for heat flow, causing heat losses during the winter and heat gain during the summer (Ortiz-Sanz et al., 2019). In IR thermography, a thermal bridge is detected as an area of temperature, usually located at the corner of the buildings or between floors (Grey & Wartman, 2017). Physical defects or missing insulation can be detected in IR thermography as areas with a temperature difference of 11°C and usually appears as patches with distinct edges that outline the non-insulated areas (Balaras & Argiriou, 2002; Chang, 1985; Grey & Wartman, 2017).

Infiltration/Exfiltration   *Thermal Bridge/ Missing Insulation*   *Thermal Bridge/ Missing Insulation*
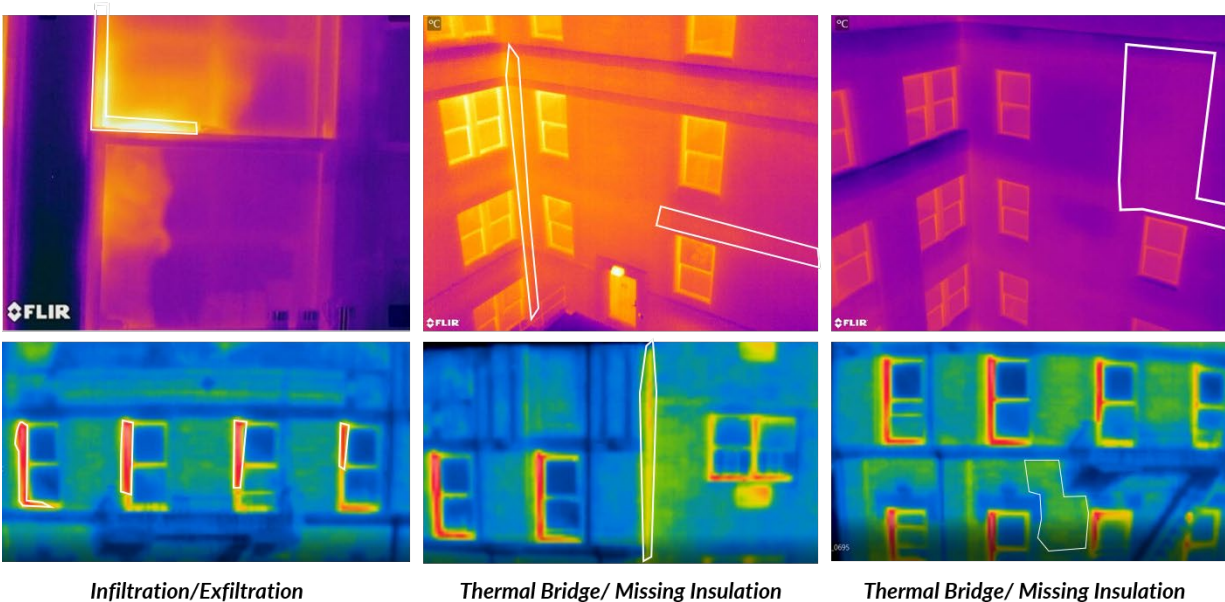
Figure 4-16: Types of thermal anomalies as they are detected in IR thermography.

A workflow using machine learning and computer vision techniques is developed to detect thermal anomalies that will assist in the general framework of heat vulnerability assessment. The proposed workflow is part of an ongoing research collaboration between MIT, Georgia Tech, and Syracuse University, and the work is funded by the U.S. Department of Energy (DOE). Thermal anomaly detection is based on Computer Vision (CV) algorithm developed by Syracuse University that outputs an IR image with detected anomalies without any additional information related to their classification. Here, the research presents a Machine Learning (ML) algorithm to classify and quantify detected thermal anomalies and their occurrence using detected anomalies as inputs and outputs anomaly classes and their probability according to two main categories: infiltration/exfiltration and thermal bridge/missing insulation. The proposed algorithm uses three input data types: RGB data for object detection and IR data and detected anomalies for anomaly classification. The object detection output from RGB will guide the anomaly probability and their classification by linking detected anomaly locations to detected envelope components. The structure of the algorithm consists of 6 components as follows: 1) object detection, 2) anomaly processing, 3) anomaly categorization, 4) geometric classification, 5) IR data processing and 6) thermal anomaly classification (Figure 4-17).
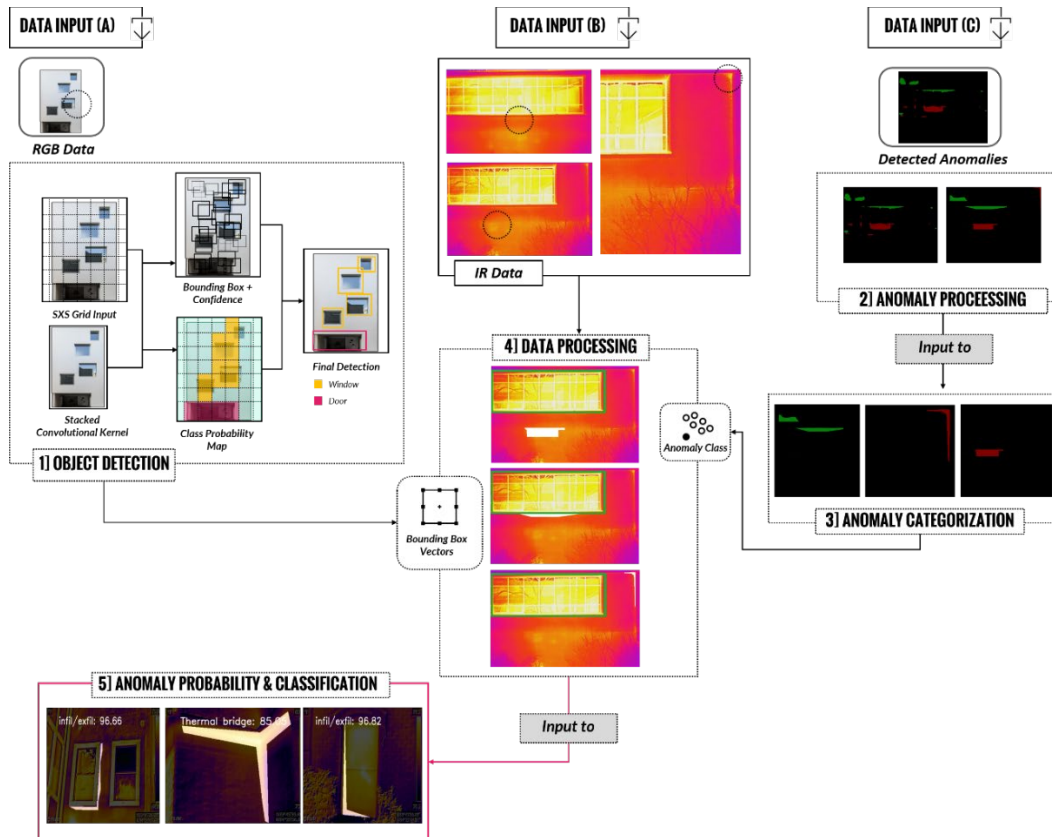
Figure 4-17: Thermal anomaly classification algorithm Structure.

4.6.4 Envelope Object Detection

Numerous research studies have focused on the extraction and segmentation of buildings' envelopes using photogrammetry and computer vision techniques. In the field of detecting building envelope objects from images, numerous models have been developed using deep learning techniques such as Recurrent Neural Networks (RNN) (Graves et al., 2008) and Convolution Neural Networks (CNN) (Krizhevsky, Sutskever, & Hinton, 2012). These models have been widely used due to their accuracy in detection that assisted in numerous fields such as object detection (Girshick, Donahue, Darrell, & Malik, 2016) and image clustering and classification (T. H. Chan et al., 2015), yet their detection rate has been slow. Redmon et al. (2016) developed a novel model called YOLO (You Only Look Once) that uses the feature map to achieve real-time detection with high accuracy. Since then, there has been an incremental upgrade to the YOLO model by integrating ResNet50 (He, Zhang, Ren, & Sun, 2016) and Feature Pyramid Network (FPN) (T.-Y. Lin et al., 2017) till the YOLO version (5) (Redmon & Farhadi, 2018).

In YOLO v5, the detection of small objects has been improved significantly, making it suitable for detecting semantic objects with repeating structures such as windows and doors in building facades. Hence, the research adopts the YOLO v5 model as the main structure algorithm for object detection using UAV's RGB and IR data. The basic structure of the YOLO model is based on an end-to-end pipeline, where an input image is divided into an SxS grid, and each cell is used to predict the object centered in that cell. The prediction process is performed by examining the center of the semantic component in each cell. Each grid produces B bounding box with a confidence score of χ (Figure 4-18).
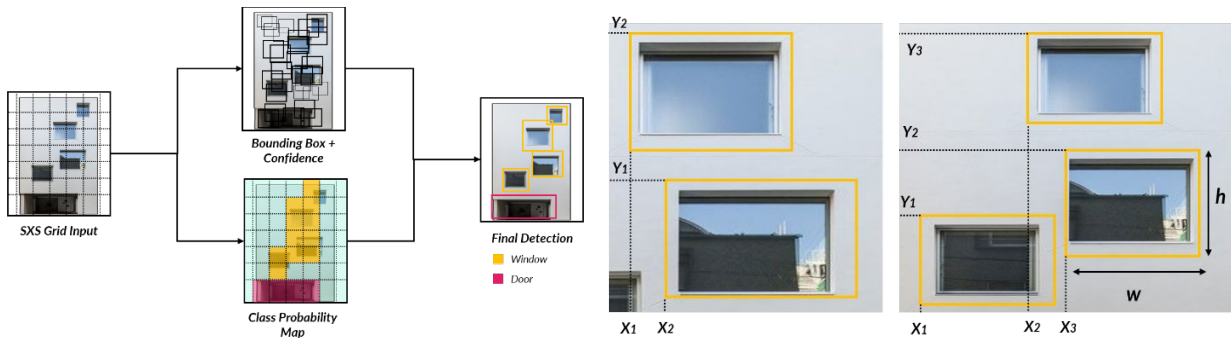
Figure 4-18: Left, Conceptual structure of YOLO model, Right, parameters of the model (Based on (Redmon et al., 2016)).

The confidence score of each predicted class is calculated using the following equation:

$$\chi = P_{class\ i} \times Q_{class\ i} \qquad (12)$$

where P is the probability of detected object in a bounding box B with accuracy score Q to account for the fitness between the predicted box and target object. There is an N bounding box for every image, and each bounding box is defined by 4 parameters (Figure 4-17). The dimensions of the bounding box are determined by w, h, and x,y represents the coordinates of the upper left corner of each bounding box.

The structure of the YOLO model is a convolutional neural network that consists of 24 convolution layers and 2 fully connected layers, as shown in Figure 4-19 (Redmon & Farhadi, 2018). The convolutional layers construct inception modules with 1x1 reduction layers followed by 3 x 3 convolutional layers (Redmon et al., 2016; Redmon & Farhadi, 2018). In the YOLO v5 model, a residual network is used as the model backbone, improving the detection accuracy significantly (He et al., 2016). Also, YOLO v5 can process images in real-time at 78 frames per second (FPS) with fewer false positives in the background (Redmon & Farhadi, 2018). Since doors and windows are considered semantic objects with varying sizes and poses, YOLO v5 is most suitable to overcome this problem by incorporating multi-scale fusion (T.-Y. Lin et al., 2017) to detect objects with good adaptability to changes in objects sizes.
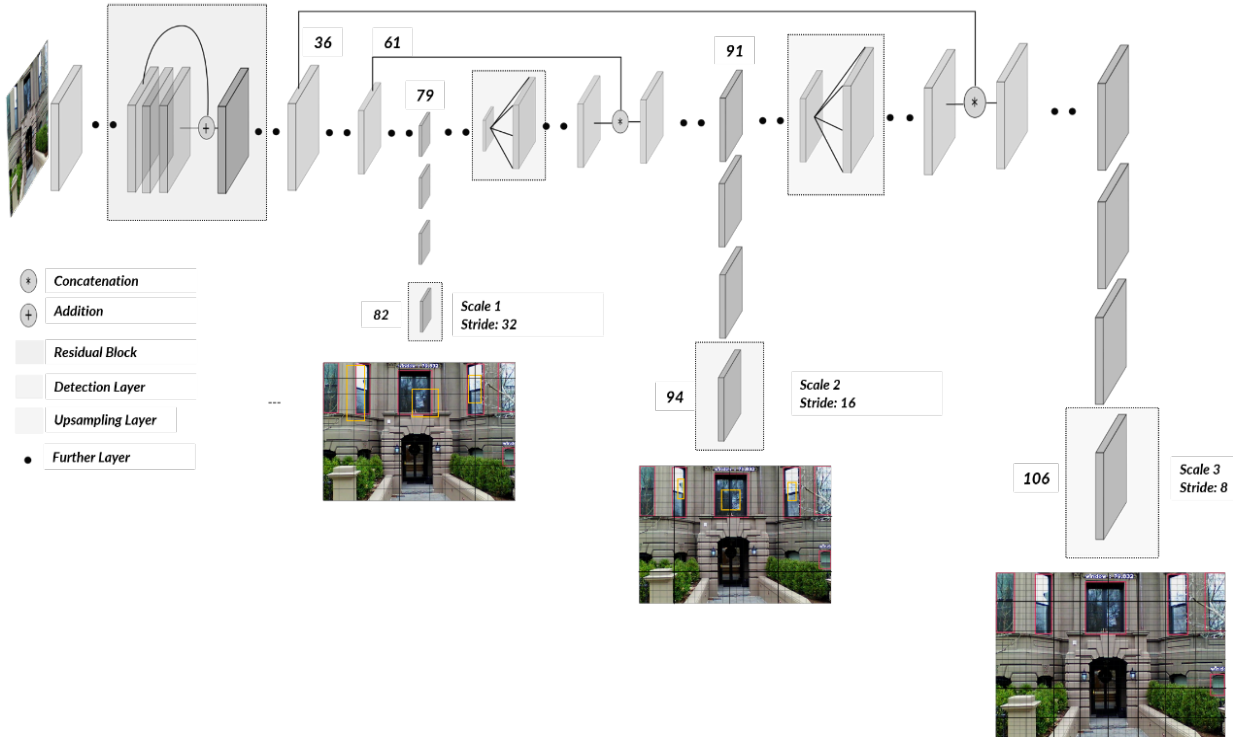
Figure 4-19: Network architecture of YOLO v5 model. (Based on (Redmon & Farhadi, 2018)).

Around 500 images collected in Boston, MA, were used as training data set with variations of doors and windows for residential buildings type. During the training process, the loss function is optimized using the following equation:

$$\lambda_{coord} \sum_{i=0}^{S^2} \sum_{j=0}^{B} d_{ij}^{obj} \left[(x_i - \hat{x}_i)^2 + (y_i - \hat{y}_i)^2 \right] +$$

$$\lambda_{coord} \sum_{i=0}^{S^2} \sum_{j=0}^{B} d_{ij}^{obj} \left[(\sqrt{w_i} - \sqrt{\hat{w}_i})^2 + (\sqrt{h_i} - \sqrt{\hat{h}_i})^2 \right] + \lambda_{coord} \sum_{i=0}^{S^2} \sum_{j=0}^{B} d_{ij}^{noobj} \left[(c_i - \hat{c}_i)^2 + \right.$$

$$\sum_{i=0}^{S^2} d_i^{obj} \sum_{c \,\epsilon\, classes} (p_i(c) - \widehat{p_i(c)})^2 \qquad (13)$$

where, in a given cell i, the center of the bounding box B is denoted as (x_i, y_i) to the bounds of the grid cell with normalized width w_i and height h_i relative to the image size. d_i^{obj} represents the existence of an object, c_i is the confidence of detection and d_{ij}^{obj} specifies that the jth bounding box performed prediction. The loss function penalizes classification errors only if an object is located in that grid cell i. Next, a binary variable ϵ [0,1] is assigned to represent the state of the selected attributes in each bounding box.
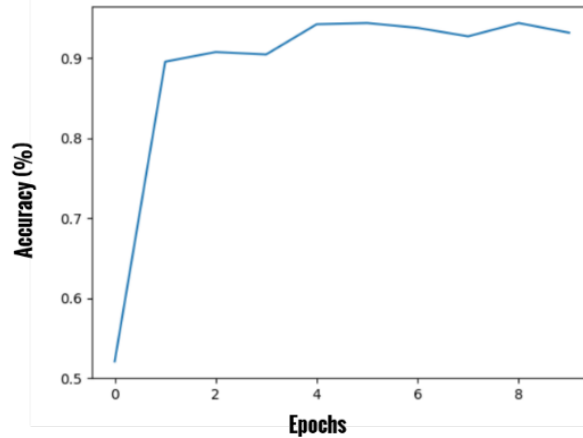
Figure 4-20: The learning rates for each of the training epochs. The magnitude of the accuracy increases after the first epoch and fluctuates around 94.4%.

The training data were manually labeled with semantic objects for two classes: doors and windows. The YOLO v5 model was then built based on Keras (Gulli & Pal, 2017), and the data were divided into 60% (300 images) for training and 40% (200 images) for testing. To assess the effectiveness of detected objects, the assessment method in (Hu, Wang, Zhang, Ding, & Zhu, 2020; Rahmani & Mayer, 2018) was adopted where every classified pixel was accounted as either false positive (FP) or true positive (TP) and the precision equals to TP/(TP+FP) and the total calculated precision was 0.93 (Figure 4-20). To assess the precision of the object detection, the model was tested with different resolutions and different layout configurations, and the model performed well with low-resolution images captured by the FLIR camera. Figure 4-21 shows the results of the detected doors and windows using the testing data set. The red frame represents the detected windows, and the green frame denotes detected doors.

Figure 4-21: Doors and windows detection results from YOLO v5 using the testing data set.

Since the YOLO model was tested against different resolutions and configurations, its output was used for window-to-wall ratio estimation. The process uses generated 3D mesh from UAV RGB data to calculate fenestration area and WWR for each façade separated. The process combines façade area segmentation and windows detection to calculate fenestration area and WWR. As explained above YOLO model will be used to detect windows in each façade side extracted from the 3D mesh. Here the research uses the Pyramid Scene Parsing Network (PSPNet) semantic segmentation algorithm proposed by Zhao et al. (2017) to estimate the façade area. PSPNet is a Scene parsing algorithm based on a semantic segmentation framework for pixel-level detection. The architecture of the algorithm uses a pre-trained ResNet model (He et al., 2016) to extract the feature map that is 1/8 of the input image's size. Then the feature map is overlayed by a Pyramid Pooling Module on top to pool the feature map to 4 different levels, each level

with a bin size of 1x1, 2x2, 3x3, and 6x6 to reduce dimensionality (Figure 4-22). Next, the pooled feature maps are convolved using a 1x1 convolution layer where the output of the convolution layer is concatenated to the original feature map. Finally, these outputs are processed by a convolutional layer to produce pixel-level detection (Figure 4-22). the PSPNet model was trained using a standard entropy loss function as follows:

$$\zeta_{ce} = \frac{1}{N} \sum_i^N \left[y_i \, \log p_i + (1 - y_i) \log(1 - p_i) \right] \quad (14)$$

where i is the pixel index, N is the number of pixels, y is the ground truth of the façade category, and p is the probability of the predicted object.
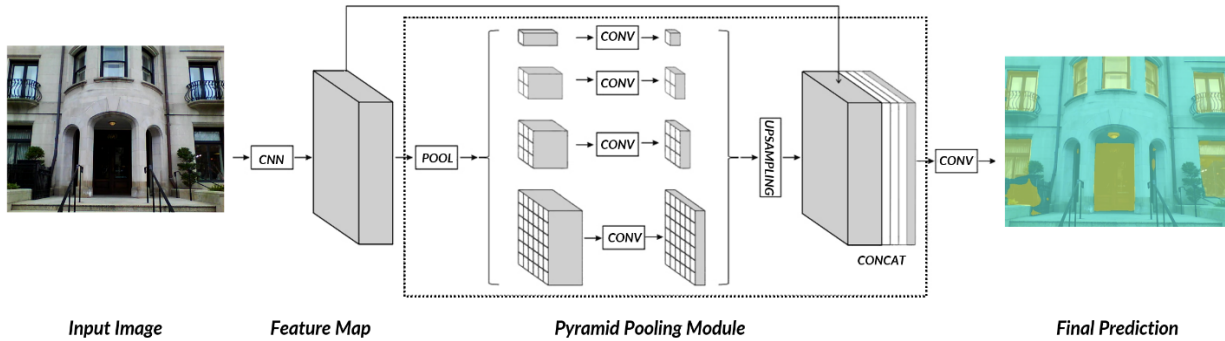
Figure 4-22: PSPNet Model architecture. (Based on (H. Zhao et al., 2017)).

the eTRIMS database (Korc & Förstner, 2009) and the "Ecole Centrale Paris Facades Database Benchmark 2011" (Teboul, Simon, Koutsourakis, & Paragios, 2010) were used to train the model. The "Ecole Centrale Paris Facades Database Benchmark 2011" contains 104 labeled images of rectified facades with 7 labels (doors, windows, sky, balcony, wall, roof, shop). The eTRIMS database contains 60 images with accurate annotations of other elements such as vegetation to test model parsing integrity against any possible noise. The research implements PSPNet based on Tensorflow and a single Google GTX 1080Ti GPU for training. The model's performance is evaluated using two of the most commonly used in image segmentation: total accuracy, mean intersection over union (IoU). Figure 4-23 shows the model's results after training using 170 images and testing for 60 images with the total accuracy of 88.27 and mean IoU 73.9.

Figure 4-23: Results from the PSPNET algorithm with segmented façade elements (walls, windows).

Next, a ratio to measure the number of pixels per detected bounding box is developed to calculate the area of the detected windows. Next, the total number of pixels of the boxes that surround windows (from

the YOLO model) was calculated and divided by the total number of pixels of the façade area detected from the PSPNet model. An image calibration was performed using the width and height ratio of the actual façade from UAV processed data as the reference object to calibrate each representative façade image. The pixel per metric (PPM) was used to estimate the ratio between the image and actual façade dimension using the following equation:

$$ppm = \frac{B_w}{f_w} \text{ in pixels} \quad (15)$$

Here, B_w is the width of the image, and F_w is the actual façade width measured from the 3D mesh, and by using that ratio, the size of all the detected bounding boxes was calculated in each façade image (Figure 4-24). The total fenestration area per each façade is calculated using the following equation:

$$WWR = \frac{\sum_{i=1}^{n} B_w \times B_h}{f_w \times f_h} \quad (16)$$

B is the detected bounding box with dimension (w,h), n is the number of detected bounding boxes in each façade image, and F is the captured image with dimensions (w,h).

Figure 4-24: Detected windows on rectified facade images.

4.6.5 Thermal Anomaly Processing & Categorization

This section discusses the process of thermal anomaly probability estimation and classification using IR data and detected thermal anomaly detection as primary data input. The workflow of thermal anomaly classification consists of four main components: 1) thermal anomaly processing, 2) anomaly categorization, 3) IR data processing, and 4) probabilistic anomaly detection and classification. The first step aims to enhance the visual integrity and reduce noise and any unwanted signals that may affect the final classification using image processing techniques. Here low pass filtering, known as smoothing, was used to remove unwanted signals and spatial noise frequencies in the detected anomaly image data. The concept of low pass filtering employs a moving window operator that affects each pixel of the image by changing its value (J. Lee, 1980; Shaikh, 2013), eliminating any unwanted noise. A low pass filter that consists of 5 x 5 pixels was used , where h is the spatial frequency, and the transfer function was carried out using the following equation:

$$y[i,j] = \sum_{m=-\infty}^{\infty} \sum_{n=-\infty}^{\infty} h[m,n] \cdot x[i-m, j-n] \quad (17)$$

Y [i.j] represents the new value of each pixel after applying the filter at row i, and column j in the image, and h[m,n] is the low pass filter with dimensions m and n. Although the naked eye cannot detect the filter's effect, it smooths out the image at the pixel level to merge the pixels of each anomaly detected.

Since each image can contain more than one anomaly, it will be challenging to assign a probability value per image as this may cause a false representation of the anomaly class detected per image. Thus, the research uses Breadth-First Search (BFS) algorithm to categorize and separate different anomalies detected in each data point (Silvela & Portillo, 2001). The concept of the BFS algorithm is grouping pixels of the same color that are connected by a continuous path of neighboring pixels of the same group. Since pixels are processed and stored in a queue connected from the low pass convolutional filter, the BFS algorithm can return a set of adjacent pixels of the same color, making this well suited to categorizing different anomalies detected in the same image. The propagation method in BFS is based on breadth-first traversal discussed by (Rayward-Smith, Cormen, Leiserson, & Rivest, 1991), where pixels are explored and stored using the function:

$$f(f(\ldots\ldots f(x)))$$

X represents the set of pixels of the same color, and this function is repeated recursively until it covers all pixels in the same image. The BFS algorithm was used on every photo to split each image into multiple versions of the same input containing only one anomaly class, as presented in Figure 4-25 below.

Figure 4-25: Left, Input segmented anomaly, right, output categorized anomalies after using the BFS algorithm.

Next, object detection output from the YOLO v5 model is combined with the categorized anomalies from the FBS model to estimate the probability of each anomaly detected. The probabilistic anomaly detection approach extends conventional object detection and categorized anomalies to quantify each anomaly's probability and class type. The process requires two data inputs, i) a presence of an anomaly and ii) a detector, to provide the classification for each anomaly detected, which is here a bounding box. The the probability distribution P is calculated for all anomaly pixels contained in an image using the following equations:

$$P_{infil/exfil} = \frac{\sum_{i,j} M_{anomaly\ i} \cdot M_{box\ i}}{\sum_i M_{anomaly j}} \qquad (18)$$

$$P_{Thermal\ Bridge} = 1 - P_{infil/exfil} \qquad (19)$$

The evaluation process examines the percentage of the anomaly pixels area that overlaps with the bounding boxes vector for both doors and windows to detect the class of the detected anomaly. In the case of infiltration/exfiltration anomalies, the probability value is assigned based on the spatial distribution of the anomaly area and a detector. For instance, if 85% of the anomaly area is located near a bounding box, the probability of this anomaly to be an infiltration/exfiltration class is 0.85, as illustrated in equation 18. The accuracy of the algorithm ranged between 80% to 85% based on a trained dataset of approximately 500 annotated images. The final output is an IR image with the anomaly class and the associated probability value, as shown in Figure 4-26 below.
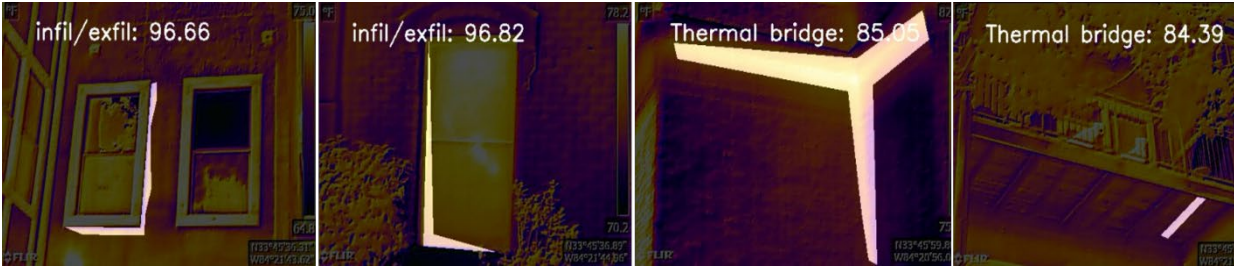
Figure 4-26: Final thermal anomaly classification and related probability.

4.7 The Case of the Bronx, NYC: Analysis Framework

This section discusses the application of rapid heat vulnerability assessment using UAV technology through a case study in Bronx Community District 6 (CD6) in New York City. The study's primary goal is to examine the applicability of the proposed framework in rapidly identifying factors associated with heat vulnerability. This is achieved by combining the socio-economic characteristics with the assessment of building envelope to identify building stocks and populations exposed to heat exposure and use that information to prioritize adaptation intervention to improve CD6 adaptive capacity against extreme heatwave events. The research also examines what role can be played through the local community in heat vulnerability assessment. The research examines a neighborhood in NYC city due to the rising concerns of extreme heat events.

The New York City Department of Health and Mental Hygiene estimates that there is an average of 13 deaths from heatstroke every year in New York City (NYC), and around 150 people are hospitalized (New York City Department of Health and Mental Hygiene, 2021). Also, in this study, the research works closely with a local community group through a research partnership between Pratt Institute and Mothers On The Move alongside the Mary Mitchell Family and Youth Center. The Bronx CD6 is a low-income residential district located in Northwest Bronx and is considered one of the densest in the United States (NY Start Smart, 2021). The total area of CD6 is 1.5 square miles and consists of 6 neighborhoods: Fordham, East Tremont, Bronx Park South, Bathgate, West Farms, and Belmont (Figure 4-27).
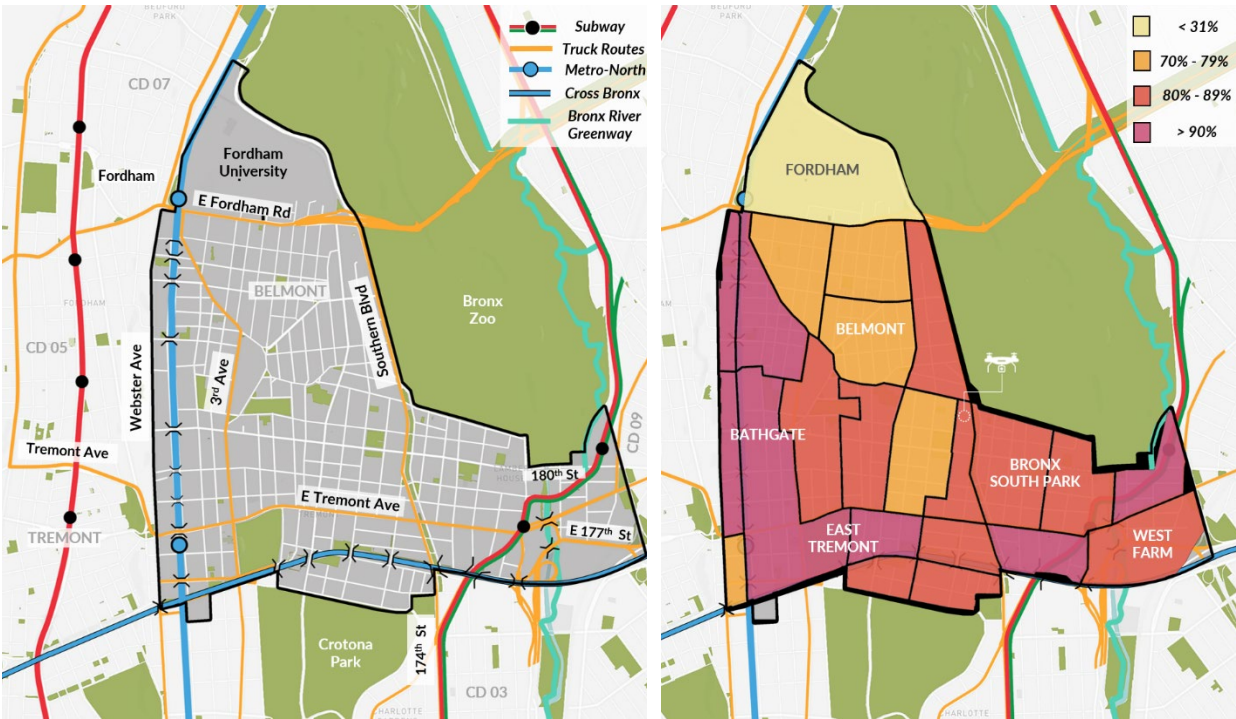
Figure 4-27: Left, The Bronx Community District (CD6) and existing infrastructure. Right, population of color distribution in CD6 (US Census Bureau, 2019).

The total population of CD6 is around 98,823 residents (DATA2GO, 2021), where 64.2% of the population are Hispanic, and 27.1% are non-Hispanic black or African American residents with the highest population of color density is located close to Bronx Zoo's southwest border (Figure 4-28). In terms of land use, there are 200 vacant lots in CD6, with 81.5% of the available lots are privately owned. There is also a high concentration of parking facilities that account for 6.2% of the total area. In comparison, recreation spaces represent 9.4%, four times lower than NYC and Bronx, limiting the adaptive capacity of CD6 residents against extreme heat exposure indoors (DATA2GO, 2021). The structure of the population in CD6 implies a higher susceptibility to heat exposure from the socio-economic perspective. The area is home to a low-income population with around 71% below the national poverty line (Figure 4-28). Also, about 37% of the population haven't completed high school, and 24% are college associate degrees (NY Start Smart, 2021). Also, most of the population are households (31,482), and the majority are single-parent households (around 10,000 single female householders) (NY Start Smart, 2021; US Census Bureau, 2019).
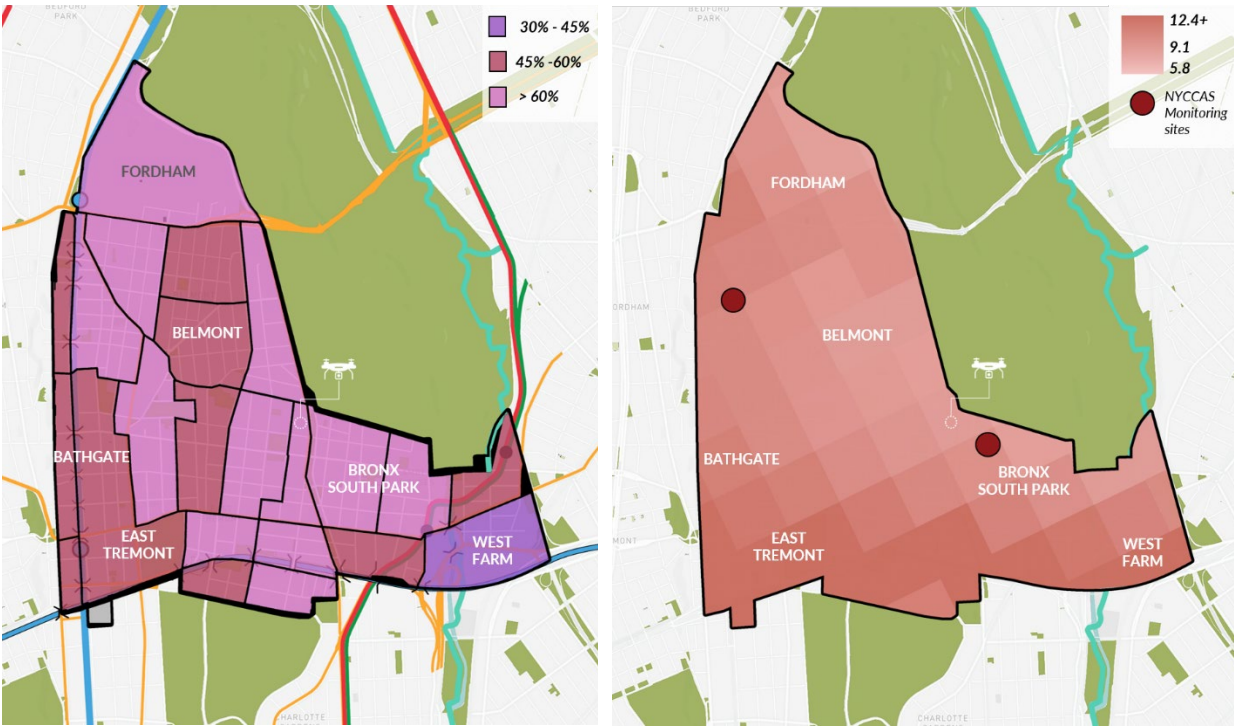
Figure 4-28: Left, CD6 population under the poverty line. Right, Average annual PM 2.5 concentration (ug/m³) in CD6 (New York City Department of Health and Mental Hygiene, 2021; US Census Bureau, 2019).

A previous assessment on heat vulnerability in CD6 indicated that the area is highly vulnerable to potential heat risks (Ortiz et al., 2018). Another factor to consider is air quality, as the concentration of PM 2,5 is relatively high in NYC, where 49% of PM 2.5 emissions are coming from buildings, and 17.5% are coming from traffic. The Bronx is considered one of the highest PM 2.5 concentrations (Figure 4-28), posing higher risks for vulnerable populations (Comptroller, Stringer, City, Heights, & Hill, 2018).

4.7.1 Data collection and Community Engagement

As discussed above, heat vulnerability in the Bronx is considered among the highest in NYC. The pilot study aims to assess how aerial thermography can provide information to guide building retrofits against heat exposure and reduce weatherization. A five-story walk-up archetype built in 1913 was selected since it has the same construction type and condition as 4156 buildings in CD6 (Figure 4-29). The building accommodates 23 residential apartments with a gross floor area of 19,523 square feet. Also, the building is part of the affordable coop housing in the Bronx and is owned and managed by the Housing Development Fund Corporation (HDFC) program in NYC. The data collection flight was conducted on April 8th, 2019, with a temperature difference of 10°C between indoor and outdoor temperatures. A strip pattern is selected with 90% frontal overlap and 80% side overlap using Mavic Pro with a dual gimbal carrying both RGB and IR simultaneously. The data collection process was carried out in collaboration with Pratt Institute and Mothers on the Move to design a community-based planning process to engage Coop Boards and residents in the building assessment. The partnership with the local community explores the opportunity to develop a pilot academy to train young people in CD6 to become drone pilots and engaged in the data collection side, as highlighted in Figure 4-13 above. This will improve the residents' employment prospects through high-paying career development, especially for young residents.

Figure 4-29: Right, exterior view for the examined building, Left, the distribution of similar archetypes in CD6.

4.8 Results

Data was collected using the workflow described above to examine the applicability of the rapid heat vulnerability framework to assess the envelope performance compared to the traditional envelope inspection and how such information can identify susceptible building stock to potential extreme heat events. From the IR data, the flight's results showed two types of thermal anomalies: infiltration/exfiltration and thermal bridge/missing insulation, with varying occurrences across the three inspected facades. Infiltration/exfiltration anomalies represented around 68.7% of the detected anomalies in both south and east façade (Figure 4-30), mainly around the window frames and AC units' boundaries. Also, thermal bridge/missing insulation is detected more in the upper floor of the west and south façade. In-person interviews with residents in different apartments were carried out to assess sources of thermal discomfort to confirm findings from thermal anomalies detection. The majority of the residents with apartments on the west-facing façade indicated an increased thermal discomfort during the wintertime, reporting that window frames are causing temperature fluctuations even when the heating system is on. These results confirm the findings from the thermal flight, which can be used as a first step of highlighting susceptible building stock rapidly and prioritize types of retrofitting interventions.
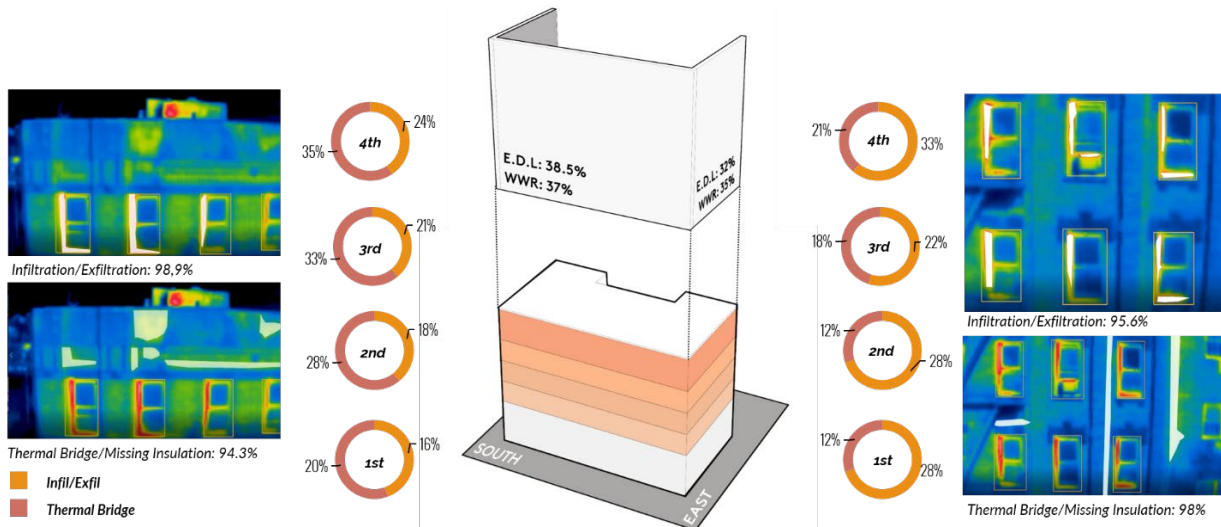
Figure 4-30: Detected thermal anomalies probabilities and their classes per floor in south and east façade.

From this analysis, the envelope's overall deterioration level was assessed from aerial thermography data. The research proposes Envelope Deterioration Level (EDL) to indicate the building's ability to regulate high outdoor temperature exposure and how susceptible the building is. EDL is calculated based on the percentage of anomalies detected over the total façade area using the following equation:

$$\frac{\sum_n^i Anomaly\ Area\ (AA)}{Facade\ Area\ (FA)} \qquad (20)$$

The overall deterioration level was estimated to be 38.6% of the total façade area, with the highest occurrence of anomalies in both south and east facades (Figure 4-31). Findings from the pilot study in CD6 highlighted the applicability of the proposed workflow in providing rapid assessment of existing building stock in a time-efficient manner. The data collection process took around two hours for 3487.5 square feet and four hours in processing time for IR data, anomaly detection, and EDL calculation. Output from RGB data was used to calculate WWR, visual assessment of material deterioration, and fenestration area (Figure 4-31). In addition to the output from the IR data processing, such information can be helpful in a further analysis of building performance, such as the development of whole building energy simulation models and estimation of thermal transmittance following the methodology discussed in the first section of this chapter.
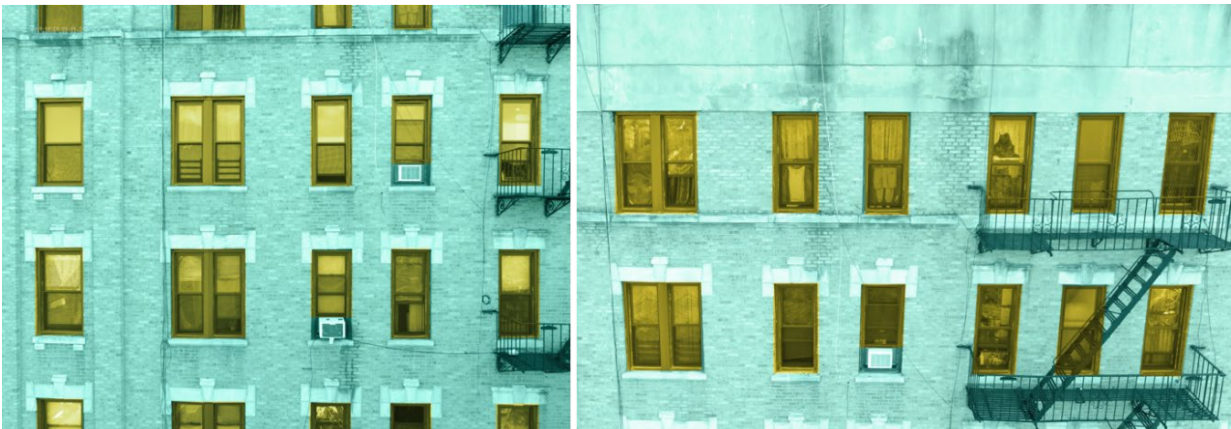
Figure 4-31: Left, Southern façade segmentation and detected windows.

Table 4-4 lists the main data outputs from the pilot study in CD6 in the Bronx. The proposed framework for rapid heat vulnerability assessment using UAVs can provide meaningful information that can also be applied in building audits, especially for ASHRAE Building Audit procedures 211P (ASHRAE, 2018). Results showed window frame replacement could play a significant role in improving the overall thermal performance of the envelope, which was evident from the several occurrences of infiltration/exfiltration anomalies in the three examined facades. New York City Housing Authority has set a target of retrofitting 87% of building stock by 2025 (NYCHA, 2018), where building envelopes representing 16% of total energy saving potentials and 18% of the total GHG emission reduction potentials. Therefore, identifying types of retrofit intervention using the proposed workflow can assist in NYC energy-saving goals from existing buildings and improve the existing stock in a time-efficient manner.

Table 4-4: Outputs from UAV data processing

Window-Wall-Ratio (WWR)	35% (Average)
Total Roof Area	3487.5 Square feet
Envelope Deterioration Level (EDL)	38.6%
Envelope Thermal Performance	61.4% (1- EDL)
Infiltration/exfiltration Occurrences	35% (Average)

4.8.1 Rapid Assessment of Urban Adaptive Capacity & Heat Adaptation Interventions

This section examines adaptive capacity at the district level by assessing the proximity of each building to surrounding urban amenities. The main goal is to rapidly evaluate how adaptive capacity conditions can better inform heat adaptation policies. The research considers available urban amenities to heat adaptation include three main categories: cooling shelter, open spaces/parks, and hospitals. To calculate proximity for each building to surrounding amenities, all pixels that carry information on the location of residential buildings and surrounding urban amenities are annotated. Annotation is divided into five main categories: residential buildings, roads, cooling shelters, open spaces/parks, and hospitals. After data annotation, BFS algorithm was used as a novel method to calculate proximity to surrounding heat adaptation amenities. The purpose of the BFS algorithm is similar to what was discussed previously in section 4.6.3.2, where it attempts to find a path by methodically examining all the neighbors of each node/pixel it examines. BFS uses a queue to track all neighboring nodes to examine, storing all assessed neighboring pixels until the queue is empty (Figure 4-32). Each examined pixel is stored in a set so that it is not examined twice and called a closed set, while pixels to be analyzed are stored in a set called open set (S. M. Kim, Peña, Moll, Bennett, & Kavraki, 2017). Thus, the BFS algorithm can annotate all road pixels from only one annotated pixel and store all groups of pixels that belong to a specific category into a separate set.
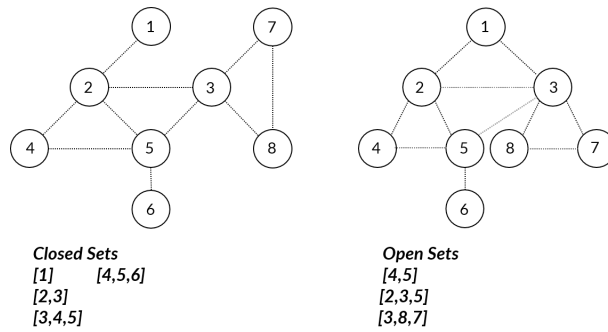
Figure 4-32: Schematic architecture of Breadth First Search (BFS) algorithm workflow (Silvela & Portillo, 2001).

All the pixels for all residential buildings are annotated and detected from the BFS algorithm and all the pixels for all nearest neighboring roads. The process of calculating the distance between each residential building and surrounding urban amenities by getting the pixels of every residential building and then the nearest road pixels the corresponds to the nearest point to each building. Then, the BFS algorithm is applied to connect the nearest point of each building to surrounding cooling shelters, open spaces/parks, and hospitals. The distance between each point and surrounding amenities is stored as a value representing the proximity of a given building and shortest path to surrounding heat adaptation amenities. This process is repeated for every building until all pixels stored in the building's set are covered. Figure 4-33 shows proximity to open spaces/parks and available health amenities in CD6 using the workflow described above. The proposed workflow can be expanded to evaluate the adaptive capacity for any given neighborhood or district based on the distribution and proximity to heat adaptation amenities and identify areas with high priority for urban intervention to improve their adaptive capacity under future heat events.
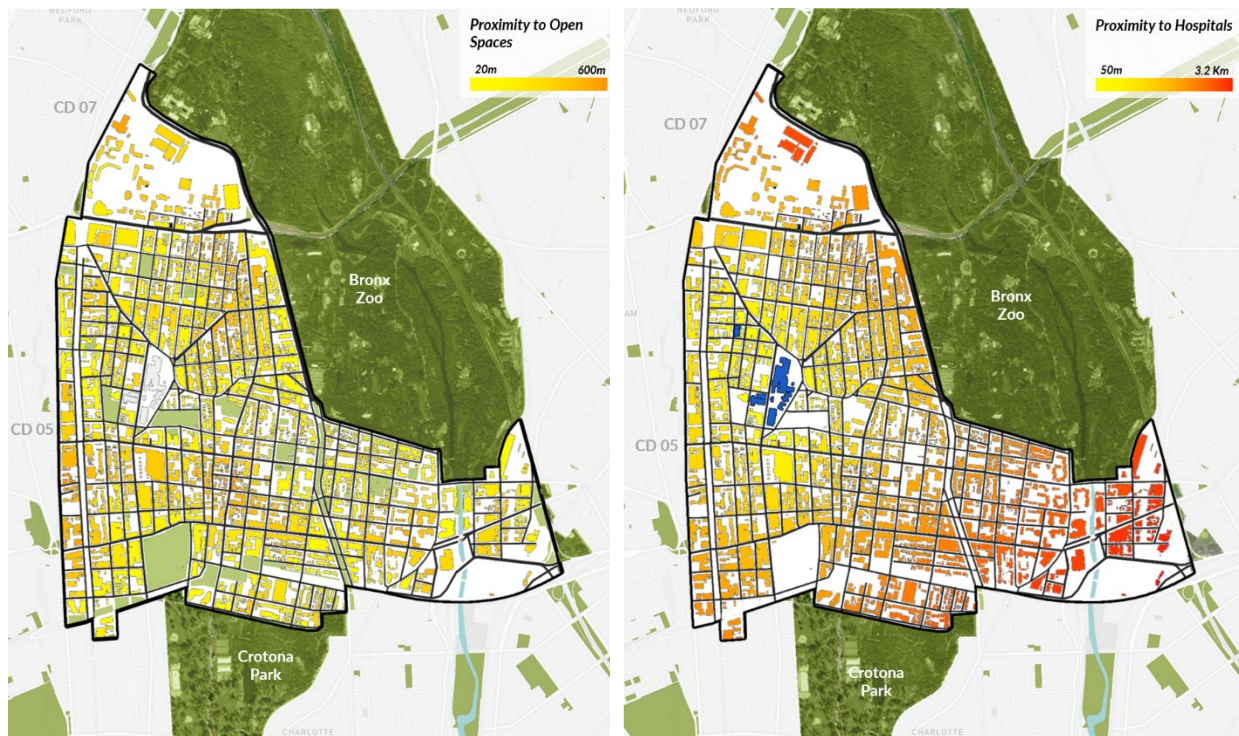
Figure 4-33: Left, proximity to existing open spaces and parks. Right, proximity to health amenities.

As it can be noted from the initial adaptive capacity assessment presented in Figure 4-33, there is limited availability of open spaces and cooling shelters. Open spaces in CD6 represent only 6.2% of the total area excluding Bronx Zoo and Crotona Park compared to 30% in the Bronx and 23% in New York City. Also, some areas have little access to open spaces that can be used as a cooling outlet during extreme heat exposure indoors and can be directly accessed by the community. Also, the lack of cooling shelters creates inequitable access to heat amenities and discourages residents from going outdoors when the indoor temperature exceeds thermal comfort limits or during power loss. Yet, there are potentials to improve access to open space by using underutilized spaces from vacant plots, curbs, and plazas that can be activated and made more accessible to the public.

Cooling centers can provide a resource to combat heat-related health impacts, especially when indoor air temperature at the building level increases. In CD6, there are 6 public facilities currently available for public residents to cool off during extreme heat events, including public libraries and senior centers, as shown in Figure 4-34. However, the capacity of existing cooling shelters can be improved by utilizing other public facilities within CD6 that can be transformed into cooling centers during extreme heat events, particularly for elderly and vulnerable residents. There are 539 public facilities in CD6 that can provide access to areas with limited access to cooling centers during a heat emergency. In addition, local community groups like Mothers on the Move can publicize the locations of these centers to residents who don't have sufficient information on heat adaptation resources during extreme heat events or heat emergencies announced by the city. Figure 4-34 illustrates improved adaptive capacity to areas of limited accessibility from the previous assessment after improving access to cooling centers.
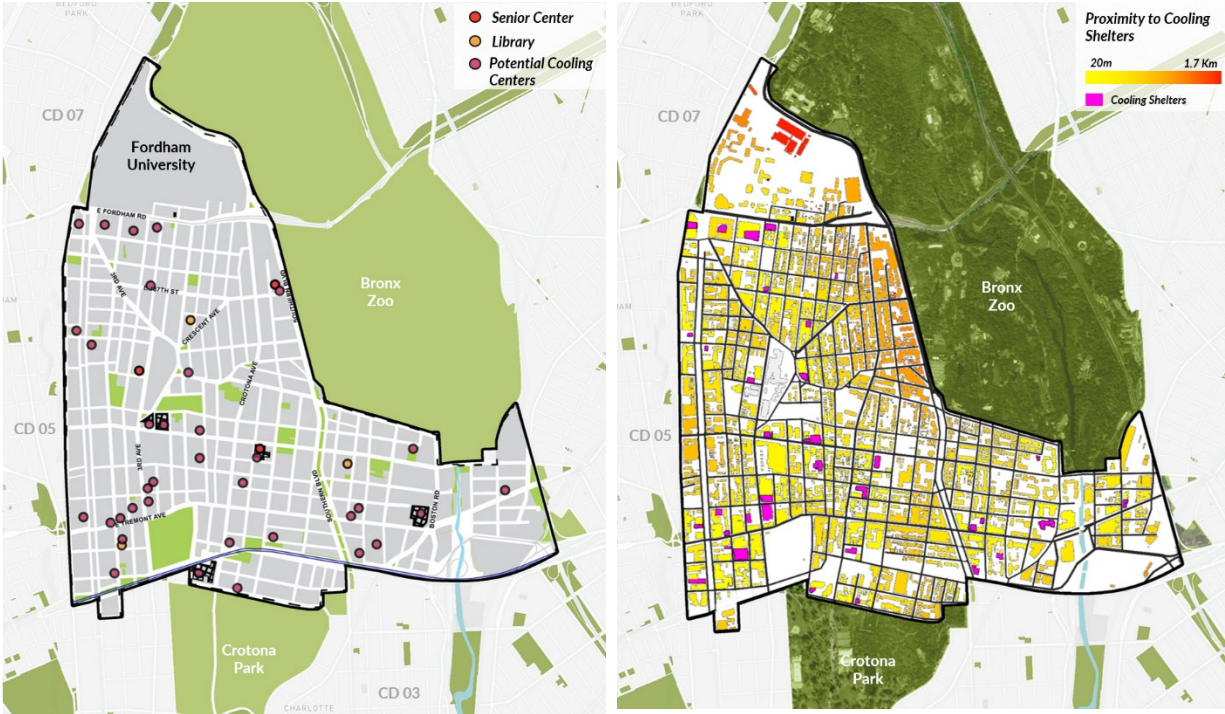
Figure 4-34: Left, Existing cooling centers in CD6. Right, improved access to cooling centers after utilizing available public buildings.

4.9 Discussion

This section presented a workflow for rapid heat vulnerability assessment using UAVs coupled with machine learning and graph theory models. The process incorporates using automated processing of IR and RGB images captured by UAVs to assess the thermal performance of building envelopes and how this can be translated to an indicator of buildings' susceptibility during extreme heat events. The proposed framework can provide helpful information in assessing building envelope with respect to anomaly classes, location, and spatial distribution across the envelope area. Also, using machine learning methods can provide reliable predictions with robustness for envelope deterioration levels that can inform better building retrofits and heat adaptation strategies. However, the main limitation of the proposed framework is assessing roof areas which can be overcome with training datasets for roof subjects. As part of the larger scope of passive survivability and heat vulnerability assessment to extreme heat events, a workflow for the adaptive capacity assessment is developed using only satellite imagery and building footprint information to understand the wide range of vulnerability disparities and access to heat adaptation amenities. The proposed workflow for the adaptive capacity assessment using the graph theory method has provided important information about the role of accessibility to heat adaptation amenities and access to other resources in heat risk reduction strategies. Findings] from CD6 in the Bronx indicate that residents have limited knowledge on the location or distribution of the closest cooling centers, which restrict their coping capacity in case of power loss at home or when the indoor temperature exceeds comfort levels. Assessing available adaptation resources to improve heat awareness plans can significantly assist decision-makers with the data to identify pathways to enhance adaptive capacity and residents' knowledge during extreme heat events at the district level.

4.10 Summary

This chapter examined the applicability of integrating aerial technology, namely UAVs, coupled with machine learning and graph theory methods in the rapid assessment of heat vulnerability at the building and district levels. The first section of this chapter proposed a framework for the detailed assessment of building thermal envelope performance using data from UAVs equipped with infrared and RGB cameras to estimate the envelope's thermal transmittance. Results from the study have shown a significant improvement in simulation models' prediction after incorporating calculated thermal transmittance. The proposed framework can also be helpful to identify types of retrofit strategies such as targeted wall insulation replacement, with less time and cost than traditional building inspection processes. The second half of this chapter presented a framework for heat vulnerability assessment at the building level using UAVs coupled with machine learning techniques and adaptive capacity evaluation at the district level using graph theory methods. The proposed methodology can provide information on the envelope's thermal performance that can impact indoor heat exposure levels. This was illustrated by the results from the pilot study in CD6 in the Bronx; by identifying the envelope's deterioration level, it can be better understood how to improve the thermal performance of building stocks that are more susceptible to future heatwaves. Also, the community engagement approach in using UAVs for building assessment can be a catalyst for the growth of job opportunities for the residents and engagement in the decision-making process. The chapter also explored graph theory and graph traversal techniques such as the BFS algorithm in evaluating adaptive capacity at the district level and how such information can assist policymakers in heat adaptation planning and heat risk awareness programs.

V. URBAN INTERVENTION AND POLICY DEVELOPMENT

Extreme heat events are increasingly affecting urban areas where the size of exposed vulnerable populations and their geographical distribution is constantly shifting due to economic development, urbanization, and demographic changes. Previous studies have illustrated that planned adaptation can significantly reduce heat-related health burdens during extreme heat events, especially among the most vulnerable populations (Liotta et al., 2018). Adaptation to climate change challenges is a complex problem encompassing various strategies triggered by extreme weather events and operates differently on spatial and temporal levels involving a broad range of actors and decision-makers (Holman, Brown, Carter, Harrison, & Rounsevell, 2019). Adaptation strategies for extreme heat events can be classified based on three main categories. First, the effect of heat risk that they target; adaptation strategies can tackle numerous heat-related effects such as a) reducing heat hazard sources either at the building level or the urban block level, b) vulnerability of the urban population through heat-awareness programs, and c) the adaptive capacity of the physical urban system such as increasing access to heat adaptation amenities and heat early warning systems. Second, the requirement for the implementing strategies, either hard (long term goals at the built environment scale) or soft adaptation (socioeconomic and institutional strategies) (Boeckmann & Rohn, 2014; Fernandez Milan & Creutzig, 2015; H. M. Füssel, 2007). Third, based on the types of actors involved in the decision-making process (Tompkins & Eakin, 2012). However, several factors can prevent the implementation and effectiveness of heat adaptation strategies. Most adaptation strategies are based on historical research rather than an accurate assessment of sectors of the population and their engagement in heat-related mortality prevention programs and are usually triggered by an extreme heat event (Heudorf & Schade, 2014; Pascal, Le Tertre, & Saoudi, 2012). In addition, there is a need to identify and design adaptation strategies that can be effective at varying levels of exposure at the physical urban system boundary and varying levels of vulnerability at the socioeconomic level of the population. The first section of this chapter presents an overview of different heat adaptation strategies for three scales: building, urban and human, and their impacts in reducing heat-related health risks. The second half explores the role of policy actors in the success and effectiveness in adaptation strategies referencing the case of 1995 Chicago heatwave using a system dynamic modelling approach.

5.1 Building Scale: Improving Coping Capacity

As mentioned in previous chapters, extreme heat poses significant risks to public health, and climate change will likely exacerbate the frequency, duration, and intensity of future heat waves. As highlighted in chapters 3 and 4, residential buildings play a vital role in mitigating indoor temperature and heat-related health impacts. Yet, heat adaptation strategies and potential climate and health benefits need to be thoroughly evaluated. This will assist future research in mapping and identifying the potentials of adaptation strategies in reducing heat-related health risks. It has been established from the literature, people spend around 90% of their time indoors (Neil E. Klepeis et al., 2001),. Thus, residential buildings play a crucial role in moderating indoor heat exposure during extreme heat events. Several studies have identified numerous factors influencing indoor heat, such as insulation level, air conditioning (AC) availability, and construction materials, which can significantly impact occupants' health during extreme heat events (Alam et al., 2016; Naughton, Henderson, Mirabelli, Kaiser, Wilhelm, et al., 2002; Quinn et al., 2014; J. Taylor et al., 2015). Therefore, heat adaptation interventions can significantly influence the magnitude of heat-related health impacts.

In addition to heat-related health impacts, buildings contribute to increased energy usage from cooling and heating demands. At the global scale, the building sector accounts for 25% of the global Greenhouse Gas (GHG) emissions (Fosas et al., 2018). Thus, improving building thermal performance lies at the heart of heat adaptation interventions and energy reduction goals (J. Li & Shui, 2015; Papadopoulos, 2016). To date, mechanical cooling is one of the primary heat adaptation strategies at the building level to combat heat-related risks during heatwaves. However, the energy cost of using air conditioning in the face of more frequent heat events is not a sustainable option. Also, the widespread blackouts during the summer months and mainly during heatwaves limit coping capacity to prolonged indoor heat exposure (Sailor, Baniassadi, O'Lenick, & Wilhelmi, 2019).

In addition, as was highlighted in chapter 3, those who are highly vulnerable to heat exposure are low-income populations who can't afford AC ownership. Therefore, improving the thermal performance of buildings' envelope has been regarded as a measure that will significantly reduce heat-related impacts on human health. Over the past 4 decades, there have been substantial efforts to reduce energy demand from the building sector through building energy codes such as ASHRAE 90.1 (ASHRAE, 2016). Also, the energy efficiency from applying these energy codes contributes to building resilience during extreme heat by improving indoor thermal comfort due to envelope improvements (Buonocore et al., 2019). This section presents an overview of strategies applied to residential buildings that can influence indoor exposure levels. Strategies to improve buildings' coping capacity are categorized into four categories: 1) strategies to limit heat gain, 2) strategies to improve heat rejection, 3) passive cooling strategies, and 4) occupants' behavior strategies (Figure 5-1).

INTERVENTIONS TO IMPROVE BUILDING COPING CAPACITY

1] Strategies To Limit Heat Gain

Building Envelope

Green Roof
Decrease indoor temperature
0.5°C to 2.0°C

Cooling Paint
Decrease Operative temperature
0.5°C to 1.6°C

Reflective Material

Night   Day

Material Selection

Thermal Mass
Stabilize peak IAT

Phase Change Material
Reduce discomfort hours by 62% to 78%

Design Strategies

Glazing Area /Ratio
Defining window sizing at early design stages

Glazing Type
Solar control films

Window Shading
Reflective internal blinds

External vertical louvers for west orientation

Fixed overhangs for South orientation

2] Strategies to Improve Heat Rejection

Air Circulation

Recirculating ventilation System
Natural ventilation is coupled with conditioning systems

Mixing ventilation system
Outdoor air is conditioned and supplied to indoor using ceiling or floor diffusers

Displacement Ventilation
Continuous extract ventilation using envelope openings

Building-integrated ventilation measures that rely on buoyancy

Secondary roof
Air flow   Water
Night   Day

Thermally active systems
Depend on buildings' thermal capacity to store heat couple with natural heat sinks to reject heat

3] Passive & Active Cooling Strategies

Evaporative Cooling
Passive Evaporative Cooling
Used in buildings where airflow through the buildings has a predefined path

Active Evaporative Cooling
Uses mechanical ventilation systems

Evaporation Pad   Fan

Bump

Mechanical Cooling
Use mechanical means to provide cool air into indoor spaces

Thermal Mass Coupled with Natural Ventilation
Cool air through both convection and radiative heat exchange between building mass and indoor spaces

4] Occupant Behavior Strategies

Knowledge on how to cope with heat exposure
When to use window blinds or curtains during sunny periods

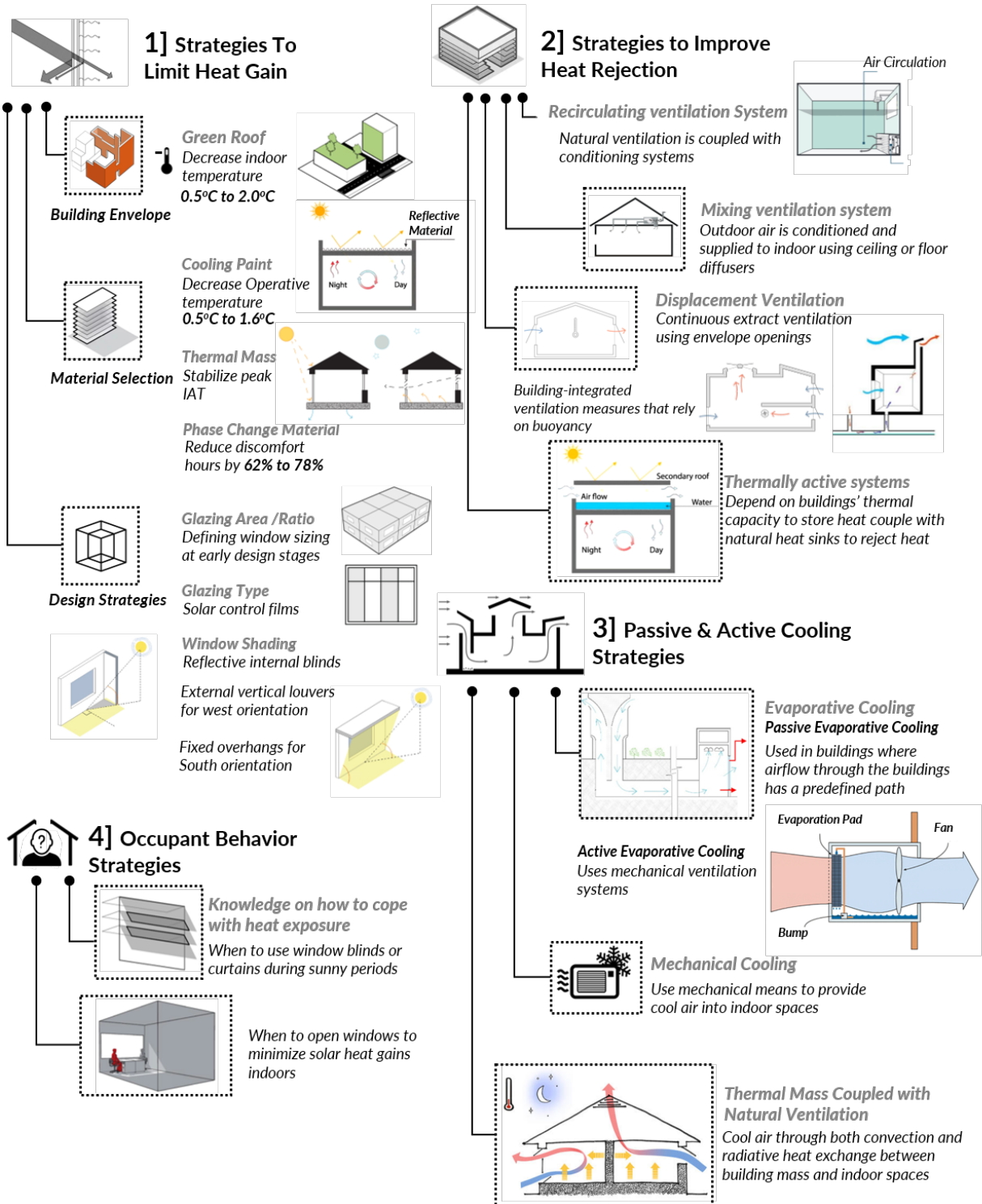When to open windows to minimize solar heat gains indoors

Figure 5-1: Coping Capacity strategies at the building scale.

5.1.1 Strategies to Limit Heat Gain

In situations of prolonged and extreme heat exposure, buildings' thermal capacity to regulate heat plays a significant role in preventing or reducing potential risks to human health. In the U.S., around 40% of heat-related morbidity happens indoors and in residential buildings (NWS, 2019). As illustrated in both case studies presented in chapters 3 and 4, building envelope thermal performance is a primary factor in heat gains during extreme heat events. Several studies have examined building envelope strategies to reduce heat gain in the face of climate change risks. From the literature, these strategies can be categorized into three main categories: i) building envelope, ii) material selection, and iii) design strategies.

A. Building Envelope: One of the explored strategies to reduce heat gain from the building envelope level is vertical greening and green roofs. Munch et al. (2018) have assessed the effect of green roofs during heatwaves. Results from the study show that green roofs generated indoor cooling 0.5°C to 2.0°C and contributed to a reduction in annual energy consumption. Another study by Virk et al. (2015) on the impacts of retrofitted green roofs on indoor microclimate found that green roofs can reduce near-surface air temperature. Another strategy is roof replacement made of highly reflective and light-colored materials that are 28°C to 36°C cooler than dark roof materials, and aged white roof materials are 20°C to 28°C cooler (Global Cool Cities Alliance (GCCA), 2012). Also, using white roofs in buildings with limited access to AC can reduce indoor air temperature for the top floor by 1°C to 2°C during extreme heatwaves. Numerous studies have investigated the impact of façade thermal insulation on heating prevention and indoor climatic conditions. Also, a vast body of literature examined the relationship between outdoor conditions and overheat concerns from thermal inertia. Kossecka and Kosny (2002) have conducted a whole building simulation analysis for six different climates in the U.S. and found that reduced heating and cooling demand from improved wall insulation surpassed 11% for continuously heated buildings. Stazi et al. have found that insulated envelopes effectively moderate heat flow to the external environment. Also, Stazi's (2017) study has found inadequate insulation layer thickness can affect heat flow and cause more overheating.

B. Material Selection: cool façade materials can contribute to indoor heat prevention and are considered among the straightforward measures to mitigate heat exposure impacts. Zinzi (18) examined the impacts of façade active cooling paint on indoor thermal conditions in Italy. The study showed that the average indoor operative temperature was reduced by 0.5°C to 1.6°C, and external surface temperature was reduced by more than 6°C. Other studies have assessed the effectiveness of using reflective materials on building thermal performance. Yang et al. (2015) have reviewed the applicability of reflective materials to prevent indoor heat exposure and found that reflective materials capability depends on numerous factors that need to be developed on a city-to-city basis. Sajjadian et al. (2015) examined the use of phase-change-materials (PCM) to mitigate heat impacts on buildings in the UK and identified that PCM could lead to a reduction in discomfort hours by 62% to 78%.

Another measure to mitigate indoor heat exposure and related to building materials is thermal mass. The use of thermal mass to improve indoor conditions has two distinct mechanisms: removing heat from air through convection when the internal air temperature is at high ranges and radiative heat exchange (Saulles, 2009). Thermal mass can be used to stabilize peak indoor air temperature, yet the level of

thermal mass exposure to air flows plays a significant role in how effectively it functions. Findings from the literature have suggested that for thermal mass to remove built-up heat from exposed thermal mass effectively, nighttime ventilation rates should be between 6 to 10 ACH (ZCH, 2016). However, in highly dense and deep urban areas, achieving high rates is challenging, especially if opening windows at night is impractical due to noise pollution levels and security. These issues need to be carefully addressed to improve thermal mass effectiveness in dense urban locations that can be more susceptible to heat exposure, as highlighted from the case study in chapter 3.

C. Design Strategies: One of the most straightforward and unfortunately rarely explored strategies to reduce heat gain is rational glazing. Rational glazing area implies simultaneously optimizing glazing area to reduce heat gain and energy demand from cooling (Kisilewicz, 2015). However, the glazing area depends significantly on multiple factors such as window orientation, thermal resistance, the layout and openness of the building interior, and the thermal capacity of the envelope (Kisilewicz, 2007). This problem can be overcome by defining window sizing at the first stage of the building design. Also, glazing type is one of the key measures that can impact heat gains from fenestration. Solar control films are one of the appropriate retrofit measures that are applied to existing glass to reduce heat gain at a relatively low cost (ZCH, 2016). Another design strategy to moderate solar heat gain through glazing is window shading, whether internal or external shading. Internal shading prevents solar radiation from directly heating internal surfaces, yet, unreflected solar radiation can get radiated back into space and back into the window, causing indoor air to warm. Therefore, the use of reflective internal blinds can be more effective than typical curtains or Venetian blinds as they can absorb shortwave radiation transmitted through windows and emit longwave radiation that the glass absorbs. External shading can be significantly more effective in reducing solar heat gain without the potential of warming indoor air from reradiated longwave heat that is absorbed by the warm glass (Stagrum, Andenæs, Kvande, & Lohne, 2020). However, the shape and location of external shading can significantly influence their performance. Fixed overhangs, for example, are more suitable for southern orientation to limit heat gains and high angel summer sun. Yet, for west elevation, where the sun is relatively lower in the summer, external vertical louvers or blinds can be more effective (Al-Tamimi & Fadzil, 2011; Zukowska, Ananida, Kolarik, Khanie, & Nielsen, 2019).

5.1.2 Strategies to Improve Heat Rejection

The second category of building intervention strategies is related to strategies of replacing indoor air with outside air when the outdoor air temperature is lower through natural ventilation. Natural ventilation relies mainly on wind speed and direction to achieve sufficient heat gain removal during peak summer months. Thus, large ventilation openings are required to provide suitable air flow rates and should be left open for long periods, even during the cooler periods of the day. In dense urban areas, leaving windows open for long periods is not practical, especially when the external environment is noisy, and there are other issues related to privacy and safety. Several studies have examined the effectiveness of natural ventilation in the face of future climate projection and during heatwaves. A recent study by Alessandrini et al. (2019) examined the use of natural ventilation during heatwaves found that natural ventilation can improve thermal comfort during normal weather conditions; however, it is not an effective coping strategy during heatwaves. Another study by Heracleous and Michael (2019) found that natural

ventilation is a viable option to cope with current heat exposure conditions but not in the future with the projected increase in temperature.

Numerous ventilation strategies can be used to minimize indoor heat exposure, such as i) recirculating ventilation, ii) mixing ventilation systems, and iii) displacement ventilation (Lipinski, Ahmad, Serey, & Jouhara, 2020). In recirculating ventilation, natural ventilation is coupled with conditioning systems (split-system air conditioning, ceiling fans, hybrid ventilation systems) used to move indoor air temperature or mix it with outdoor air before pumping into the room. This ventilation method generates turbulent air flows with stale air recirculated back into the room. In mixing ventilation systems, outdoor air is conditioned and supplied to indoor spaces through ducts using ceiling or floor diffusers (Emmerich, Dols, & Axley, 2001). Mechanical ventilation with heat recovery (MVHR) systems is used to reduce ventilation-related heat loss. Finally, displacement ventilation systems are categorized into 1) continuous extract ventilation that uses envelope openings to replace indoor air with outdoor air utilizing negative pressure, and 2) building-integrated ventilation measures that rely on buoyancy to displace hot air using elements such as windows, solar chimney, or passive stacks (Lipinski et al., 2020).

As discussed above, thermal mass can store heat and reduce peak summer temperature. However, stored heat needs to be removed later from exposed surfaces with night ventilation or other forms of active cooling. There are alternatives to overcome thermal mass heat storage release during the nighttime, such as thermally active systems that use water-based cooling as an alternative to cool down building structures. These systems depend on buildings' thermal capacity to store heat coupled with natural heat sinks such as groundwater or reverse cycle heat pumps to reject heat (Stazi, 2017). A roof pond is one example that uses large volumes of exposed water to cool down spaces beneath.

5.1.3 Passive & Active Cooling Strategies

One of the passive cooling strategies that can be utilized to reduce or prevent heat-related risks during heatwaves is evaporative cooling, classified into passive and active evaporative cooling methods (Addante, Iannone, & Rinaldi, 2015). Passive evaporative cooling can be used in buildings where airflow through the buildings has a predefined path and a well-established wind pattern. On the other hand, active evaporative cooling uses mechanical ventilation methods to pass the air through a wetted medium and can be used in any building (ZCH, 2016). There are two types of active evaporative cooling: i) direct evaporative cooling, where the air is cooled directly by evaporating water into the air stream, yet, this method increases levels of relative humidity in the air pumped into space, and ii) indirect evaporative cooling that cools air supply through an air heat exchanger. Indirect evaporative cooling is less effective than cooling, but it doesn't increase relative humidity levels in air supplied to indoor spaces (Addante et al., 2015).

Active cooling strategies that can be used for heat adaptation intervention at the building scale include mechanical free cooling, mechanical cooling, and direct cooling. Mechanical free cooling strategies use mechanical means to provide cool air into indoor spaces (Zukowski, Sadowska, & Sarosiek, 2011). Earth tube is one of the free cooling strategies that draw air through earth tubes buried in the ground. In the summer months, earth tubes are generally cooler than the outdoor air temperature, thus providing a potential to reduce incoming air temperature and provide cooler air into indoor spaces (Morley, 2017).

The main limitations with earth tubes are the required large land areas and concerns regarding potential mold growth in air supply ducts due to condensation. As discussed above, there is a potential for thermal mass coupled with natural ventilation to cool air through both convection and radiative heat exchange between building mass and indoor spaces. There are two approaches that link thermal mass to mechanical cooling systems: 1) passing air through a void on one side of the building's thermal mass like raised floors or false ceiling allowing airspeed to stay high and with a controlled airflow rate, and 2) passing air through hollow cores within the thermal mass of the building (Sajjadian et al., 2015; Saulles, 2009). Finally, mechanical cooling is one of the most commonly used strategies to reduce indoor heat exposure and minimize heat risks during extreme heatwaves. In addition to their energy-intensive profile, mechanical cooling has high costs either from ongoing maintenance costs over the operation time of the system or running costs affected by the size of the system, how it is used, and outdoor air temperature (Lundgren-Kownacki, Hornyanszky, Chu, Olsson, & Becker, 2018). In reality, mechanical cooling systems during extreme heat events will operate for more extended periods, resulting in higher running costs and increased heat rejected to the local urban climate and contributing more to Urban Heat Island (UHI) effect. Some studies have also found that air conditioning (AC) negatively influences human heat acclimatization ability after continuous exposure to AC for two weeks (Lundgren-Kownacki et al., 2018).

5.1.4 Occupant Behavior Strategies

Occupant behavior is considered one of the leading causes of uncertainty in building performance (Hoes, Hensen, Loomans, de Vries, & Bourgeois, 2009; J. Kim et al., 2017). During extreme heat events, occupants' knowledge of building design features that can influence heat gain and rejection is crucial to the effectiveness of the strategies presented above. Studies from the literature have shown that most buildings' occupants are unaware of heat gain sources, whether from windows or building structures (Delzendeh, Wu, Lee, & Zhou, 2017). There are various behavioral strategies that can contribute to heat gain reduction at the building level, such as using window blinds or curtains during sunny periods of the day or when the sun is directly shining on the windows.

Another occupant behavior measure that can lead to increased indoor heat exposure is changing window covering positions during the day. Studies on occupant behavior and indoor conditions (DOE, 2013) found that between 75% and 84% of the window covering of the examined sample remains in the same position throughout the day. Also, 56% and 71% of surveyed households didn't adjust window covering daily or throughout the week when the outdoor air temperature increases. The same study showed that most building occupants are unaware of how to operate window blinds or open windows to minimize solar heat gains indoors. Therefore, heat awareness programs at the building level should be an integral part of building strategies to combat heat-related health risks during extreme heat events.

5.2 Urban Scale: Adaptive Capacity and Heat Adaptation Amenities

There are numerous strategies to reduce heat risk impacts at the urban level. As discussed in chapter 2, urban adaptive capacity denotes resource availability to reduce heat-related health risks at the urban level. Strategies to improve urban adaptive capacity can be categorized into three types, 1) strategies to combat Urban Heat Island (UHI) effect, 2) urban design strategies, and 3) strategies to decrease population vulnerability (Figure 5-2). As was discussed in chapter 2 and 3, urban areas tend to be warmer

than rural areas at night, due to the concentration of building, physical infrastructure, and energy use (Lapola et al., 2019b).

5.2.1 Strategies to combat UHI Effect

At the urban level, strategies to combat UHI are primarily influenced by the physical layout of the built environment that affects sun and daylight availability, the degree of shading, and the potentials for natural ventilation (Wang & Akbari, 2016). Also, transportation infrastructure can often be a barrier to opening windows at the building level due to air pollution or noise. The presence of vegetation and permeable paving can also mitigate the UHI effect alongside the availability of open water bodies to cool down air at the urban canyon level. The US Environment Protection Agency (EPA) reported that foliage coupled with shading could help significantly reduce peak air temperature during the summer. It was also found that suburban areas with trees are 2 °C to 3°C cooler than suburbs without trees (US EPA, 2008). A detailed study by Knight et al. (2016) has found that urban greening strategies such as parks or planting trees have affected air temperature within the surrounding urban areas. Another study by Doick et al. (2013) has identified a minimum area of one hectare (10,000 m2) of green spaces to achieve a cooling effect at distances beyond the vegetation site.

Surface Albedo: At the local urban level, the solar reflectivity of urban surfaces can largely influence the heat absorbed by the urban structure (buildings, pavements, roads) and the release of heat back into the local climate. Morini et al. (2016) have identified a potential decrease in air temperature by 2°C and 4°C at the local climate by changing the albedo of paving and roofing materials in urban areas. In addition to urban surface albedo, there are other strategies such as green roofs (vegetation), white roofs (cooling paint), and blue roofs (roof ponds) that can contribute to the reduction of air temperature at the urban level. Although green roofs can significantly influence air temperature at the local climate in urban areas, installation and maintenance costs should be carefully assessed in heat adaptation planning.

5.2.2 Urban Design Strategies

The configuration of the urban form and its physical characteristics can impact the amount of solar heat gains and losses. Numerous studies that examined the role of urban form in heat mitigation have found that in hot climates, urban areas with narrow streets have lower solar access and more shading potentials during the day (Ferwati, Skelhorn, Ferwati, Shandas, & Makido, 2020). However, deep urban canyons can negatively influence airflow movement and thus limit the potential for natural ventilation, as illustrated in the case study discussed in chapter 3. Also, the ratio between a building's surface area and volume directly impacts heat losses; for example, compact forms reduce envelope heat losses (Y. Li, Schubert, Kropp, & Rybski, 2020). Heat adaptation strategies that target urban layout need to be carefully addressed at the planning level, where design decisions at the city scale can have a local influence on reducing impacts from future heat risks. Another planning strategy that can significantly influence heat risks at the city level is the orientation of buildings. These strategies are specifically important to minimize summer and mid-season heat gains while utilizing winter solar gains. Building height is another important factor that influences wind speed and potentials for wind-driven ventilation at the building level, as are the sizing and area of the windows to allow a suitable airflow rate.

5.2.3 Strategies to Decrease Population Vulnerability

In addition to heat adaptation strategies at the level of the physical urban system, there are other strategies in the aspect of heat risk that target improving the population's capacity against heat exposure. These strategies aim to improve occupants' awareness of coping with heat exposure, such as heat-related social programs (cooling shelters and assistance programs to subsidize electricity bills for low-income populations) and social networks at the neighborhood level. These strategies primarily target reducing human vulnerability to heat exposure through three main pathways. **First, strategies to improve access to heat adaptation amenities**. These strategies aim to increase access to heat adaptation resources at both the building level, such as access to AC at the building level through energy subsidies in collaboration with local energy programs, and at the urban level by increasing access to public cooling shelters through information campaigns to raise awareness about locations of nearest cooling centers (Hayden et al., 2017a). **Second, strategies to decrease poverty-related vulnerability.** These strategies aim to decrease socioeconomic inequalities, the number of households below the poverty line, and increase employment rates in low-income communities. They also aim to improve urban services for low-income communities, such as public transportation, to reduce residential segregation and thus promoting job stability (Rohat et al., 2019). T**hird, strategies to decrease social isolation.** Vulnerability due to social isolation is tackled by strengthening community social networks such as active monitoring programs that aim to improve social relationship networks or neighborhood-based programs to visit and communicate and visit most vulnerable populations (elderly, elderly living alone, elderly with medical history) during extreme heat events (Fernandez Milan & Creutzig, 2015).
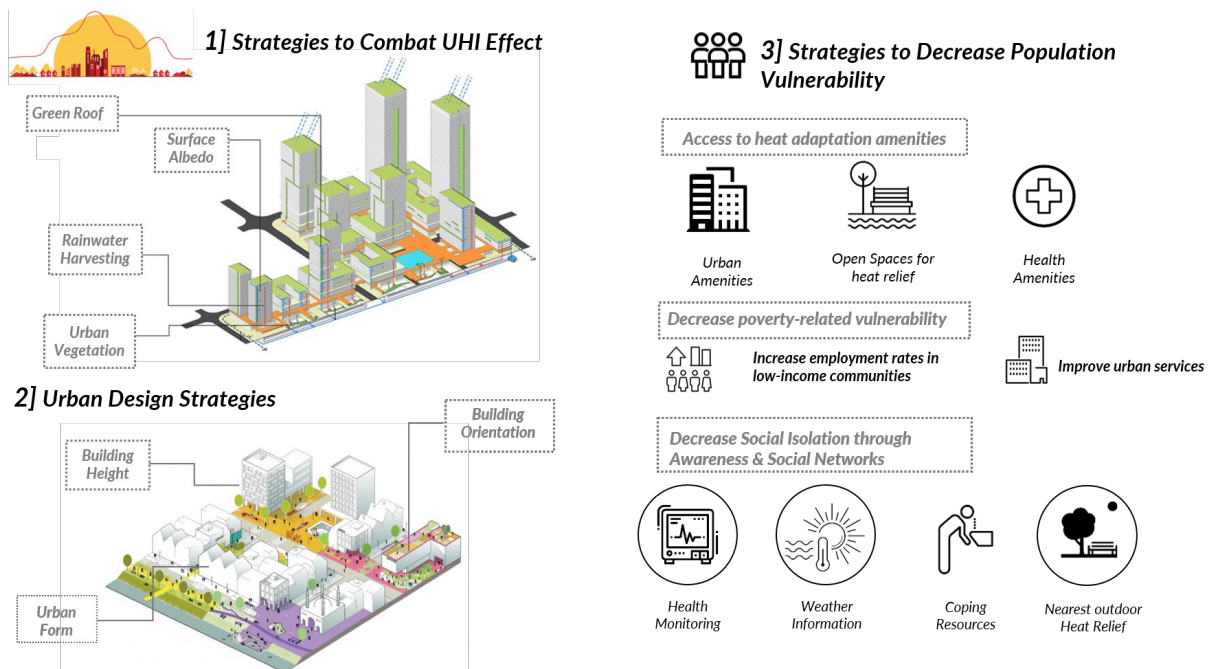

Figure 5-2: Heat Adaptation interventions at the urban level.

5.3 Human Scale: Impacts of Community and Social Capital

Social capital has been identified as a significant contributor to climate change adaptation and positive climate-related health outcomes. During extreme weather events, populations struggle to maintain behavioral patterns or access to social support that can affect their vulnerability against climate risk, similar to what happened during the heatwave in Chicago (Bernier & Meinzen-Dick, 2014; Davies et al., 2013; Naughton, Henderson, Mirabelli, Kaiser, Wilhelm, et al., 2002). Studies on social capital and climate adaptation classified social capital into three main classes. First, bonding social capital is represented in the relationship between individuals from the same social identity and characterized by strong ties and localized trust. For instance, networks between members of the same family, friends, or neighbors sharing the same social or demographic characteristics (Adger, 2003; Pelling, 2011). Second, bridging social capital links distinct groups and is characterized by weak ties such as social networks between people with similar political views or economic status. Third, linking social capital takes the form of trust networks with authority gradients and is characterized by weak ties of reciprocity, for example, social links between residents and individuals with political power, such as government officials or policymakers (Woolcock, 2001).

In social sciences, human vulnerability to climate hazards is strongly tied to the social capital of the population (Cutter, Boruff, & Shirley, 2003). A significant body of literature identified three indicators of how social capital can impact community resilience during extreme weather events—first, support networks as an indicator of strong social relationships between community members (Forbes & Wainwright, 2001). Second, social and economic discrepancies as an indicator of poor health outcomes (Wilkinson, 1996). Finally, access to resources for adaptation governs potential health outcomes during extreme weather events (Muntaner, Lynch, & Smith, 2007). In this context, social capital plays a crucial role in residents' survival during extreme weather events and can positively accelerate the recovery process and long-term adaptation plans. Individuals with strong social ties, either with neighbors, friends, or a sense of attachment, are more likely to contribute to the support networks during a catastrophe (Aldrich & Sawada, 2015).

Also, strong social capital can seek changes in political regimes or planned policies that can reduce potential climate impacts and create more sustainable and resilient societal practices. There are numerous approaches to improve social capital, such as community currency to encourage involvement and strengthen trust between community members and time banking programs, that have been proven to be effective in building social ties (Brune & Bossert, 2009) and improving the community's collective role through engagement in planning and support existing social structure such as engagement of local community groups in adaptation planning. Finally, social and communications technologies can strengthen coordination between local communities, government, and policy officials (Aldrich, Page-Tan, & Paul, 2016).

5.4 Policy Role in Heat Adaptation Strategies

Because extreme heat events are expected to increase worldwide within the next 20 years, there is a need to improve adaptation policies and policymakers' responses to potential heat-related impacts on human health. Studies on heat adaptation strategies can assist in identifying types of adequate measures based on quantifiable assessment, yet, the central part to the success of this process is tied to government policies, planning, and the decision-making process. Efforts to adapt to various climate change risks are often based on the technical assessment of different climate stressor impacts as the driver of change. However, enabling adaptation policies requires navigating political realities and interests and institutional incentives to influence governments' policies in programming. This section examines the role of policymakers in shaping adaptation success or failure and how the delay in policy implementation can influence the level and magnitude of risk during extreme weather events. The 1995 Chicago heatwave is used as a model to examine how policies can negatively or positively affect the portion of the population exposed to climate stress and how adaptation strategies could help mitigate potential risks before, during, and after the exposure to an extreme heat event.

In the United States, around 400 people die from extreme heat events each year, with the risk of heatwaves increasing even further due to climate change. Many cities still lack a proper heat response plan despite the growing risks of heat-related mortality and morbidity. The root cause of this problem is tied to the underestimated attention from public health in the United States to heat-related mortality (Changnon, Pielke, Changnon, Sylves, & Pulwarty, 2000; McGeehin & Mirabelli, 2001). There are several best practices to improve the built environment and alleviate surrounding conditions during heat exposure; however, how can policy play a role in disaster preparedness?

For natural disasters like hurricanes, the economic damage of expensive properties is so intense that the policy action is immediate as it generates strong public attention and media coverage. Yet, heatwaves receive little public attention not only because they fail to generate the massive property damage produced by other natural disasters like hurricanes and storms, but also most of the heatwave victims are primarily lower income individuals, the elderly, social outcasts and isolated individuals. The series of deadly heatwaves that the U.S. witnessed in the early 1980s indicated a connection between vulnerability to heat, policy, and state retrenchment (Klinenberg, 2003a). Most of the studies that have looked at heat-related mortality and morbidity examined the link of heat-related deaths to environmental factors with little emphasis on the policy role. The notion of policy action delay or delayed impact from a specific policy on increased vulnerability is still limited. Thus, the focus of this section is to investigate the implications of policy action delays and delayed impacts from specific policies on heat vulnerability and heat-related mortality and morbidity. The central hypothesis is that heat-related vulnerability is a function of three parameters: people susceptibility, available adaptive capacity, and exposure to heat as a result of the surrounding built environment conditions. The research hypothesizes that availability and quality of adaptive capacity are driven by policy action, which is triggered with a delay by the number of people at risk from heatwave or in the real-world death tolls from heat. Also, susceptibility is a function of the population's socioeconomic factors developed over time due to misplaced policies that led to an increase in poverty indirectly or gaps in available adaptive capacity with a delayed impact, as illustrated in Figure 5-3 below.
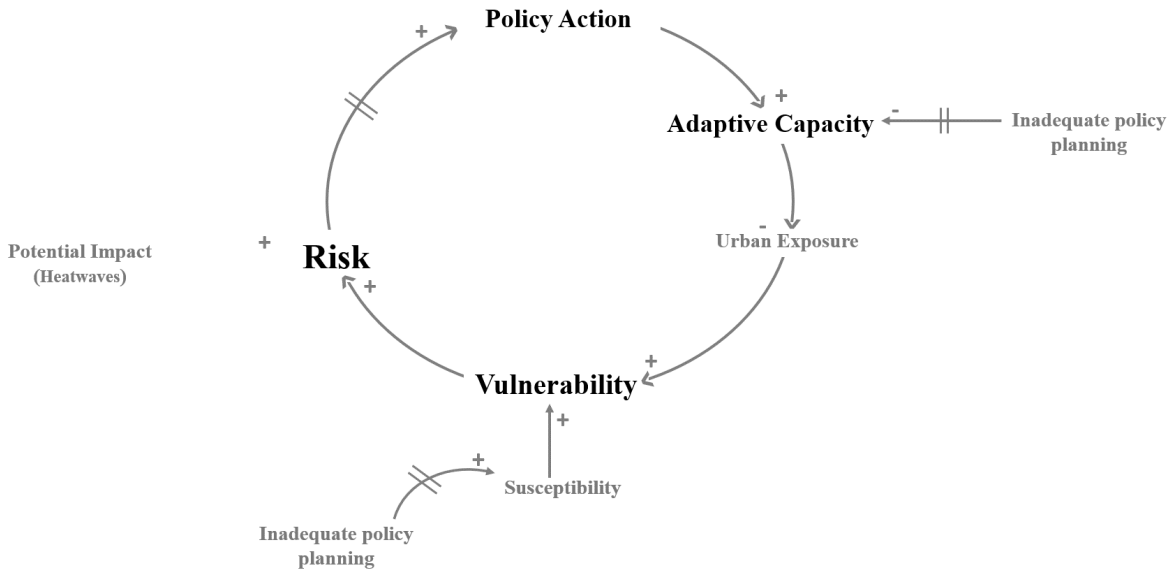
Figure 5-3: Causal Loop Diagram of the hypothesis of policy impacts and heat risk within the city boundary.

5.4.1 The Case of Chicago Heatwave 1995

During the summer of 1995, specifically between July and August, the city of Chicago witnessed the tragic death of more than 739 people from heat-related causes (Kaiser et al., 2007). The 1995 disaster was considered one of the most extreme heat events that the U.S has ever witnessed, yet, such disaster wouldn't have been so deadly without the extreme surrounding conditions of the city's most residents, alongside the state of poverty and inadequacy of the city's response. Scientific evidence indicated that the mortality rates recorded during the 1995 heatwave compared to earlier heatwaves were not only attributable to weather (Klinenberg, 2003a). This raises the question of the nature of the surrounding conditions that led to such devastating losses in human lives. Eric Klinenberg (2003a) explains that the unprecedented death tolls were strongly attributable to some socio-spatial features and political structures; however, no scientific studies have attempted to find them.

Factors associated with vulnerability to heat exposure have been widely studied over the past decade (Schwartz, 2005); generally, people at most risk include the elderly, infants, socially isolated urban residents, chronically ill patients, and populations with limited access to coping mechanisms such as air conditioning (Lapola et al., 2019b). From the environmental perspective, a heatwave is tied to factors such as duration, intensity, air temperature, relative humidity, and the extent to which the heatwave is different from the climatic norm experienced by the population (Di Napoli et al., 2018; Palmer et al., 2014). Although such factors were all present during the 1995 heatwave in Chicago, the geography of mortality indicates an urban inequality. The west and south side of the city witnessed the largest concentration of deaths, specifically, neighborhoods with primarily black populations and widespread unemployment, poverty, institutional abandonment, and depopulation. What allowed the heatwave disaster to happen is a more complicated process of social policy and institutional indifference that produced the conditions that cause such extreme death tolls during the heatwave. The literal isolation of a growing poor population with segregation in services made these two areas most vulnerable to heat exposure. Other factors attributable to the excess deaths in Chicago during the 1995 heatwave that are strongly tied to

the policy are the deterioration of public services thanks to privatization and the "No-Go" neighborhoods that have caused depopulation and business abandonment in the long terms dropping these areas from the city safety net.

System dynamics modeling using causal loop diagrams (CLD) is utilized to assess policy-related causes that contributed to increased vulnerability during the 1995 heatwave in Chicago. The research focuses on four primary policy and policy delayed impacts mechanisms that have contributed to the conditions around the 1995 heatwave as follows:

1- "No-Go Neighborhood" policy impact
2- "Funding cuts" for the Department of Aging.
3- "Market-Model" Strategy for public services.
4- "Congress Cuts for the budget of the Low-Income Home Energy Assistance Program (HILEAP)."

"No-Go Neighborhood" Policy Impact

By the late 1980s, Chicago has declared several neighborhoods on the west and south side of the city as no-go zones due to the increased crime rates; simultaneously, these were the same areas that accommodate the Black and Hispanic population. This segregation of specific neighborhoods as danger zones has caused a massive surge in business abandonment, which as a result, led to an increase in unemployment, poverty, and as a result, higher crime rates. The long-term effect of this policy has strongly affected the growth in poverty with social isolation, as initial residents started to age with their children leaving the neighborhood looking for job opportunities. This mixture of social isolation with poverty was one of the main factors that caused the excess number of death tolls during the 1995 heatwave, as explained by Eric Klinenberg (2002). Figure 5-4 illustrates the cause-effect dynamics of the "No-Go Neighborhood" policy's impact on increased poverty-related vulnerability and social isolation.
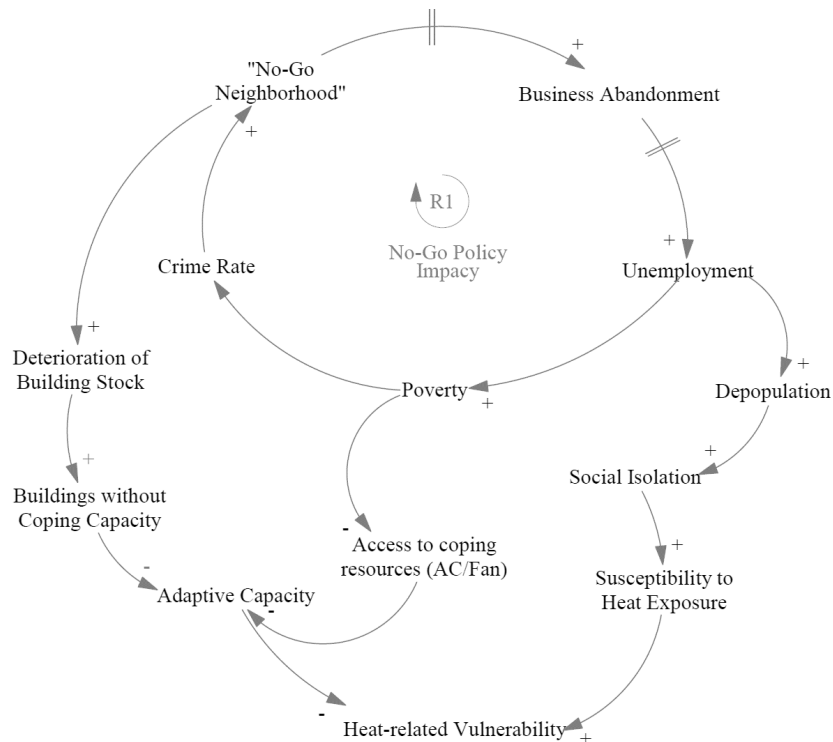
Figure 5-4: CLD of the "No-Go Neighborhood" policy impact on heat-related vulnerability.

"Funding cuts" for the Department of Aging

During the heatwave of 1995, most of the death tolls were from elderly urban residents despite that the department of the aging program in Chicago was one of the earliest programs in the U.S. By the mid-1990s, Chicago's elderly population was exploding, and the department funds were shrinking. This has caused the department to turn to private foundations for support, reducing full-time employees with more reliance on part-time and temporary employees. This cut in department capacity has caused a gap in the service capacity relative to the number of elderly residents that needed assistance at that time (Klinenberg, 2003a). The result was neglect of elderly poor who lacked access to support from the city system, as illustrated in Figure 5-5 below.
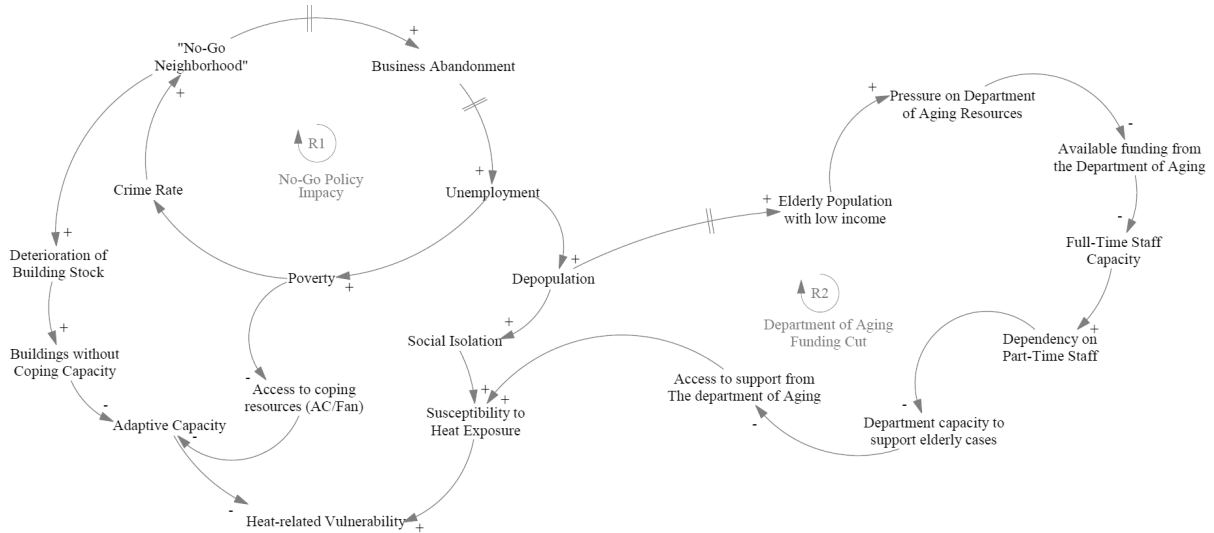
Figure 5-5: CLD of the "Funding Cuts" for the Department of Aging impacts heat-related vulnerability.

"Market-Model" Strategy for Public Services

Around the same time of cutting the Aging fund, the city officials adopted an entrepreneurial model to provide public services (Whitman et al., 1997), with the idea of empowerment to the residents and consumers of the city who cannot act effectively unless they have helpful information. Despite the expensive advertisement effort to promote this new model, Chicago's residents who need public assistance were mostly elderly who are isolated and with the lowest level of education that led them to be the ones with the weakest ties to the mainstream institutions. This framework, as a result, has caused most vulnerable urban residents to become the worst prepared to claim public services such as health care to which they are entitled to as the "Market Model" required to seek access to information and service providers actively. This strategy has caused stress on these populations, posing more significant threats to their survival capacity under extreme weather events. The dynamics of the Market-Model strategy and its relationship to increased vulnerability from other policies are illustrated in Figure 5-6.
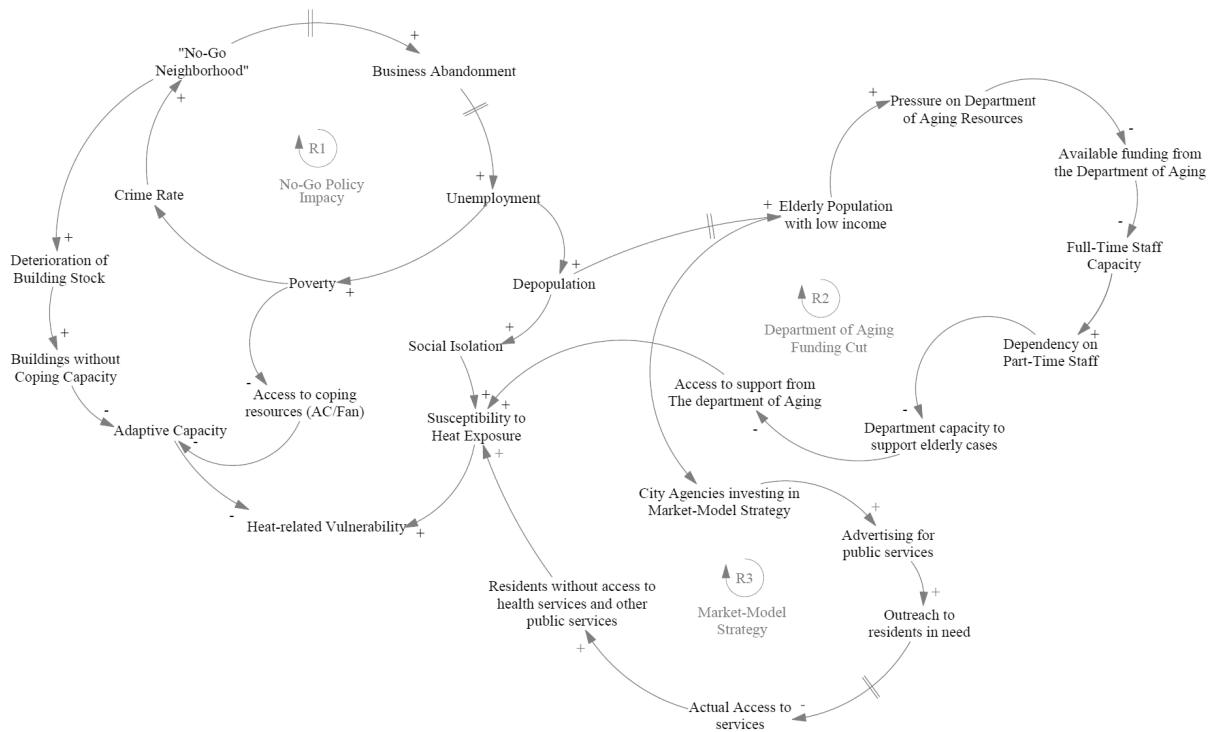
Figure 5-6: CLD of the "Market Model Strategy" and its impacts on heat-related vulnerability.

Congress Cuts For The Low-Income Home Energy Assistance Program (HILEAP)

During the 1990s, Congress cut the budget of the Low-Income Home Energy Assistance Program (LIHEAP). The program was designed to support energy bills for low-income populations in Chicago (Gilbert, 1996). The combination of low-income urban residents living in an energy crisis has placed a lot of pressure on using air conditioning units or fans when it gets warm outside. With energy costs rising, fixed income, and escalating unemployment, people in pilot programs to provide air conditioners to the poor started to sell the units rather than install them. Also, from the interviews conducted by Eric Klinenberg in 1995, he noted that seniors kept their light off during the day with minimized used of air conditioning to save on their electricity bill. The threat of losing power altogether with rising temperatures has deteriorated conditions at the building level made the 1995 heatwave far more extreme. These conditions have limited the elderly population's capacity to use air conditioning, alongside high crime rates have caused some of the residents not to open windows when indoor temperature increased. The conditions described here are strongly linked to the high death tolls, especially in these neighborhoods. Thus, understanding the underlying policies that have generated these conditions is essential in planning heat adaptation strategies. Figure 5-7 shows the dynamics of the energy subsidy cut and its impact on increased heat risk.
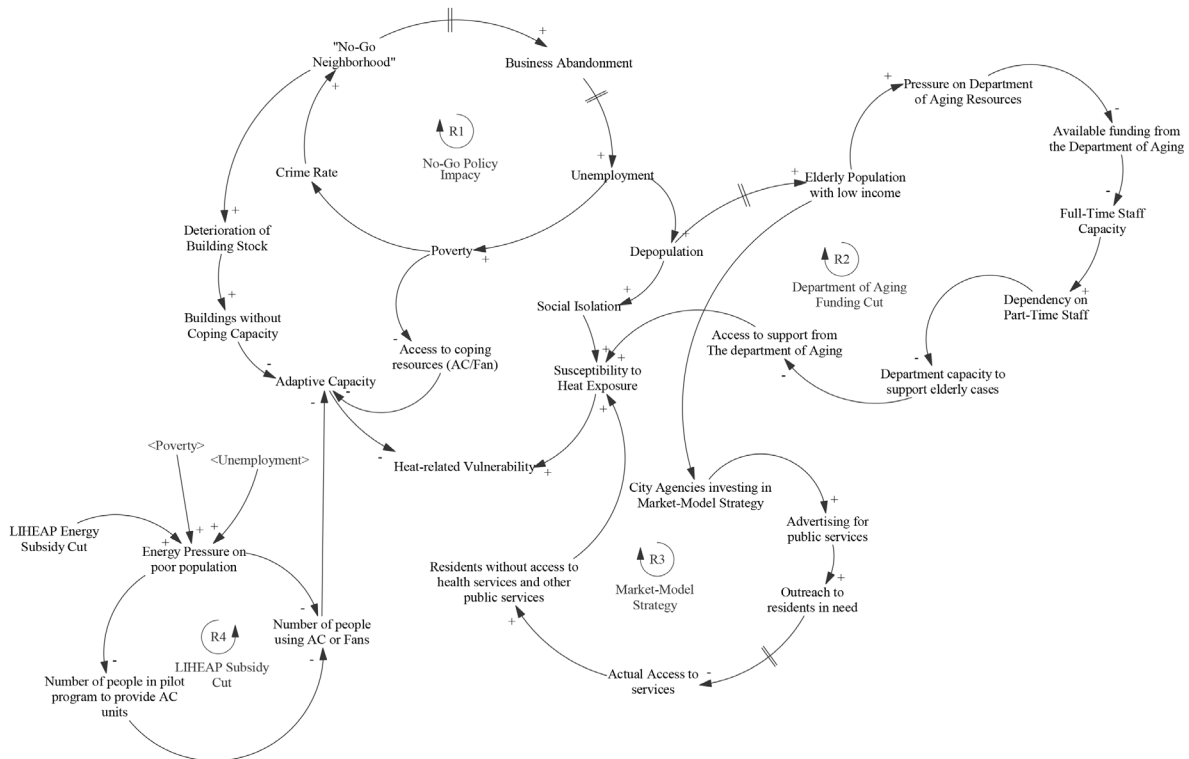
Figure 5-7: CLD of the four proposed policy strategy and their effect on heat-related vulnerability.

The strategies presented above illustrate how population structure and socioeconomic characteristics have contributed to an increase in population at risk during the 1995 heatwave. As discussed above, the population in the west and south Chicago during the 1930s was less affected by crime rates as they were relatively lower. Thus, they were able to leave windows and doors open when the indoor temperature increased. Also, most elderly populations during the 1930s lived with families that cared for them, while in 1995, more elderly were living alone. The delayed effect between 1936 and 1995 shows how policies can indirectly influence the surrounding social and economic environment cause a shift in population structure over time to transition from susceptible to vulnerable under heat exposure. After the city experienced several deaths during 1995 and 1999 heatwaves (Naughton, Henderson, Mirabelli, Kaiser, & Wilhelm, 2002), Chicago's officials have recognized the importance of community preparedness supported by adequate policies to decrease deaths during extreme heat events and improve the city's adaptive capacity to heat risks. Findings from this analysis for the case of the 1995 heatwave in Chicago indicate how policies play a significant role in the success of heat adaptation strategies. As it has been indicated from Klinenberg's analysis (2003a), delay in policymakers' response, inadequate provision of public services have, and lack of an effective system for organizing and coordinating the city's adaptation services contributed to the increase in death tolls in Cook County during the 1995 heatwave. This was evident in the city's failure in coordinating an emergency public health response plan to the heatwave despite the severity of the crisis. These findings indicate the need to support decision-making processes on the dynamics of heat-related risks at a broader scale and how planned adaptation strategies can mitigate future risks, especially for highly vulnerable populations. Thus, this chapter aims to develop a system dynamic model to capture the impact of planned policies on increased or decreased heat-related

risks during heatwaves and how government response can accelerate or delay the effectiveness of planned strategies over time.

5.4.2 Methods: Time Delay and Heat Vulnerability

The system dynamics model is developed to examine policy impact on the vulnerability of the urban system during heat events and how delays in the public policy response to extreme heat can increase risk. This is explored through three different scenarios for policy's impacts on heat risks. First, mis-planned policies have produced conditions associated with increased susceptibilities, such as increased poverty rates, unemployment, depopulation, or a gap in available urban services in the form of adaptive capacity. Second, during a heat event, a delay in the policy response might cause more risk to an already vulnerable population. Third, after a heat event, delay in planning and execution might lead to an increased risk for the following years if the same heatwave event hits again with more vigorous intensity.

The mechanism of policies' impact on heat vulnerability is based on three primary components. First, susceptibility, which depends on population socio-economic conditions that would increase their vulnerability to heat as discussed in chapter 2. Second, adaptive capacity that includes available adaptation amenities during heat exposure at the dwelling level (access to fan, air conditioning unit) and the urban block-level (access to cooling shelter, and access to health care service). Finally, policy delays, which is measure of time-based policies that can either positively or negatively influence the vulnerability level of the population and potential risks. Policy delay is modeled based on three potential scenarios: i) delay between reported cases and media coverage, ii) the delay between media first response and policy initial action to the number of death tolls, and iii) policy delay in planning and execution phase post-disaster. Vulnerability to heat is expressed as a function of exposure to heat events, susceptibility, and available adaptive capacity, while heat risk is vulnerability multiplied by potential impact from an increased level of exposure.

Heat exposure is expressed as the days where the outdoor heat index is above the caution level. For the scope of this dissertation, the research focuses on developing the system dynamics model that captures delays after the heat event, more significantly, the delay from policy actions and response. The effectiveness of policy measures during or after heatwave events must consider the political and administrative framework, which profoundly affects the success of the planned strategies. For simplification, all regulatory and legislative frameworks are abstracted where the focus is given to the dynamics that might result from delayed policy actions. Indicators considered in the system dynamic model are listed in Table 5-1 below.

Table 5-1: System Variables in the case of a heat event and their indicators.

Variable		Indicator
Exposure		No. of days when the outdoor heat index is above the caution level (> 39ºC).
Susceptibility	Age	No. of urban residents >60 years old or <5 years old
	Health Condition	No. of urban residents who are chronically ill (heart problem or respiratory conditions)
	Income	No. of urban residents below the poverty line
	Social Isolation	No. of urban residents >60 years old and living alone
Adaptive Capacity	Buildings without coping capacity	No. of building with poor insulation and AC system
	Cooling Shelters	No. of Cooling Shelters available
	Health Care	No. of emergency health care units
Policy Delays	Risk Impact on Policy	No. of days for a policy to take immediate response
	Policy Impact on Planning	No. of days between policy response and action planning (number of days that would be reduced if the risk is high between planning and execution)
	Cooling shelter	No. of days required to plan a cooling shelter
		No. of days required to construct a cooling shelter
	Building retrofit	No. of days required to plan for retrofitting / building
		No. of days required to do the actual retrofit

The key stocks in the model are coping capacity, cooling shelters, the elderly population, and infants. The coping capacity and cooling shelters are an annual input to the model, and their value is calculated based on the relationship between available funding and the delay between the actual planning and execution. The initial coping capacity value is set as an input value corresponding to the number of existing buildings with poor insulation and AC systems. Also, the value of cooling shelters is based on the available vacant plots for cooling shelter construction. The elderly population stock represents the fraction of the population older than 55 years and increased by the aging time to become 60 years or older. Other initial variables, such as available funding/investments for retrofitting and cooling shelter construction, is an input variable that is set depending on the context and the institutional structure examined. Cooling shelter capacity represents the occupancy density per cooling shelter, where the average occupancy density is assumed to be 25 people / 100 m². Table 5-2 lists the model's parameters and their formulation.

Table 5-2: Formulation of model variables and their units.

A. Coping capacity: the number of buildings that are well insulated and equipped with air conditioning units		
Coping Capacity	Building Retrofit – Building Decay	Amenity
Building Retrofit	Coping Gap / Retrofitting Time	Amenity/Day
Coping Gap	MAX (0, Desired Coping Capacity-Coping Capacity)	Amenity
Desired Coping Capacity	IF THEN ELSE (Available Coping Investments/Cost of Building Retrofit>Initial Stock, Initial Stock, Available Coping Investments/Cost of Building Retrofit)	Amenity
Initial Stock	Total number of existing buildings within a neighborhood	Amenity
Available coping investments	Amount of investment available for building retrofit that is allocated according to the city stakeholders	USD
Cost of building retrofit	The average cost of a simple retrofitting strategy including the replacement of the windows' frame and changing ac units.	USD/Amenity
Retrofitting Time	Average retrofitting time* desired coping capacity	Day

Average retrofitting time	Building retrofitting time + Policy Impact	Days/Amenity
Building Retrofitting Time	No. of days to retrofit a single building	15 Days/Amenity
Policy Impact	Risk Impact on policy Delay*Retrofitting Planning Delay	Days/Amenity
Retrofitting Planning Delay	the time required to identify buildings that need immediate intervention, picking the best practices, and selecting contractors	300 Days
Buildings without coping capacity	Initial Stock – Coping Capacity	Amenity
B. Cooling Shelters: Number of cooling shelter available for the neighborhood residents		
Cooling Shelters (CS)	New Cooling shelters- cooling shelter decay	Amenity
New Cooling Shelter	Cooling Shelter gap/ Planning Time	Amenity
Cooling Shelter Gap	MAX (0, Desired CS-"Cooling Shelters (CS)")	Amenity
Planning Time	Desired CS*Average Construction Time	Days
Average Construction Time	Policy Planning Delay + Policy Impact	Days/Amenity
Policy planning delay	The time required to identify the location of the cooling shelter and selecting a contractor	Days/Amenity
Cooling Shelter Gap	MAX (0, Desired CS-"Cooling Shelters (CS)")	Amenity
Desired CS	MIN (Vacant Plot for CS, Available Investments for CS/Cost of CS)	Amenity
Vacant Plot for CS	Available land areas for cooling shelters	Amenity
Cost of CS	Amount of investment available for cooling shelter provision that is allocated according to the city stakeholders	USD/Amenity
Available investments for CS	Amount of investment available for cooling shelter provision that is allocated according to the city stakeholders	USD
CS Capacity	"Cooling Shelters (CS)"*CS Density	Person
CS Density	Number of people that a cooling shelter can accommodate	Person/Amenity
C. Adaptive capacity: number of people who have access to coping capacity on the building level and the urban block level		
Adaptive capacity	Population W CC+CS Capacity	Person
Population with CC	Population Density*Coping Capacity	Person
Population Density	The average number of people living in a building	Person/Amenity
D. Elderly Population: Number of elderly residents in a neighborhood		
Elderly Population	Aging Rate – The death rate	Person
Aging Rate	(Population wo CC*"Fraction of Population <55")/Time to age	Person/Day
Time to age	Time to become 60 years or older	Day
Death Rate	Elderly Population/Life Expectancy	Person/Day
Life Expectancy	Time to reach an average age of life expectancy	Day
E: Susceptibility: number of urban residents with conditions that may cause increased risks under heat exposure.		
Susceptibility	Infants+(Elderly Population-Population with Chronic Disease) +(Elderly Population+ (Population wo CC-Elderly Population-Population with Chronic Disease))	Person
Population with chronic diseases	Elderly Population*Fraction with Chronic Disease	Person
The fraction with Chronic Disease	Percentage of an elderly population with chronic diseases	Dimensionless (Dmnl)
Infants	Births- Growing Up Rate	Person
F. Vulnerability: Number of urban residents that are susceptible and lacking adaptive capacity		

Vulnerability	(Exposure+ Susceptibility)-Adaptive Capacity	Person
G. Exposure: days where the heat index is above caution level (normalized based on heat index values above 90 F		
Risk	Vulnerability * Potential Impact	Person
Risk Impact on Policy	Risk impact on policy response, represented by the number of people at extreme risk to alter policymakers to take immediate actions to cut delays in planning and execution time	
	IF THEN ELSE (Risk>=Total Population, 0.5, 1)	Dimensionless (Dmnl)

Figure 5-8 represents the cause-effect relationship and the system structure between the various parameters of the proposed system dynamics model.
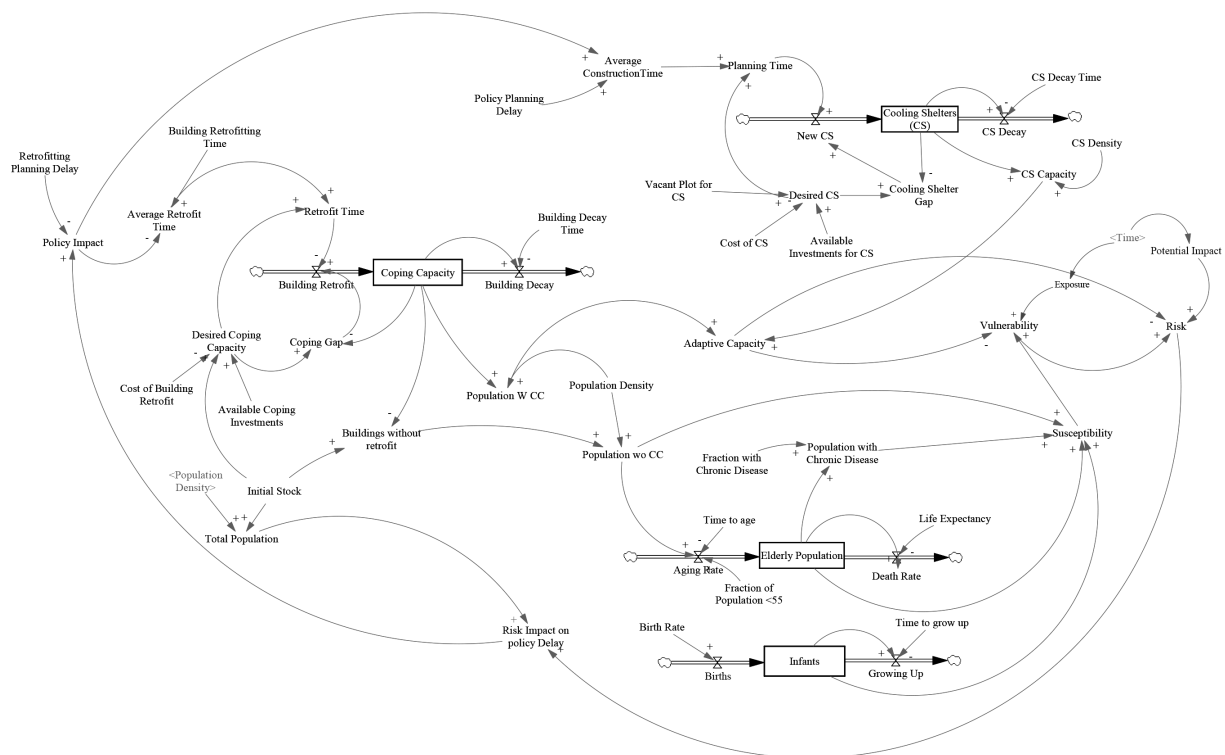
Figure 5-8: Dynamics of the model in the case of a heatwave shock

The initial values in the modeling process are based on a conceptual neighborhood of 1500 residents and a population density of 15 people/building. Using a conceptual neighborhood, the model examines how policy delay can significantly influence people under high-risk conditions away from the complexity of political and administrative, and institutional framework in the real world.

Testing the Model Behavior: The relationship between Policy variables and Heat risk

The model is examined under two main scenarios. First, the delayed policy response, where the planning process is decoupled from the number of people at risk from heat exposure. Second, the immediate policy response is represented by less time spent planning as a function of the population at risk exceeding a specific threshold. Delay in planning time is modeled as six months, which is the time spent identifying best practices, allocating funding resources, and selecting contractors to start construction. In the immediate response scenario, this time is reduced by 50% to examine how policy delay may impact the

number of urban residents under risk. The model is tested over five years to account for increased adaptive capacity over time, aging population, and change in population's susceptibility. Heat exposure is assumed to be constant over the five years, meaning that the neighborhood will experience similar heatwave conditions every year without a change in intensity, duration, or frequency.

5.5. Results

Figure 5-9 shows delayed policy response impact (base simulation) on the number of people accessing adaptive capacity resources. As a result, the total population at risk over five years has slowly decreased at an annual rate of 1.48% even though decision-makers are acting, and there are investments in place to improve adaptive capacity. Over time, the increase in adaptive capacity is influenced by the available funding and the total number of required amenities added to the existing adaptive capacity stock. These dynamics are vital to understand the impact of planned strategies over time and pinpoint the leading causes of delay throughout the planning and execution processes. The second policy scenario is short-term and thus oriented to an immediate policy response assuming policies are planned and executed after the number of people at risk reaches a specific threshold (triggered policy actions). Here it is assumed that policymakers act after the number of urban residents at risk reach 250 persons with a decrease in planning time by 50% to represent the sensitivity of the policy planning process to risk levels. Results from the simulation indicate that by cutting delay time in policy response, the number of urban residents at risk decreased faster by 5% annually compared to the delayed policy response scenario.
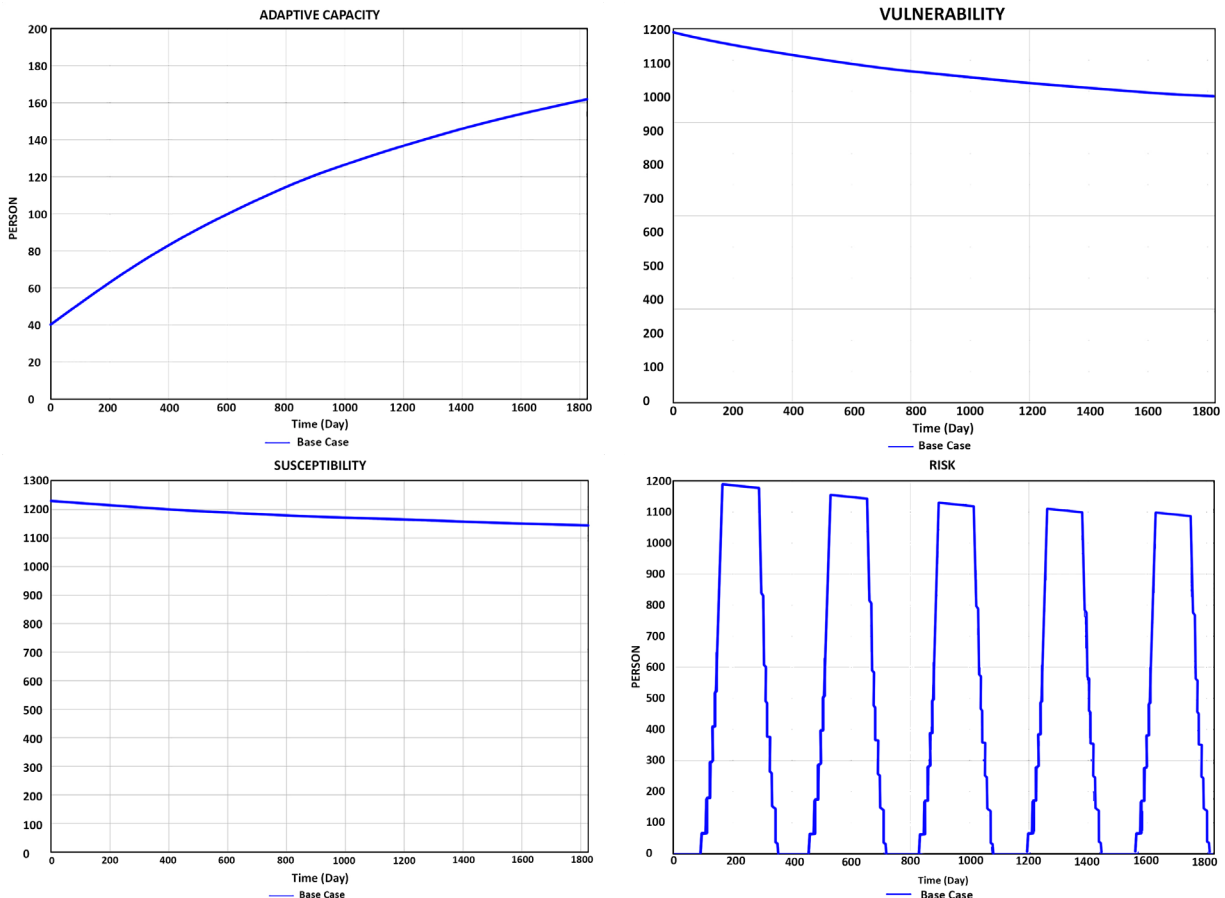
Figure 5-9: Simulation results for policy delayed response scenario in planning and execution during a heatwave.

Figure 5-10 shows the results from immediate policy response. It can be noted that the number of urban residents getting access to adaptation resources (represented by adaptive capacity) has increased at a faster rate of 109% annually than 60.4% in the delayed policy response scenario.
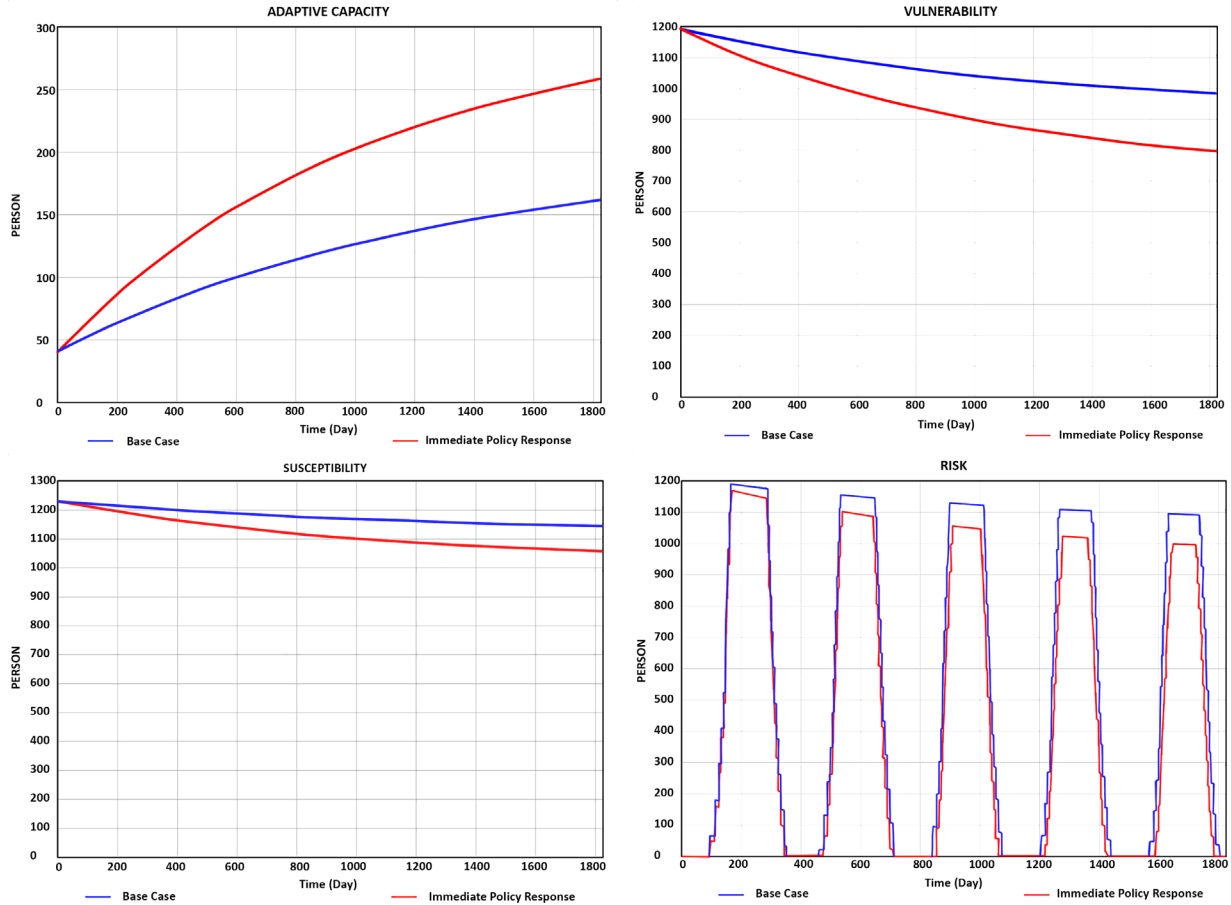
Figure 5-10: Simulation results for **Immediate Policy response scenario** in planning and execution during a heatwave.

To test the model behavior in representing policy impacts on increased risks during heatwaves, a scenario of an extreme heatwave for one week is modeled to examine the model behavior in mimicking the policy delay impact during the 1995 heatwave in Chicago. Here the research is focusing on testing the model structure in generating the same trend rather than producing the absolute number of actual death tolls in 1995, as this process will be far more complex and will require detailed information on the types of available amenities, delay in policy response between the occurrence of the heatwave and reported deaths and population access during the heatwave. Thus, a new parameter is added to the model, **heat warning**. This model examines heat warning under two scenarios: 1) heat warning with a delay and heat warning under policy preparedness. Under the delay scenario, heat warning is a function of exposure with a delay step of two days after the actual temperature peak occurrence, similar to what was experienced during the heatwave in Chicago. Findings from other studies that examined the heatwave in Chicago reported that most of the deaths reported in the second and third days after the peak temperatures were mainly linked to the time when bodies were found, which underline the impact of delayed policy response (Semenza et al., 1996a). Finally, exposure is modeled using the heat index record during the 1995

heatwave in Chicago (Semenza et al., 1996a). Figure 5-11 shows the population at risk and normalized heat exposure and the actual death tolls trend during the 1995 heatwave in Chicago with the heat warning delay (area in red) between exposure peak and risk peak. It can be noted that the model produced a similar trend to what was experienced in the 1995 heatwave, where risk peaks two days after peak temperatures are reached.
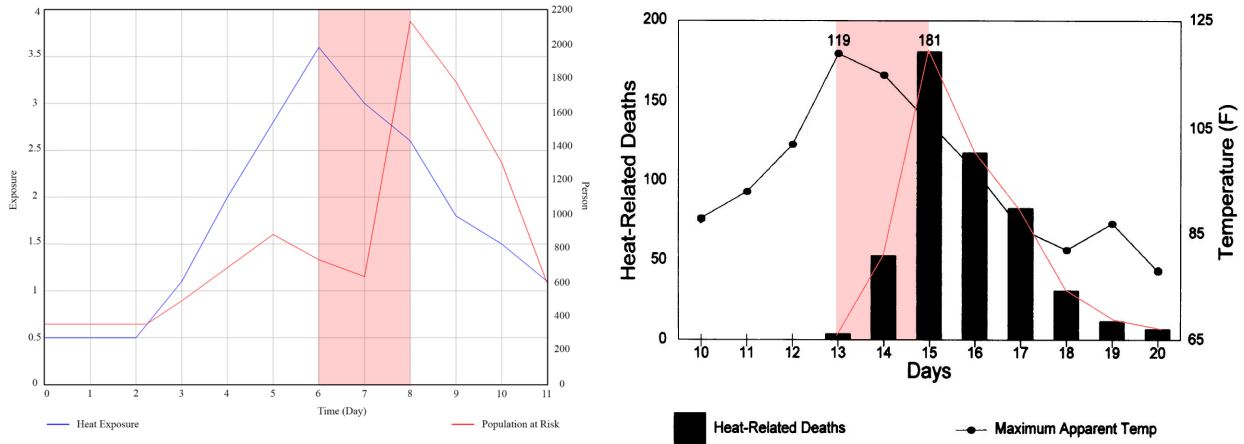
Figure 5-11: Left, the potential population at risk from the SD model, Right heat-related deaths during 1995 heatwave.

Next, the impact of changes in heat warning delay is examined by testing the model behavior under the scenario of policy preparedness. Heat warning is modeled as a policy trigger for decision-makers to execute heat response plans to examine how it can contribute to reduced risk during and after the occurrence of a heatwave. A new parameter is added to the model, **heat response impact**, and modeled as a percentage decrease in the population at risk due to increased adaptive capacity when heat warning is bigger than 0. Thus, it is assumed that heat response impact will increase adaptive capacity by 50% for the population at risk and is triggered by heat warning.

Figure 5-12 shows the change in risk due to heat response impact. In the immediate policy response scenario, activating the preparedness plan has contributed to positive change in the risk trend from the delay response scenario discussed above. The total population at risk has decreased by 87.6% compared to the delayed response scenario. It should be highlighted that the reduction in the population at risk is modeled as a function of the increase in access to the adaptive capacity measures. If this model is to be used for policy planning, decision-makers can assess what types of additional measures to be introduced to the heat preparedness plan to contribute to a more significant reduction in the population at risks ahead of heatwave occurrence.
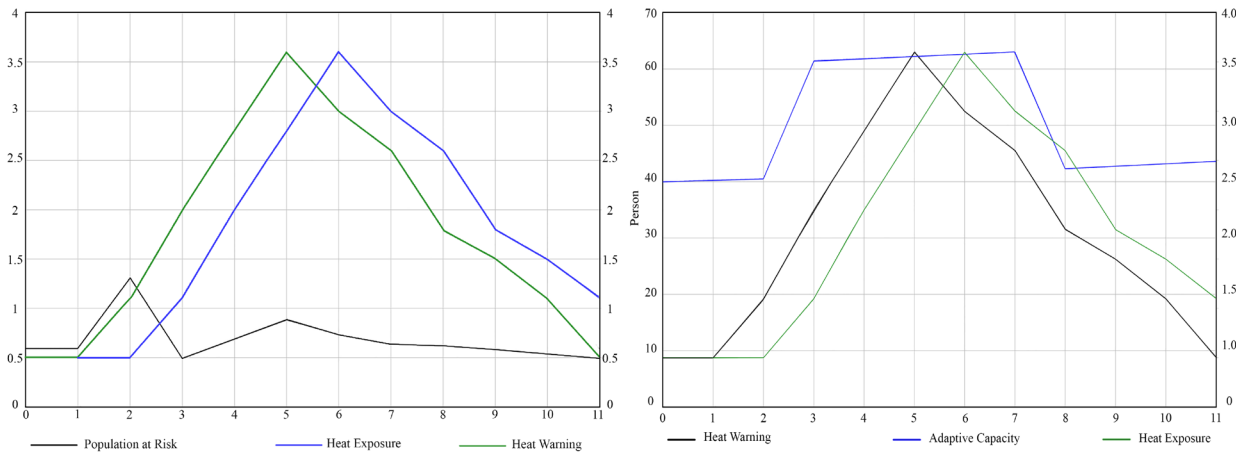
Figure 5-12: Left, the population at risk under heat warning and policy preparedness scenario and increased adaptive capacity (right).

The proposed SD model focused on examining the impact of policy delay on heat-related risks. The results indicated that delay in policy action and planning has a significant impact on the success of adaptation preparedness plans. Some policy implications can be drawn from this analysis. First, it is fundamental for policymakers to have a prompt and effective policy planning framework. Second, allocating and designing adaptation strategies doesn't necessarily mean they will effectively reduce risk; adaptation plans need to be tied more to how the institutional framework responds to crisis and allocate suitable investments with a proper timeframe. Third, to improve adaptive capacity during extreme heat events, it is required from the policy side to understand the time required to become available and accessible to the vulnerable population, with respect to the potential change in the intensity and frequency of future heat events.

5.6 Discussion

This chapter examined types of adaptation strategies to reduce heat-related risks during extreme heatwaves. The first section of this chapter reviewed sets of adaptation strategies at the building level, urban level, and the role of social capital in mitigating heat-related impacts. Through literature, the research assessed the potentials of specific adaptation strategies to reduce future heat vulnerability. The adaptation strategies presented in this chapter highlight how heat adaptation planning requires a broad range of measures and data to facilitate effective strategies to reduce heat risks at different levels of the urban system. Also, the diversity of adaptation measures implies no single approach is considered to be most effective in reducing risks. Yet, there is a need for policy flexibility to apply different approaches relevant to the socioeconomic complexity of the urban population and the performance of the urban system. Another vital measure in heat adaptation planning is the coping range of existing urban conditions where the population becomes vulnerable outside this range. What can be drawn from the coping range is the adaptation often arises from extreme exposure that is well beyond the coping range, causing more significant health risks to urban populations. Thus, adaptation measures, vulnerability, and current coping ranges should be considered jointly during policy planning.

Most heat adaptation assessments assume that adaptation measures can all be implemented in the short term without considering resource constraints. Hence, the second half of this chapter examined the

dynamics of vulnerability considering policy and heat adaptation planning and how these dynamics challenge the effectiveness of planned strategies. A system dynamics modeling is used to understand how the delay in the policy response to heat hazard plays a role in the potential increase in heat-related risks, referencing policy impacts during the 1995 heatwave in Chicago. The primary motivation behind this assessment is to understand how policy actions that reduce vulnerability to current climate risks can still contribute to future changes. As illustrated in the causal loop diagrams, policies can change the context for vulnerability and introduce new risks into the system with a delayed effect. Findings from the proposed SD model indicated that heat adaptation planning is strongly linked to the institutional capacity to measure the extent to which planned adaptation strategies can be effective in heat risk relief and stakeholders' understanding of the complexity of adaptation planning.

This chapter has summarized the current adaptation strategies to extreme heat events and how policy contributes to the success of planned strategies. Lesson learned from the pertinent literature and analysis carried out are:

- Adaption to extreme heat events is context-specific and depends on various factors, including environmental, social, economic, urban, and political.
- There has been a growing advancement in heat adaptation technologies that have emerged in the past two decades.
- Adaptation planning requires close collaboration between policymakers, climate scientists, the local community, practitioners, and other stakeholders.
- Adaptation to heat risks involves a broad range of measures with various levels of complexity that should be carefully considered during policy planning and implementation.
- There is a need to establish a dialogue between policy-makers and climate scientists where heat assessment is carried out collaboratively, and intervention strategies are identified with the relevant stakeholder.
- The need for suitable utilization strategies of the city's resources to implement effective adaptation strategies and means for knowledge can be exchanged with the local community throughout the planning process.

VI. CONCLUSIONS

Heat vulnerability assessment in the built environment is a complex process with multiple dynamics and components of human-natural systems and their interaction with the surrounding built environment. These dynamics include social, demographics, urban growth, environmental changes, access to public services, and policy impacts. This dissertation examines different methodologies to develop an integrated framework for heat vulnerability analytics in the built environment. The work presented in this dissertation is developed around the premise that there is a need for a multivalent framework to assess heat vulnerability in urban settings. The proposed framework can help broaden the understanding of heat vulnerability assessment using various approaches of building assessment coupled with Machine Learning (ML) methods to examine heat exposure variation and related vulnerability at the district level. The work presented in this dissertation is driven by the need to examine the dynamics of urban heat vulnerability and human health impacts at a detailed level which was addressed through the work in Cairo, Egypt. The detailed assessment highlighted the need to develop a technological approach for assessing the built environment that would lend meaningful information in a rapid way and how community engagement can assist in the development of these new approaches examined in the work presented in Chapter four. Finally, these sets of analytics were then used to examine how policy can influence the success or failure of heat adaptation strategies examined in Chapter five. The proposed sets of assessment methods in this dissertation can help identify types of buildings that are more susceptible to heat-related impacts and how the distribution of adaptation resources can mitigate potential risks from future extreme heat events. Also, the heat vulnerability framework aims to provide vital information in the planning and designing of heat adaptation strategies at multiple levels serving different purposes through three distinct levels: i) preliminary assessment of heat vulnerability to support the primary analysis phase in the adaptation planning process; ii) detailed assessment of heat exposure at the building level to assist in the definition of adaptation strategies and prioritization of high-risk urban areas, and iii) urban intervention and policy development to support policymakers in implementing and monitoring adaptation measures. Each chapter of the dissertation provides detailed procedures and a thorough analysis of the three assessment levels and determines the most suitable portfolio of methods at each level. The framework aims to capture the complex and dynamic components of heat vulnerability that can influence the formation and shift of heat-related health risks and guide adaptation planning processes.

6.1 Comprehension of Vulnerability

The research developed as part of this dissertation started with a review of the current state of the art in the nascent field of Heat Vulnerability Assessment in Chapter 2. As a result of the review, the basic foundation of the heat vulnerability framework was developed around the assessment of three distinct components: Susceptibility (S), Exposure (E), and Adaptive Capacity (AC). These three components are examined and combined to capture the vulnerability of an urban population to a climate hazard (UNFCCC, 2016). In this dissertation's context, heat vulnerability was assessed as a function of an urban area's susceptibility to heat exposure based on the characteristics of the urban population and the surrounding built environment and the available resources for coping and adapting during extreme heat exposure. The review presented in Chapter 2 assisted in developing the proposed heat vulnerability assessment framework and the components of each level. The framework intends to support the heat adaptation planning process by better understanding the local dimension of heat vulnerability distribution that can increase risks during extreme heat events. The proposed framework for vulnerability assessment involves analyzing the physical parameters of the urban space, indoor exposure at the building level, and occupants' adaptive capacity using spatial information, building performance simulations, in-person surveys, and aerial data coupled with ML methods for building and urban assessment. This mix of spatial data, simulation models, and occupants' assessment is designed to support policymakers in developing adaptation strategies informed by the distribution of high-risk urban areas that accommodate highly exposed building stock to high temperatures and home to vulnerable populations.

6.2 Indoor Heat Exposure & Adaptive Capacity Limits

Chapter 3 offered a detailed assessment of heat vulnerability at the building level and a thorough analysis of simulation results using a case study of a low-income neighborhood in Cairo, Egypt. The work presented in chapter 3 addressed a critical area of concern for indoor heat exposure and human health impacts to determine indoor conditions threshold that can potentially pose a risk, especially for vulnerable populations. The simulation workflow carried out an in-depth investigation of potential health risks associated with increased indoor overheating for vulnerable populations with limited mechanical ventilation access. The goal was to investigate the threshold for indoor conditions that could result in health risks, specifically for elderly residents. Residents examined in AlDarb Al Ahmar were exposed to similar ambient conditions. Still, their buildings and surrounding resources have played a role in exacerbating or mitigating heat exposure risks. Analysis revealed the complexities of heat vulnerability, where numerous direct and indirect factors influence how an individual responds to heat stress. The analysis contained within Chapter 3 demonstrates how buildings can significantly modify indoor conditions and how physiologic markers like heart rate can be negatively impacted by heat exposure and its duration. These results demonstrated that the available adaptive capacity resources for examined residents in AlDarb Al Ahmar were not equally adequate in overcoming high temperatures exposure. Thus, Chapter 3 offered an analysis workflow that combines whole building energy simulation models and ML-based methods to examine the adaptive capacity and related heat vulnerability at the district level. The workflow presented in Chapter 3 overcomes challenges of heat vulnerability assessment at the district level by incorporating ML and image processing techniques as a novel approach to examine heat vulnerability and related risks at the district level. Results from the case study in Cairo demonstrate that

improving adaptive capacity in an approach that strategically prioritizes the most vulnerable populations and buildings can positively impact vulnerability levels and related risks. The ML-based method is significant as it can provide information at the district level to prioritize which buildings are more susceptible to future heat exposure, the capacity of available heat adaptation amenities, and types of intervention strategies to mitigate heat-related risks.

6.3 Rapid vulnerability analytics

Chapter 4 examined the applicability of integrating aerial technology, namely, UAVs coupled with machine learning and graph theory methods, in the rapid assessment of heat vulnerability at the building and district levels. The work presented in Chapter 4 was devised around two main research components. First, developing a methodology for the detailed assessment of building thermal envelope performance using data from UAVs equipped with infrared and RGB cameras to estimate the envelope's thermal transmittance using a case study in Cambridge, MA. The analysis showed a significant improvement in simulation models' prediction, which will be helpful to identify types of retrofit strategies such as targeted wall insulation replacement, with less time and cost than traditional building inspection processes. The second component relates to developing a framework for integrating UAVs' data coupled with ML and graph theory techniques to assess heat vulnerability and associated adaptive capacity at the district level using a case study in Bronx, NYC. The proposed methodology can provide information on the envelope's thermal performance that can impact indoor heat exposure levels. The framework includes a community engagement approach in using UAVs for building assessment as a catalyst for the growth of job opportunities for the residents and engagement in the decision-making process. Results from the adaptive capacity assessment provided helpful information to assist policymakers in heat adaptation planning and heat risk awareness programs.

6.4 Heat adaptation and Policy Impacts

As climate change poses risks to human health through more intense and more prolonged heatwaves, adaptation and mitigation strategies will help urban populations cope with these growing challenges. Chapter 5 examines the role of policy in heat adaptation planning and intervention strategies to mitigate heat risks. The first section of Chapter 5 presented an overview of heat adaptation interventions at three scales: building, urban and human, and their impacts in reducing heat-related health risks. Through literature, Chapter 5 assessed the potentials of specific adaptation strategies to reduce future heat vulnerability. Assessment of the various adaptation strategies underlined that heat adaptation planning requires a broad range of measures and data to facilitate effective strategies to reduce heat risks at different levels of the urban system. Also, it has been identified that most heat adaptation assessments assume that adaptation measures can all be implemented in the short term without considering resource constraints. Hence, the second half of Chapter 5 examined how policy actions can impact vulnerability to current climate risks and contribute to future changes using System Dynamics (SD) modeling. Results from the proposed SD approach indicated that heat adaptation planning is strongly linked to the institutional capacity to measure the extent to which planned adaptation strategies can be effective in heat risk relief and stakeholders' understanding of the complexity of adaptation planning.

6.5 Research Outlook

Results described in this dissertation provide important contributions to the field of vulnerability assessment, especially for low-income neighborhoods with limited access to AC, as well as the field of building performance and adaptation planning. Findings from work presented in chapters 2 through chapter 5 contribute important knowledge on how social, urban adaptive capacity, and building-related factors jointly influence heat vulnerability. The workflows and methods presented in this dissertation offer opportunities to be integrated in pairwise combinations or solely in heat vulnerability assessment. The following section organizes direction for future work into three main categories: policy planning and heat vulnerability, UAV technology in climate change risk assessment, and community engagement in climate risk planning.

6.5.1 Policy Planning and Heat Vulnerability

Findings from this dissertation indicate that cities can take significant steps to improve their adaptive capacity and preparedness against heat risks. These steps require communication between policymakers, planners, government officials, and other stakeholders involved in the heat-health assessment. Implications from work presented in this dissertation can help adaptation planning through three main pathways as follows.

1. **Localized heat vulnerability:** methods presented in Chapters 3 and 4 can be expanded to assist policy planning in determining place-based indicators associated with local heat vulnerability at the neighborhood level and locate areas of high risk. Also, adaptation policies need to account for contextual effects and other socioeconomic factors that make neighborhoods more or less resilient to heat exposure.

2. **Develop Strategies for Vulnerable Populations:** As discussed in Chapters 2 and 5, low-income and socially isolated individuals are considered highly vulnerable to heat exposure. Thus, there is a need for proactive policies alongside urban adaptation interventions to support vulnerable populations, such as funding programs for socially isolated to strengthen social ties and heat awareness campaigns to offer knowledge on mitigating and avoiding heat risks. Also, strategies to reduce social inequality and provision of equal access to adaptation resources.

3. **Targeted Adaptation Policies:** Findings from the heat vulnerability assessment presented in this dissertation demonstrates that effective adaptation strategies need to incorporate multiple interconnected factors. These factors include: i) socioeconomic characteristics of the communities it targets, ii) type and intensity of heat risk that the policy targets and iii) location where strategies are implemented.

6.5.2 UAVs in Climate Change Risk Assessment

UAVs are an emerging technology with the potential to be utilized in various climate change fields and provide a broad range of information. The use of UAVs in this dissertation for heat vulnerability assessment has proven the potential of using this technology in other climate risk assessments. Future work can expand UAVs technology coupled with additional sources of information such as Open Street Maps and satellite data for modeling and assessing large-scale urban areas. The data obtained from UAVs can inform numerous building analyses such as building energy modeling and integration with building energy audit workflows such as ASHRAE 211P. Also, UAV data can be combined with IoT devices to

perform various analytics at the city level, such as transportation system management, air quality monitoring, and carbon accounting at the neighborhood level. Within the humanitarian community, UAVs have improved the assessment and monitoring of large areas in a time-efficient manner to provide information on displaced communities, temporary settlements, and mapping affected areas after climate hazard occurrence. UAVs can be utilized in other climate change risk assessments such as landslide monitoring, deforestation assessment, glacier analysis, mapping water bodies, and climate modeling.

6.5.3 ML-based Approaches for Building Analytics

Chapters 3 and 4 presented the potentials of using ML-based methods in building performance and heat vulnerability assessment. ML methods have been proven to be effective in modeling existing conditions using simulation data and assessing urban services using 2D image data. Future work can expand on ML methods presented in this dissertation to address other fields such as building energy forecast and UHI assessment. The framework of envelope assessment presented in Chapter 4 can be expanded to an automated real-time assessment to detect and process key data critical for building performance. Also, the object detection model presented in chapter 4 can be coupled with image segmentation models to perform rapids documentation of large urban areas and provide information that is useful for district-level urban energy modeling.

6.6 Concluding Remarks

Extreme heat is considered one of the most growing climate threats to human health. To date, much of the existing literature on heat vulnerability has focused on societal and economic risk factors. Yet, the physical characteristics of the built environment determine the majority of human's exposure to heat, either exacerbating or mitigating temperature, whether at the building scale or the urban scale. Further, most heat adaptation interventions have relied on human usage of AC or improving indoor conditions with building control measures which are limited in their equity and resilience under future climate risks and energy challenges. UAVs data and machine learning algorithms explored in this dissertation attempt to capitalize on research advancement as we look to find ways to assess future climate impacts on our existing urban environment. However, the applicability of these new approaches in the developing world may be limited by the lack of regulations on how to deploy these technologies in assessing the built environment. Finally, the procedures and workflows outlined in this dissertation have helped to set up "MENA Heatwave platform" which contains **100 years of heatwave archive** documenting historic heatwaves since the 1800s till 2019, and **Built Environment Heat Vulnerability Analytics**, which is an online platform of vulnerability analytics to share and visualize research findings and outputs for the two case studies presented in this dissertation with the public audience, stakeholders and policymakers in these two neighborhoods. Given the multiple levels of details of information produced through the proposed heat vulnerability framework, the work can contribute to the planning process on multiple fronts: i) adaptation planning preparatory phase by increasing access of information, ii) the development of strategies and interventions on where and how to implement the adequate adaptation interventions, iii) the implementation phase to assess and adjust adaptation strategies using the proposed SD modeling approach, and finally iv) the monitoring phase, considering the proposed ML and UAV technologies to update and assess changes over time and perform prediction rapidly to assess the effects of the implementation of adaptation measures.

REFERENCES

A. Young. (2021). UTCI Universal Thermal Climate Index Documents. Retrieved January 2, 2021, from http://www.utci.org/utci_doku.php

Abdel-Ghany, A. M., Al-Helal, I. M., & Shady, M. R. (2013). Human thermal comfort and heat stress in an outdoor urban arid environment: A case study. *Advances in Meteorology*, *2013*(i). https://doi.org/10.1155/2013/693541

Addante, G., Iannone, F., & Rinaldi, A. (2015). Evaporative Cooling and Ventilation Control Strategies for a Kindergarten in Evaporative Cooling and Ventilation Control Strategies for a Kindergarten in Mediterranean Climate, (September).

Adger, W. N. (2003). Social capital, collective action, and adaptation to climate change. *Economic Geography*, *79*(4), 387–404. https://doi.org/10.1111/j.1944-8287.2003.tb00220.x

AECOM. (2012). *Investigation into Overheating in Homes: Literature Review. Communities*. Retrieved from https://www.gov.uk/government/uploads/system/uploads/attachment_data/file/7604/2185850.pdf

AECOM. (2019). *Middle East Property & Construction Handbook*.

Afroz, Z., Urmee, T., Shafiullah, G. M., & Higgins, G. (2018). Real-time prediction model for indoor temperature in a commercial building. *Applied Energy*, *231*(August), 29–53. https://doi.org/10.1016/j.apenergy.2018.09.052

Aga Khan Foundation. (2013). Historic Cities Support Programme. *Sites The Journal Of 20Th Century Contemporary French Studies*, (April).

Aga Khan Trust for Culture (AKTC). (2005). *Cairo : Urban Regeneration in the Darb al-Ahmar District*.

Aga Khan Trust for Culture (AKTC). (2013). *Urban Conservation and Regeneration of Heritage Areas in Egypt Aga Khan Darb Al-Ahmar Project Model*. Geneva, Switzerland.

Aivalioti, S. (2015). *Electricity Sector Adaptation to Heat*. Columbia Law School.

Al-Tamimi, N. A., & Fadzil, S. F. S. (2011). The potential of shading devices for temperature reduction in high-rise residential buildings in the tropics. *Procedia Engineering*, *21*, 273–282.

https://doi.org/10.1016/j.proeng.2011.11.2015

AlAhram. (2015, August 20). Egypt's Heatwave Death Toll reaches 110.pdf. *AlAhmram Online*.

Alam, M., Sanjayan, J., Zou, P. X. W., Stewart, M. G., & Wilson, J. (2016). Modelling the correlation between building energy ratings and heat-related mortality and morbidity. *Sustainable Cities and Society*, *22*(April), 29–39. https://doi.org/10.1016/j.scs.2016.01.006

Albatici, R., Tonelli, A. M., & Chiogna, M. (2015). A comprehensive experimental approach for the validation of quantitative infrared thermography in the evaluation of building thermal transmittance. *Applied Energy*, *141*, 218–228. https://doi.org/10.1016/j.apenergy.2014.12.035

Aldrich, D. P., Page-Tan, C. M., & Paul, C. J. (2016). Social Capital and Climate Change Adaptation. *Oxford Research Encyclopedia of Climate Science*. https://doi.org/10.1093/acrefore/9780190228620.013.342

Aldrich, D. P., & Sawada, Y. (2015). The physical and social determinants of mortality in the 3.11 tsunami. *Social Science and Medicine*, *124*(Cdc), 66–75. https://doi.org/10.1016/j.socscimed.2014.11.025

Alele, F., Malau-Aduli, B., Malau-Aduli, A., & Crowe, M. (2020). Systematic review of gender differences in the epidemiology and risk factors of exertional heat illness and heat tolerance in the armed forces. *BMJ Open*, *10*(4), 1–10. https://doi.org/10.1136/bmjopen-2019-031825

Alessandrini, J. M., Ribéron, J., & Da Silva, D. (2019). Will naturally ventilated dwellings remain safe during heatwaves? *Energy and Buildings*, *183*(January), 408–417. https://doi.org/10.1016/j.enbuild.2018.10.033

Allard, F., Ghiaus, C., & Szucs, A. (2009). Natural ventilation in cities, 137–162.

American Public Health Association (APHA). (2016). *Making The Connection: Climate Changes Children's Health*.

American Society of Heating, R. and A.-, & Conditioning Engineers (ASHRAE). (2017). *Standard 55- Thermal Comfort*. https://doi.org/10.1007/978-3-642-15790-5_3

Anderson, B. G., & Bell, M. L. (2009a). Weather-related mortality: How heat, cold, and heat waves affect mortality in the United States. *Epidemiology*, *20*(2), 205–213. https://doi.org/10.1097/EDE.0b013e318190ee08

Anderson, B. G., & Bell, M. L. (2009b). Weather-Related Mortality. *Epidemiology*, *20*(2), 205–213. https://doi.org/10.1097/ede.0b013e318190ee08

Anggraini, A. R., & Oliver, J. (2019). Mapping the Vulnerability of Human Health to Extreme Heat in the United States. *Journal of Chemical Information and Modeling*, *53*(9), 1689–1699.

AP. (2015). Egypt says heat wave death toll c. Retrieved March 13, 2020, from https://www.timesofisrael.com/egypt-says-heat-wave-death-toll-climbs-to-106/

Apotsos, A. (2019). Mapping relative social vulnerability in six mostly urban municipalities in South Africa. *Applied Geography*, *105*, 86–101. https://doi.org/10.1016/j.apgeog.2019.02.012

Arbuthnott, K., Hajat, S., Heaviside, C., & Vardoulakis, S. (2016). Changes in population susceptibility to heat and cold over time: Assessing adaptation to climate change. *Environmental Health: A Global Access Science Source*, *15*, 1–70. https://doi.org/10.1186/s12940-016-0102-7

Arnaud, J.-L., & Depaule, J.-C. (2020). Redefining Urban Spaces in Cairo at the Turn of the 19th and 20th Centuries. *Sensibilities of the Islamic Mediterranean*. https://doi.org/10.5040/9780755610167.ch-016

Arulmozhi, E., Moon, B. E., Basak, J. K., Sihalath, T., Park, J., & Kim, H. T. (2021). Machine learning-based microclimate model for indoor air temperature and relative humidity prediction in a swine building. *Animals*, *11*(1), 1–24. https://doi.org/10.3390/ani11010222

ASHRAE. (2016). *Energy Standard for Buildings Except Low-Rise Residential Buildings. The American Society of Heating, Refrigerating and Air-Conditioning Engineers (ASHRAE)*.

ASHRAE. (2017a). *ASHRAE Handbook - Fundamentals (SI Edition)*. Atlanta, Georgia.

ASHRAE. (2017b). ASHRAE Handbook Fundamentals. *Atlanta, GA*, 1014.

ASHRAE. (2018). Standard for Commercial Building Energy Audits, *8400*.

ASTM International. (2018). *Standard Practice for Measuring and Compensating for Reflected Temperature Using Infrared Imaging Radiometers* (Vol. 97). West Conshohocken, PA.

Attia, S., Evrard, A., & Gratia, E. (2012). Development of benchmark models for the Egyptian residential buildings sector. *Applied Energy*, *94*(2012), 270–284. https://doi.org/10.1016/j.apenergy.2012.01.065

Attia, S., & Wanas, O. (2012). the Database of Egyptian Building Envelopes (Debe): a Database for Building Energy Simulations. In *Fifth National Conference of IBPSA-USA* (pp. 96–103). Madison, Wisconsin.

Aubrecht, C., & Özceylan, D. (2013). Identification of heat risk patterns in the U.S. National Capital Region by integrating heat stress and related vulnerability. *Environment International*, *56*, 65–77. https://doi.org/10.1016/j.envint.2013.03.005

Auliciems;, A., & Szokolay, S. V. (2014). *Thermal Comfort. Passive and Low Energy Architecture International (PLEA)*. https://doi.org/10.4324/9781315074467

Auliciems, A., & Skinner, J. L. (1989). Cardiovascular deaths and temperature in subtropical Brisbane. *International Journal of Biometeorology*, *33*(4), 215–221. https://doi.org/10.1007/BF01051080

Avdelidis, N. P., & Moropoulou, A. (2003). *Emissivity considerations in building thermography*. *Energy and Buildings* (Vol. 35). https://doi.org/10.1016/S0378-7788(02)00210-4

Aydinalp, M., Ismet Ugursal, V., & Fung, A. S. (2002). Modeling of the appliance, lighting, and space-cooling energy consumptions in the residential sector using neural networks. *Applied Energy*, *71*(2), 87–110. https://doi.org/10.1016/S0306-2619(01)00049-6

Azuatalam, D., Lee, W.-L., de Nijs, F., & Liebman, A. (2020). Reinforcement learning for whole-building HVAC control and demand response. *Energy and AI*, *2*, 100020. https://doi.org/10.1016/j.egyai.2020.100020

Baccini, M., Biggeri, A., Accetta, G., Kosatsky, T., Katsouyanni, K., Analitis, A., … Michelozzi, P. (2008). Heat effects on mortality in 15 European cities. *Epidemiology*, *19*(5), 711–719. https://doi.org/10.1097/EDE.0b013e318176bfcd

Baker, D. G. (2002). Multiple sclerosis and thermoregulatory dysfunction. *Journal of Applied Physiology*, *92*(5), 1779–1780. https://doi.org/10.1152/japplphysiol.01251.2001

Bala, B. K., Arshad, F. M., & Noh, K. M. (2018). System dynamics: Modelling and simulation. *Springer*, 287.

Balaras, C. A., & Argiriou, A. A. (2002). Infrared thermography for building diagnostics. *Energy and Buildings*, *34*(2), 171–183. https://doi.org/10.1016/S0378-7788(01)00105-0

Balbus, J. M., & Malina, C. (2009). Identifying vulnerable subpopulations for climate change health effects in the United States. *Journal of Occupational and Environmental Medicine*, *51*(1), 33–37. https://doi.org/10.1097/JOM.0b013e318193e12e

Baldwin, J. W., Dessy, J. B., Vecchi, G. A., & Oppenheimer, M. (2019). Temporally Compound Heat Wave Events and Global Warming: An Emerging Hazard. *Earth's Future*, *7*(4), 411–427. https://doi.org/10.1029/2018EF000989

Banerjee, P., Singh, V. S., Chatttopadhyay, K., Chandra, P. C., & Singh, B. (2011). Artificial neural network model as a potential alternative for groundwater salinity forecasting. *Journal of Hydrology*, *398*(3–4), 212–220. https://doi.org/10.1016/j.jhydrol.2010.12.016

Baniassadi, A. (2019). *Vulnerability of U . S . Residential Building Stock to Heat*. Arizona State University.

Baniassadi, A., Sailor, D. J., O'Lenick, C. R., Wilhelmi, O. V., Crank, P. J., Chester, M. V., & Reddy, A. T. (2020). Effectiveness of Mechanical Air Conditioning as a Protective Factor Against Indoor Exposure to Heat Among the Elderly. *ASME Journal of Engineering for Sustainable Buildings and Cities*, *1*(1), 1–57. https://doi.org/10.1115/1.4045678

Bankoff, G., Hillorst, D., & Frerks, G. (2004). *Mapping Vulnerability Disasters, Development and People* (1st Editio). London, United Kingdom: Routledge.

Banwell, C., Dixon, J., Bambrick, H., Edwards, F., & Kjellström, T. (2012). Socio-cultural reflections on heat in Australia with implications for health and climate change adaptation. *Global Health Action*, *5*(1), 1–4. https://doi.org/10.3402/gha.v5i0.19277

Barclay, M., Sharples, S., Kang, J., & Watkins, R. (2012). The natural ventilation performance of buildings under alternative future weather projections. *Building Services Engineering Research and Technology*, *33*(1), 35–50. https://doi.org/10.1177/0143624411427460

Bark, N. (1998). Deaths of Pyschiatric Patients During Heatwaves. *Pyshiatric Services*, *49*(8), 1088–1090.

Barreca, A., Clay, K., Deschenes, O., Greenstone, M., & Shapiro, J. S. (2016). Adapting to climate change: The remarkable decline in the US temperature-mortality relationship over the Twentieth Century. *Journal of Political Economy*, *124*(1), 105–159. https://doi.org/10.1086/684582

Barreca, A. I. (2012). Climate change, humidity, and mortality in the United States. *Journal of Environmental Economics and Management*, *63*(1), 19–34. https://doi.org/10.1016/j.jeem.2011.07.004

Barreira, E., de, V. P., Delgado, J. M. P. Q., & Ramos, N. M. M. (2012). Thermography Applications in the Study of Buildings Hygrothermal Behaviour. *Infrared Thermography*. https://doi.org/10.5772/28282

Barriopedro, D., Fischer, E. M., Luterbacher, J., Trigo, R. M., & García-Herrera, R. (2011). The hot summer of 2010: Redrawing the temperature record map of Europe. *Science*, *332*(6026), 220–224. https://doi.org/10.1126/science.1201224

Basu, R. (2009). High ambient temperature and mortality: A review of epidemiologic studies from 2001 to 2008. *Environmental Health: A Global Access Science Source*, *8*(1). https://doi.org/10.1186/1476-

069X-8-40

Basu, R., Pearson, D., Malig, B., Broadwin, R., & Green, R. (2012). The effect of high ambient temperature on emergency room visits. *Epidemiology*, *23*(6), 813–820. https://doi.org/10.1097/EDE.0b013e31826b7f97

Basu, R., & Samet, J. M. (2002). An exposure assessment study of ambient heat exposure in an elderly population in Baltimore, Maryland. *Environmental Health Perspectives*, *110*(12), 1219–1224. https://doi.org/10.1289/ehp.021101219

Bates, G., & Miller, V. (2002). Empirical validation of a new heat stress index. *Journal of Occupational Health Safety*, *18*(2), 145–153.

Battisti, D. S., & Naylor, R. L. (2009). Historical Warnings of Future Food Insecurity with Unprecedented Seasonal Heat. *Science*, *341*(September), 1387–1391.

BBC. (2015a). Egypt heatwave leaves 61 people dead. *BBC News*.

BBC. (2015b, August 12). Egypt heatwave leaves 61 people dead.pdf. *BBC News*.

Behr, J. G., & Diaz, R. (2013). Disparate health implications stemming from the propensity of elderly and medically fragile populations to shelter in place during severe storm events. *Journal of Public Health Management and Practice*, *19*(5 SUPPL. 2), 10–12. https://doi.org/10.1097/PHH.0b013e318297226a

Bell, M. L., O'Neill, M. S., Ranjit, N., Borja-Aburto, V. H., Cifuentes, L. A., & Gouveia, N. C. (2008). Vulnerability to heat-related mortality in Latin America: A case-crossover study in São Paulo, Brazil, Santiago, Chile and Mexico City, Mexico. *International Journal of Epidemiology*, *37*(4), 796–804. https://doi.org/10.1093/ije/dyn094

Bernier, Q., & Meinzen-Dick, R. S. (2014). *Networks for resilience: The role of social capital. International Food Research Policy Institute (IFPRI)*. Retrieved from http://ebrary.ifpri.org/utils/getfile/collection/p15738coll2/id/128152/filename/128363.pdf

Besada, J. A., Campana, I., Bergesio, L., Bernardos, A. M., & De Miguel, G. (2019). Drone Flight Planning for Safe Urban Operations: UTM Requirements and Tools. *2019 IEEE International Conference on Pervasive Computing and Communications Workshops, PerCom Workshops 2019*, (June), 924–930. https://doi.org/10.1109/PERCOMW.2019.8730856

Bethea, D., & Parsons, K. (2002). The development of a practical heat stress assessment methodology for use in UK industry stress assessment methodology for use in UK industry. *Research Report 008*, 214 pages.

Blazejczyk, K., & Błażejczyk, A. (2014). Assessment of Bioclimatic Variability on Regional and Local Scales in Central Europe Using Ucti, *60*(March 2015), 82.

Blazejczyk, K., Epstein, Y., Jendritzky, G., Staiger, H., & Tinz, B. (2012). Comparison of UTCI to selected thermal indices. *International Journal of Biometeorology*, *56*(3), 515–535. https://doi.org/10.1007/s00484-011-0453-2

Bleta, A., Nastos, P. T., & Matzarakis, A. (2014). Assessment of bioclimatic conditions on Crete Island, Greece. *Regional Environmental Change*, *14*(5), 1967–1981. https://doi.org/10.1007/s10113-013-0530-7

Boeckmann, M., & Rohn, I. (2014). Is planned adaptation to heat reducing heat-related mortality and illness? A systematic review. *BMC Public Health*, *14*(1), 1–13. https://doi.org/10.1186/1471-2458-14-1112

Borden, K. A., Schmidtlein, M. C., Emrich, C. T., Piegorsch, W. W., & Cutter, S. L. (2007). Vulnerability of U.S. cities to environmental hazards. *Journal of Homeland Security and Emergency Management*, *4*(2). https://doi.org/10.2202/1547-7355.1279

Borrell, C., Marí-Dell'Olmo, M., Rodríguez-Sanz, M., Garcia-Olalla, P., Caylà, J. A., Benach, J., & Muntaner, C. (2006). Socioeconomic position and excess mortality during the heat wave of 2003 in Barcelona. *European Journal of Epidemiology*, *21*(9), 633–640. https://doi.org/10.1007/s10654-006-9047-4

Bouchama, A., Dehbi, M., Mohamed, G., Matthies, F., Shoukri, M., & Menne, B. (2012). Prognostic Factors in Heat Wave – Related Deaths. *Archives of Internal Medicine*, *167*(20), 2170–2176.

Bourdeau, M., Zhai, X. qiang, Nefzaoui, E., Guo, X., & Chatellier, P. (2019). Modeling and forecasting building energy consumption: A review of data-driven techniques. *Sustainable Cities and Society*, *48*(February), 101533. https://doi.org/10.1016/j.scs.2019.101533

Brake, R., & Bates, G. (2002). A valid method for comparing rational and empirical heat stress indices. *Annals of Occupational Hygiene*, *46*(2), 165–174. https://doi.org/10.1093/annhyg/mef030

Briley, L., Brown, D., & Kalafatis, S. E. (2015). Overcoming barriers during the co-production of climate information for decision-making. *Climate Risk Management*, *9*, 41–49. https://doi.org/10.1016/j.crm.2015.04.004

Brooke Anderson, G., & Bell, M. L. (2011). Heat waves in the United States: Mortality risk during heat waves and effect modification by heat wave characteristics in 43 U.S. communities. *Environmental Health Perspectives*, *119*(2), 210–218. https://doi.org/10.1289/ehp.1002313

Brown, S., & Walker, G. (2008). Understanding heat wave vulnerability in nursing and residential homes. *Building Research and Information*, *36*(4), 363–372. https://doi.org/10.1080/09613210802076427

Brune, N. E., & Bossert, T. (2009). Building social capital in post-conflict communities: Evidence from Nicaragua. *Social Science and Medicine*, *68*(5), 885–893. https://doi.org/10.1016/j.socscimed.2008.12.024

Bueno, B., Norford, L., Hidalgo, J., & Pigeon, G. (2013). The urban weather generator. *Journal of Building Performance Simulation*, *6*(4), 269–281. https://doi.org/10.1080/19401493.2012.718797

Buonocore, J. J., Hughes, E. J., Michanowicz, D. R., Heo, J., Allen, J. G., & Williams, A. (2019). Climate and health benefits of increasing renewable energy deployment in the United States. *Environmental Research Letters*, *14*(11). https://doi.org/10.1088/1748-9326/ab49bc

Burdziakowski, P., Specht, C., Dabrowski, P. S., Specht, M., Lewicka, O., & Makar, A. (2020). Using UAV photogrammetry to analyse changes in the coastal zone based on the sopot tombolo (Salient) measurement project. *Sensors (Switzerland)*, *20*(14), 1–21. https://doi.org/10.3390/s20144000

Buzug, T., Schumann, S., Pfaffmann, L., Reinhold, U., & Ruhlmann, J. (2006). *Functional Infrared Imaging for Skin-Cancer Screening*. *Conference proceedings : ... Annual International Conference of the IEEE Engineering in Medicine and Biology Society. IEEE Engineering in Medicine and Biology Society. Conference* (Vol. 1). https://doi.org/10.1109/IEMBS.2006.259895

C. Tanner, B. Lehmann, T. Frank, K. G. W. (2011). A proposal for standardized thermal images. *Bauphysik*, *33*, 345–356.

C.Clark, W., Jager, J., & Corell, R. (2000). *Assessing Vulnerability to Global Environmental Risks*.

Cai, Z., Tang, Y., Chen, K., & Han, G. (2019). Assessing the heat vulnerability of different local climate zones in the old areas of a Chinese megacity. *Sustainability (Switzerland)*, *11*(7). https://doi.org/10.3390/su11072032

CDC. (1996). *Heat-wave-related mortality Milwaukee, Wisconsin*. Atlanta, GA.

CDC. (2013). Heat illness and deaths - new york city, 2000-2011. *MMWR, Morbidity and Mortality Weekly Report*, *62*(31), 617–621. Retrieved from http://www.ncbi.nlm.nih.gov/pubmed/23925170

Cedeño Laurent, J. G., Williams, A., Oulhote, Y., Zanobetti, A., Allen, J. G., & Spengler, J. D. (2018a). Reduced cognitive function during a heat wave among residents of non-air-conditioned buildings: An observational study of young adults in the summer of 2016. *PLoS Medicine*, *15*(7). https://doi.org/10.1371/journal.pmed.1002605

Cedeño Laurent, J. G., Williams, A., Oulhote, Y., Zanobetti, A., Allen, J. G., & Spengler, J. D. (2018b). Reduced cognitive function during a heat wave among residents of non-air-conditioned buildings: An observational study of young adults in the summer of 2016. *PLoS Medicine*, *15*(7), 1–20. https://doi.org/10.1371/journal.pmed.1002605

Chae, Y. T., Horesh, R., Hwang, Y., & Lee, Y. M. (2016). Artificial neural network model for forecasting sub-hourly electricity usage in commercial buildings. *Energy and Buildings*, *111*, 184–194. https://doi.org/10.1016/j.enbuild.2015.11.045

Chan, E. Y. Y., Goggins, W. B., Kim, J. J., & Griffiths, S. M. (2012). A study of intracity variation of temperature-related mortality and socioeconomic status among the Chinese population in Hong Kong. *Journal of Epidemiology and Community Health*, *66*(4), 322–327. https://doi.org/10.1136/jech.2008.085167

Chan, T. H., Jia, K., Gao, S., Lu, J., Zeng, Z., & Ma, Y. (2015). PCANet: A Simple Deep Learning Baseline for Image Classification? *IEEE Transactions on Image Processing*, *24*(12), 5017–5032. https://doi.org/10.1109/TIP.2015.2475625

Chang, M. (1985). Evaluation of the Thermal Integrity of the Building Envelopes of Eight Federal.

Changnon, S. A., Pielke, R. A., Changnon, D., Sylves, R. T., & Pulwarty, R. (2000). Human factors explain the increased losses from weather and climate extremes. *Bulletin of the American Meteorological Society*, *81*(3), 437–442. https://doi.org/10.1175/1520-0477(2000)081<0437:HFETIL>2.3.CO;2

Chatzidimitriou, A., & Axarli, K. (2017). Street Canyon Geometry Effects on Microclimate and Comfort; A Case Study in Thessaloniki. *Procedia Environmental Sciences*, *38*(December), 643–650. https://doi.org/10.1016/j.proenv.2017.03.144

Chaudhuri, T., Soh, Y. C., Li, H., & Xie, L. (2019). A feedforward neural network based indoor-climate control framework for thermal comfort and energy saving in buildings. *Applied Energy*, *248*(February), 44–53. https://doi.org/10.1016/j.apenergy.2019.04.065

CHO., Y. K., Leite, F., Behzadan, A., & Wang, C. (2019). Opportunities for Applying Camera-Equipped Drones towards Performance Inspections of Building Facades. In *Computing in Civil Engineering* (pp.

105–113). Reston, VA: American Society of Civil Engineers. Retrieved from http://toc.proceedings.com/49478webtoc.pdf

Chong, D., Zhu, N., Luo, W., & Zhang, Z. (2019). Broadening human thermal comfort range based on short-term heat acclimation. *Energy*, *176*, 418–428. https://doi.org/10.1016/j.energy.2019.04.007

Chong, T. W. H., & Castle, D. J. (2004). Layer upon layer: Thermoregulation in schizophrenia. *Schizophrenia Research*, *69*(2–3), 149–157. https://doi.org/10.1016/S0920-9964(03)00222-6

Chow, W. T. L., Chuang, W. C., & Gober, P. (2012). Vulnerability to Extreme Heat in Metropolitan Phoenix: Spatial, Temporal, and Demographic Dimensions. *Professional Geographer*, *64*(2), 286–302. https://doi.org/10.1080/00330124.2011.600225

Christensen, J. J. (2013). Hurricane preparedness of community-dwelling dementia. *Dissertation Abstracts International Section A: Humanities and Social Sciences*, (January).

CIBSE. (2013). The limits of thermal comfort : avoiding overheating in European buildings. *CIBSE Tm52*, 1–25.

CIBSE. (2017). Design methodology for the assessment of overheating risk in homes. *Technical Memoranda 59*.

Coakley, D., Raftery, P., & Keane, M. (2014). A review of methods to match building energy simulation models to measured data. *Renewable and Sustainable Energy Reviews*, *37*, 123–141. https://doi.org/10.1016/j.rser.2014.05.007

Comptroller, C., Stringer, S. M., City, S., Heights, W., & Hill, M. (2018). *Addressing the Harms of Prohibition : What NYC Can do to Support an Equitable Cannabis Industry*.

Corsi, C. (2010). History highlights and future trends of infrared sensors. *Journal of Modern Optics*, *57*(18), 1663–1686. https://doi.org/10.1080/09500341003693011

Cosma, A. C., & Simha, R. (2019). Machine learning method for real-time non-invasive prediction of individual thermal preference in transient conditions. *Building and Environment*, *148*(July 2018), 372–383. https://doi.org/10.1016/j.buildenv.2018.11.017

Costello, A., Abbas, M., Allen, A., Ball, S., Bell, S., Bellamy, R., … Patterson, C. (2009). Managing the health effects of climate change. Lancet and University College London Institute for Global Health Commission. *The Lancet*, *373*(9676), 1693–1733. https://doi.org/10.1016/S0140-6736(09)60935-1

Crandall, C. G., & González-Alonso, J. (2010). Cardiovascular function in the heat-stressed human. *Acta Physiologica*, *199*(4), 407–423. https://doi.org/10.1111/j.1748-1716.2010.02119.x

Crump, D. (2011). Climate change – health impacts due to changes in the indoor environment ; Research needs, (February).

Curriero, F. C., Heiner, K. S., Samet, J. M., Zeger, S. L., Strug, L., & Patz, J. A. (2002). Temperature and mortality in 11 cities of the eastern United States. *American Journal of Epidemiology*, *155*(1), 80–87. https://doi.org/10.1093/aje/155.1.80

Cusack, L., de Crespigny, C., & Athanasos, P. (2011). Heatwaves and their impact on people with alcohol, drug and mental health conditions: A discussion paper on clinical practice considerations. *Journal of Advanced Nursing*, *67*(4), 915–922. https://doi.org/10.1111/j.1365-2648.2010.05551.x

Cutter, S. L., Boruff, B. J., & Shirley, W. L. (2003). Social vulnerability to environmental hazards. *Social Science Quarterly*, *84*(2), 242–261. https://doi.org/10.1111/1540-6237.8402002

D'Ippoliti, D, Michelozzi, P., Marino, C., D'Ovidio, M., Kirchmayer, U., & Menne, B. (2007). The Role of Gender in the Impact Evaluation of Heat Waves on Mortality in European Cities. *Epidemiology*, *27*(5), 371–378.

D'Ippoliti, Daniela, Michelozzi, P., Marino, C., De'Donato, F., Menne, B., Katsouyanni, K., … Perucci, C. A. (2010). The impact of heat waves on mortality in 9 European cities: Results from the EuroHEAT project. *Environmental Health: A Global Access Science Source*, *9*(1), 1–9. https://doi.org/10.1186/1476-069X-9-37

Dall'O', G., Sarto, L., & Panza, A. (2013). Infrared screening of residential buildings for energy audit purposes: Results of a field test. *Energies*, *6*(8), 3859–3878. https://doi.org/10.3390/en6083859

DATA2GO. (2021). Mass Incarceration Rates By Community District.

Davies, M., Béné, C., Arnall, A., Tanner, T., Newsham, A., & Coirolo, C. (2013). Promoting Resilient Livelihoods through Adaptive Social Protection: Lessons from 124 programmes in South Asia. *Development Policy Review*, *31*(1), 27–58. https://doi.org/10.1111/j.1467-7679.2013.00600.x

Davila Delgado, J. M., Oyedele, L., Ajayi, A., Akanbi, L., Akinade, O., Bilal, M., & Owolabi, H. (2019). Robotics and automated systems in construction: Understanding industry-specific challenges for adoption. *Journal of Building Engineering*, *26*(July), 100868. https://doi.org/10.1016/j.jobe.2019.100868

Dawson, B., Bridle, J., & Lockwood, R. J. (1994). Thermoregulation of paraplegic and able bodied men during prolonged exercise in hot and cool climates. *Paraplegia*, *32*(12), 860–870. https://doi.org/10.1038/sc.1994.132

de Dear, R., & Brager, G. S. (1998). Thermal Adaptation in the Built Environment : A Literature Review. *Energy and Buildings*, *27*(83), 83–96. https://doi.org/10.1201/b14052

de Munck, C., Lemonsu, A., Masson, V., Le Bras, J., & Bonhomme, M. (2018). Evaluating the impacts of greening scenarios on thermal comfort and energy and water consumptions for adapting Paris city to climate change. *Urban Climate*, *23*(2018), 260–286. https://doi.org/10.1016/j.uclim.2017.01.003

de Sherbinin, A., Schiller, A., & Pulsipher, A. (2007). The vulnerability of global cities to climate hazards. *Environment and Urbanization*, *19*(1), 39–64. https://doi.org/10.1177/0956247807076725

Delzendeh, E., Wu, S., Lee, A., & Zhou, Y. (2017). The impact of occupants' behaviours on building energy analysis: A research review. *Renewable and Sustainable Energy Reviews*, *80*(May), 1061–1071. https://doi.org/10.1016/j.rser.2017.05.264

Deschênes, O., & Greenstone, M. (2011). Climate change, mortality, and adaptation: Evidence from annual fluctuations in weather in the US. *American Economic Journal: Applied Economics*, *3*(4), 152–185. https://doi.org/10.1257/app.3.4.152

Di Napoli, C., Pappenberger, F., & Cloke, H. L. (2018). Assessing heat-related health risk in Europe via the Universal Thermal Climate Index (UTCI). *International Journal of Biometeorology*, *62*(7), 1155–1165. https://doi.org/10.1007/s00484-018-1518-2

Di Napoli, C., Pappenberger, F., & Cloke, H. L. (2019). Verification of heat stress thresholds for a health-based heat-wave definition. *Journal of Applied Meteorology and Climatology*, *58*(6), 1177–1194.

https://doi.org/10.1175/JAMC-D-18-0246.1

Dilling, L., Daly, M. E., Travis, W. R., Wilhelmi, O. V., & Klein, R. A. (2015). The dynamics of vulnerability: why adapting to climate variability will not always prepare us for climate change. *Wiley Interdisciplinary Reviews: Climate Change*, *6*(4), 413–425. https://doi.org/10.1002/wcc.341

Dino, I. G., Sari, A. E., Iseri, O. K., Akin, S., Kalfaoglu, E., Erdogan, B., … Alatan, A. A. (2020). Image-based construction of building energy models using computer vision. *Automation in Construction*, *116*(March), 103231. https://doi.org/10.1016/j.autcon.2020.103231

DJI. (n.d.). DJI Inspire 1.

DOE. (2013). *Residential Windows and Window Coverings: A Detailed View of the Installed Base and User Behavior*.

Department of Energy (DOE), (2015). Quadrennial Technology Review An Assessment Of Energy Technologies And Research, Chapter 2: Energy Sectors And Systems., (September), 39.

Doick, K., & Hutchings, T. (2013). Air temperature regulation by urban trees and green infrastructure. *Research {Note} - {Forestry} {Commission}*, (February), 10 pp.--10 pp. Retrieved from http://www.forestry.gov.uk/pdf/FCRN012.pdf/$FILE/FCRN012.pdf

Dominianni, C., Ahmed, M., Johnson, S., Blum, M., Ito, K., & Lane, K. (2018). Power Outage Preparedness and Concern among Vulnerable New York City Residents. *Journal of Urban Health*, *95*(5), 716–726. https://doi.org/10.1007/s11524-018-0296-9

Dong, W., Liu, Z., Zhang, L., Tang, Q., Liao, H., & Li, X. (2014). Assessing heat health risk for sustainability in Beijing's urban heat island. *Sustainability (Switzerland)*, *6*(10), 7334–7357. https://doi.org/10.3390/su6107334

Dufour, A., & Candas, V. (2007). Ageing and thermal responses during passive heat exposure: Sweating and sensory aspects. *European Journal of Applied Physiology*, *100*(1), 19–26. https://doi.org/10.1007/s00421-007-0396-9

E., G., P., B., G., C., & Peron, F. (2010). R-value estimation by local thermographic analysis. In *Proceedings of SPIE* (pp. 6–11). Thermosense XXXII.

E.Grinzatoa, V.Vavilov, & T.Kauppinenc. (1998). Quantitative infrared thermography in Buildings. *Energy and Buildings*, *29*(13), 1–9. https://doi.org/10.21611/qirt.1998.001

Ebi, K. L. (2004). Heat Watch / Warning Systems. *Society*, (August), 1067–1073.

Eckle, K., & Schmidt-Hieber, J. (2019). A comparison of deep networks with ReLU activation function and linear spline-type methods. *Neural Networks*, *110*, 232–242. https://doi.org/10.1016/j.neunet.2018.11.005

Edenhofer, O., Pichs-Madruga, R., Sokona, Y., Minx, J. C., Farahani, E., Susanne, K., … Zwickel, T. (2014). *Climate Change 2014: Mitigation of Climate Change*. *Working Group III Contribution to the Fifth Assessment Report of the Intergovernmental Panel on Climate Change*. https://doi.org/10.1017/CBO9781107415416

Environmental Protection Agency (EPA). (2011). *Reducing Urban Heat Islands: Compendium of strategies*. *Urban Heat Island Basics*.

Egondi, T., Kyobutungi, C., Kovats, S., Muindi, K., Ettarh, R., & Rocklöv, J. (2012). Time-series analysis of weather and mortality patterns in Nairobi's informal settlements. *Global Health Action*, *5*(SUPPL.), 23–32. https://doi.org/10.3402/gha.v5i0.19065

Elkatsha, M. (2000). *The Evolution Of Al-Azhar Street*. Massachusetts Institute of Technology.

Emmerich, S., Dols, W., & Axley, J. (2001). Natural ventilation review and plan for design and analysis tools. *National Institute of Standards and Technology*, *NIS*, 64. Retrieved from http://www.bfrl.nist.gov/IAQanalysis/docs/NISTIR_6781_NatVentTool.pdf

Enander, A. E., & Hygge, S. (1990). Thermal stress and human performance. *The Scandinavian Journal of Work, Environment & Health*, *16*, 44–50.

Engelland, R. E., Hemingway, H. W., Tomasco, O. G., Olivencia-Yurvati, A. H., & Romero, S. A. (2020). Neural control of blood pressure is altered following isolated leg heating in aged humans. *American Journal of Physiology - Heart and Circulatory Physiology*, *318*(4), H976–H984. https://doi.org/10.1152/ajpheart.00019.2020

Epstein, Y., & Moran, D. S. (2006). Thermal Comfort and the Heat Stress Indices. *Industrial Health*, *44*, 388–398.

F. Altmayer, E., Bauman, F., Gadgil, A., & C. Kammerud, R. (1982). *Correlations for convective heat transfer from room surfaces*. *NASA STI/Recon Technical Report N* (Vol. 89).

Fadare, D. A. (2009). Modelling of solar energy potential in Nigeria using an artificial neural network model. *Applied Energy*, *86*(9), 1410–1422. https://doi.org/10.1016/j.apenergy.2008.12.005

Fahim, B. K., & Thomas, M. (2014). Blackouts in Egypt Prompt Accusations. Retrieved March 15, 2020, from https://www.nytimes.com/2014/08/23/world/middleeast/blackouts-in-egypt-prompt-accusations.html

Falorca, J. F., & Lanzinha, J. C. G. (2020). Facade inspections with drones–theoretical analysis and exploratory tests. *International Journal of Building Pathology and Adaptation*, *39*(2), 235–258. https://doi.org/10.1108/IJBPA-07-2019-0063

Fernandez Milan, B., & Creutzig, F. (2015). Reducing urban heat wave risk in the 21st century. *Current Opinion in Environmental Sustainability*, *14*, 221–231. https://doi.org/10.1016/j.cosust.2015.08.002

Ferwati, S., Skelhorn, C., Ferwati, S., Shandas, V., & Makido, Y. (2020). *Urban Adaptation to Climate Change Urban Form and Variation in Temperatures*. Springer.

Fiala, D., Havenith, G., Bröde, P., Kampmann, B., & Jendritzky, G. (2012). UTCI-Fiala multi-node model of human heat transfer and temperature regulation. *International Journal of Biometeorology*, *56*(3), 429–441. https://doi.org/10.1007/s00484-011-0424-7

Ficken, G. W. (1978). Beating the heat: Keeping UK building cool in a warming climate. *The Physics Teacher*, *16*, 175.

Field, C. B., Barros, V., Stocker, T. F., Dahe, Q., Jon Dokken, D., Ebi, K. L., … Midgley, P. M. (2012). Managing the risks of extreme events and disasters to advance climate change adaptation: Special report of the intergovernmental panel on climate change. *Managing the Risks of Extreme Events and Disasters to Advance Climate Change Adaptation: Special Report of the Intergovernmental Panel on Climate Change*, *9781107025*(Chapter 2), 1–582. https://doi.org/10.1017/CBO9781139177245

FLIR Systems. (n.d.). FLIR Systems: FLIR Tools+.

FLIR Systems. (2011). *Thermal Imaging Guidebook for building and renewable energy applications*. *Guid book*. Retrieved from www.flir.com%5Cnwww.flirmedia.com/MMC/THG/Brochures/.../T820264_APAC.pdf

FLIR Systems. (2016). *Zenmuse XT User Manual*.

FLIR Systems. (2019). How Does Emissivity Affect Thermal Imaging ?

Foam-Tech. (2015). Building Envelope Theory. Retrieved October 29, 2018, from http://www.foam-tech.com/toc_NEW.htm

Forbes, A., & Wainwright, S. P. (2001). On the methodological, theoretical and philosophical context of health inequalities research: A critique. *Social Science and Medicine*, *53*(6), 801–816. https://doi.org/10.1016/S0277-9536(00)00383-X

Foroni, M., Salvioli, G., Rielli, R., Goldoni, C. A., Orlandi, G., Sajani, S. Z., … Mussi, C. (2007). A retrospective study on heat-related mortality in an elderly population during the 2003 heat wave in Modena, Italy: The Argento Project. *Journals of Gerontology - Series A Biological Sciences and Medical Sciences*, *62*(6), 647–651. https://doi.org/10.1093/gerona/62.6.647

Forrester, J. W. (1961). *Industrial Dynamics*. Cambridge, MA, USA: MIT Press. https://doi.org/10.5749/minnesota/9780816683314.003.0008

Forrester, J. W. (1990). *Principles of Systems*. Portland, OR, USA: Productivity Press.

Fosas, D., Coley, D. A., Natarajan, S., Herrera, M., Fosas de Pando, M., & Ramallo-Gonzalez, A. (2018). Mitigation versus adaptation: Does insulating dwellings increase overheating risk? *Building and Environment*, *143*(May), 740–759. https://doi.org/10.1016/j.buildenv.2018.07.033

Foster, K. G., Ellis, F. P., Doré, C., Exton-smtth, A. N., & Weiner, J. S. (1976). Sweat Responses in The Aged. *Age and Ageing*, *5*(2), 91–101. https://doi.org/10.1093/ageing/5.2.91

Fouillet, A., Rey, G., Laurent, F., Pavillon, G., Bellec, S., Guihenneuc-Jouyaux, C., … Hémon, D. (2006). Excess mortality related to the August 2003 heat wave in France. *International Archives of Occupational and Environmental Health*, *80*(1), 16–24. https://doi.org/10.1007/s00420-006-0089-4

Fouillet, A., Rey, G., Wagner, V., Laaidi, K., Empereur-Bissonnet, P., Le Tertre, A., … Hémon, D. (2008). Has the impact of heat waves on mortality changed in France since the European heat wave of summer 2003? A study of the 2006 heat wave. *International Journal of Epidemiology*, *37*(2), 309–317. https://doi.org/10.1093/ije/dym253

Fox, M., Coley, D., Goodhew, S., & De Wilde, P. (2014). Thermography methodologies for detecting energy related building defects. *Renewable and Sustainable Energy Reviews*, *40*, 296–310. https://doi.org/10.1016/j.rser.2014.07.188

Francesco, A., Giorgio, baldinelli, & Francesco, B. (2011). A quantitative methodology to evaluate thermal bridges in buildings. *Applied Energy*, *xxx*(May), 1241–1252. Retrieved from http://www.scopus.com/results/results.url?sort=plf-f&src=s&st1=A+quantitative+methodology+to+evaluate+thermal+bridges+in+buildings&sid=hCw9z 1NyoK8_DHCYyqc-tN5%3A30&sot=b&sdt=b&sl=82&s=TITLE-ABS-KEY%28A+quantitative+methodology+to+evaluate+thermal+bridges+

Frey, S. E., Destaillats, H., Cohn, S., Ahrentzen, S., & Fraser, M. P. (2014). Characterization of indoor air quality and resident health in an Arizona senior housing apartment building. *Journal of the Air and Waste Management Association*, *64*(11), 1251–1259. https://doi.org/10.1080/10962247.2014.937513

Frumkin, H., McMichael, A. J., & Hess, J. J. (2008). Climate Change and the Health of the Public. *American Journal of Preventive Medicine*, *35*(5), 401–402. https://doi.org/10.1016/j.amepre.2008.08.031

Fuhrmann, C. M., Sugg, M. M., Konrad, C. E., & Waller, A. (2016). Impact of Extreme Heat Events on Emergency Department Visits in North Carolina (2007–2011). *Journal of Community Health*, *41*(1), 146–156. https://doi.org/10.1007/s10900-015-0080-7

Füssel, H. M. (2007). Adaptation planning for climate change: Concepts, assessment approaches, and key lessons. *Sustainability Science*, *2*(2), 265–275. https://doi.org/10.1007/s11625-007-0032-y

Füssel, Hans Martin, & Klein, R. J. T. (2006). Climate change vulnerability assessments: An evolution of conceptual thinking. *Climatic Change*, *75*(3), 301–329. https://doi.org/10.1007/s10584-006-0329-3

Gallagher, N. B. (2013). Savitzky–Golay filter for smoothing and differentiation. *Signal Processing*, (January), 2–6. Retrieved from https://doi.org/10.1016/j.sigpro.2005.02.002

Gamble, J. L., Hurley, B. J., Schultz, P. A., Jaglom, W. S., Krishnan, N., & Harris, M. (2013). Climate change and older Americans: State of the science. *Environmental Health Perspectives*, *121*(1), 15–22. https://doi.org/10.1289/ehp.1205223

Gaskin, C. J., Taylor, D., Kinnear, S., Mann, J., Hillman, W., & Moran, M. (2017). Factors associated with the climate change vulnerability and the adaptive capacity of people with disability: A systematic review. *Weather, Climate, and Society*, *9*(4), 801–814. https://doi.org/10.1175/WCAS-D-16-0126.1

Gasparrini, A., Guo, Y., & Hashizume, M. (2015). Mortalité attribuable au froid et à la chaleur : Analyse multi-pays. *Environnement, Risques et Sante*, *14*(6), 464–465. https://doi.org/10.1016/S0140-6736(14)62114-0

Gasparrini, Antonio, & Armstrong, B. (2011). The impact of heat waves on mortality. *Epidemiology*, *22*(1), 68–73. https://doi.org/10.1097/EDE.0b013e3181fdcd99

Gilbert, N. (1996). *Welfare Justice: Restoring Social Equity.* (Vol. 25). Yale University Press. https://doi.org/10.2307/2077096

Gillespie, K. L., Cowan, J. D., Frazell, C. W., Haberl, J. S., Heinemeier, K. H., Kummer, J. P., … Montgomery, R. D. (2002). Measurement of Energy and Demand Savings. Guide 14. ASHRAE, *8400*, 170.

Girshick, R., Donahue, J., Darrell, T., & Malik, J. (2016). Region-Based Convolutional Networks for Accurate Object Detection and Segmentation. *IEEE Transactions on Pattern Analysis and Machine Intelligence*, *38*(1), 142–158. https://doi.org/10.1109/TPAMI.2015.2437384

Glass, K., Tait, P. W., Hanna, E. G., & Dear, K. (2015). Estimating risks of heat strain by age and sex: A population-level simulation model. *International Journal of Environmental Research and Public Health*, *12*(5), 5241–5255. https://doi.org/10.3390/ijerph120505241

Gleeds. (2020). *Egypt Construction Market Report*. *Gleeds*.

Global Cool Cities Alliance (GCCA). (2012). *A Practical Guide to Cool Roofs and Cool Pavements*.

Goromosov, M. S., Solomonovic, M., & World Health Organization. (1968). *The Physiological Basis of Health Standards for Dwellings*. Geneva, Switzerland: World Health Organization (WHO).

Goromosov, M., & WHO. (1968). *The physiological basis of health standards for dwellings*. Retrieved from http://apps.who.int/iris/handle/10665/39749

Gosling, S. N., Lowe, J. A., McGregor, G. R., Pelling, M., & Malamud, B. D. (2009). *Associations between elevated atmospheric temperature and human mortality: A critical review of the literature*. *Climatic Change* (Vol. 92). https://doi.org/10.1007/s10584-008-9441-x

Gotanda, H., Fogel, J., Husk, G., Levine, J. M., Peterson, M., Baumlin, K., & Habboushe, J. (2015). Hurricane sandy: Impact on emergency department and hospital utilization by older adults in Lower Manhattan, New York (USA). *Prehospital and Disaster Medicine*, *30*(5), 496–502. https://doi.org/10.1017/S1049023X15005087

Goudarzi, H., Hine, D., & Richards, A. (2019). Mission Automation for Drone Inspection in Congested Environments. *2019 International Workshop on Research, Education and Development on Unmanned Aerial Systems, RED-UAS 2019*, 305–314. https://doi.org/10.1109/REDUAS47371.2019.8999719

Gover, M. (1938). Mortality during Periods of Excessive Temperature. *Public Health Reports*, *53*(27), 1122–1143.

Graves, A., Liwicki, M., Fernandez, S., Bertolami, R., Bunke, H., & Schmidhuber, J. (2008). A Novel Connectionist System for Unconstrained Handwriting Recognition. *IEEE Transactions on Pattern Analysis and Machine Intelligence*, *31*(5), 855–868.

Green, J. M., Bishop, P. A., Muir, I. H., & Lomax, R. G. (2000). Gender differences in sweat lactate. *European Journal of Applied Physiology*, *82*(3), 230–235. https://doi.org/10.1007/s004210050676

Grey, C. N., & Wartman, E. C. (2017). Infrared Technology application in Building Envelopes: Applications, ASTM Standards, and Limitations. *ITC User Conference*, 1–10. Retrieved from http://www.sgh.com/sites/default/files/downloads/Knowledge-Sharing/11_grey.pdf

Groffman, P. M., Kareiva, P., Carter, S., Grimm, N. B., Lawler, J., Mack, M., … Tallis, H. (2014). *Ch. 8: Ecosystems, Biodiversity, and Ecosystem Services. Climate Change Impacts in the United States: The Third National Climate Assessment*. *Climate Change Impacts in the United States: The Third National Climate Assessment.* (Vol. 841). Retrieved from https://nca2014.globalchange.gov/downloads

Gromosov, M. S. (1963). Microclimate in Living Quarters and Its Hygienic Investigations. *Gig Sanit*, (8), 3–11.

Gronlund, C. J. (2014). Racial and Socioeconomic Disparities in Heat-Related Health Effects and Their Mechanisms: a Review. *Current Epidemiology Reports*, *1*(3), 165–173. https://doi.org/10.1007/s40471-014-0014-4

Gulli, A., & Pal, S. (2017). *Deep Learning with Keras* (Vol. 78). Packt Publishing Ltd. Retrieved from p

Guo, Y., Gasparrini, A., Armstrong, B. G., Tawatsupa, B., Tobias, A., Lavigne, E., … Tong, S. (2017). Heat wave and mortality: A multicountry, multicommunity study. *Environmental Health Perspectives*, *125*(8), 1–11. https://doi.org/10.1289/EHP1026

Guresen, E., Kayakutlu, G., & Daim, T. U. (2011). Using artificial neural network models in stock market

index prediction. *Expert Systems with Applications*, *38*(8), 10389–10397. https://doi.org/10.1016/j.eswa.2011.02.068

Haines, A., & Ebi, K. (2019). The Imperative for Climate Action to Protect Health. *New England Journal of Medicine*, *380*(3), 263–273. https://doi.org/10.1056/nejmra1807873

Hajat, S., & Kosatky, T. (2010). Heat-related mortality: A review and exploration of heterogeneity. *Journal of Epidemiology and Community Health*, *64*(9), 753–760. https://doi.org/10.1136/jech.2009.087999

Hajat, S., O'Connor, M., & Kosatsky, T. (2010). Health effects of hot weather: from awareness of risk factors to effective health protection. *The Lancet*, *375*(9717), 856–863. https://doi.org/10.1016/S0140-6736(09)61711-6

Hallegatte, S., & Corfee-Morlot, J. (2011). Understanding climate change impacts, vulnerability and adaptation at city scale: An introduction. *Climatic Change*, *104*(1), 1–12. https://doi.org/10.1007/s10584-010-9981-8

Hansen, A., Bi, L., Saniotis, A., & Nitschke, M. (2013). Vulnerability to extreme heat and climate change: Is ethnicity a factor? *Global Health Action*, *6*(1). https://doi.org/10.3402/gha.v6i0.21364

Hansen, A., Bi, P., Nitschke, M., Pisaniello, D., Newbury, J., & Kitson, A. (2011). Perceptions of heat-susceptibility in older persons: Barriers to adaptation. *International Journal of Environmental Research and Public Health*, *8*(12), 4714–4728. https://doi.org/10.3390/ijerph8124714

Hansen, A., Bi, P., Nitschke, M., Ryan, P., Pisaniello, D., & Tucker, G. (2008). The effect of heat waves on mental health in a temperate Australian City. *Environmental Health Perspectives*, *116*(10), 1369–1375. https://doi.org/10.1289/ehp.11339

Haralambopoulos, D. A., & Paparsenos, G. F. (1998). Assessing the thermal insulation of old buildings—The need for in situ spot measurements of thermal resistance and planar infrared thermography. *Energy Conversion and Management*, *39*(1–2), 65–79. https://doi.org/10.1016/s0196-8904(96)00176-8

Harlan, S. L., Brazel, A. J., Prashad, L., Stefanov, W. L., & Larsen, L. (2006). Neighborhood microclimates and vulnerability to heat stress. *Social Science and Medicine*, *63*(11), 2847–2863. https://doi.org/10.1016/j.socscimed.2006.07.030

Harlan, S. L., Chowell, G., Yang, S., Petitti, D. B., Butler, E. J. M., Ruddell, B. L., & Ruddell, D. M. (2014). Heat-related deaths in hot cities: Estimates of human tolerance to high temperature thresholds. *International Journal of Environmental Research and Public Health*, *11*(3), 3304–3326. https://doi.org/10.3390/ijerph110303304

Havenith, G., & Fiala, D. (2016). Thermal indices and thermophysiological modeling for heat stress. *Comprehensive Physiology*, *6*(1), 255–302. https://doi.org/10.1002/cphy.c140051

Hayden, M. H., Brenkert-Smith, H., & Wilhelmi, O. V. (2011). Differential Adaptive Capacity to Extreme Heat: A Phoenix, Arizona, Case Study. *Weather, Climate, and Society*, *3*(4), 269–280. https://doi.org/10.1175/WCAS-D-11-00010.1

Hayden, M. H., Wilhelmi, O. V., Banerjee, D., Greasby, T., Cavanaugh, J. L., Nepal, V., … Gower, S. (2017a). Adaptive capacity to extreme heat: Results from a household survey in Houston, Texas. *Weather, Climate, and Society*, *9*(4), 787–799. https://doi.org/10.1175/WCAS-D-16-0125.1

Hayden, M. H., Wilhelmi, O. V., Banerjee, D., Greasby, T., Cavanaugh, J. L., Nepal, V., … Gower, S. (2017b). Adaptive Capacity to Extreme Heat: Results from a Household Survey in Houston, Texas. *Weather, Climate, and Society*, WCAS-D-16-0125.1. https://doi.org/10.1175/WCAS-D-16-0125.1

Haykin, S. (1999). *Neural Networks: A Comprehensive Foundation*. Prentice Hall.

He, K., Zhang, X., Ren, S., & Sun, J. (2016). Deep residual learning for image recognition. *Proceedings of the IEEE Computer Society Conference on Computer Vision and Pattern Recognition*, *2016-Decem*, 770–778. https://doi.org/10.1109/CVPR.2016.90

Henderson, S. B., Wan, V., & Kosatsky, T. (2013). Differences in heat-related mortality across four ecological regions with diverse urban, rural, and remote populations in British Columbia, Canada. *Health and Place*, *23*, 48–53. https://doi.org/10.1016/j.healthplace.2013.04.005

Heracleous, C., & Michael, A. (2019). Experimental assessment of the impact of natural ventilation on indoor air quality and thermal comfort conditions of educational buildings in the Eastern Mediterranean region during the heating period. *Journal of Building Engineering*, *26*(November). https://doi.org/10.1016/j.jobe.2019.100917

Heudorf, U., & Schade, M. (2014). Heat waves and mortality in Frankfurt am Main, Germany, 2003-2013: what effect do heat-health action plans and the heat warning system have? *Zeitschrift Für Gerontologie Und Geriatrie*, *47*(6), 475–482. https://doi.org/10.1007/s00391-014-0673-2

Hg, E., Iru, S., Upgpulf, R. X., Prgho, W. K. H., Zlwk, D. Q. G., Ylghrv, W. K. H., … Frqvwuxfwlrq, W. K. H. (2019). BIM-based Mixed Reality Application for Supervision of Construction, *63*, 1903–1907.

Hippert, H. s., & Pedreira, C. E. (2004). Estimating temperature profiles for short-term load forecasting: Neural networks compared to linear models. *IEE Proceedings-Generation, Transmission and …*, *151*(3), 201–212. https://doi.org/10.1049/ip-gtd

Hoegh-Guldberg et al. (2018). Chapter 3: Impacts of 1.5°C global warming on natural and human systems. In: Global Warming of 1.5 °C. An IPCC special report on the impacts of global warming of 1.5 °C above preindustrial levels and related global greenhouse gas emission pathways [...]. *Special Report, Intergovernmental Panel on Climate Change*, (ISBN 978-92-9169-151-7), 175–311.

Hoes, P., Hensen, J. L. M., Loomans, M. G. L. C., de Vries, B., & Bourgeois, D. (2009). User behavior in whole building simulation. *Energy and Buildings*, *41*(3), 295–302. https://doi.org/10.1016/j.enbuild.2008.09.008

Holman, I. P., Brown, C., Carter, T. R., Harrison, P. A., & Rounsevell, M. (2019). Improving the representation of adaptation in climate change impact models. *Regional Environmental Change*, *19*(3), 711–721. https://doi.org/10.1007/s10113-018-1328-4

Holmes, S. H., Phillips, T., & Wilson, A. (2016a). Overheating and passive habitability : indoor health and heat indices, *44*(1), 1–19.

Holmes, S. H., Phillips, T., & Wilson, A. (2016b). Overheating and passive habitability: Indoor health and heat indices. *Building Research and Information*, *44*(1), 1–19. https://doi.org/10.1080/09613218.2015.1033875

Honda, Y. (1995). Air-conditioning and mortality in hot weather. *American Journal of Epidemiology*, *142*(1), 99. https://doi.org/10.1093/oxfordjournals.aje.a117551

Hondula, D. M., Davis, R. E., Leisten, M. J., Saha, M. V., Veazey, L. M., & Wegner, C. R. (2012). Fine-scale spatial variability of heat-related mortality in Philadelphia County, USA, from 1983-2008: A case-series analysis. *Environmental Health: A Global Access Science Source*, *11*(1), 1–51. https://doi.org/10.1186/1476-069X-11-16

Hondula, D. M., Davis, R. E., Saha, M. V., Wegner, C. R., & Veazey, L. M. (2015). Geographic dimensions of heat-related mortality in seven U.S. cities. *Environmental Research*, *138*, 439–452. https://doi.org/10.1016/j.envres.2015.02.033

Hu, H., Wang, L., Zhang, M., Ding, Y., & Zhu, Q. (2020). Fast and Regularized Reconstruction of Building Facades from Street-View Images Using Binary Integer Programming. *ISPRS Annals of the Photogrammetry, Remote Sensing and Spatial Information Sciences*, *5*(2), 365–371. https://doi.org/10.5194/isprs-annals-V-2-2020-365-2020

IEA. (2018). *The Future of Cooling: Opportunities for Energy-efficient Air Conditioning*. https://doi.org/10.1787/9789264301993-en

Iglesias, C., Martínez Torres, J., García Nieto, P. J., Alonso Fernández, J. R., Díaz Muñiz, C., Piñeiro, J. I., & Taboada, J. (2014). Turbidity Prediction in a River Basin by Using Artificial Neural Networks: A Case Study in Northern Spain. *Water Resources Management*, *28*(2), 319–331. https://doi.org/10.1007/s11269-013-0487-9

Inostroza, L., Palme, M., & De La Barrera, F. (2016). A heat vulnerability index: Spatial patterns of exposure, sensitivity and adaptive capacity for Santiago de Chile. *PLoS ONE*, *11*(9), 1–26. https://doi.org/10.1371/journal.pone.0162464

Intergovernmental Panel on Climate Change (IPCC). (2013). *IPCC, 2013: Climate Change 2013: The Physical Science Basis. Contribution of Working Group I to the Fifth Assessment Report of the Intergovernmental Panel on Climate Change*. the Fifth Assessment Report of the Intergovernmental Panel on Climate Change (Vol. AR5). Cambridge, UK.

International Standards Organization. (1983). *Thermal insulation -- Qualitative detection of thermal irregularities in building envelopes -Infrared method*.

IPCC. (2014a). *Climate Change 2014: Synthesis Report. Contribution of Working Groups I, II and III to the Fifth Assessment Report of the Intergovernmental Panel on Climate Change*. Geneva, Switzerland. https://doi.org/10.1177/0002716295541001010

IPCC. (2014b). *Technical Summary- Climate Change: Impacts, Adaptation, and Vulnerability*. *Climate Change 2014: Impacts, Adaptation, and Vulnerability. Part A: Global and Sectoral Aspects. Contribution of Working Group II to the Fifth Assessment Report of the Intergovernmental Panel on Climate Change*. Geneva, Switzerland. https://doi.org/10.1016/j.renene.2009.11.012

Irizarry, J., Gheisari, M., & Walker, B. N. (2012). Usability assessment of drone technology as safety inspection tools. *Electronic Journal of Information Technology in Construction*, *17*(September 2012), 194–212.

Jakovljević, M., Mück-Šeler, D., Pivac, N., Ljubičić, D., Bujas, M., & Dodig, G. (1997). Seasonal influence on platelet 5-HT levels in patients with recurrent major depression and schizophrenia. *Biological Psychiatry*, *41*(10), 1028–1034. https://doi.org/10.1016/S0006-3223(96)00212-0

Jänicke, B., Holtmann, A., Kim, K. R., Kang, M., Fehrenbach, U., & Scherer, D. (2019). Quantification and evaluation of intra-urban heat-stress variability in Seoul, Korea. *International Journal of*

Biometeorology, *63*(1), 1–12. https://doi.org/10.1007/s00484-018-1631-2

Jendritzky, G., de Dear, R., & Havenith, G. (2012). UTCI-Why another thermal index? *International Journal of Biometeorology*, *56*(3), 421–428. https://doi.org/10.1007/s00484-011-0513-7

Jentsch, M. F., James, P. A. B., Bourikas, L., & Bahaj, A. B. S. (2013). Transforming existing weather data for worldwide locations to enable energy and building performance simulation under future climates. *Renewable Energy*, *55*, 514–524. https://doi.org/10.1016/j.renene.2012.12.049

Johnson, D. P., Stanforth, A., Lulla, V., & Luber, G. (2012). Developing an applied extreme heat vulnerability index utilizing socioeconomic and environmental data. *Applied Geography*, *35*(1–2), 23–31. https://doi.org/10.1016/j.apgeog.2012.04.006

Johnson, D. P., Wilson, J. S., & Luber, G. C. (2009). Socioeconomic indicators of heat-related health risk supplemented with remotely sensed data. *International Journal of Health Geographics*, *8*, 57. https://doi.org/10.1186/1476-072X-8-57

Jordan, S., Moore, J., Hovet, S., Box, J., Perry, J., Kirsche, K., … Tse, Z. T. H. (2018). State-of-the-art technologies for UAV inspections. *IET Radar, Sonar and Navigation*, *12*(2), 151–164. https://doi.org/10.1049/iet-rsn.2017.0251

Jurgilevich, A., Räsänen, A., Groundstroem, F., & Juhola, S. (2017). A systematic review of dynamics in climate risk and vulnerability assessments. *Environmental Research Letters*, *12*(1). https://doi.org/10.1088/1748-9326/aa5508

Kaiser, R., Le Tertre, A., Schwartz, J., Gotway, C. A., Daley, W. R., & Rubin, C. H. (2007). The effect of the 1995 heat wave in Chicago on all-cause and cause-specific mortality. *American Journal of Public Health*, *97 Suppl 1*, 158–162. https://doi.org/10.2105/AJPH.2006.100081

Kajl, S., Roberge, M.-A., Lamarche, L., & Malinowski, P. (1997). Evaluation of Building Energy Consumption Based on. *Oceedings of Clima 2000 Conference, Held Brussels, August 30th to September 2nd*, (1), 1–10.

Keatinge, W. R., Donaldson, G. C., Cordioli, E., Martinelli, M., Kunst, A. E., Mackenbach, J. P., … Vuori, I. (2000). Heat related mortality in warm and cold regions of Europe: Observational study. *British Medical Journal*, *321*(7262), 670–673. https://doi.org/10.1136/bmj.321.7262.670

Keller, R. C. (2013). Place matters: Mortality, space, and urban form in the 2003 Paris heat wave disaster. *French Historical Studies*, *36*(2), 299–330. https://doi.org/10.1215/00161071-1960682

Kenney, W. L. (2001). Decreased cutaneous vasodilation in aged skin: Mechanisms, consequences and interventions. *Journal of Thermal Biology*, *26*(4–5), 263–271. https://doi.org/10.1016/S0306-4565(01)00029-8

Kenny, G. P., Flouris, A. D., Yagouti, A., & Notley, S. R. (2018). Towards establishing evidence-based guidelines on maximum indoor temperatures during hot weather in temperate continental climates. *Temperature*, *8940*(May), 1–26. https://doi.org/10.1080/23328940.2018.1456257

Kenny, G. P., Flouris, A. D., Yagouti, A., & Notley, S. R. (2019). Towards establishing evidence-based guidelines on maximum indoor temperatures during hot weather in temperate continental climates. *Temperature*, *6*(1), 11–36. https://doi.org/10.1080/23328940.2018.1456257

Kenny, G. P., Poirier, M. P., Metsios, G. S., Boulay, P., Dervis, S., Friesen, B. J., … Flouris, A. D. (2017).

Hyperthermia and cardiovascular strain during an extreme heat exposure in young versus older adults. *Temperature*, *4*(1), 79–88. https://doi.org/10.1080/23328940.2016.1230171

Kenny, G. P., Yardley, J., Brown, C., Sigal, R. J., & Jay, O. (2010). Heat stress in older individuals and patients with common chronic diseases. *Cmaj*, *182*(10), 1053–1060. https://doi.org/10.1503/cmaj.081050

Ketterer, C., & Matzarakis, A. (2014). Human-biometeorological assessment of the urban heat island in a city with complex topography - The case of Stuttgart, Germany. *Urban Climate*, *10*(P3), 573–584. https://doi.org/10.1016/j.uclim.2014.01.003

Kim, J., Hong, T., Jeong, J., Lee, M., Lee, M., Jeong, K., … Jeong, J. (2017). Establishment of an optimal occupant behavior considering the energy consumption and indoor environmental quality by region. *Applied Energy*, *204*(October), 1431–1443. https://doi.org/10.1016/j.apenergy.2017.05.017

Kim, M., Chun, C., & Han, J. (2010). A study on bedroom environment and sleep quality in Korea. *Indoor and Built Environment*, *19*(1), 123–128. https://doi.org/10.1177/1420326X09358031

Kim, S. M., Peña, M. I., Moll, M., Bennett, G. N., & Kavraki, L. E. (2017). A review of parameters and heuristics for guiding metabolic pathfinding. *Journal of Cheminformatics*, *9*(1), 1–13. https://doi.org/10.1186/s13321-017-0239-6

Kim, Y.-M., Kim, S., Cheong, H.-K., Ahn, B., & Choi, K. (2012). Effects of Heat Wave on Body Temperature and Blood Pressure in the Poor and Elderly. *Environmental Health and Toxicology*, *27*, e2012013. https://doi.org/10.5620/eht.2012.27.e2012013

Kirimtat, A., & Krejcar, O. (2018). A review of infrared thermography for the investigation of building envelopes: Advances and prospects. *Energy and Buildings*, *176*, 390–406. https://doi.org/10.1016/j.enbuild.2018.07.052

Kisilewicz, T. (2007). Computer simulation in solar architecture design. *Architectural Engineering and Design Management*, *3*(2), 106–123. https://doi.org/10.1080/17452007.2007.9684635

Kisilewicz, T. (2015). Passive control of indoor climate conditions in low energy buildings. *Energy Procedia*, *78*, 49–54. https://doi.org/10.1016/j.egypro.2015.11.113

Klein Rosenthal, J., Kinney, P. L., & Metzger, K. B. (2014). Intra-urban vulnerability to heat-related mortality in New York City, 1997-2006. *Health and Place*, *30*, 45–60. https://doi.org/10.1016/j.healthplace.2014.07.014

Klepeis, N E, Nelson, W. C., Ott, W. R., Robinson, J. P., Tsang, A. M., Switzer, P., … Engelmann, W. H. (2001). *The National Human Activity Pattern Survey*. *Lawrence Berkeley National Laboratory* (Vol. 11). https://doi.org/10.1038/sj.jea.7500165 T4 - A resource for assessing exposure to environmental pollutants Y3 - 20/2/2017 U6 - 10.1038/sj.jea.7500165 M4 - Citavi

Klepeis, Neil E., Bellettiere, J., Hughes, S. C., Nguyen, B., Berardi, V., Liles, S., … Hovell, M. F. (2017). Fine particles in homes of predominantly lowincome families with children and smokers: Key physical and behavioral determinants to inform indoor-Air-quality interventions. *PLoS ONE*, *12*(5), 1–24. https://doi.org/10.1371/journal.pone.0177718

Klepeis, Neil E., Nelson, W. C., Ott, W. R., Robinson, J. P., Tsang, A. M., Switzer, P., … Engelmann, W. H. (2001). The National Human Activity Pattern Survey (NHAPS): A resource for assessing exposure to environmental pollutants. *Journal of Exposure Analysis and Environmental Epidemiology*, *11*(3), 231–252. https://doi.org/10.1038/sj.jea.7500165

Klinenberg, E. (2002). Heat Wave: Death Comes to the City of Extremes. *The Baffler*, *15*(15), 65–70. https://doi.org/10.1162/bflr.2002.15.65

Klinenberg, E. (2003a). *Heat Wave: A Social Autopsy of Disaster in Chicago. The University of Chicago Press*. https://doi.org/10.1001/jama.289.12.1573

Klinenberg, E. (2003b). *Heat Wave: Social Autopsy of Disaster in Chicago* (Vol. 348). Chicago, IL: University of Chicago Press. https://doi.org/10.1056/nejm200302133480721

Knight, T., Price, S., Bowler, D., & King, S. (2016). How effective is "greening" of urban areas in reducing human exposure to ground-level ozone concentrations, UV exposure and the "urban heat island effect"? A protocol to update a systematic review. *Environmental Evidence*, *5*(1), 1–6. https://doi.org/10.1186/s13750-016-0054-y

Knowlton, K., Rotkin-Ellman, M., Geballe, L., Max, W., & Solomon, G. M. (2011). Six climate change-related events in the United States accounted for about $14 billion in lost lives and health costs. *Health Affairs*, *30*(11), 2167–2176. https://doi.org/10.1377/hlthaff.2011.0229

Kolendowicz, L., Półrolniczak, M., Szyga-Pluta, K., & Bednorz, E. (2018). Human-biometeorological conditions in the southern Baltic coast based on the universal thermal climate index (UTCI). *Theoretical and Applied Climatology*, *134*(1–2), 363–379. https://doi.org/10.1007/s00704-017-2279-2

Korc, F., & Förstner, W. (2009). eTRIMS Image Database for Interpreting Images of Man-Made Scenes, (1).

Kossecka, E., & Kosny, J. (2002). Influence of insulation configuration on heating and cooling loads in a continuously used building. *Energy and Buildings*, *34*(4), 321–331. https://doi.org/10.1016/S0378-7788(01)00121-9

Kovats, R. S., & Hajat, S. (2008). Heat stress and public health: A critical review. *Annual Review of Public Health*, *29*, 41–55. https://doi.org/10.1146/annurev.publhealth.29.020907.090843

Kravchenko, J., Abernethy, A. P., Fawzy, M., & Lyerly, H. K. (2013). Minimization of heatwave morbidity and mortality. *American Journal of Preventive Medicine*, *44*(3), 274–282. https://doi.org/10.1016/j.amepre.2012.11.015

Kreuzer, P., Landgrebe, M., M. Wittmann, M. Schecklmann, T. B., Poeppl, G. H., & Langguth, B. (2012). Hypothermia Associated with Antipsychotic Drug Use: A Clinical Case Series and Review of Current Literature. *Clinical Pharmacol*, *52*, 1090– 1097.

Krizhevsky, A., Sutskever, I., & Hinton, G. E. (2012). ImageNet Classification with Deep Convolutional Neural Networks. In *Advances in neural information processing systems* (pp. 1097–1105). https://doi.org/10.1201/9781420010749

Kuras, E. R., Richardson, M. B., Calkins, M. M., Ebi, K. L., Hess, J. J., Kintziger, K. W., … Hondula, D. M. (2017). Opportunities and challenges for personal heat exposure research. *Environmental Health Perspectives*, *125*(8). https://doi.org/10.1289/EHP556

Kwok, A. G., & Rajkovich, N. B. (2010). Addressing climate change in comfort standards. *Building and Environment*, *45*(1), 18–22. https://doi.org/10.1016/j.buildenv.2009.02.005

Kylili, A., Fokaides, P. A., Christou, P., & Kalogirou, S. A. (2014). Infrared thermography (IRT) applications for building diagnostics: A review. *Applied Energy*, *134*, 531–549.

https://doi.org/10.1016/j.apenergy.2014.08.005

Lancet, T. (2015). Health professionals: Be prepared for heatwaves. *The Lancet*, *386*(9990), 219. https://doi.org/10.1016/S0140-6736(15)61261-2

Lapola, D. M., Braga, D. R., Di Giulio, G. M., Torres, R. R., & Vasconcellos, M. P. (2019a). *Heat stress vulnerability and risk at the (super) local scale in six Brazilian capitals*. *Climatic Change* (Vol. 154). https://doi.org/10.1007/s10584-019-02459-w

Lapola, D. M., Braga, D. R., Di Giulio, G. M., Torres, R. R., & Vasconcellos, M. P. (2019b). Heat stress vulnerability and risk at the (super) local scale in six Brazilian capitals. *Climatic Change*, *154*(3–4), 477–492. https://doi.org/10.1007/s10584-019-02459-w

Larrieu, S., Carcaillon, L., Lefranc, A., Helmer, C., Dartigues, J. F., Tavernier, B., … Filleul, L. (2008). Factors associated with morbidity during the 2003 heat wave in two population-based cohorts of elderly subjects: PAQUID and Three City. *European Journal of Epidemiology*, *23*(4), 295–302. https://doi.org/10.1007/s10654-008-9229-3

Laska, S., & Morrow, B. H. (2006). Social vulnerabilities and Hurricane katrina: An unnatural disaster in new Orleans. *Marine Technology Society Journal*, *40*(4), 16–26. https://doi.org/10.4031/002533206787353123

Lazrus, H., Morrow, B. H., Morss, R. E., & Lazo, J. K. (2012). Vulnerability beyond stereotypes: Context and agency in hurricane risk communication. *Weather, Climate, and Society*, *4*(2), 103–109. https://doi.org/10.1175/WCAS-D-12-00015.1

Lee, D. C., Smith, S. W., Carr, B. G., Doran, K. M., Portelli, I., Grudzen, C. R., & Goldfrank, L. R. (2016). Geographic Distribution of Disaster-Specific Emergency Department Use after Hurricane Sandy in New York City. *Disaster Medicine and Public Health Preparedness*, *10*(3), 351–361. https://doi.org/10.1017/dmp.2015.190

Lee, J. (1980). Digital image enhancement and noise filtering by use of local statistics. *IEEE Transactions on Pattern Analysis and Machine Intelligence*, (2), 1978–1981.

Lee, J. Y., Kim, H., Gasparrini, A., Armstrong, B., Bell, M. L., Sera, F., … Guo, Y. (2019). Predicted temperature-increase-induced global health burden and its regional variability. *Environment International*, *131*(July). https://doi.org/10.1016/j.envint.2019.105027

Lee, K., & Lee, D. (2015). The relationship between indoor and outdoor temperature in two types of residence. *Energy Procedia*, *78*, 2851–2856. https://doi.org/10.1016/j.egypro.2015.11.647

Lee, S., Lee, H., Myung, W., Kim, E. J., & Kim, H. (2018). Mental disease-related emergency admissions attributable to hot temperatures. *Science of the Total Environment*, *616–617*, 688–694. https://doi.org/10.1016/j.scitotenv.2017.10.260

Leech, J. A., Nelson, W. C., Burnett, R. T., Aaron, S., & Raizenne, M. E. (2002a). It's about time: A comparison of Canadian and American time-activity patterns. *Journal of Exposure Analysis and Environmental Epidemiology*, *12*(6), 427–432. https://doi.org/10.1038/sj.jea.7500244

Leech, J. A., Nelson, W. C., Burnett, R. T., Aaron, S., & Raizenne, M. E. (2002b). It's about time: A comparison of Canadian and American time-activity patterns. *Journal of Exposure Analysis and Environmental Epidemiology*, *12*(6), 427–432. https://doi.org/10.1038/sj.jea.7500244

LEED. (2021). Passive Survivability and Back- up Power During Disruptions. Retrieved from https://www.usgbc.org/credits/passivesurvivability?view=resources

Li, B., Du, C., Tan, M., Liu, H., Essah, E., & Yao, R. (2018). A modified method of evaluating the impact of air humidity on human acceptable air temperatures in hot-humid environments. *Energy and Buildings*, *158*, 393–405. https://doi.org/10.1016/j.enbuild.2017.09.062

Li, F., Chen, W., Zeng, Y., Zhao, Q., & Wu, B. (2014). Improving estimates of grassland fractional vegetation cover based on a pixel dichotomy model: A case study in Inner Mongolia, China. *Remote Sensing*, *6*(6), 4705–4722. https://doi.org/10.3390/rs6064705

Li, H., Tang, X., Wang, R., Lin, F., Liu, Z., & Cheng, K. (2016). Comparative study on theoretical and machine learning methods for acquiring compressed liquid densities of 1,1,1,2,3,3,3-heptafluoropropane (R227ea) via Song and Mason equation, support vector machine, and artificial neural networks. *Applied Sciences (Switzerland)*, *6*(1), 1–12. https://doi.org/10.3390/app6010025

Li, J., & Shui, B. (2015). A comprehensive analysis of building energy efficiency policies in China: Status quo and development perspective. *Journal of Cleaner Production*, *90*, 326–344. https://doi.org/10.1016/j.jclepro.2014.11.061

Li, Y., Schubert, S., Kropp, J. P., & Rybski, D. (2020). On the influence of density and morphology on the Urban Heat Island intensity. *Nature Communications*, *11*(1), 1–9. https://doi.org/10.1038/s41467-020-16461-9

Lin, S., Fletcher, B. A., Luo, M., Chinery, R., & Hwang, S. A. (2011). Health impact in New York City during the Northeastern blackout of 2003. *Public Health Reports*, *126*(3), 384–393. https://doi.org/10.1177/003335491112600312

Lin, T.-Y., Dollar, P., Girshick, R., He, K., Hariharan, B., & Belongie, S. (2017). Feature Pyramid Networks for Object Detection. *CVPR*, 1500–1504. https://doi.org/10.1109/ISPA-BDCloud-SustainCom-SocialCom48970.2019.00217

Lindemann, U., Stotz, A., Beyer, N., Juha, O., Skelton, D. A., Becker, C., … Klenk, J. (2017). Effect of indoor temperature on physical performance in older adults during days with normal temperature and heat waves. *International Journal of Environmental Research and Public Health*, *14*(2), 1–9. https://doi.org/10.3390/ijerph14020186

Liotta, G., Inzerilli, M. C., Palombi, L., Madaro, O., Orlando, S., Scarcella, P., … Marazzi, M. C. (2018). Social interventions to prevent heat-related mortality in the older adult in Rome, Italy: A quasi-experimental study. *International Journal of Environmental Research and Public Health*, *15*(4), 1–13. https://doi.org/10.3390/ijerph15040715

Lipinski, T., Ahmad, D., Serey, N., & Jouhara, H. (2020). Review of ventilation strategies to reduce the risk of disease transmission in high occupancy buildings. *International Journal of Thermofluids*, *7–8*, 100045. https://doi.org/10.1016/j.ijft.2020.100045

Lobell, D. B., Schlenker, W., & Costa-Roberts, J. (2011). Climate Trends and Global Crop Production Since 1980. *Science*, *29*(July), 616–621. https://doi.org/10.5040/9780755621101.0007

Loenhout, J. A. F. Van, Grand, A., Duijm, F., Greven, F., Vink, N. M., Hoek, G., & Zuurbier, M. (2016). The Effect of High Indoor Temperatures on Self- Perceived Health of Elderly Persons. *Environmental Research*, (146), 27–34. https://doi.org/10.1016/j.envres.2015.12.012

Lomas, K. J., & Kane, T. (2013). Summertime temperatures and thermal comfort in UK homes. *Building Research and Information*, *41*(3), 259–280. https://doi.org/10.1080/09613218.2013.757886

Lomas, Kevin J., & Porritt, S. M. (2017). Overheating in buildings: lessons from research. *Building Research and Information*, *45*(1–2), 1–18. https://doi.org/10.1080/09613218.2017.1256136

Loughnan, M. E., Nicholls, N., & Tapper, N. J. (2010). When the heat is on: Threshold temperatures for AMI admissions to hospital in Melbourne Australia. *Applied Geography*, *30*(1), 63–69. https://doi.org/10.1016/j.apgeog.2009.08.003

Loughnan, M., Nicholls, N., & Tapper, N. (2010). Mortality-temperature thresholds for ten major population centres in rural Victoria, Australia. *Health and Place*, *16*(6), 1287–1290. https://doi.org/10.1016/j.healthplace.2010.08.008

Loughnan ME, T. N., Phan, T., Lynch, K., & McInnes, J. A. (2013). *A spatial vulnerability analysis of urban populations during extreme heat events in Australian capital cities, National Climate Change Adaptation Research Facility, Gold Coast, Australia*.

Lucchi, E. (2018). Applications of the infrared thermography in the energy audit of buildings: A review. *Renewable and Sustainable Energy Reviews*, *82*(July 2017), 3077–3090. https://doi.org/10.1016/j.rser.2017.10.031

Lundgren-Kownacki, K., Hornyanszky, E. D., Chu, T. A., Olsson, J. A., & Becker, P. (2018). Challenges of using air conditioning in an increasingly hot climate. *International Journal of Biometeorology*, *62*(3), 401–412. https://doi.org/10.1007/s00484-017-1493-z

Luo, M., de Dear, R., Ji, W., Bin, C., Lin, B., Ouyang, Q., & Zhu, Y. (2016). The dynamics of thermal comfort expectations: The problem, challenge and impication. *Building and Environment*, *95*, 322–329. https://doi.org/10.1016/j.buildenv.2015.07.015

M. Vollmer, K. -p. M. (2002). *Infrared Thermal Imaging: Fundamentals, Research and Applicagions. Wiley-VCH*. Weinheim, Germany: Wiley-VCH.

Ma, L., Li, M., Tong, L., Wang, Y., & Cheng, L. (2014). Using unmanned aerial vehicle for remote sensing application. *International Conference on Geoinformatics*. https://doi.org/10.1109/Geoinformatics.2013.6626078

Ma, W., Chen, R., & Kan, H. (2014). Temperature-related mortality in 17 large Chinese cities: How heat and cold affect mortality in China. *Environmental Research*, *134*, 127–133. https://doi.org/10.1016/j.envres.2014.07.007

Ma, W., Yang, C., Tan, J., Song, W., Chen, B., & Kan, H. (2012). Modifiers of the temperature-mortality association in Shanghai, China. *International Journal of Biometeorology*, *56*(1), 205–207. https://doi.org/10.1007/s00484-011-0406-9

Macpherson, R. K. (1973). Thermal stress and thermal comfort. *Ergonomics*, *16*(5), 611–623. https://doi.org/10.1080/00140137308924552

Madding, R. (2008). Finding R-values of Stud-Frame Constructed Houses with IR Thermography Finding R-Values of Stud Frame Constructed Houses with IR Thermography. In *Proceedings of InfraMation*. Reno, USA.

Madrigano, J., Mittleman, M. A., Baccarelli, A., Goldberg, R., Melly, S., Von Klot, S., & Schwartz, J. (2013).

Temperature, myocardial infarction, and mortality: Effect modification by individual-and area-level characteristics. *Epidemiology*, *24*(3), 439–446. https://doi.org/10.1097/EDE.0b013e3182878397

Magoulès, F., & Zhao, H.-X. (2016). *Data Mining and Machine Learning in Building Energy Analysis*. Wiley-ISTE.

Maller, C. J., & Strengers, Y. (2011). Housing, heat stress and health in a changing climate: Promoting the adaptive capacity of vulnerable households, a suggested way forward. *Health Promotion International*, *26*(4), 492–498. https://doi.org/10.1093/heapro/dar003

Maltais, D., Wilk, B., Unnithan, V., & Bar-Or, O. (2004). Responses of children with cerebral palsy to treadmill walking exercise in the heat. *Medicine and Science in Sports and Exercise*, *36*(10), 1674–1681. https://doi.org/10.1249/01.MSS.0000142312.43629.D8

Maragno, D., Fontana, M. D., & Musco, F. (2020). Mapping heat stress vulnerability and risk assessment at the neighborhood scale to drive Urban adaptation planning. *Sustainability (Switzerland)*, *12*(3). https://doi.org/10.3390/su12031056

Martiello, M. A., & Giacchi, M. V. (2010). Review Article: High temperatures and health outcomes: A review of the literature. *Scandinavian Journal of Public Health*, *38*(8), 826–837. https://doi.org/10.1177/1403494810377685

Martin-Latry, K., Goumy, M. P., Latry, P., Gabinski, C., Bégaud, B., Faure, I., & Verdoux, H. (2007). Psychotropic drugs use and risk of heat-related hospitalisation. *European Psychiatry*, *22*(6), 335–338. https://doi.org/10.1016/j.eurpsy.2007.03.007

Martinez, M., Devenport, L., Saussy, J., & Martinez, J. (2020). Drug-associated heat stroke, *95*(8), 2–3.

Massachusetts Institute of Technology. (2019). Capital Projects, 1–67.

Mateo-Garcia, M., Ahmed, A., & McGough, D. (2017). Non-invasive approaches for low-energy retrofit of buildings: Implementation, monitoring and simulation in a living lab case study. *WIT Transactions on the Built Environment*, *171*(August), 183–193. https://doi.org/10.2495/STR170161

Mateo, F., Carrasco, J. J., Sellami, A., Millán-Giraldo, M., Domínguez, M., & Soria-Olivas, E. (2013). Machine learning methods to forecast temperature in buildings. *Expert Systems with Applications*, *40*(4), 1061–1068. https://doi.org/10.1016/j.eswa.2012.08.030

Matthews, T. (2017). "Canyon Effect" in Australian cities. *PolicyInnoHub*, (September).

Matzarakis, A., Muthers, S., & Rutz, F. (2014). Application and comparison of UTCI and pet in temperate climate conditions. *Finisterra*, *49*(98), 21–31. https://doi.org/10.18055/Finis6453

Mauriello, M. L., Norooz, L., & Froehlich, J. E. (2015). Understanding the role of thermography in energy auditing: Current practices and the potential for automated solutions. *Conference on Human Factors in Computing Systems - Proceedings*, *2015-April*, 1993–2002. https://doi.org/10.1145/2702123.2702528

Mavrogianni, A., Davies, M., Wilkinson, P., & Pathan, A. (2010a). London Housing and Climate Change : Impact on Comfort and Health - Preliminary Results of a Summer Overheating Study. *Open House International*, *35*(2).

Mavrogianni, A., Davies, M., Wilkinson, P., & Pathan, A. (2010b). London Housing and Climate Change: Impact on Comfort and Health. *Open House International*, *35*(2), 49–59. Retrieved from

www.infra.kth.se/BBAwww.bsu.edu/caphttp:w3.uniroma1.it/housinglabwww.bme.huhttp://portal.psz.utm.my/psz/

Mayrhuber, E. A. S., Dückers, M. L. A., Wallner, P., Arnberger, A., Allex, B., Wiesböck, L., … Kutalek, R. (2018). Vulnerability to heatwaves and implications for public health interventions – A scoping review. *Environmental Research*, *166*(10), 42–54. https://doi.org/10.1016/j.envres.2018.05.021

Mba, L., Meukam, P., & Kemajou, A. (2016). Application of artificial neural network for predicting hourly indoor air temperature and relative humidity in modern building in humid region. *Energy and Buildings*, *121*, 32–42. https://doi.org/10.1016/j.enbuild.2016.03.046

Mbokodo, I., Bopape, M. J., Chikoore, H., Engelbrecht, F., & Nethengwe, N. (2020). Heatwaves in the future warmer climate of South Africa. *Atmosphere*, *11*(7), 1–18. https://doi.org/10.3390/atmos11070712

McGeehin, M. A., & Mirabelli, M. (2001). The potential impacts of climate variability and change on temperature-related morbidity and mortality in the United States. *Environmental Health Perspectives*, *109*(SUPPL. 2), 185–189. https://doi.org/10.2307/3435008

McGill, G., Sharpe, T., Robertson, L., Gupta, R., & Mawditt, I. (2017). Meta-analysis of indoor temperatures in new-build housing. *Building Research and Information*, *45*(1–2), 19–39. https://doi.org/10.1080/09613218.2016.1226610

McGregor, G. R., & Vanos, J. K. (2018). Heat: a primer for public health researchers. *Public Health*, *161*(August), 138–146. https://doi.org/10.1016/j.puhe.2017.11.005

McMichael, A. J., Wilkinson, P., Kovats, R. S., Pattenden, S., Hajat, S., Armstrong, B., … Nikiforov, B. (2008). International study of temperature, heat and urban mortality: The "ISOTHURM" project. *International Journal of Epidemiology*, *37*(5), 1121–1131. https://doi.org/10.1093/ije/dyn086

McNeel. (2021). Rhinoceros version 6.0. Retrieved from https://www.rhino3d.com

Mechaqrane, A., & Zouak, M. (2004). A comparison of linear and neural network ARX models applied to a prediction of the indoor temperature of a building. *Neural Computing and Applications*, *13*(1), 32–37. https://doi.org/10.1007/s00521-004-0401-8

Medina-Ramón, M., & Schwartz, J. (2007). Temperature, temperature extremes, and mortality: A study of acclimatisation and effect modification in 50 US cities. *Occupational and Environmental Medicine*, *64*(12), 827–833. https://doi.org/10.1136/oem.2007.033175

Meerburg, B. G., Verhagen, A., Jongschaap, R. E. E., Franke, A. C., Schaap, B. F., Dueck, T. A., & Van Der Werf, A. (2009). Do nonlinear temperature effects indicate severe damages to US crop yields under climate change? *Proceedings of the National Academy of Sciences of the United States of America*, *106*(43), 15594–15598. https://doi.org/10.1073/pnas.0910618106

Mehnert, P., Bröde, P., & Griefahn, B. (2002). Gender-related difference in sweat loss and its impact on exposure limits to heat stress. *International Journal of Industrial Ergonomics*, *29*(6), 343–351. https://doi.org/10.1016/S0169-8141(02)00073-2

Merte, S. (2017). Estimating heat wave-related mortality in Europe using singular spectrum analysis. *Climatic Change*, *142*(3–4), 321–330. https://doi.org/10.1007/s10584-017-1937-9

Messina, G., Peña, J. M., Vizzari, M., & Modica, G. (2020). A comparison of UAV and satellites multispectral

imagery in monitoring onion crop. An application in the 'Cipolla Rossa di Tropea' (Italy). *Remote Sensing*, *12*(20), 1–27. https://doi.org/10.3390/rs12203424

Metzger, K. B., Ito, K., & Matte, T. D. (2010). Summer heat and mortality in New York City: How hot is too hot? *Environmental Health Perspectives*, *118*(1), 80–86. https://doi.org/10.1289/ehp.0900906

Michelozzi, P., de Donato, F., Bisanti, L., Russo, A., Cadum, E., DeMaria, M., … Perucci, C. A. (2005). The impact of the summer 2003 heat waves on mortality in four Italian cities. *Euro Surveillance : Bulletin Européen Sur Les Maladies Transmissibles = European Communicable Disease Bulletin*, *10*(7), 161–165. https://doi.org/10.2807/esm.10.07.00556-en

Minson, C. T., Wladkowski, S. L., Cardell, A. F., Pawelczyk, J. A., & Kenney, W. L. (1998). Age alters the cardiovascular response to direct passive heating. *Journal of Applied Physiology*, *84*(4), 1323–1332. https://doi.org/10.1152/jappl.1998.84.4.1323

Mora, C., Dousset, B., Caldwell, I. R., Powell, F. E., Geronimo, R. C., Bielecki, C. R., … Trauernicht, C. (2017a). Global risk of deadly heat. *Nature Climate Change*, *7*(7), 501–506. https://doi.org/10.1038/nclimate3322

Mora, C., Dousset, B., Caldwell, I. R., Powell, F. E., Geronimo, R. C., Bielecki, C. R., … Trauernicht, C. (2017b). Global risk of deadly heat. *Nature Climate Change*, *7*(7), 501–506. https://doi.org/10.1038/nclimate3322

Moradzadeh, A., & Pourhossein, K. (2019). Early Detection of Turn-to-Turn Faults in Power Transformer Winding: An Experimental Study. *Proceedings 2019 International Aegean Conference on Electrical Machines and Power Electronics, ACEMP 2019 and 2019 International Conference on Optimization of Electrical and Electronic Equipment, OPTIM 2019*, 199–204. https://doi.org/10.1109/ACEMP-OPTIM44294.2019.9007169

Morini, E., Touchaei, A. G., Castellani, B., Rossi, F., & Cotana, F. (2016). The impact of albedo increase to mitigate the urban heat island in Terni (Italy) using the WRF model. *Sustainability (Switzerland)*, *8*(10), 1–14. https://doi.org/10.3390/su8100999

Morley, M. (2017). Investigating the use of earth tubes for passive cooling and ventilation through thermal modelling, (June).

Muntaner, C., Lynch, J., & Smith, G. D. (2007). Social capital and the third way in public health. *Critical Perspectives in Public Health*, 35–46. https://doi.org/10.4324/9780203938980

Mustafaraj, G., Chen, J., & Lowry, G. (2010). Thermal behaviour prediction utilizing artificial neural networks for an open office. *Applied Mathematical Modelling*, *34*(11), 3216–3230. https://doi.org/10.1016/j.apm.2010.02.014

Muzet, A., Ehrhart, J., Candas, V., Libert, J. P., & Vogt, J. J. (1983). Rem sleep and ambient temperature in man. *International Journal of Neuroscience*, *18*(1–2), 117–125. https://doi.org/10.3109/00207458308985885

N. Lacetera, U. Bernabucci, H.H. Khalifa, B. R. and A. N. (2003). *Interactions between climate and animal production* (EAAP Techn). Wageningen Academic.

Nagpal, S., Mueller, C., Aijazi, A., & Reinhart, C. F. (2019). A methodology for auto-calibrating urban building energy models using surrogate modeling techniques. *Journal of Building Performance Simulation*, *12*(1), 1–16. https://doi.org/10.1080/19401493.2018.1457722

Nahlik, M. J., Chester, M. V., Pincetl, S. S., Eisenman, D., Sivaraman, D., & English, P. (2017). Building Thermal Performance, Extreme Heat, and Climate Change. *Journal of Infrastructure Systems*, *23*(3), 04016043. https://doi.org/10.1061/(asce)is.1943-555x.0000349

Nasser, I. M., & Abu-Naser, S. S. (2019). Predicting Tumor Category Using Artificial Neural Networks. *International Journal of Academic Health and Medical Research*, *3*(2), 1–7. Retrieved from www.ijeais.org/ijahmr

Nastos, P. T., & Matzarakis, A. (2012). The effect of air temperature and human thermal indices on mortality in Athens, Greece. *Theoretical and Applied Climatology*, *108*(3–4), 591–599. https://doi.org/10.1007/s00704-011-0555-0

National Renewable Energy Laboratory (NREL). (2012). *Building America Residential System Research Results: Achieving 30% Whole House Energy Savings Level in Hot-Dry and Mixed-Dry Climates Building Technologies Program*.

Naughton, M. P., Henderson, A., Mirabelli, M. C., Kaiser, R., & Wilhelm, J. L. (2002). Heat-Related Mortality during a 1999 Hea Wave in Chicago. *American Journal of Preventive Medicine*, *22*(4), 221–227. https://doi.org/10.1080/10643389.2012.728825

Naughton, M. P., Henderson, A., Mirabelli, M. C., Kaiser, R., Wilhelm, J. L., Kieszak, S. M., … McGeehin, M. A. (2002). Heat-related mortality during a 1999 heat wave in Chicago. *American Journal of Preventive Medicine*, *22*(4), 221–227. https://doi.org/10.1016/S0749-3797(02)00421-X

Németh, Á. (2011). Changing Thermal Bioclimate in Some Hungarian Cities, (January 2011), 93–101.

Neto, A. H., & Fiorelli, F. A. S. (2008). Comparison between detailed model simulation and artificial neural network for forecasting building energy consumption. *Energy and Buildings*, *40*(12), 2169–2176. https://doi.org/10.1016/j.enbuild.2008.06.013

New York City Department of Health and Mental Hygiene. (2021). *Community Health Improvement Plan: Take Care New York 2024*. Retrieved from www.nyc.gov/health

Nicholls, N., Skinner, C., Loughnan, M., & Tapper, N. (2008). A simple heat alert system for Melbourne, Australia. *International Journal of Biometeorology*, *52*(5), 375–384. https://doi.org/10.1007/s00484-007-0132-5

Nicol, J. F., & Humphreys, M. A. (2002). Adaptive thermal comfort and sustainable thermal standards for buildings, *34*, 563–572.

Nitschke, M., Hansen, A., Bi, P., Pisaniello, D., Newbury, J., Kitson, A., … Dal Grande, E. (2013). Risk factors, health effects and Behaviour in older people during extreme heat: A survey in South Australia. *International Journal of Environmental Research and Public Health*, *10*(12), 6721–6733. https://doi.org/10.3390/ijerph10126721

Nordon, C., Martin-Latry, K., De Roquefeuil, L., Latry, P., Bégaud, B., Falissard, B., … Verdoux, H. (2009). Risk of death related to psychotropic drug use in older people during the european 2003 heatwave: A population-based case-control study. *American Journal of Geriatric Psychiatry*, *17*(12), 1059–1067. https://doi.org/10.1097/JGP.0b013e3181b7ef6e

NWS. (2019). Weather Related Fatality and Injury Statistics. *National Weather Service*, 2020. Retrieved from https://www.weather.gov/hazstat/

NY Start Smart. (2021). Fact Sheets – Start SMART New York. Retrieved May 12, 2021, from http://smart-ny.com/resources/fact-sheets/

NYCHA. (2018). *Data for Savings Opportunities Turning Data Into Action*.

O'Grady, M., Lechowska, A. A., & Harte, A. M. (2017). Quantification of heat losses through building envelope thermal bridges influenced by wind velocity using the outdoor infrared thermography technique. *Applied Energy*, *208*(April), 1038–1052. https://doi.org/10.1016/j.apenergy.2017.09.047

O'Neill, M. S., Zanobetti, A., & Schwartz, J. (2003). Modifiers of the temperature and mortality association in seven US cities. *American Journal of Epidemiology*, *157*(12), 1074–1082. https://doi.org/10.1093/aje/kwg096

O'Neill, M. S., Zanobetti, A., & Schwartz, J. (2005). Disparities by race in heat-related mortality in four US cities: The role of air conditioning prevalence. *Journal of Urban Health*, *82*(2), 191–197. https://doi.org/10.1093/jurban/jti043

Ogunlade Davidson, E. (2014). Summary for Policymakers Summary for Policymakers. *International Panel on Climate Change*, (April 2007), 1–161. Retrieved from http://ebooks.cambridge.org/ref/id/CBO9781107415416A011

Önder, S., & Akay, A. (2014). The Roles of Plants on Mitigating the Urban Heat Islands' Negative Effects. *International Journal of Agriculture and Economic Development*, *2*(2), 18–32.

Oniga, E., Breaban, A., & Statescu, F. (2018).   Determining the optimum number of ground control points for obtaining high precision results based on UAS images, 5165. https://doi.org/10.3390/ecrs-2-05165

Oppenheimer, M., Campos, M., Warren, R., Birkmann, J., Luber, G., O'Neill, B., & Takahashi, K. (2014). Emergent Risks and Key Vulnerabilities. *Climate Change 2014: Impacts, Adaptation, and Vulnerability. Part A: Global and Sectoral Aspects. Contribution of Working Group II to the Fifth Assessment Report of the Intergovernmental Panel on Climate Change*, 1039–1099.

Ormandy, D., & Ezratty, V. (2012). Health and thermal comfort: From WHO guidance to housing strategies. *Energy Policy*, *49*, 116–121. https://doi.org/10.1016/j.enpol.2011.09.003

Ortiz-Sanz, J., Gil-Docampo, M., Arza-García, M., & Cañas-Guerrero, I. (2019). IR thermography from UAVs to monitor thermal anomalies in the envelopes of traditional wine cellars: Field test. *Remote Sensing*, *11*(12). https://doi.org/10.3390/rs11121424

Ortiz, L. E., Gonzalez, J. E., Wu, W., Schoonen, M., Tongue, J., & Bornstein, R. (2018). New York City impacts on a regional heat wave. *Journal of Applied Meteorology and Climatology*, *57*(4), 837–851. https://doi.org/10.1175/JAMC-D-17-0125.1

Oudin Åström, D., Bertil, F., & Joacim, R. (2011). Heat wave impact on morbidity and mortality in the elderly population: A review of recent studies. *Maturitas*, *69*(2), 99–105. https://doi.org/10.1016/j.maturitas.2011.03.008

Palatini, P., & Julius, S. (1999). The physiological determinants and risk correlations of elevated heart rate. *American Journal of Hypertension*, *12*(1 SUPPL. 1), 3S-8S. https://doi.org/10.1016/S0895-7061(98)00207-6

Palme, M., Carrasco, C., Ángel Gálvez, M., & Inostroza, L. (2017). Natural Ventilation: A Mitigation Strategy

to Reduce Overheating in Buildings under Urban Heat Island Effect in South American Cities. *IOP Conference Series: Materials Science and Engineering*, *245*(7). https://doi.org/10.1088/1757-899X/245/7/072046

Palmer, J., Bennetts, H., Pullen, S., Zuo, J., Ma, T., & Chileshe, N. (2014). Adaptation of Australian houses and households to future heat waves. *7th Australasian Housing Researchers' Conference, AHRC 2013: Refereed Proceedings*, (October 2014).

Pan, M., Linner, T., Pan, W., Cheng, H., & Bock, T. (2020). Structuring the context for construction robot development through integrated scenario approach. *Automation in Construction*, *114*(March), 103174. https://doi.org/10.1016/j.autcon.2020.103174

Papadopoulos, A. M. (2016). Forty years of regulations on the thermal performance of the building envelope in Europe: Achievements, perspectives and challenges. *Energy and Buildings*, *127*(2016), 942–952. https://doi.org/10.1016/j.enbuild.2016.06.051

Parsons, & Kenneth, C. (2011). Assessment of Heat Stress and Heat Stress Indices. In *Encyclopedia of Occupational Health and Safety* (pp. 1–12). Geneva, Switzerland: International Labor Organization.

Pascal, M., Le Tertre, A., & Saoudi, A. (2012). Quantification of the heat wave effect on mortality in nine French cities during summer 2006. *PLoS Currents*. https://doi.org/10.1371/currents.RRN1307

Patz, J. A., McGeehin, M. A., Bernard, S. M., Ebi, K. L., Epstein, P. R., Grambsch, A., … Trtanj, J. (2001). The potential health impacts of climate variability and change for the United States: Executive summary of the report of the health sector of the U.S. National Assessment. *Journal of Environmental Health*, *64*(2), 20–28. https://doi.org/10.2307/3454357

Pearson, C. (2011). *Thermal Imaging of Building Fabric*. BSRIA.

Peer, N., Lombard, C., Steyn, K., & Levitt, N. (2020). Elevated resting heart rate is associated with several cardiovascular disease risk factors in urban-dwelling black South Africans. *Scientific Reports*, *10*(1), 1–8. https://doi.org/10.1038/s41598-020-61502-4

Pelling, M. (2011). *Adaptation to Climate Change: From resilience to transformation*. Routledge.

Pengelly, L. D., Campbell, M. E., Cheng, C. S., Fu, C., Gingrich, S. E., & Macfarlane, R. (2007). Anatomy of heat waves and mortality in Toronto: Lessons for public health protection. *Canadian Journal of Public Health*, *98*(5), 364–368. https://doi.org/10.1007/bf03405420

Perkins-Kirkpatrick, S. E., & Gibson, P. B. (2017). Changes in regional heatwave characteristics as a function of increasing global temperature. *Scientific Reports*, *7*(1), 1–12. https://doi.org/10.1038/s41598-017-12520-2

Perkins, S. E., Alexander, L. V., & Nairn, J. R. (2012). Increasing frequency, intensity and duration of observed global heatwaves and warm spells. *Geophysical Research Letters*, *39*(20), 1–5. https://doi.org/10.1029/2012GL053361

Phil, D. A. M. (2005). Dwelling temperatures and comfort during the August 2003 heat wave, *4*(August 2003).

Pillai, S. K., Noe, R. S., Murphy, M. W., Vaidyanathan, A., Young, R., Kieszak, S., … Wolkin, A. F. (2014). Heat illness: Predictors of hospital admissions among emergency department visits - Georgia, 2002-2008. *Journal of Community Health*, *39*(1), 90–98. https://doi.org/10.1007/s10900-013-9743-4

PIX4D. (2020). Image acquisition. https://doi.org/10.4324/9780080477275-10

Prezant, D. J., Clair, J., Belyaev, S., Alleyne, D., Banauch, G. I., Davitt, M., … Kalkut, G. (2005). Effects of the August 2003 blackout on the New York City healthcare delivery system: A lesson for disaster preparedness. *Critical Care Medicine*, *33*(1 SUPPL.), 1–3. https://doi.org/10.1097/01.CCM.0000150956.90030.23

Pyrgou, A., Castaldo, V. L., Pisello, A. L., Cotana, F., & Santamouris, M. (2017). On the effect of summer heatwaves and urban overheating on building thermal-energy performance in central Italy. *Sustainable Cities and Society*, *28*(January), 187–200. https://doi.org/10.1016/j.scs.2016.09.012

Quinn, A., Tamerius, J. D., Perzanowski, M., Jacobson, J. S., Goldstein, I., Acosta, L., & Shaman, J. (2014). Predicting indoor heat exposure risk during extreme heat events. *Science of the Total Environment*, *490*(August), 686–693. https://doi.org/10.1016/j.scitotenv.2014.05.039

Rahmani, K., & Mayer, H. (2018). High Quality Facade Segmentation Based On Structured Random Forest, Region Proposal Network And Rectangular Fitting. *ISPRS Annals of the Photogrammetry, Remote Sensing and Spatial Information Sciences*, *4*(2), 223–230. https://doi.org/10.5194/isprs-annals-IV-2-223-2018

Rakha, T., & Gorodetsky, A. (2018a). Review of Unmanned Aerial System (UAS) applications in the built environment: Towards automated building inspection procedures using drones. *Automation in Construction*, *93*(January), 252–264. https://doi.org/10.1016/j.autcon.2018.05.002

Rakha, T., & Gorodetsky, A. (2018b). Review of Unmanned Aerial System (UAS) applications in the built environment: Towards automated building inspection procedures using drones. *Automation in Construction*, *93*(September), 252–264. https://doi.org/10.1016/j.autcon.2018.05.002

Rakha, T., Liberty, A., Gorodetsky, A., Kakillioglu, B., & Velipasalar, S. (2018). Heat Mapping Drones: An Autonomous Computer-Vision-Based Procedure for Building Envelope Inspection Using Unmanned Aerial Systems (UAS). *Technology|Architecture + Design*, *2*(1), 30–44. https://doi.org/10.1080/24751448.2018.1420963

Ramamurthy, P., González, J., Ortiz, L., Arend, M., & Moshary, F. (2017). Impact of heatwave on a megacity: An observational analysis of New York City during July 2016. *Environmental Research Letters*, *12*(5). https://doi.org/10.1088/1748-9326/aa6e59

Ramírez, N., & El Habashi, A. (2020). reGREENeration of Historic Cairo. Hara al-Nabawiya and Bayt Madkour in al-Darb Al-Ahmar. *The Journal of Public Space*, *5*(Vol. 5 n. 1), 51–74. https://doi.org/10.32891/jps.v5i1.1251

Ramsey, J. D. (1995). Task performance in heat: A review. *Ergonomics*. https://doi.org/10.1080/00140139508925092

Ramsey, J. D., & Chai, C. P. (1983). Inherent variability in heat-stress decision rules. *Ergonomics*, *26*(5), 495–504. https://doi.org/https://doi.org/10.1080/00140138308963365

Rayward-Smith, V. J., Cormen, T. H., Leiserson, C. E., & Rivest, R. L. (1991). *Introduction to Algorithms*. *The Journal of the Operational Research Society* (Vol. 42). https://doi.org/10.2307/2583667

Reckien, D., Wildenberg, M., & Bachhofer, M. (2013). Subjective realities of climate change: How mental maps of impacts deliver socially sensible adaptation options. *Sustainability Science*, *8*(2), 159–172. https://doi.org/10.1007/s11625-012-0179-z

Reddy, T. A., & Maor., I. (2006). Procedures for Reconciling Computer-Calculated Results With Measured Energy Data. *ASHRAE Research Project 1051- RP*, (iii). Retrieved from http://www.eeperformance.org/uploads/8/6/5/0/8650231/ashrae_rp1051.pdf

Redmon, J., Divvala, S., Girshick, R., & Farhadi, A. (2016). You only look once: Unified, real-time object detection. *Proceedings of the IEEE Computer Society Conference on Computer Vision and Pattern Recognition*, *2016-Decem*, 779–788. https://doi.org/10.1109/CVPR.2016.91

Redmon, J., & Farhadi, A. (2018). YOLOv3: An Incremental Improvement. Retrieved from http://arxiv.org/abs/1804.02767

Reid, C. E., O'Neill, M. S., Gronlund, C. J., Brines, S. J., Brown, D. G., Diez-Roux, A. V., & Schwartz, J. (2009). Mapping community determinants of heat vulnerability. *Environmental Health Perspectives*, *117*(11), 1730–1736. https://doi.org/10.1289/ehp.0900683

Reinhart, C. F., Dogan, T., Jakubiec, J. A., Rakha, T., & Sang, A. (2013). UMI - An Urban Simulation Environment for Building Energy Use, Daylighting and Walkability. In *13th Conference of International Building Performance Simulation Association* (pp. 79–82). Chambery. France. https://doi.org/10.1016/bs.pbr.2015.01.004

Ren, C., O'Neill, M. S., Park, S. K., Sparrow, D., Vokonas, P., & Schwartz, J. (2011). Ambient temperature, air pollution, and heart rate variability in an aging population. *American Journal of Epidemiology*, *173*(9), 1013–1021. https://doi.org/10.1093/aje/kwq477

Reuters. (2014). Preventing summer blackouts in Egypt is " impossible " -minister. Retrieved March 2, 2020, from https://www.reuters.com/article/egypt-energy/preventing-summer-blackouts-in-egypt-is-impossible-minister-idUSL6N0N407L20140412?feedType=RSS&feedName=utilitiesSector

Rinner, C., Patychuk, D., Bassil, K., Nasr, S., Gower, S., & Campbell, M. (2010). The role of maps in neighborhood-level heat vulnerability assessment for the city of toronto. *Cartography and Geographic Information Science*, *37*(1), 31–44. https://doi.org/10.1559/152304010790588089

Roaf, S., & Nicol, F. (2017). Running buildings on natural energy: design thinking for a different future. *Architectural Science Review*, *60*(3), 145–149. https://doi.org/10.1080/00038628.2017.1303924

Robaa, S. M. (2013). Some aspects of the urban climates of Greater Cairo Region, Egypt. *International Journal of Climatology*, *33*(15), 3206–3216. https://doi.org/10.1002/joc.3661

Robine, J. M., Cheung, S. L. K., Le Roy, S., Van Oyen, H., Griffiths, C., Michel, J. P., & Herrmann, F. R. (2008). Death toll exceeded 70,000 in Europe during the summer of 2003. *Comptes Rendus - Biologies*, *331*(2), 171–178. https://doi.org/10.1016/j.crvi.2007.12.001

Robinson, C., Dilkina, B., Hubbs, J., Zhang, W., Guhathakurta, S., Brown, M. A., & Pendyala, R. M. (2017). Machine learning approaches for estimating commercial building energy consumption. *Applied Energy*, *208*(September), 889–904. https://doi.org/10.1016/j.apenergy.2017.09.060

Rohat, G., Flacke, J., Dosio, A., Pedde, S., Dao, H., & van Maarseveen, M. (2019). Influence of changes in socioeconomic and climatic conditions on future heat-related health challenges in Europe. *Global and Planetary Change*, *172*(February 2018), 45–59. https://doi.org/10.1016/j.gloplacha.2018.09.013

Romero-Lankao, P., Qin, H., & Dickinson, K. (2012). Urban vulnerability to temperature-related hazards: A meta-analysis and meta-knowledge approach. *Global Environmental Change*, *22*(3), 670–683.

https://doi.org/10.1016/j.gloenvcha.2012.04.002

Romero Lankao, P., & Qin, H. (2011). Conceptualizing urban vulnerability to global climate and environmental change. *Current Opinion in Environmental Sustainability*, *3*(3), 142–149. https://doi.org/10.1016/j.cosust.2010.12.016

Ruiz, J. M., Steffen, P., & Smith, T. B. (2013). Hispanic mortality paradox: A systematic review and meta-analysis of the longitudinal literature. *American Journal of Public Health*, *103*(3), 10–11. https://doi.org/10.2105/AJPH.2012.301103

Saez, M., Sunyer, J., Castellsagué, J., Murillo, C., & Antó, J. M. (1995). Relationship between weather temperature and mortality: A time series analysis approach in Barcelona. *International Journal of Epidemiology*, *24*(3), 576–582. https://doi.org/10.1093/ije/24.3.576

Sailor, D. J., Baniassadi, A., O'Lenick, C. R., & Wilhelmi, O. V. (2019). The growing threat of heat disasters. *Environmental Research Letters*, *14*(5). https://doi.org/10.1088/1748-9326/ab0bb9

Sajjadian, S. M., Lewis, J., & Sharples, S. (2015). The potential of phase change materials to reduce domestic cooling energy loads for current and future UK climates. *Energy and Buildings*, *93*(2015), 83–89. https://doi.org/10.1016/j.enbuild.2015.02.029

Sakka, A., Santamouris, M., Livada, I., Nicol, F., & Wilson, M. (2012). On the thermal performance of low income housing during heat waves. *Energy and Buildings*, *49*, 69–77. https://doi.org/10.1016/j.enbuild.2012.01.023

Salata, F., Golasi, I., Petitti, D., de Lieto Vollaro, E., Coppi, M., & de Lieto Vollaro, A. (2017). Relating microclimate, human thermal comfort and health during heat waves: An analysis of heat island mitigation strategies through a case study in an urban outdoor environment. *Sustainable Cities and Society*, *30*(April), 79–96. https://doi.org/10.1016/j.scs.2017.01.006

Sampson, N. R., Gronlund, C. J., Buxton, M. A., Catalano, L., White-Newsome, J. L., Conlon, K. C., … Parker, E. A. (2013). Staying cool in a changing climate: Reaching vulnerable populations during heat events. *Global Environmental Change*, *23*(2), 475–484. https://doi.org/10.1016/j.gloenvcha.2012.12.011

Santamouris, M., Haddad, S., Saliari, M., Vasilakopoulou, K., Synnefa, A., Paolini, R., … Fiorito, F. (2018). On the energy impact of urban heat island in Sydney: Climate and energy potential of mitigation technologies. *Energy and Buildings*, *166*, 154–164. https://doi.org/10.1016/j.enbuild.2018.02.007

Saulles, T. de. (2009). *Thermal Mass Explained*. *Wookware*. Retrieved from http://wookware.org/files/MB_Thermal_Mass_Explained_Feb09.pdf

Schlader, Z. J., Wilson, T. E., & Crandall, C. G. (2015). Mechanisms of Orthostatic Intolerance During Heat Stress. *Neuroscience*, *196*, 37–46.

Schwartz, J. (2005). Who is sensitive to extremes of temperature? A case-only analysis. *Epidemiology*, *16*(1), 67–72. https://doi.org/10.1097/01.ede.0000147114.25957.71

Schwoegler, M. (2006). *Infrared Thermography Basics*. Stockholm.

Seghier, T. E., Lim, Y. W., Ahmad, M. H., & Samuel, W. O. (2017). Building Envelope Thermal Performance Assessment Using Visual Programming and BIM, based on ETTV requirement of Green Mark and GreenRE. *International Journal of Built Environment and Sustainability*, *4*(3), 227–235. https://doi.org/10.11113/ijbes.v4.n3.216

Semenza;, J. C., Rubin, C. H., Falter, K. H., Selanikio, J. D., Flanders, D., Howe, H. L., & Wilhelm, J. L. (1996). Heat-Related Deaths During The July 1995 Heat Wave In Chicago. *New England Journal of Medicine*, (July 1995).

Semenza, J. C. (1996). Heat-Related Deaths during the July 1995 Heat Wave in Chicago. *Environmental Health*, (July 1995).

Semenza, J. C., McCullough, J. E., Flanders, W. D., McGeehin, M. A., & Lumpkin, J. R. (1999). Excess hospital admissions during the July 1995 heat wave in Chicago. *American Journal of Preventive Medicine*, *16*(4), 269–277. https://doi.org/10.1016/S0749-3797(99)00025-2

Semenza, J. C., Rubin, C. H., Falter, K. H., Selanikio, J. D., Flanders, D., Howe, H. L., & Wilhelm, J. L. (1996a). Heat-Related Deaths During the July 1995 Heatwave in Chicago. *The New England Journal of Medicine*.

Semenza, J. C., Rubin, C. H., Falter, K. H., Selanikio, J. D., Flanders, W. D., Howe, H. L., & Wilhelm, J. L. (1996b). Heat-Related Deaths during the July 1995 Heat Wave in Chicago. *New England Journal of Medicine*, *335*(2), 84–90. https://doi.org/10.1056/nejm199607113350203

Sen, J., & Nag, P. K. (2019). Effectiveness of human-thermal indices: Spatio–temporal trend of human warmth in tropical India. *Urban Climate*, *27*(February 2018), 351–371. https://doi.org/10.1016/j.uclim.2018.11.009

Seo, D. K., & Eo, Y. D. (2019). Multilayer perceptron-based phenological and radiometric normalization for high-resolution satellite imagery. *Applied Sciences (Switzerland)*, *9*(21). https://doi.org/10.3390/app9214543

Seth H. Holmes, T. P. & A. W. (2016). Overheating and passive habitability: indoor health and heat indices. *Building Research & Information*, *44*(1), 1–19. https://doi.org/10.1080/09613218.2015.1033875

Seyedzadeh, S., Rahimian, F. P., Glesk, I., & Roper, M. (2018). Machine learning for estimation of building energy consumption and performance: a review. *Visualization in Engineering*, *6*(1). https://doi.org/10.1186/s40327-018-0064-7

Shaikh, N. R. (2013). Smoothing of a Noisy Image Using Different Low Pass Filters. *International Journal of Computer Science Trends and Technology (IJCST)*, *5*(2), 261–264. Retrieved from www.ijcstjournal.org

Shapiro, I. (2009). Energy audits in large commercial office buildings. *ASHRAE Journal*, *51*(1), 1–7.

Sharma, H. S. (2007). Methods to produce hyperthermia-induced brain dysfunction. *Progress in Brain Research*, *162*(06), 173–199. https://doi.org/10.1016/S0079-6123(06)62010-4

Sharma, J., Murthy, I. K., Esteves, T., Negi, P., S, S., Dasgupta, S., … Ravindranath, N. H. (2016). *Climate Vulnerability and Risk Assessment: Framework, Methods and Guidelines*. *Indian Himalayas Climate Adaptation*. Retrieved from http://www.ghbook.ir/index.php?name=فرهنگ و رسانه های نوین&option=com_dbook&task=readonline&book_id=13650&page=73&chkhashk=ED9C9491B4&Itemid=218&lang=fa&tmpl=component

Shen, T., Howe, H. L., Alo, C., & Moolenaar, R. L. (1998). Toward a broader definition of heat-related death: Comparison of mortality estimates from medical examiners' classification with those from total death differentials during the July 1995 heat wave in Chicago, Illinois. *American Journal of Forensic Medicine and Pathology*, *19*(2), 113–118. https://doi.org/10.1097/00000433-199806000-00003

Sheridan, S. C. (2007). A survey of public perception and response to heat warnings across four North American cities: An evaluation of municipal effectiveness. *International Journal of Biometeorology*, *52*(1), 3–15. https://doi.org/10.1007/s00484-006-0052-9

Sherwood, S. C., & Huber, M. (2010). An adaptability limit to climate change due to heat stress. *Proceedings of the National Academy of Sciences of the United States of America*, *107*(21), 9552–9555. https://doi.org/10.1073/pnas.0913352107

Silvela, J., & Portillo, J. (2001). Breadth-first search and its application to image processing problems. *IEEE Transactions on Image Processing*, *10*(8), 1194–1199. https://doi.org/10.1109/83.935035

Simister, J., & Cooper, C. (2005). Thermal stress in the U.S.A.: Effects on violence and on employee behaviour. *Stress and Health*, *21*(1), 3–15. https://doi.org/10.1016/j.gmhc.2013.04.007

Singaravel, S., Suykens, J., & Geyer, P. (2018). Deep-learning neural-network architectures and methods: Using component-based models in building-design energy prediction. *Advanced Engineering Informatics*, *38*(June), 81–90. https://doi.org/10.1016/j.aei.2018.06.004

Slobodan, S. P., & Simonović, P. S. (2012). *Understanding City Resilience through through System Dynamics Simulation*.

Smargiassi, A., Goldberg, M. S., Plante, C., Fournier, M., Baudouin, Y., & Kosatsky, T. (2009). Variation of daily warm season mortality as a function of micro-urban heat islands. *Journal of Epidemiology and Community Health*, *63*(8), 659–664. https://doi.org/10.1136/jech.2008.078147

Smargiassi, Audrey, Fournier, M., Griot, C., Baudouin, Y., & Kosatsky, T. (2008). Prediction of the indoor temperatures of an urban area with an in-time regression mapping approach. *Journal of Exposure Science and Environmental Epidemiology*, *18*(3), 282–288. https://doi.org/10.1038/sj.jes.7500588

Snell, J., Spring, R., & Montpelier, V. (2008). *Testing Building Envelope Systems Using Infrared Thermography*. *The Snells Group*. Retrieved from http://www.cebq.org/documents/Infraredthermographyforbuildingenvelopes.pdf

SODA SRD. (2020). Maps of Irradiation - Africa. Retrieved from http://www.soda-is.com/eng/map/maps_for_free.html#pvgis-africa

Spengler, J. D. (2012). Climate change, indoor environments, and health. *Indoor Air*, *22*(2), 89–95. https://doi.org/10.1111/j.1600-0668.2012.00768.x

Stafoggia, M., Forastiere, F., Agostini, D., Biggeri, A., Bisanti, L., Cadum, E., … Perucci, C. A. (2006). Vulnerability to heat-related mortality: A multicity, population-based, case-crossover analysis. *Epidemiology*, *17*(3), 315–323. https://doi.org/10.1097/01.ede.0000208477.36665.34

Stagrum, A. E., Andenæs, E., Kvande, T., & Lohne, J. (2020). Climate change adaptation measures for buildings-A scoping review. *Sustainability (Switzerland)*, *12*(5). https://doi.org/10.3390/su12051721

Stapleton, J. M., Larose, J., Simpson, C., Flouris, A. D., Sigal, R. J., & Kenny, G. P. (2014). Do older adults experience greater thermal strain during heat waves? *Applied Physiology, Nutrition and Metabolism*, *39*(3), 292–298. https://doi.org/10.1139/apnm-2013-0317

Stazi, F. (2017). Thermal Inertia in Energy Efficient Building Envelopes. *Thermal Inertia in Energy Efficient Building Envelopes*, 1–358. https://doi.org/10.1016/C2016-0-00641-1

Stepanić, J., & Lesičar, J. Ć. (2019). Prospective Configurations Of Optical Systems For Smart Remote Visual

Testing Conducted With The Unmanned Aerial Vehicles. *International Journal of Advanced Research and …*, *3*(3), 147–152. Retrieved from http://www.ijarp.org/published-research-papers/mar2019/Prospective-Configurations-Of-Optical-Systems-For-Smart-Remote-Visual-Testing-Conducted-With-The-Unmanned-Aerial-Vehicles.pdf

Stone, J. (2012). The City and the Coming Climate. *The City and the Coming Climate*, 5–6. https://doi.org/10.1017/cbo9781139061353

Streutker, D. R. (2003). Satellite-measured growth of the urban heat island of Houston, Texas. *Remote Sensing of Environment*, *85*(3), 282–289. https://doi.org/10.1016/S0034-4257(03)00007-5

Sun, J. G. (2006). Analysis of Pulsed Thermography Methods for Defect Depth Prediction. *Journal of Heat Transfer*, *128*(4), 329. https://doi.org/10.1115/1.2165211

Taylor, J., Wilkinson, P., Davies, M., Armstrong, B., Chalabi, Z., Mavrogianni, A., … Bohnenstengel, S. I. (2015). Mapping the effects of urban heat island, housing, and age on excess heat-related mortality in London. *Urban Climate*, *14*(December), 517–528. https://doi.org/10.1016/j.uclim.2015.08.001

Taylor, N. A. S. (2006). Ethnic differences in thermoregulation: Genotypic versus phenotypic heat adaptation. *Journal of Thermal Biology*, *31*(1-2 SPEC. ISS.), 90–104. https://doi.org/10.1016/j.jtherbio.2005.11.007

Taylor, N. A. S. (2014). Human heat adaptation. *Comprehensive Physiology*, *4*(1), 325–365. https://doi.org/10.1002/cphy.c130022

Teboul, O., Simon, L., Koutsourakis, P., & Paragios, N. (2010). Segmentation of building facades using procedural shape priors. *Proceedings of the IEEE Computer Society Conference on Computer Vision and Pattern Recognition*, 3105–3112. https://doi.org/10.1109/CVPR.2010.5540068

Tejedor, B., Casals, M., & Gangolells, M. (2018). *Assessing the influence of operating conditions and thermophysical properties on the accuracy of in-situ measured U-values using quantitative internal infrared thermography*. *Energy and Buildings* (Vol. 171). https://doi.org/10.1016/j.enbuild.2018.04.011

Tham, S., Thompson, R., Landeg, O., Murray, K. A., & Waite, T. (2020). Indoor Temperature and Health: a global Systematic Review. *Public Health*, (179), 9–17.

The Guardian. (2015a). Egypt heatwave death toll rises as temperatures reach 46C. *The Guardian*, 1–8. Retrieved from https://www.theguardian.com/world/2015/aug/12/egypt-heatwave-death-toll-rises

The Guardian. (2015b). Your privacy Egypt heatwave death toll rises as temperatures reach 46C. Retrieved March 13, 2020, from https://www.theguardian.com/world/2015/aug/12/egypt-heatwave-death-toll-rises

Thimm, G., & Fiesler, E. (1997). High-order and multilayer perceptron initialization. *IEEE Transactions on Neural Networks*, *8*(2), 349–359. https://doi.org/10.1109/72.557673

Thomas, B., & Soleimani-Mohseni, M. (2007). Artificial neural network models for indoor temperature prediction: Investigations in two buildings. *Neural Computing and Applications*, *16*(1), 81–89. https://doi.org/10.1007/s00521-006-0047-9

Thumann, P.E., C.E.M., A., & Younger, C.E.M., W. J. (2017). *Handbook of Energy Audits*. *Handbook of*

Energy Audits. https://doi.org/10.4324/9780203912584

Tmušić, G., Manfreda, S., Aasen, H., James, M. R., Gonçalves, G., Ben-Dor, E., … McCabe, M. F. (2020). Current practices in UAS-based environmental monitoring. *Remote Sensing*, *12*(6). https://doi.org/10.3390/rs12061001

Tomlinson, C. J., Chapman, L., Thornes, J. E., & Baker, C. J. (2011). Including the urban heat island in spatial heat health risk assessment strategies: a case study for Birmingham, UK. *International Journal of Health Geographics*, *10*(41), 118–124. https://doi.org/10.1080/00049670.1997.10755790

Tompkins, E. L., & Eakin, H. (2012). Managing private and public adaptation to climate change. *Global Environmental Change*, *22*(1), 3–11. https://doi.org/10.1016/j.gloenvcha.2011.09.010

Totel, G. L. (1974). Physiological responses to heat of resting man with impaired sweating capacity. *Journal of Applied Physiology*, *37*(3), 346–352. https://doi.org/10.1152/jappl.1974.37.3.346

Tourneux, P., Libert, J.-P., Ghyselen, L., Léké, A., Delanaud, S., Dégrugilliers, L., & Bach, V. (2009). Heat Exchange and Thermoregulation in Newborns. *Pediatrics Archives*, *16*(7), 1057–1062.

Tran, K. V., Azhar, G. S., Nair, R., Knowlton, K., Jaiswal, A., Sheffield, P., … Hess, J. (2013). A cross-sectional, randomized cluster sample survey of household vulnerability to extreme heat among slum dwellers in Ahmedabad, India. *International Journal of Environmental Research and Public Health*, *10*(6), 2515–2543. https://doi.org/10.3390/ijerph10062515

Trang, P. M., Rocklöv, J., Giang, K. B., Kullgren, G., & Nilsson, M. (2016). Heatwaves and hospital admissions for mental disorders in Northern Vietnam e0155609. *PLoS ONE*, *11*(5), 1–20. https://doi.org/10.1371/journal.pone.0155609

Tso, G. K. F., & Yau, K. K. W. (2007). Predicting electricity energy consumption: A comparison of regression analysis, decision tree and neural networks. *Energy*, *32*(9), 1761–1768. https://doi.org/10.1016/j.energy.2006.11.010

Turner, B. L., Kasperson, R. E., Matsone, P. A., McCarthy, J. J., Corell, R. W., Christensene, L., … Schiller, A. (2003). A framework for vulnerability analysis in sustainability science. *Proceedings of the National Academy of Sciences of the United States of America*, *100*(14), 8074–8079. https://doi.org/10.1073/pnas.1231335100

Turner, L. R., Barnett, A. G., Connell, D., & Tong, S. (2012). Ambient temperature and cardiorespiratory morbidity: A systematic review and meta-analysis. *Epidemiology*, *23*(4), 594–606. https://doi.org/10.1097/EDE.0b013e3182572795

Uejio, C. K., Tamerius, J. D., Vredenburg, J., Asaeda, G., Isaacs, D. A., Braun, J., … Freese, J. P. (2016). Summer indoor heat exposure and respiratory and cardiovascular distress calls in New York City, NY, U.S. *Indoor Air*, (26), 594–604. https://doi.org/10.1111/ina.12227

Uejio, Christopher K., Wilhelmi, O. V., Golden, J. S., Mills, D. M., Gulino, S. P., & Samenow, J. P. (2011). Intra-urban societal vulnerability to extreme heat: The role of heat exposure and the built environment, socioeconomics, and neighborhood stability. *Health and Place*, *17*(2), 498–507. https://doi.org/10.1016/j.healthplace.2010.12.005

UNDP. (2016). Climate change and labour: Impacts of heat in the workplace, 36. Retrieved from http://www.undp.org/content/undp/en/home/librarypage/climate-and-disaster-resilience-/tackling-challenges-of-climate-change-and-workplace-heat-for-dev.html

UNESCO. (2012). UNESCO World Heritage Centre - Management of World Heritage Sites in Egypt Urban Regeneration Project for Historic Cairo, (July 2010), 135.

UNFCCC. (2016). *Opportunities and options for enhancing adaptation actions and supporting their implementation: reducing vulnerability and mainstreaming adaptation*. *UNFCC* (Vol. FCCC/TP/20).

UNISDR. (2009). Terminology on Disaster Risk Reduction. *International Stratergy for Disaster Reduction (ISDR)*, 1–30. Retrieved from www.unisdr.org/publications

United Nation Environment Programme (UNEP). (2004). *Impacts of Summer 2003 heat wave in Europe*. *Environment Alert Bulletin*. Nairobi, Kenya. https://doi.org/10.3886/ICPSR35021.v1

United Nations. (2018). *The World 's Cities*.

Urban, A., & Kyselý, J. (2014). Comparison of UTCI with other thermal indices in the assessment of heat and cold effects on cardiovascular mortality in the Czech Republic. *International Journal of Environmental Research and Public Health*, *11*(1), 952–967. https://doi.org/10.3390/ijerph110100952

US Census Bureau. (2019). 2018 Data Profiles - American Community Survey. Retrieved from https://www.census.gov/acs/www/data/data-tables-and-tools/data-profiles/2018/

US EPA. (2008). *Reducing Urban Heat Islands: Compendium of Strategies. Cool Pavements*. *EPA*. Retrieved from http://www.epa.gov/hiri/resources/compendium.htm%5Cnpapers2://publication/uuid/30F84843-04A3-4904-A3DF-AC06915537C0

Valleron, A. J., & Boumendil, A. (2004). Épidémiologie et canicules: Analyses de la vague de chaleur 2003 en France. *Comptes Rendus - Biologies*, *327*(12), 1125–1141. https://doi.org/10.1016/j.crvi.2004.09.009

van der Wiel, K., Kapnick, S. B., Vecchi, G. A., Cooke, W. F., Delworth, T. L., Jia, L., … Zeng, F. (2016). The resolution dependence of contiguous U.S. precipitation extremes in response to CO2 forcing. *Journal of Climate*, *29*(22), 7991–8012. https://doi.org/10.1175/JCLI-D-16-0307.1

Vandentorren, S., Bretin, P., Zeghnoun, A., Mandereau-Bruno, L., Croisier, A., Cochet, C., … Ledrans, M. (2006). August 2003 heat wave in France: Risk factors for death of elderly people living at home. *European Journal of Public Health*, *16*(6), 583–591. https://doi.org/10.1093/eurpub/ckl063

Vardoulakis, S., Dear, K., Hajat, S., Heaviside, C., Eggen, B., & McMichael, A. J. (2015). Comparative assessment of the effects of climate change on heat- and cold-related mortality in the United Kingdom and Australia. *Environmental Health Perspectives*, *122*(12), 1285–1292. https://doi.org/10.1289/ehp.1307524

Villa, T., Gonzalez, F., Miljevic, B., Ristovski, Z. D., & Morawska, L. (2016). An overview of small unmanned aerial vehicles for air quality measurements: Present applications and future prospectives. *Sensors (Switzerland)*, *16*(7), 12–20. https://doi.org/10.3390/s16071072

Virk, G., Jansz, A., Mavrogianni, A., Mylona, A., Stocker, J., & Davies, M. (2015). Microclimatic effects of green and cool roofs in London and their impacts on energy use for a typical office building. *Energy and Buildings*, *88*, 214–228. https://doi.org/10.1016/j.enbuild.2014.11.039

Walker, S. F. (1990). A brief history of connectionism and its psychological implications. *AI & Society*, *4*(1),

17–38. https://doi.org/10.1007/BF01889762

Walton, Z. L., Poudyal, N. C., Hepinstall-Cymerman, J., Johnson Gaither, C., & Boley, B. B. (2016). Exploring the role of forest resources in reducing community vulnerability to the heat effects of climate change. *Forest Policy and Economics*, *71*(October), 94–102. https://doi.org/10.1016/j.forpol.2015.09.001

Wang, Y., & Akbari, H. (2016). Analysis of urban heat island phenomenon and mitigation solutions evaluation for Montreal. *Sustainable Cities and Society*, *26*(October), 438–446. https://doi.org/10.1016/j.scs.2016.04.015

Watts, N., Amann, M., Arnell, N., Ayeb-Karlsson, S., Belesova, K., Boykoff, M., … Montgomery, H. (2019). The 2019 report of The Lancet Countdown on health and climate change: ensuring that the health of a child born today is not defined by a changing climate. *The Lancet*, *394*(10211), 1836–1878. https://doi.org/10.1016/S0140-6736(19)32596-6

Weber, S., Sadoff, N., Zell, E., & de Sherbinin, A. (2015). Policy-relevant indicators for mapping the vulnerability of urban populations to extreme heat events: A case study of Philadelphia. *Applied Geography*, *63*, 231–243. https://doi.org/10.1016/j.apgeog.2015.07.006

Wei, Y., Zhang, X., Shi, Y., Xia, L., Pan, S., Wu, J., … Zhao, X. (2018). A review of data-driven approaches for prediction and classification of building energy consumption. *Renewable and Sustainable Energy Reviews*, *82*(May 2017), 1027–1047. https://doi.org/10.1016/j.rser.2017.09.108

White-Newsome, J. L., Sánchez, B. N., Jolliet, O., Zhang, Z., Parker, E. A., Timothy Dvonch, J., & O'Neill, M. S. (2012). Climate change and health: Indoor heat exposure in vulnerable populations. *Environmental Research*, *112*(January), 20–27. https://doi.org/10.1016/j.envres.2011.10.008

White-Newsome, J. L., Sánchez, B. N., Parker, E. A., Dvonch, J. T., Zhang, Z., & O'Neill, M. S. (2011). Assessing heat-adaptive behaviors among older, urban-dwelling adults. *Maturitas*, *70*(1), 85–91. https://doi.org/10.1016/j.maturitas.2011.06.015

White-Newsomea, J. L., Sánchezb, B. N., Jollietc, O., Zhangb, Z., Parkerd, E. A., Dvonche, J. T., & O'Neillf, M. S. (2012). Climate Change and Health: Indoor heat Exposure in Vulnerable Populations. *Environmental Research*, (112), 20–27. https://doi.org/10.1016/j.envres.2011.10.008.Climate

Whitman, S., Good, G., Donoghue, E. R., Benbow, N., Shou, W., & Mou, S. (1997). Mortality in Chicago attributed to the July 1995 heat wave. *American Journal of Public Health*, *87*(9), 1515–1518. https://doi.org/10.2105/AJPH.87.9.1515

Wilhelmi, O., de Sherbinn, A., & Hayden, M. (2012). Exposure to Heat Stress in Urban Environments. In *Ecologies and Politics of Health* (Vol. 28, p. 1). Oxon, UK: Routledge.

Wilhelmi, O., & Hayden, M. (2016). Reducing Vulnerability to Extreme Heat Through Interdisciplinary Research and Stakeholder Engagement, (1), 165–186. https://doi.org/10.1007/978-3-319-30626-1_8

Wilkinson, R. G. (1996). *Unhealthy Societies: The Afflictions of Inequality*. Routledge.

Williams, A. A., Spengler, J. D., Catalano, P., Allen, J. G., & Cedeno-laurent, J. G. (2019). Building Vulnerability in a Changing Climate : Indoor Temperature Exposures and Health Outcomes in Older Adults Living in Public Housing during an Extreme Heat Event in Cambridge , MA.

Williams, C. (2002). Transforming the Old : Cairo's New Medieval City. *The Middle East Journal*, *56*(3), 457–475.

Wilson, A. (2006). Passive Survivability: A New Design Criterion for Buidlings. *Environmental Building News*, *15*(6).

Wolf, T., McGregor, G., & Analitis, A. (2014). Performance assessment of a heat wave vulnerability index for Greater London, United Kingdom. *Weather, Climate, and Society*, *6*(1), 32–46. https://doi.org/10.1175/WCAS-D-13-00014.1

Wolkoff, P. (2018). Indoor air humidity, air quality, and health – An overview. *International Journal of Hygiene and Environmental Health*, *221*(3), 376–390. https://doi.org/10.1016/j.ijheh.2018.01.015

Woodruff, R. E., McMichael, T. ., Butler, C. ., & Hales, S. . (2006). Action on Climate Change: The Health Risks of Procrastinating. *Australian and New Zealand Journal of Public Health*, *30*(26), 567–571. https://doi.org/10.1016/j.gmhc.2013.04.007

Woolcock, M. (2001). The place of social capital in understanding social and economic outcomes. *Canadian Journal of Policy Research*, *2*(1), 1–35.

World Health Organization (WHO). (2011). *Public Health Advice on Preventing Health Effects of Heat*. Copenhagen, Denmark. Retrieved from http://www.euro.who.int/__data/assets/pdf_file/0007/147265/Heat_information_sheet.pdf?ua=1

World Health Organization (WHO). (2018). *Climate Change and Health Security*. *Climate Change, New Security Challenges and the United Nations*. https://doi.org/10.4324/9781315272085-4

Wright, A. J., Young, A. N., & Natarajan, S. (2005). Dwelling temperatures and comfort during the August 2003 heat wave. *Building Services Engineering Research and Technology*, *26*(4), 285–300. https://doi.org/10.1007/0-306-48581-8_80

Wu, Z., Li, N., Peng, J., Cui, H., Liu, P., Li, H., & Li, X. (2018). Using an ensemble machine learning methodology-Bagging to predict occupants' thermal comfort in buildings. *Energy and Buildings*, *173*, 117–127. https://doi.org/10.1016/j.enbuild.2018.05.031

Xu, R., Zhao, Q., Coelho, M. S. Z. S., Saldiva, P. H. N., Abramson, M. J., Li, S., & Guo, Y. (2020). Socioeconomic level and associations between heat exposure and all-cause and cause-specific hospitalization in 1,814 Brazilian cities: A nationwide case-crossover study. *PLoS Medicine*, *17*(10), 1–18. https://doi.org/10.1371/journal.pmed.1003369

Yang, J., Wang, Z. H., & Kaloush, K. E. (2015). Environmental impacts of reflective materials: Is high albedo a "silver bullet" for mitigating urban heat island? *Renewable and Sustainable Energy Reviews*, *47*, 830–843. https://doi.org/10.1016/j.rser.2015.03.092

Yang, Y., Pan, M., & Pan, W. (2019). 'Co-evolution through interaction' of innovative building technologies: The case of modular integrated construction and robotics. *Automation in Construction*, *107*(July), 102932. https://doi.org/10.1016/j.autcon.2019.102932

Yardley, J., Sigal, R. J., & Kenny, G. P. (2011). Heat health planning: The importance of social and community factors. *Global Environmental Change*, *21*(2), 670–679. https://doi.org/10.1016/j.gloenvcha.2010.11.010

Yardley, J., Stapleton, J., Carter, M., Sigal, R., & Kenny, G. (2013). Is Whole-Body Thermoregulatory

Function Impaired in Type 1 Diabetes Mellitus? *Current Diabetes Reviews*, *9*(2), 126–136. https://doi.org/10.2174/1573399811309020004

Ye, X., Wolff, R., Yu, W., Vaneckova, P., Pan, X., & Tong, S. (2012). Ambient temperature and morbidity: A review of epidemiological evidence. *Environmental Health Perspectives*, *120*(1), 19–28. https://doi.org/10.1289/ehp.1003198

Yu, J., Ouyang, Q., Zhu, Y., Shen, H., Cao, G., & Cui, W. (2012). A comparison of the thermal adaptability of people accustomed to air-conditioned environments and naturally ventilated environments. *Indoor Air*, *22*(2), 110–118. https://doi.org/10.1111/j.1600-0668.2011.00746.x

Zamanian, Z., Sedaghat, Z., Hemehrezaee, M., & Khajehnasiri, F. (2017). Evaluation of environmental heat stress on physiological parameters. *Journal of Environmental Health Science and Engineering*, *15*(1), 1–8. https://doi.org/10.1186/s40201-017-0286-y

Zanobetti, A., O'Neill, M. S., Gronlund, C. J., & Schwartz, J. D. (2013). Susceptibility to mortality in weather extremes: Effect modification by personal and small-area characteristics. *Epidemiology*, *24*(6), 809–819. https://doi.org/10.1097/01.ede.0000434432.06765.91

ZCH. (2016). *Solutions to overheating in homes: Evidence review report*.

Zeng, Q., Li, G., Cui, Y., Jiang, G., & Pan, X. (2016). Estimating temperature-mortality exposure-response relationships and optimum ambient temperature at the multi-city level of China. *International Journal of Environmental Research and Public Health*, *13*(3). https://doi.org/10.3390/ijerph13030279

Zhang, S., & Lin, Z. (2020). Standard effective temperature based adaptive-rational thermal comfort model. *Applied Energy*, *264*(April), 2001–2002. https://doi.org/10.1016/j.apenergy.2020.114723

Zhang, Y., Nitschke, M., & Bi, P. (2013). Risk factors for direct heat-related hospitalization during the 2009 Adelaide heatwave: A case crossover study. *Science of the Total Environment*, *442*(January 2013), 1–5. https://doi.org/10.1016/j.scitotenv.2012.10.042

Zhang, Z. (2016). Introduction to machine learning: K-nearest neighbors. *Annals of Translational Medicine*, *4*(11). https://doi.org/10.21037/atm.2016.03.37

Zhao, H., Shi, J., Qi, X., Wang, X., & Jia, J. (2017). Pyramid scene parsing network. *Proceedings - 30th IEEE Conference on Computer Vision and Pattern Recognition, CVPR 2017*, *2017-Janua*, 6230–6239.

Zhao, Y., Genovese, P. V., & Li, Z. (2020). Intelligent thermal comfort controlling system for buildings based on IoT and AI. *Future Internet*, *12*(2). https://doi.org/10.3390/fi12020030

Zhu, Q., Liu, T., Lin, H., Xiao, J., Luo, Y., Zeng, W., … Ma, W. (2014). The spatial distribution of health vulnerability to heat waves in guangdong province, China. *Global Health Action*, *7*(1).

Zukowska, D., Ananida, M., Kolarik, J., Khanie, M. S., & Nielsen, T. R. (2019). Solar control solutions for reducing overheating risks in retrofitted Danish apartment buildings from the period 1850-1900 - A simulation-based study. *E3S Web of Conferences*, *111*(201 9), 1–8.

Zukowski, M., Sadowska, B., & Sarosiek, W. (2011). Assessment of the cooling potential of an earth-tube heat exchanger in residential buildings. *8th International Conference on Environmental Engineering, ICEE 2011*, (May 2015), 830–834.